

**Efficient transition metal oxides-based catalysts
for the catalytic oxidation of volatile organic
compounds (VOCs)**

Jing Wang

Graduate School of Science and Technology

Hirosaki University

2020

ABSTRACT

Volatile organic compounds (VOCs) are a large group of carbon-based chemicals which mainly come from human activities of industrial production and transportation. Their toxic properties and easily vaporized nature under atmospheric pressure make them the main contributor to the serious environmental pollution, and the second pollution of ozone, photochemical smog and aerosols, causing further threat to life on earth. It is urgent to remove VOCs by environmental and economical strategies. Catalytic oxidation is one of the most efficient and environmentally friendly pathways to convert VOCs into harmless substances of water (H_2O), carbon dioxide (CO_2) and other less harmful chemicals. Normally, two types of noble metal-based catalysts and transition metal oxides-based catalysts are widely investigated and developed for the catalytic oxidation of VOCs.

In this work, transition metal oxides-based catalysts were investigated and used for the catalytic oxidation of VOCs. Herein, toluene was chosen as the model VOCs, the catalytic performance of toluene oxidation was carried out in a fixed-bed reactor at the atmospheric pressure, accompanied by detected the reaction products using a gas chromatograph equipped with a flame ionization detector (FID), meanwhile, the outgoing products from the reactor were analyzed on an on-line FTIR gas analyzer. In order to improve the catalytic activity of $\text{Co}_3\text{O}_4/\text{NF}$ (Nickel foam) catalyst, firstly, we prepared a series of hetero-metal doped Co-based catalysts by using facile electrodeposition method, and the effect of different metal doping on the catalytic performance of toluene was investigated. It was found that hetero-metal doping significantly influenced the morphology and surface elemental compositions of Co-based catalyst, but over doping of hetero-metals such as Ni and Mn elements content made a negative influence on the catalyst structure. H_2 -TPR and O_2 -TPD analysis results suggested that the hetero-metal doping enhanced the low temperature reducibility and resulted in the formation of lattice defects, which are favorable to generate more easily reducible species and facilitate the oxygen mobility, thereby improved the performance for the catalytic oxidation of toluene. Especially, when compared with pure $\text{Co}_3\text{O}_4/\text{NF}$ catalyst, mixed metal oxides based catalyst

of Co-Cu/NF exhibited much lower toluene conversion (T_{90}) of around 248 °C, which should be contributed by its low-temperature reducibility, increased surface and lattice oxygen species, and high content of active Co^{3+} species promoted by the interaction of the mixed metal oxides. Moreover, the Co-Cu/NF also performed excellent catalytic stability and high selectivity to CO_2 in the presence and absence of water vapor for the catalytic combustion of toluene for a long-term test.

Based on the first work, we used the same method to prepare Ce modified Co-based catalysts for the catalytic oxidation of toluene. The catalysts of Co-Ce mixed oxides supported on three-dimensional NF by using a unipolar pulse electro-deposition (UPED) in the solutions of $\text{Co}(\text{NO}_3)_2 \cdot 6\text{H}_2\text{O}$ and $\text{Ce}(\text{NO}_3)_3 \cdot 6\text{H}_2\text{O}$ with molar ratios of Co to Ce (Co/Ce) of 15:1, 10:1, and 5:1, respectively. The experimental results showed that Co-Ce mixed oxide with a well nanosheet structure could be uniformly deposited on NF support. H_2 -TPR analysis indicated that Ce doping improved the reducibility of Co-Ce/NF catalyst due to the synergistic effect between Co and Ce. In the toluene catalytic oxidation, the 10Co-Ce/NF catalyst prepared with a molar ratio of Co/Ce at 10 in the initial solution achieved the best catalytic performance among all the catalysts with a complete toluene conversion temperature of 268 °C and CO_2 selectivity of 100%. This can be contributed to the superior physiochemical properties of uniform nanosheet structure, increase of surface and lattice active oxygen species at low temperatures, high content of Co^{3+} active species with high oxygen vacancies and $\text{Ce}^{4+}/\text{Ce}^{3+}$ redox couples in the catalyst. Furthermore, the 10Co-Ce/NF catalyst exhibited long-term stability in the presence of water vapor.

Cerium oxide (CeO_2) has been proved to be active to the catalytic oxidation because of its excellent oxygen storage and release ability, especially the redox couple of $\text{Ce}^{4+}/\text{Ce}^{3+}$ is favorable to the generation of active oxygen species for VOCs oxidation. Consequently, in this part, CeO_2 dominated catalysts of Ag- CeO_2 @CNWs/CF were designed and applied for the catalytic oxidation of toluene. The Ag- CeO_2 @CNWs/CF catalysts with different Ag loading amount was prepared by applying a three-step electrochemical process, in which copper nanowires (CNWs) were generated on the surface of CF by an electro-oxidization process at first and then, CeO_2 was uniformly coated

on the CNWs by a UPED method and finally highly dispersed Ag nanoparticles were embedded on the surface of CeO₂ using a constant voltage electrodeposition method. It is found that the suitable Ag loading amount effectively enhanced the low-temperature reducibility, the generation of oxygen vacancies, and distribution of surface acid sites, which are favorable to the catalytic oxidation of toluene. Especially, the obtained 80Ag-CeO₂@CNWs/CF catalyst with an electrodeposition time of 80 s for Ag loading exhibited the best catalytic activity with the T₁₀, T₅₀ and T₉₀ of toluene conversion at 222, 240 and 256 °C, respectively. Long-term stability tests with and without water vapor further indicated that the 80Ag-CeO₂@CNWs/CF catalyst had good stability and water resistance ability during the catalytic oxidation of toluene.

In the first three parts of work, NF and CF were applied as the catalyst supports, hence, in order to investigate the influence of the catalyst supports of NF and CF on the catalytic performance of the prepared catalysts, the Mn-Co mixed metal oxides as active species were prepared and applied for the catalytic oxidation of toluene. We fabricated a series of Mn-Co/CF catalysts with different molar ratio of Mn/Co in the initial solution for the electrodeposition. SEM images displayed that Mn-Co mixed metal oxides were uniformly coated on the Cu nanowires by the electrochemical method. The intimate contact between Mn and Co nanocrystals was found by HRTEM, which is important for realizing synergetic effects on improving catalytic activity. Meanwhile, the formation of the active surface oxygen species and the increase of the active species of Mn⁴⁺ and Co³⁺ were considered to make significant contribution to the catalytic oxidation of toluene. The catalyst with Mn-Co mixed metal oxides exhibited higher performance than the single metal oxides, and especially 0.10Mn-0.01Co/CF catalyst with the Mn/Co molar ratio of 10:1 in the initial solution for the electrodeposition achieved the highest catalytic activity with a low toluene conversion temperature (T₉₀) of 251 °C, and displayed excellent catalytic stability even in the presence of water vapor. However, Mn-Co mixed oxides based catalysts which prepared by using unpretreated CF (without electro-oxidation) and NF supports performed poor catalytic activity when compared the optimum catalysts of 0.10Mn-0.01Co/CF. Consequently, catalysts prepared by CF support which possesses

nanowires was more favorable to the catalytic oxidation of toluene in this part of work.

In summary, efficient transition metal oxides-based catalysts which prepared by the time-saving method of electrodeposition and three-dimensional (3D) catalyst supports of NF and CF and used for the catalytic oxidation of toluene, all of them performed excellent catalytic activity, long-term stability and water resistance in the presence and absence of water vapor. It is expected that such a simply-electrodeposited mixed metal oxides-based catalysts could be applied for the oxidation of volatile organic compounds (VOCs) in a practical process.

ACKNOWLEDGMENTS

First and foremost, I would like to thank my profound and respectable academic mentor, Professor Dr. Guoqing Guan, who gives me an opportunity to study towards Ph. D in his laboratory, and his valuable, academical and professional suggestions are extremely important to my three-year Ph. D program.

I would like to thank Professor Dr. Abuliti Abudula, Graduate School of Science and Technology, Hirosaki University, his kind support helps me a lot for my study.

I would like to thank Associate Professor Dr. Akihiro Yoshida helps me setting up the experimental device, as well as his useful advices on my research.

I would like to thank Professor Dr. Xiaogang Hao, Department of Chemical Engineering, Taiyuan University of Technology, China, for his introduction to continue my PhD study in this laboratory, and his help to the regarding to the application of X-ray photoelectron spectroscopy.

I would like to thank all professors and staff in Energy Conversion Engineering Laboratory Institute of Regional Innovation (IRI), and at Graduated School of Science and Technology, Hirosaki University, for their kind helps and support in my study.

I would like to thank all members in our groups, including seniors who have graduated, for their warm and kind advice and helps to my study and daily life.

I would like to thank my all family members, friends and my boyfriend Wu Zhijun, for their support, understanding, help and encouragement during my study and daily life.

Finally, I would like to give my deep thanks to Jiku Chemical Co. Ltd., Japan, for their kind support to my research.

Thank you all very much

Jing Wang

TABLE OF CONTENTS

ABSTRACT.....	I
ACKNOWLEDGMENTS	V
TABLE OF CONTENTS	VI
LIST OF TABLES	X
LIST OF FIGURES	XI
CHAPTER 1 Introduction.....	1
1.1 Classification and influence of VOCs.....	1
1.2 Strategies of VOCs removal	2
1.3 Mechanisms of VOCs catalytic oxidation	4
1.4 Development of catalysts for VOCs catalytic oxidation.....	6
1.4.1 Single-noble-metal-based catalysts.....	6
1.4.2 Mixed-noble-metals-based catalysts	8
1.4.3 Supported transition-metal-oxide-based catalysts	13
1.4.4 Unsupported mesoporous transition-metal-oxide-based catalysts.....	14
1.5 Deactivation/regeneration of catalysts	19
1.6 Experimental performance of VOCs catalytic oxidation.....	22
1.7 Objective of this study	23
1.8 Scope of this dissertation	23
References.....	26
CHAPTER 2 Stable hetero-metal doped Co-based catalysts prepared by electrodeposition method for low temperature combustion of toluene.....	42
2.1 Introduction.....	42
2.2 Experimental	44

2.2.1 Chemicals and Materials.....	44
2.2.2 Catalyst preparation	44
2.2.3 Characterizations.....	45
2.2.4 Catalytic performance test	45
2.3. Results and discussion	46
2.3.1 Morphology, surface composition and crystal phase	46
2.3.2 Redox properties	49
2.3.3 Surface composition and metal oxidation state	52
2.3.4 Catalytic performance	55
2.3.5 Long-term stability test on stream	57
2.4 Conclusions.....	59
References.....	60
CHAPTER 3 Catalytic oxidation of volatile organic compound over Ce modified Co-based mixed oxide catalysts synthesized by electrodeposition method.....	65
3.1 Introduction.....	65
3.2 Experimental.....	67
3.2.1 Chemicals and Materials.....	67
3.2.2 Preparation of catalysts	67
3.2.3 Characterizations.....	68
3.2.4 Catalytic activity test.....	69
3.3 Results and discussion	70
3.3.1 SEM analysis	70
3.3.2 XRD analysis	72
3.3.3 TEM analysis	74
3.3.4 H ₂ -TPR analysis.....	75
3.3.5 O ₂ -TPD analysis.....	79

3.3.6 XPS analysis	80
3.3.7 Catalytic activity	83
3.3.8 Effect of supported Co-Ce loading amount, WHSV and GHSV	87
3.3.9 Effect of water in long-term stability evaluation	89
3. 4. Conclusions.....	92
References.....	93
CHAPTER 4 Highly dispersed Ag nanoparticles embedded on the surface of CeO ₂ /CF nanowires derived from three-dimensional structured Cu foam for toluene catalytic oxidation.....	
4.1 Introduction.....	99
4.2 Experimental.....	101
4.2.1 Chemicals and Materials.....	101
4.2.2 Catalyst preparation	101
4.2.3 Characterizations.....	102
4.2.4 Catalytic activity test.....	104
4.3 Results and discussion	105
4.3.1 XRD analysis and SEM/TEM characterizations.....	105
4.3.2 Redox performance	109
4.3.3 XPS analysis	113
4.3.4 Surface acidity	116
4.3.5 Catalytic performance.....	117
4.3.6 Stability.....	123
4.4 Conclusions.....	125
References.....	126
CHAPTER 5 Mn-Co oxide decorated on Cu nanowires as efficient catalysts for catalytic oxidation of toluene.....	
5.1 Introduction.....	132

5.2 Experimental	134
5.2.1 Chemicals and Materials	134
5.2.2 Electrodeposition of Mn-Co mixed metal oxides	135
5.2.3 Characterizations	135
5.2.4 Catalytic activity test	136
5.3. Results and discussion	137
5.3.1 SEM analysis	137
5.3.2 TEM analysis	140
5.3.3 XRD analysis	141
5.3.4 H ₂ -TPR analysis	143
5.3.5 O ₂ -TPD analysis	145
5.3.6 XPS analysis	146
5.3.7 Catalytic activity	148
5.3.8 Long-term on-stream stability test	153
5.4. Conclusions	154
References	156
CHAPTER 6 Conclusions and Prospects	161
6.1 Conclusions	161
6.2 Prospects	163
List of publications and presentations	166

LIST OF TABLES

Table 1.1 Typical single-noble-metal-based catalysts reported in the literatures.....	11
Table 1.2 Typical mixed-noble-metals-based catalysts reported in the literatures.....	12
Table 1.3 Supported single-transition-metal catalyst reported in the literatures.	16
Table 1.4 Supported mixed-transition-metal catalyst reported in the literatures.	17
Table 1.5 Unsupported transition-metal-based catalysts reported in the literatures.....	18
Table 2.1 Hetero-metal contents on the prepared catalyst surfaces.	47
Table 2.2 Hydrogen consumptions of the prepared Co-based catalysts in H ₂ -TPR analyses.	51
Table 2.3 Surface elemental compositions and valence states of Co-based catalysts based on XPS analysis.....	54
Table 2.4 Performance test results for the prepared Co-based catalysts for the catalytic combustion of toluene.....	57
Table 3.1 Loading amounts of catalysts on NF.	68
Table 3.2 Elemental compositions on the surfaces of Co-Ce/NF catalysts prepared with different initial molar ratios of Co/Ce.	71
Table 3.3 Hydrogen consumption and O ₂ desorption of Co-Ce/NF catalysts.....	78
Table 3.4 Surface elemental compositions of Co-Ce/NF catalysts.	78
Table 3.5 Results of catalytic oxidation of toluene over Co-Ce/NF catalysts.....	86
Table 3.6 Comparison of common Co-Ce mixed oxide catalysts for toluene catalytic oxidation reported in the literature with this work.....	87
Table 4.1 Surface elemental compositions of Ag-CeO ₂ @CNWs/CF catalysts prepared with the electrodeposition time varied from 40 to 100 s for Ag loading.	107
Table 4.2 Hydrogen consumption and oxygen desorption of various Ag-CeO ₂ @CNWs/CF catalysts for H ₂ -TPR and O ₂ -TPD analyses.....	111
Table 4.3 Surface element compositions and valence states of Ag-CeO ₂ /CF catalysts tested by XPS	

technique.	115
Table 4.4 Summary of the results on the catalytic oxidation of toluene over the prepared Ag-CeO ₂ @CNWs/CF catalysts.	121
Table 5.1 Surface elemental compositions of Mn-Co/CF catalysts prepared with different initial molar ratios of Mn/Co in the electrodeposition solutions.	138
Table 5.2 Hydrogen consumption of Mn-Co/CF catalysts for H ₂ -TPR analysis	145
Table 5.3 Surface element compositions and valence states of Mn-Co/CF catalysts.	148
Table 5.4 Results of catalytic oxidation of toluene over Mn-Co/CF catalysts.	150

LIST OF FIGURES

Fig. 1.1. Schematic illustration of mechanism for VOCs catalytic oxidation.	4
Fig. 1.2. Experimental performance of VOCs catalytic oxidation.	22
Fig. 2.1. SEM images of the prepared hetero-metal doped Co-based catalysts with different metals.	48
Fig. 2.2. XRD patterns of the prepared hetero-metal doped Co-based catalysts.	49
Fig. 2.3. H ₂ -TPR profiles of the prepared Co-based catalysts.	51
Fig. 2.4. O ₂ -TPD profiles of the prepared Co-based catalysts.	52
Fig. 2.5. XPS spectra of Ni 2p, Mn 2p and Cu 2p (a), Co 2p (b) and O1s (c) for pure Co ₃ O ₄ /NF, hetero-metal doping catalysts of Co-Ni/NF, Co-Mn/NF, and Co-Cu/NF.	54
Fig. 2.6. Catalytic performances of the prepared Co-based catalysts for catalytic combustion of toluene.	56
Fig. 2.7. Long-term stability test in the absence and presence of water vapor for the catalytic combustion of toluene.	58
Fig. 2.8. Surface elemental compositions of the spent Co-Cu/NF catalyst after the long-term stability test (The weight percent of wt % for O, Co, Ni and Cu were taken by EDX analysis).	58
Fig. 3.1. SEM images of the surfaces of various Co-Ce/NF catalysts (Insets: the enlarged ones).	71

Fig. 3.2. SEM image (a) and EDX analysis (b) of the spent 10Co-Ce/NF catalysts (Inset: the enlarged image).	72
Fig. 3.3. XRD patterns of as-prepared Co-Ce/NF catalysts.	73
Fig. 3.4. TEM and HRTEM images of Co ₃ O ₄ /NF catalyst (a, b), 5Co-Ce/NF catalyst(c, d), 10Co-Ce/NF catalyst (e, f) and 15Co-Ce/NF catalyst (g, h).....	74
Fig. 3.5. H ₂ -TPR profiles of Co-Ce/NF catalysts.	77
Fig. 3.6. O ₂ -TPD profiles of Co-Ce/NF catalysts.....	77
Fig. 3.7. XPS spectra of Co-Ce/NF catalysts: Co 2p (a), Ce 3d (b) and O 1s (c).....	83
Fig. 3.8. Catalytic activity of nickel foam for the catalytic oxidation of toluene.....	84
Fig. 3.9. Performances of Co-Ce/NF catalysts for the catalytic oxidation of toluene: (a) Toluene conversion; (b) CO ₂ selectivity.	85
Fig. 3.10. Catalytic performance of 10Co-Ce/NF catalyst with different loading amounts prepared by different pulse cycles for the catalytic oxidation of toluene: (a) 500 cycles, (b) 1000 cycles and (c) 1500 cycles.....	88
Fig. 3.11. SEM images of 10Co-Ce/NF catalysts prepared by different pulse cycles; (a, b) 1000 cycles and (c, d) 1500 cycles.	89
Fig. 3.12. Effects of WHSV (a) and GHSV (b) on the catalytic oxidation of toluene over 10Co-Ce/NF catalyst.....	89
Fig. 3.13. Recycled catalytic performances of 10Co-Ce/NF catalyst on-stream for catalytic oxidation of toluene (WHSV=30,000 mL·g ⁻¹ ·h ⁻¹ , toluene concentration = 900 ppm, water vapor content = 5.0 vol%).....	90
Fig. 3.14. Long time evaluation on-stream of toluene catalytic oxidation over 10Co-Ce/NF catalyst (WHSV=30,000 mL g ⁻¹ h ⁻¹ , toluene concentration = 900 ppm, reaction temperature = 262 °C, reaction time = 1660 min).....	91
Fig. 3.15. Long-term evaluation of toluene catalytic oxidation on 10Co-Ce/NF catalyst (WHSV=30,000 mL·g ⁻¹ ·h ⁻¹ , toluene concentration = 900 ppm, reaction temperature was set at 250 °C	

in order to maintain the conversion >90%, reaction time =2500 min).	91
Fig. 4.1. SEM images of (a) Cu nanowires on Cu foam (CF) and (b) CeO ₂ @CNWs/CF catalyst (Insets: the enlarged images).	102
Fig. 4.2. XRD patterns of Ag-CeO ₂ @CNWs/CF catalysts prepared with the electrodeposition time varied from 40 to 100 s for Ag loading.	107
Fig. 4.3. SEM images of the prepared Ag-CeO ₂ @CNWs/CF catalysts (Insets: the enlarged images).	108
Fig. 4.4. SEM image of the spent 80Ag-CeO ₂ @CNWs/CF catalyst (Inset: the enlarged image).	108
Fig. 4.5. TEM images of (a) bare single CNWs, (b) CeO ₂ @CNWs and (c-f) Ag-CeO ₂ @CNWs catalysts.	109
Fig. 4.6. HRTEM images of the prepared Ag-CeO ₂ @CNWs/CF catalysts.	109
Fig. 4.7. H ₂ -TPR profiles of the prepared Ag-CeO ₂ @CNWs/CF catalysts with different Ag loading amounts.	111
Fig. 4.8. O ₂ -TPD profiles of the prepared Ag-CeO ₂ @CNWs/CF catalysts.	113
Fig. 4.9. XPS profiles of Ce 3d, Ag 3d and O 1s of the prepared Ag-CeO ₂ @CNWs/CF catalysts.	116
Fig. 4.10. NH ₃ -TPD profiles of the prepared Ag-CeO ₂ @CNWs/CF catalysts.	117
Fig. 4.11. (a) Toluene conversion, (b) toluene consumption rate per gram of catalyst and (c) Arrhenius plots of the prepared Ag-CeO ₂ @CNWs/CF catalysts for catalytic oxidation of toluene.	121
Fig. 4.12. Catalytic activity of 3.7wt% Ag-CeO ₂ @CNWs/CF catalyst prepared by a wet impregnation method for catalytic oxidation of toluene.	122
Fig. 4.13. SEM image of 3.7wt% Ag-CeO ₂ @CNWs/CF catalyst prepared by a wet impregnation method.	122
Fig. 4.14. CO ₂ selectivity of 80Ag-CeO ₂ @CNWs/CF for the catalytic oxidation of toluene.	123
Fig. 4.15. Long-term on-stream evaluation of 80Ag-CeO ₂ @CNWs/CF catalyst for the catalytic oxidation of toluene in the presence and absence of water vapor (Reaction conditions: toluene concentration = 961 ppm, WHSV=30,000 mL g ⁻¹ h ⁻¹ , reaction temperature=280 °C, reaction	

time=2625 min).....	124
Fig. 4.16. Stability test of 80Ag-CeO ₂ @CNWs/CF catalyst for the catalytic oxidation of toluene in the absence of water vapor with a lower toluene conversion (Reaction conditions: toluene concentration = 961 ppm, WHSV=30,000 mL g ⁻¹ h ⁻¹ , reaction temperature = 257 °C, reaction time=2730 min).....	124
Fig. 5.1. SEM images of Cu foam (CF) possesses nanowires after electro-oxidation.	134
Fig. 5.2. SEM images of various Mn-Co/CF catalysts (Insets: the enlarged images).	139
Fig. 5.3. SEM images of 0.15Mn-0.01Co/CF catalyst.	139
Fig. 5.4. TEM images of single 0.01Co/CF (a) and 0.10Mn/CF (b) catalysts and the corresponding HRTEM images (c, d).....	140
Fig. 5.5. TEM images of 0.01Mn-0.01Co/CF (a), 0.05Mn-0.01Co/CF (b) and 0.10Mn-0.01Co/CF (c) catalysts and (d, e, f) are the corresponding HRTEM images of (a, b, c).	141
Fig. 5.6. XRD patterns of 0.01Co/CF, 0.01Mn/CF and three Mn-Co/CF catalysts.	143
Fig. 5.7. H ₂ -TPR (a) and O ₂ -TPD (b) profiles of the prepared catalysts.	144
Fig. 5.8. XPS profiles of Mn 2p (a), Co 2p (b), O 1s (c) of 0.01Co/CF, 0.10Mn/CF and Mn-Co/CF catalysts and linear relationship between Mn ⁴⁺ /Mn ³⁺ and Co ³⁺ /Co ²⁺ tested by XPS (d).....	148
Fig. 5.9. Catalytic performances of Mn-Co/CF catalysts for the toluene oxidation: (a) Toluene conversion and (b) CO ₂ selectivity.	150
Fig. 5.10. Catalytic performances of 0.10Mn-0.01Co/CF catalyst (CF without electro-oxidation) (a), 0.10Mn-0.01Co/NF catalyst was prepared by using nickel foam (NF) support (b).	151
Fig. 5.11. SEM images of (a) 0.10Mn-0.01Co/CF catalyst (CF without electro-oxidation) and (b) 0.10Mn-0.01Co/ NF (nickel foam) catalyst was prepared by using NF support.	152
Fig. 5.12. TOFs based on the surface Mn species of the prepared catalysts at 222 °C and 232 °C...	152
Fig. 5.13. Long-term on-stream evaluation of 0.10Mn-0.01Co/CF catalyst for the catalytic oxidation of toluene in the presence of water vapor (Reaction conditions: toluene concentration = 978 ppm, WHSV=30,000 mL g ⁻¹ h ⁻¹ , reaction temperature=261 °C, reaction time=1500 min).....	153
Fig. 5.14. Long-term evaluation of 0.10Mn-0.01Co/CF catalyst for the catalytic oxidation of toluene in	

the absence of water vapor (Reaction conditions: toluene concentration = 978 ppm, WHSV=30,000 mL g⁻¹ h⁻¹, reaction temperature = 237 °C, reaction time=3100 min).....154

CHAPTER 1 Introduction

1.1 Classification and influence of VOCs

Volatile organic compounds (VOCs) are a large group of easily-evaporated carbon-based organic chemicals with high vapor pressure (>10 Pa) and low boiling points ($50-260^{\circ}\text{C}$) under atmospheric pressure[1]. The easily vaporized nature and low water solubility make them main contributor to the environmental pollution[2]. VOCs are harmful to human health and the environment as a result of their toxicity, irritation, teratogenicity and carcinogenicity, especially the second pollution of ozone, photochemical smog and aerosols causing further threat to life on earth [3-6]. VOCs are always existed into air by a series of human activities like extensive use of organic solutions in building materials, decorative materials, fiber materials, chemical industries, and transportation section [7-10].

Depending on the chemical structures of VOCs, which can be classified into various types such as alkanes, aromatics, alkenes, halocarbons, esters, aldehydes, and ketones [11]. The most common alkane is methane, it is widely used as fuel in our daily life and industrial process, meanwhile, the synthesis of ammonia, urea and carbon black also and raw materials of is a byproduct exist in the exhaust of the syngas production and natural gas power plants. The excessive emissions of methane will lead to serious greenhouse effect in the world [12]. Aromatics of toluene, benzene and xylene are not only the petroleum products, but also the main raw material for the industrial products such as medicine, paint, oily coatings, and inks etc., while their toxic properties could cause serious impact on the human health. Importantly, the emission of aromatics into air also can make significant influence on the ozone layer, and therefore leading to environmental pollution problem of photochemical smog formation[13]. Alkenes are one class of unsaturated hydrocarbons, which are the main raw material for the production of polyolefin and synthetic rubbers through organic synthesis[14]. However, styrene as an unsaturated hydrocarbon which is easily volatilizes into the air, and small amount of styrene could damage the respiratory system and the central nervous system of

human being, therefore it is classified in the carcinogen list [15]. Sub-class VOCs of halocarbons are derived from compounds in which a hydrogen atom in a hydrocarbon molecule is replaced by a halogen atom, they are well known for their strong toxic properties of anti-biodegradability and carcinogenicity[16]. It is commonly found that chlorine containing VOCs are prevalent in drinking water, refrigerants and cleaning agents, which are huge hidden dangers to the environment and humans[17]. Esters are widespread in nature (e.g., plants, fruits and animals), which formed by the reactions between acid (carboxylic acid or inorganic oxo acid) and alcohol. Aldehydes are famous for formaldehyde, especially its excessive production and utilization in decoration materials is the main cause of many diseases and photochemical smog[18]. Ketones can be classified as fatty ketones, alicyclic ketones, aromatic ketones, saturated ketones, and unsaturated ketones. They are widely applied in the field of cosmetics such as nail polish, perfumes, aerosols and so on, which are harmful and toxic as other VOCs. In addition, VOCs come from wastewater treatment, automobile exhaust or burning fossil fuels always containing hetero elements of sulfide and nitrogen, the excessive emissions of sulfide and nitrogen compounds could lead to the second pollution of acid rain, acidification and eutrophication of surface water [19].

As a result, VOCs are proved to be harmful to the environment and human health, it is important not only to reduce VOCs emissions, but also to remove VOCs as soon as possible. The development of our society depends on the natural environment, and more efforts needed to be made to protect the environment.

1.2 Strategies of VOCs removal

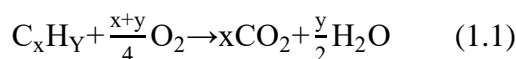
For decades, various approaches including thermal incineration, membrane separation, condensation, adsorption, absorption, biochemical, photo-catalysis, ozone-catalytic oxidation, plasma-catalysis and catalytic oxidation have been developed and applied for the VOCs removal[1]. The commonly used method for VOCs removal is thermal incineration, which is suitable for the removal of high concentrated VOCs, however, the required temperatures for complete VOCs destruction is usually in the high temperature range of 800~1200°C, leading to the high operating

costs[20]. Membrane separation is facile way to remove VOCs from industry exhaust, the process is flexible depending on the selected membrane, while its high cost and unstable property limit the widespread utilization in industrial process[21]. VOCs removal by condensation is an energy consuming way, which also restricted by the treatment of coolants after the condensation process[22]. Adsorption is widely used for the selected adsorption of highly diluted VOCs in gas stream, in which zeolite or activated carbon can be applied as the effective adsorbent, the limitation of this method is the high cost and the regeneration of the used adsorbent[23]. On the contrary, absorption is employed to eliminate the high concentrated of water-soluble VOCs, the difficulty is removing VOCs with a suitable solvent[7]. Biochemical method is an environmental way which could convert VOCs to CO₂ and H₂O without using natural gas fuel, while the existed interaction within the mixed VOCs will lead to inhibition or competition during this process [24]. Photocatalysis technique is a cost-effective strategy for the degradation of indoor VOCs, by which VOCs from liquid and gas phase could be transferred into CO₂ in the presence of ultra-violet (UV) light and semiconductor, the disadvantage is that the organic intermediate products may cause the second pollution[25, 26]. Ozone-catalytic oxidation is another promising method to eliminate VOCs assisted by ozone, which could be conducted under relatively mild conditions, while the accumulation of organic byproducts on the surface of catalysts can easily cause catalyst deactivation[27, 28]. Hazardous VOCs also can be degraded by the method of plasma-catalysis, which is a low-temperature oxidation process, the main influence factors are the selection of applied materials and the selectivity of CO₂ product[29]. However, compared with these methods, catalytic oxidation is an effective and economically feasible way for the removal of VOCs, which can completely transform organic contaminant into harmless substances such as carbon dioxide (CO₂) and water (H₂O) at relatively low temperatures (< 500 °C)[7]. In terms of the catalytic oxidation of VOCs, the most important issue is how to design rational catalyst with high activity and stability but low cost and environmentally friendly. For instance, Peng *et al.* prepared Pt/CeO₂ catalysts for the catalytic oxidation of toluene, by which toluene could be completely converted into CO₂ at low temperature of 160 °C [30]. Meanwhile,

Zhao *et al.* synthesized non-precious catalysts of $\text{Co}_3\text{O}_4@\text{MnO}_x\text{-NF}$ for the catalytic oxidation of acetone, ethyl acetate and toluene, the complete conversion temperatures were 180, 210 and 240 °C, respectively[31]. Notably, these outstanding catalysts also exhibited good stability and water-resistance during the oxidation process. As a result, both supported noble metal based catalysts and transition metal oxides based catalysts are active to the catalytic oxidation of VOCs, and which has already been proved by numbers of works in the reported literatures[32].

1.3 Mechanisms of VOCs catalytic oxidation

Simply, complete oxidation of VOCs can be expressed by the following equation:



When this reaction occurs over the catalyst, three mechanisms have been proposed (listed in **Fig. 1.1**): (1) Eley-Rideal (E-R) mechanism, which demonstrates that the reaction is controlled by the absorbed molecules and the molecule in the gas phase; (2) Langmuir-Hinshelwood (L-H) mechanism, which explains that the reaction is promoted by the absorbed VOCs and the absorbed oxygen; and (3) Mars-van Krevelen (MVK) mechanism, which indicates that the reaction takes place between the absorbed VOCs molecules and the lattice oxygen in the catalyst [33, 34].

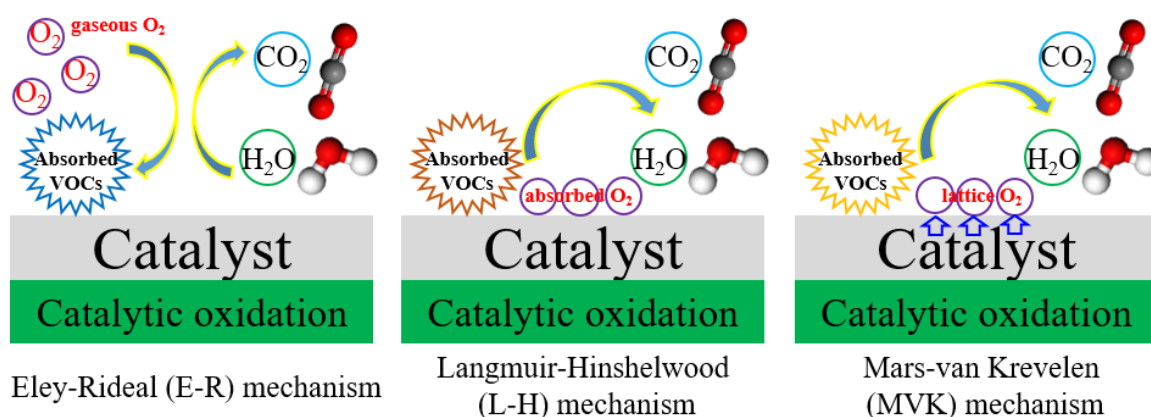


Fig. 1.1. Schematic illustration of mechanism for VOCs catalytic oxidation.

In general, oxidation of VOCs over different catalysts should follow different mechanisms [35]. For examples, Minicò *et al.* [36] performed the catalytic oxidations of 2-propanol, methanol, ethanol, acetone and toluene, respectively, over $\text{Au/Fe}_2\text{O}_3$ catalysts, and found that the high catalytic activity

was related to the lattice oxygen, thus they considered that the reaction followed the MVK mechanism. However, Burgos *et al.* [37] confirmed that the catalytic oxidation of alcohol over Pt/Al₂O₃/Al monolith catalysts followed the E-R mechanism since the alcohol was chemisorbed on the Al₂O₃ and directly oxidized by the chemisorbed oxygen atom from the gas phase. Moreover, Chen *et al.* [38] prepared mesoporous Cr₂O₃-supported platinum (Pt@M-Cr₂O₃) catalysts for the catalytic oxidation of toluene, which followed the L-H mechanism, namely, the adsorbed O₂ molecules was dissociated on Pt nanoparticles to form active oxygen atom and reacted with the chemisorbed toluene molecules, resulting the rapid transformation of benzylic and aldehydic species into benzoate species, while benzoates were converted into maleic anhydrides and then transferred into CO species adsorbed on Pt nanoparticles and finally oxidized to CO₂ by O₂.

Additionally, the reaction mechanism for the oxidation of VOCs can be also affected by the types of VOCs because of their different nucleophilic characteristics. Especially, the unsaturated hydrocarbon can be strongly adsorbed on the active sites of Pt or Pd surface through their π -bonds [39]. As such, the most favored reaction mechanism over noble-metal-based catalysts should be the L-H mechanism, and the controlling step is the adsorptions of the VOCs and oxygen molecules on the active sites. Moreover, the L-H mechanism can also be classified into the single-site L-H model (adsorptions occur on the similar active sites) and the dual-site L-H model (adsorptions occur on the two different types of active sites) [8].

Meanwhile, the reaction mechanism over the transition-metal-oxide-based catalysts can also be possibly explained by the MVK mechanism. In this case, the adsorbed VOCs molecule will react with the oxygen species from the catalyst, which leads to the reduction of the metal oxide. Then, the reduced metal oxide will be oxidized by the oxygen from the gas phase again. As such, the MVK mechanism over the transition-metal-oxide-based catalysts is also known as the redox mechanism [40]. The possible reaction process over Co/Sr-CeO₂ catalyst as the following steps: firstly, active surface oxygen species of O₂⁻ and O⁻ were generated by oxygen vacancies and Co²⁺ ions, then Phenyl was adsorbed on Co ions by the big π bonds derived from toluene, leading to the interaction

of methyl and phenyl groups with the adsorbed active oxygen species. Subsequently, nondestructive by-products of toluene selective oxidation were generated by utilizing nucleophilic O^{2-} inserted oxygen into toluene, and transient surface oxygen species such as O^{2-} and O^- reacted with carbon atoms and weakened the C–C bonds, the weaker C–C bond was cleaved and intermediate product benzene was generated. Finally, the carbon atoms were further oxidized by O^- and $ads-O^{2-}$ to form destructive products and eventually converted into CO_2 and H_2O [41]. Other reaction mechanisms should be also existed for the oxidation of VOCs over the transition-metal-oxide-based catalysts. It is still necessary to have a clear understanding on the mechanism so that the novel effective catalysts can be better designed.

1.4 Development of catalysts for VOCs catalytic oxidation

Up to now, two typical catalysts have been widely reported for the catalytic oxidation of VOCs. One is the supported noble metals, such as Pt, Pd, Au and Ag, which always show excellent performance at low temperatures. However, their high cost and limited availability restrict their large-scale applications [42]. The other one is the transition metal oxide based catalysts, which not only have low cost, but also exhibit high performance and sometimes comparable to the noble-metal-based catalysts if we can well design their structure and fully use their active sites [43]. It is reported that fabrication of transition metal oxide based catalysts with porous structure and special morphologies such as nanorod, nanowire, nanotube and nanoflower-like structure could expose more high-energy crystal faces with active sites to improve the adsorption and diffusion of the involved reactants and activate them for the further complete conversion [44]. As the most effective and economical way for the removal of VOCs, the catalytic oxidations over various catalysts have been widely investigated. Herein, the recent progress of catalytic oxidation of VOCs over both noble metal and transition metal oxides-based catalysts will be stated in this part.

1.4.1 Single-noble-metal-based catalysts

Single noble metal (e.g., Au, Pt, Pd and Ru) based catalysts have been confirmed to have high activity for the complete conversion of VOCs to harmless substances of CO_2 and H_2O at low

temperature [45]. To date, a large number of works have already been done on the investigation of the catalytic performance of supported single noble metal-based catalysts for the catalytic oxidation of VOCs. **Table 1.1** summarizes some typical works reported in recent years. For instance, Zhang *et al.* synthesized noble metal catalyst of Pt/TiO₂ and applied for the catalytic oxidation of formaldehyde, it showed that formaldehyde could be complete converted into harmless CO₂ at room temperature when the Pt/TiO₂ catalyst with proper Pt loading of 1 wt.% (weight percent) [46]. Activated carbon is well known its large surface area, which is favorable to the dispersion of the supported active species. Herein, Abdelouahab-Reddam *et al.* [47] supported metals of Pt and Ce on the activated carbon, the result demonstrated that both Pt and Ce were highly dispersed as a result of the large surface area of activated carbon, which resulted in the complete conversions of ethanol and toluene to CO₂ and H₂O at 160 and 180 °C, respectively. It was proved that the excellent catalytic performance was assigned to the optimum synergistic interaction between the well-dispersed Pt nanoparticles and Ce species. However, catalyst of Pt/CeO₂ with a low surface area accompanied by the low catalytic activity when compared with that of sample Pt/10Ce-C in this work, indicating that the surface area of the support and the well dispersion of Pt active species were very important for the catalytic oxidation of VOCs. It is found that immobilizing and/or well dispersing of noble metal nanoparticles on the catalyst support with porous structure and high surface area could improve the catalytic performance greatly [48]. For example, Bendahou *et al.* [49] supported Pd and Pt catalysts on the lanthanum (La)-doped SBA-15, both of which completely converted toluene to CO₂ and H₂O at a temperature as low as 200 °C. Herein, it should be noted that the La doping also modified the electronic density of the noble metal and increased the Pd (or Pt)–O bonding strength, which was conducive to the improvement of catalytic activity. Meanwhile, Wang *et al.* [50] supported ruthenium (Ru) oxide on a cobalt phosphate-SiO₂ mesostructured cellular foam (CoPO-MCF) for the catalytic oxidation of vinyl chloride. Since the CoPO-MCF support possessed an ordered mesoporous structure, and the active species of Ru was well dispersed on its surface, the prepared Ru/CoPO-MCF catalyst exhibited excellent catalytic performance in the oxidation reactions, namely,

a low conversion temperature for $T_{90\%}$ (the conversion temperature for 90% of vinyl chloride) around 313 °C was achieved with high stability for a long-term test. This could be contributed to the improved reducibility and acidity of CoPO-MCF support and the interaction of ruthenium oxide nanoparticles and the support.

In addition, the preparation method could also play an important role in the tuning of physiochemical properties of catalysts, and therefore influence their catalytic performance. For example, Lamallem *et al.* [51] synthesized Au/Ce-Ti-O catalysts by using different preparation methods of deposition-precipitation and impregnation. The experimental results showed that the temperature for the complete conversion of propene on the catalyst prepared by the deposition-precipitation method was 300 °C, nevertheless, uncomplete conversion of propene occurred on the catalyst which prepared by impregnation method even the reaction temperature increased to 400 °C. The similar work conducted by Yang *et al.* [52], in which single-atom Pt supported on mesoporous Fe_2O_3 (meso- Fe_2O_3) by a polyvinyl alcohol-protected reduction route for benzene combustion. The obtained catalyst of 0.25Pt/meso- Fe_2O_3 (with a 0.25 wt% of Pt loading amount) exhibited the best catalytic activity with 90% conversion ($T_{90\%}$) at low temperature of 198 °C in the catalytic combustion of benzene, which was contributed to the well dispersed and good utilize Pt atoms. Furthermore, the strong interaction between Pt and meso- Fe_2O_3 also made huge contributions to the superior catalytic stability. For comparison, as Pt nanoparticles rather than Pt atoms were supported on the mesoporous Fe_2O_3 (Pt_{NP} /meso- Fe_2O_3) by using the general method, the obtained catalysts showed much higher conversion temperature of $T_{90\%}=250$ °C. Thus, the performance of the single-noble-metal-based catalysts could be enhanced by the improved preparation method.

1.4.2 Mixed-noble-metals-based catalysts

To improve the catalytic performance of the noble-metal-based catalysts for the catalytic oxidation of VOCs, mixed-noble-metals-based catalysts were also designed and applied. The synergistic effect between the different noble metals was found to be favorable for the catalytic

activity [53, 54]. **Table 1.2** summaries the reported typical mixed-noble-metals-based catalysts. For examples, Kim *et al.* [55] found that mixed noble based catalyst of Pt-Pd/ γ -Al₂O₃ was more active than the single noble metal based catalysts of Pt/ γ -Al₂O₃ and Pd/ γ -Al₂O₃ in the benzene combustion. Additionally, the added Pt with proper amount improved the stability and catalytic activity of Pt-Pd/ γ -Al₂O₃ catalyst, as a result of the improved distribution of noble metal nanoparticles and the interaction between Pd and the γ -Al₂O₃ support. Subsequently, Xia *et al.* [56] loaded Au-Pd mixed metals on α -MnO₂ nanotubes for various types of VOCs oxidation, the favorable interaction between Au-Pd mixed metals and catalyst support of α -MnO₂ nanotubes enhanced the reactivity of lattice oxygen of the catalyst, by which Au-Pd/ α -MnO₂ catalyst achieved the excellent catalytic activity in the catalytic oxidation of VOCs. Mesoporous materials with large surface area and uniform pore size distribution are proved to be helpful to enhance the active species dispersion and mass transport during the reaction process. For instance, Hosseini *et al.* [57] supported Au and Pd together on the mesoporous TiO₂, which performed better catalytic activity than that of the catalysts prepared by the conventional TiO₂, in which mesoporous TiO₂ was conducive to the formation of the smaller Au and Pt nanoparticles. Additionally, mixed metals based catalyst of Pd-Au/TiO₂ with optimum metal loading (0.5% Pd and 1% Au) exhibited lower toluene conversion temperatures (50% conversion, T_{50%} for propene = 208 °C, and T_{50%} for toluene = 219 °C) than those of single metal based ones of Pd/TiO₂ (T_{50%} for propene = 250 °C, and T_{50%} for toluene = 230 °C) and Au/TiO₂ (T_{50%} for propene = 332 °C, and T_{50%} for toluene = 367 °C), respectively. Matějová *et al.* [58] and Silva *et al.* [59] also proved the similar results. Meanwhile, Chen *et al.* [60] synthesized mesoporous γ -Al₂O₃ to prepare Pd-Pt mixed noble metals based catalysts for the catalytic oxidation of benzene, and also found that the obtained catalysts exhibited better catalytic activity than the corresponding single-noble-metal-based catalysts. Additionally, the catalytic activity and stability were found to be further improved by doping appropriate cerium (Ce) since Ce enhanced the ability of physical adsorption/chemisorption of benzene to the nanoalloy of Pd-Pt, as well as the oxygen storage and oxygen release capacity of the catalyst. Barakat *et al.* [61] also proved this result, in which they

doped Nb and V for the enhancement of the catalytic performance. To date, large amounts of efforts have already been made on noble metal supported catalysts for the catalytic oxidation of VOCs, especially on the investigation of catalyst support effect, which is one of the pivotal factors to affect the supported active species.

Table 1.1 Typical single-noble-metal-based catalysts reported in the literatures.

Catalyst	VOCs	VOCs concentration	Temperature (°C)	Conversion (%)	References
Pt/ γ -Al ₂ O ₃	N-hexane	250 ppm	~320	100	2004[62]
Pt/HFAU zeolite	Methyl-isobutyl-ketone	1340 ppmv	180	100	2005[63]
Pt/TiO ₂	Formaldehyde	100 ppm	20	100	2006[46]
Au/TiO ₂	N-hexane	125 vppm	110	360	2007[64]
Pd/SBA-15	Toluene	1000 ppm	167	50	2008[49]
Au/Ce-Ti-O	Propene, toluene	6000 ppm, 1000 ppm	~230, ~330	100	2009[65]
Pd/ZSM-5/MCM-48	Benzene	1500 ppm	209	90	2010[66]
Pt/Al ₂ O ₃ -CeO ₂	Toluene	1000 ppm	250	100	2011[67]
Pt/CeO ₂ -Al ₂ O ₃	Dichloromethane	3000 ppm	410	100	2012[68]
Au/Ce oxides	Ethyl acetate, ethanol, toluene	~466 ppm, ~930 ppm, ~266 ppm	230, 250, 300	100	2012[69]
Pt/Nb-TiO ₂	Toluene, butan-1-ol	1000 ppm, 1000 ppm	147, 147	90	2013[70]
Au/Co ₃ O ₄	Benzene, toluene, o-xylene	1000 ppm	189, 138, 162	90	2014[71]
Pt-CeO ₂ /activated carbon	Ethanol, toluene	1000 ppm	160, 180	100	2015[47]
Au/CeO ₂ -Al ₂ O ₃	CH ₃ SSCH ₃	500 ppm	525	90	2016[72]
Pd-Ni/SBA-15	Benzene	1000 ppm	260	100	2017[73]
Pd/CoO	O-xylene	1000 ppm	173	90	2018[74]
Pt-W/CeO ₂	Chlorobenzene	1000 ppm	343	90	2019[75]
Au@SiO ₂	Formaldehyde	500 ppm	100	100	2020[76]

Table 1.2 Typical mixed-noble-metals-based catalysts reported in the literatures.

Catalyst	VOCs	VOCs concentration	Temperature (°C)	Conversion (%)	References
Pt-Pd/ γ -Al ₂ O ₃	Benzene	1000 ppm	275	100	2005[55]
Pd-Au/TiO ₂	Toluene, propene	1000 ppm, 1000 ppm	219, 208	50	2007[57]
Pt-Au/ZnO/Al ₂ O ₃	Toluene	1.8 mol%	182	80	2009[77]
Ru-Au/SiO ₂	Methanol	1000 ppm	185	90	2010[78]
Pd-Au/TiO ₂ -ZrO ₂	Toluene, propene	1000 ppm, 3000 ppm	202,193	50	2011[54]
Pt-Pd/Al ₂ O ₃ -Ce	Ethanol, toluene	1000 vpm,1000 vpm	212, 285	90	2012[58]
Pd-Au/Nb doped TiO ₂	Toluene	1000 ppm	204	50	2012[61]
Au-Pt-Pd/TiO ₂	N-hexane	1000 ppm	286	50	2014[79]
Au-Pd/Co ₃ O ₄	Toluene	1000 ppm	168	90	2015[80]
Au-Pd/MCM-41	Benzene, toluene, <i>o</i> -xylene	1.2 g m ⁻³ , 0.7 g m ⁻³ , 0.5 gm ⁻³	~213, 300, ~485	50	2015[59]
Au-Pd/Cr ₂ O ₃	Toluene	1000 ppm	165	90	2016[81]
Pt-Pd/MCM-41	Toluene	500 ppm	180	100	2016[82]
Pd-Pt/SiO ₂	Toluene	1000 ppm	160	98	2017[83]
Pd-Pt/CeO ₂ -Al ₂ O ₃ -TiO ₂	Methanol	1.0 vol. %	75	90	2017[84]
Au-Pd/ α -MnO ₂ nanotubes	Toluene, m-xylene, ethyl acetate, acetone.	1000 ppm	185, 220, 187, 180	90	2018[56]
Pd-Pt/Ce/ γ -Al ₂ O ₃	Benzene	1000 ppm	200	100	2019[60]
Ag@Pd/MnO ₂	Toluene	1.0 g m ⁻³	185	99.3	2019[85]
Pt-Ru/ZrO ₂	Toluene	50 ppm	160	100	2020[86]

1.4.3 Supported transition-metal-oxide-based catalysts

Transition-metal-based catalysts have already been widely investigated and applied in the catalytic oxidation of VOCs, and some of typical works on the supported transition-metal-based catalysts are summarized in **Tables 1.3** and **1.4**, respectively. For examples, Gaur *et al.* [87] impregnated single transition metals (i.e., Co, Cr, Ni, and Cu) on the active carbon fiber (ACF) and applied them to the catalytic oxidations of toluene and m-xylene, and found that the Ni oxide based catalysts with a proper loading amount exhibited the best catalytic performance among all the prepared single transition metal based catalysts, however, a higher loading amount would block the micro and mesopores of ACF support, and therefore hindered the mass transfer during the reaction process. Chuang *et al.* [88] demonstrated that the single-transition-metal-based catalyst of Cu/SBA-15 was the most active ones to the catalytic oxidation of toluene. Moreover, as they doped the second metal of Mn together with Cu on SBA-5, they found that the catalytic activity was further improved significantly. Recently, more works have been focused on the mixed-transition-metals-based catalysts in the field of VOCs removal (as the examples shown in **Table 1.3**). For instances, Yu *et al.* [89] supported $\text{MnO}_x\text{-CeO}_2$ mixed oxide on mesoporous TiO_2 , which converted 89.4% of toluene into CO_2 and H_2O at a temperature as low as 180 °C and the complete toluene conversion temperature was 40 °C lower than that over corresponding Ce-free catalysts, suggesting that Ce addition can significantly improve the catalyst performance. Subsequently, Ma *et al.* prepared Fe-Mn/Cordierite catalysts for toluene oxidation, the best catalytic activity was achieved when Fe/Mn molar ratio of 4/1 and metal loading of 10 wt%, which was much active than the powder-typed samples of Fe-Mn oxides [90]. Additionally, Yang *et al.* [91] synthesized Cr-Ce mixed oxide and loaded it on the modified HZSM-5 zeolite for the catalytic oxidation of chlorinated VOCs, and found that the interaction between CeO_2 and Cr_2O_3 promoted the formation of Cr^{6+} active species, which in turn enhanced the mobility of active oxygen species and improved the catalytic performance of the catalysts.

Transition metal oxides can not only be supported on other mesoporous materials as the catalysts, but can be also applied as the catalyst supports. Metals such as cerium oxide, which is a promising material for catalytic oxidation of VOCs. For instances, Wang *et al.* [92] synthesized rod-, cube- and polyhedron-structured CeO₂ to support La_{0.8}Ce_{0.2}MnO₃ perovskite and used for the catalytic oxidation of toluene. It was found that the catalytic activity of morphology La_{0.8}Ce_{0.2}MnO₃/CeO₂ significantly influenced by the CeO₂ support, the best catalytic activity was obtained on the sample of La_{0.8}Ce_{0.2}MnO₃/CeO₂ nanopolyhedra, which possessed the lowest conversion temperature of 240 °C for 90% toluene. However, Kustov *et al.* [93] encapsulated LaCoO_x perovskite nanoparticles in the mesoporous matrix of ZrO₂ and used for the catalytic oxidation of methanol. It is found that 80% of methanol was converted at a temperature as low as 150 °C. Herein, the mesoporous structure of the ZrO₂ support provided the possibility to form nano-sized particles in it and therefore improved the catalytic performance. Furthermore, Doggali *et al.* [94] made a deep investigation on the mesoporous support, they supported Cu–Mn mixed oxide catalysts on different mesoporous supports of Al₂O₃, TiO₂ and ZrO₂ for the catalytic oxidation of benzene and acetaldehyde, and found that Cu–Mn/TiO₂ and Cu–Mn/ZrO₂ catalysts had higher catalytic performance than Cu–Mn/Al₂O₃ due to their improved mass transfer and better redox properties. Thus, it is important to consider the synergistic effects between different transition metal oxides, as well as the interaction between active species and the catalyst support in order to get the optimum mixed transition metal oxide based catalysts for the oxidation of VOCs.

1.4.4 Unsupported mesoporous transition-metal-oxide-based catalysts

Unsupported transition-metal-oxide-based catalysts could be synthesized directly so that they are not necessary to support on catalyst supports, and their morphology can be easily controlled and modified by the *in-situ* preparation methods. As summarized in **Table 1.4**, various transition-metal-oxide-based catalysts with special morphologies have been reported for the catalytic oxidation of VOCs. For instances, Hosseini *et al.* [95] used sol-gel auto combustion method to

synthesize NiMn_2O_4 catalyst with nanocrystalline for 2-propanol and toluene oxidation, which could completed convert propanol and toluene into CO_2 at low temperatures of 250 and 350 °C, respectively. Meanwhile, He *et al.* [96] prepared mesoporous $\text{CuO}_x\text{--CeO}_2$ catalysts with ordered structure through a hard template method, and found that the most active catalysts converted epichlorohydrin into CO_2 with a superior selectivity (>99%) and stability for long-term evaluation of 50 h, which was mainly assigned to the well dispersion of active phase, high amount of surface active oxygen and good reducibility at low temperatures. Deng *et al.* [97] also prepared $\text{MnO}_2\text{@NiO}$ composite with a core@shell structure, the experimental results confirmed that the hetero-interface constructed between MnO_2 and NiO in the core@shell nanostructure could effectively enhance the low-temperature reducibility and increased the surface oxygen active species of the catalyst, so that the catalytic activity and stability of core@shell structured $\text{MnO}_2\text{@NiO}$ catalyst for benzene oxidation were better than that of single MnO_2 . Additionally, CoMnO_x composite is one kind of widely used catalysts for the catalytic oxidation of VOCs. As it reported by Li *et al.* [98], it can be synthesized with a mesoporous coral-like morphology and active to the catalytic oxidation of benzene, which exhibited better catalytic activity than that of single-transition-metal-based catalysts of Mn_3O_4 and Co_3O_4 , as a result of its higher surface area, better low-temperature reducibility and more surface active oxygen species. Meanwhile, MnCoO_x catalysts also can be obtained with a flower-like morphology, its excellent catalytic activity for toluene oxidation was contributed to the interaction between Co and Mn, high concentration of surface oxygen species and rich surface oxygen vacancies of the catalyst [99]. Therefore, it is a promising way to directly design and synthesize transition-metal-based catalysts with special morphologies for the catalytic oxidation of VOCs.

Table 1.3 Supported single-transition-metal catalyst reported in the literatures.

Catalyst	VOCs	VOCs concentration	Temperature (°C)	Conversion (%)	References
MnO _x /H-ZSM-5	Dichloromethane, trichloroethylene	1000 ppm	500, 500	100	2003[100]
WO _x /Activated carbon	Toluene	500 ppm	350	87	2004[101]
Ni/Activated carbon fiber	Toluene	2000 ppm	300	~90	2005[87]
Co/Porous carbons	Toluene	150 ppm	250	100	2009[102]
Cu/SBA-15	Toluene	200 ppm	250	~70	2010[88]
CrO _x /Al ₂ O ₃	Dichloromethane	3000 ppm	350	100	2011[103]
VO _x /TiO ₂	Chlorobenzene, dichlorobenzene, dichloromethane, trichloroethylene	1000 ppm	262, 288, 313, 377	90	2012[104]
CaCO ₃ /α-Fe ₂ O ₃	1,2-dichlorobenzene	100 ppmv	450	100	2013[105]
Co ₃ O ₄ /Carbon nanotubes	Toluene	850 ppm	257	100	2013[106]
NiO/SiO ₂	Toluene	80 ppm	< 200	100	2014[107]
VO _x /CeO ₂	Chlorobenzene	1000 ppm	307	90	2015[108]
CuO _x /TiO ₂ -carbon nanotubes	1,2-dichlorobenzene	120 ppm	150	77	2016[109]
Cu/CeO ₂	Ethyl acetate	466.7 ppm	275	100	2017[110]
Cr-O/HZSM-5	Dichloromethane	1000 ppm	320	95	2017[111]
MnO _x /SBA-15	Toluene	500 ppm	230	>90	2018[112]
MnO _x /Cr ₂ O ₃	Toluene	1000 ppm	268	90	2019[113]
Co ₃ O ₄ @MnO _x	Acetone, ethyl acetate, toluene	900, 1000, 780 ppm	195,200, 222	90	2019[114]
CuO/CeO ₂	Toluene	500 ppm	240	100	2020[115]

Table 1.4 Supported mixed-transition-metal catalyst reported in the literatures.

Catalyst	VOCs	VOCs concentration	Temperature (°C)	Conversion (%)	References
Cr-Cu/H-ZSM-5	Chlorinated VOCs	2500 ppm	400	100	2006[116]
Cu-Mn/MCM-41	Toluene	0.35 vol.%	320	90	2006[117]
LaCoO ₃ /Ce _{1-x} Zr _x O ₂	Benzene, toluene	1700 ppm	337, 268	50	2007[118]
LaCoO ₃ /SBA-15	Toluene, ethyl acetate	1000 ppm, 1000 ppm	284, 290	100	2009[119]
MnCuO _x /TiO ₂	Chlorobenzene	500 ppm	350	100	2009[120]
Cr-Ce/Ti-pillared interlayered clays	Nitrogen-containing VOCs	1000 ppm	180	50	2010[121]
Mn-Ce/ γ -Al ₂ O ₃	Toluene, propane	1000 ppm	~280, ~440	90	2011[122]
Cu-Mn/Al ₂ O ₃	Ethanol, toluene	1000 vpm, 1000 vpm	184, 301	90	2012[58]
Cu-Mn/TiO ₂	Benzene, acetaldehyde	900 ppm, 500 ppm	350, 200	100	2012[94]
Cr-CeO ₂ /HZSM-5	Chlorinated VOCs	1000 ppm	269	100	2013[91]
MnCeO _x /Crdierite	Benzene	150 ppm	300	99	2013[123]
Cu-Mn/ γ -Al ₂ O ₃	Toluene	1000 ppm	320	90	2014[124]
Cu-Co/Halloysite	Toluene	600 ppm	301	90	2015[125]
La _{0.8} Ce _{0.2} MnO ₃ /CeO ₂	Toluene	300 mg·m ⁻³	240	100	2016[92]
Co-Ce/USY zeolite	Benzene	1000 ppm	~250	100	2017[126]
Mn-Ce/Silica	Benzene	100 ppm	216	90	2018[127]
CoMn/SBA-15	Propane, n-hexane	2000 ppm, 1000 ppm	~318, ~314	98 ^a , 100 ^b	2019[128]
Co-Fe/Iron-mesh	Toluene	500 ppm	345	90	2020[129]

Table 1.5 Unsupported transition-metal-based catalysts reported in the literatures.

Catalyst	VOCs	VOCs concentration	Temperature (°C)	Conversion (%)	References
3D Chromium oxide	Toluene	100 ppm	280–300	100	2005[130]
Mn-Cu mixed oxides	Ethanol, propane	2%, 1%	217, 377	100	2006[131]
Mn pillared TiP	Diethyl ether	1200-1500 ppm	290	100	2007[132]
CuO-CeO ₂ mixed oxides	Benzene	1000 ppm	230	100	2008[133]
Mesoporous chromia	Toluene, acetate	1000 ppm, 1000ppm	290, 250	100	2009[134]
Cerium oxides	Naphthalene	450 ppm	275	90	2010[135]
MnO _x	Ethanol, ethyl acetate, toluene	4000 mg C·m ⁻³	215, 213, 283	100	2011[136]
Iron oxide	Acetone, methanol	1000 ppm, 1000 ppm	186, 189	90	2011[137]
NiMn ₂ O ₄	2-propanol, toluene	0.2%	250, 350	100	2012[95]
CuO _x -CeO ₂	Heteroatom-containing VOCs	-	174	90	2013[96]
SnO _x -MnO _x -TiO ₂	Chlorobenzene	2500 mg·m ⁻³	177	90	2014[138]
CeO ₂ -based catalysts	Chlorinated VOCs	~1000 ppm	224	90	2015[139]
Mn-Ce-Fe	1,2-dichlorobenzene	400-600 ppm	400	100	2016[140]
Co ₃ O ₄	O-xylene	1000 ppm	240	83	2017[141]
MnO _x -CeO _y	Toluene, chlorobenzene, o-xylene, Benzene	1000 ppm	239, 355, 268, 210	90	2018[142]
MnO ₂ @NiO	Benzene	1000 ppm	320	100	2018[97]
CoMnO _x	Benzene	1000 ppm	210	100	2019[98]
Fe-Mn mixed oxides	1,2-dichlorobenzene	50 ppm	400	100	2020[143]

1.5 Deactivation/regeneration of catalysts

In a practical process for the catalytic oxidation of VOCs, the stability and the reusability of a catalysts are more important than the activity. Thus, catalyst deactivation always receives extensive attention when considering an industrial catalyst. Generally, fouling, poisoning, thermal degradation, vapor-solid and/or solid-solid reactions, vapor compound formation accompanied by transport, and attrition/crushing are the six main reasons for the deactivation of catalysts [144]. Herein, some examples will be given to discuss the deactivation of noble-metal-based catalysts and transition-metal-oxide based catalysts in the catalytic oxidation of VOCs and the strategies to solve the catalyst deactivation as well as to regenerate the spent catalysts.

One of common reasons of the deactivation of noble-metal-based catalysts is sintering, which is also an irreversible process. As reported by Cui *et al.* [145], the catalytic activity of the aged Pd/Al₂O₃ catalyst and aged Pd/H-Al₂O₃ catalyst was significantly decreased for the catalytic oxidation of CH₄, which was assigned to the agglomeration of Pd nanoparticles, and the high temperature aging led to the particle size increasing from 7 to 13 nm. To solve this problem, a protecting layer of Al₂O₃ deposited on the Pd/Al₂O₃, which effectively resisted the sintering even at a high temperature of 700 °C. Therefore, how to avoid the sintering during the reactions and/or catalyst preparation stage at a high temperature should be considered for the VOCs removal catalysts. Meanwhile, poisoning is another main reason for the catalyst deactivation. During the catalytic oxidation of VOCs, especially for those VOCs containing halogen, sulfur, nitrogen elements and/or some other impurities, some inactive species such as sulfur could be strongly chemisorbed on the active sites of the catalyst so that the catalysts are poisoned and lose the activity [144]. In a practical process, the VOCs emissions from industries always contain airborne pollutants, such as sulfur, chlorine, or nitrogen, would easily lead to the catalyst deactivation. Gélin *et al.* [146] investigated the effect of H₂S on the performances of Pt/Al₂O₃ and Pd/Al₂O₃ catalysts for the complete oxidation of methane, and found that the Pt/Al₂O₃ had higher poisoning-resistance to sulfur than Pd/Al₂O₃. Especially, the presence of H₂S resulted in irreversible deactivation of Pd/Al₂O₃ catalysts. Cao *et al.*

[147] supported Pt, Pd and Ru on the TiO₂ support for the catalytic oxidation of dichloromethane, and found that the obtained Pt/TiO₂ and Pd/TiO₂ catalysts had serious deactivation problems during the reaction process, which was assigned to the chlorine poisoning and carbon species deposition. In contrast, the Ru/TiO₂ catalyst displayed the best catalytic performance and high stability in a long-term test among these three catalysts since the carbon and chlorine species can be effectively removed by RuO₂. They also pointed out that the suitable pore-size distribution of the catalyst should be benefit for the by-product desorption during the reaction. As a result, the catalyst deactivation by poisoning could be avoided by using suitable active species and catalyst supports. In order to avoid the catalyst deactivation, Ma *et al.* [148] supported Pd on mesoporous SBA-15 for the catalytic oxidation of n-butylamine, and found that Pd nanoparticles can be confined in the channels of SBA-15 with well dispersion, which led to the low-temperature oxidation of n-butylamine. Additionally, the high porosity and the micropore of the catalyst made a large contribution to the low production of NO_x. The similar work was also conducted by Darif *et al.* [149], who found that the acid properties of the catalyst support significantly enhanced the resistance of catalysts for sulfur poisoning, and thus enhanced the catalytic performance in the oxidation of dimethyl disulfide.

The deactivation also always occurs for the transition-metal-oxide-based catalysts. Huang *et al.* [121] used Cr-Ce/silica-pillared clay catalysts for the deep oxidation of nitrogen-containing VOCs, and found that the -NH₂ group of VOCs was easily absorbed on the acid sites of catalysts and destructed, resulting in a sudden decrease of the catalytic activity. Water vapor in the VOCs flow also has a significant effect on the VOCs removal efficiency due to the competitive adsorption with VOCs molecules on the active sites [113, 148]. For example, Chen *et al.* [150] obtained CeO₂ catalyst from a Ce-MOF precursor for the catalytic oxidation of toluene, which displayed excellent catalytic performance with 100% conversion at a low temperature of 260 °C with excellent stability. However, the toluene conversion decreased lower than 100% when water vapor was introduced, it was assigned to the competition between water and toluene molecules on the active sites of catalyst. Consequently, the existence of water had a negative effect on the catalytic oxidation of VOCs.

Fortunately, it is noted that the catalytic activity of the catalyst would be recovered after stopping the water vapor introduction. Coke formation is also one of the main reasons of catalyst deactivation because VOCs are carbon-based chemicals. Yang *et al.* [151] synthesized mesoporous $\text{CeO}_2\text{--CrO}_x$ catalysts for the deep oxidation of chlorinated VOCs, in which the partial Cr element was inserted into the lattice of CeO_2 to form a Ce–Cr–O mixed oxide, and the strong interaction between CeO_2 and CrO_x enhanced the catalytic activity. However, obvious deactivation occurred during the durability test due to the coke formation and the adsorption of Cl species on the catalyst surface, and this situation could be improved by increasing the reaction temperature.

Deactivation is generally unavoidable phenomenon in an industrial process. How to regenerate the deactivated catalyst is also an important issue during the catalyst development. For example, it is found that the H_2S -poisoned $\text{Pd/Al}_2\text{O}_3$ catalyst can be only partly regenerated under the O_2/He atmosphere at a temperature range of 673–873 K [146]. Herein, the sulphate species were re-distributed on the surface of the catalyst so that the active species of PdO were partly regenerated after the regeneration. Moreover, the poisoned-catalyst could still be not regenerated completely even the temperature was increased to as high as 923 K. It was found that H_2S could result in the irreversible deactivation of $\text{Pd/Al}_2\text{O}_3$ because of the formation of the inactive species of PdSO_4 during the reaction process. Thus, even some noble metal-based catalysts could not be regenerated after deactivated. Currently, strategies for the regeneration of the catalysts include heat treatment, oxygen plasma treatment, chemical swing treatment, ozone injection treatment, radio frequency (RF) plasma treatment and pin-to-plate dielectric barrier discharge treatment [152]. For an industrial process, the regeneration process should be simple and cost efficient. Most importantly, the best approach is to prevent catalyst deactivation before the reaction occurs, rather than the regeneration of catalysts after the reaction.

1.6 Experimental performance of VOCs catalytic oxidation

Usually, the catalytic performance of VOCs oxidation is conducted on a fixed bed system as it displayed in **Fig. 1.2**. In this work, for each of catalyst evaluation, the catalyst and the silica sand are mixed and sealed in the middle of the reaction tube, the involved reaction gas of nitrogen (N_2) and oxygen (O_2) generated by the gas cylinders with a flow rate ratio of 4:1, respectively, which is similar to air composition. Toluene as the model VOCs was introduced into reactor by N_2 gas flow from a saturated water bubbler with toluene in an ice-water mixing bath. During the reaction process, the reaction temperature is programmed to increase by the heater controller. Moreover, the inlet and outlet concentrations of toluene can be analyzed by a gas chromatograph (Shimadzu-2014), it is also equipped with a flame ionization detector (FID), and simultaneously, the outgoing products from the reactor are also analyzed over an on-line FTIR gas analyzer (Horiba, FG-120). The evaluation of water effect on the catalyst is also generated water vapor by bubbler which is filled with water, the content of the introduced water vapor is adjusted by the heating temperature.

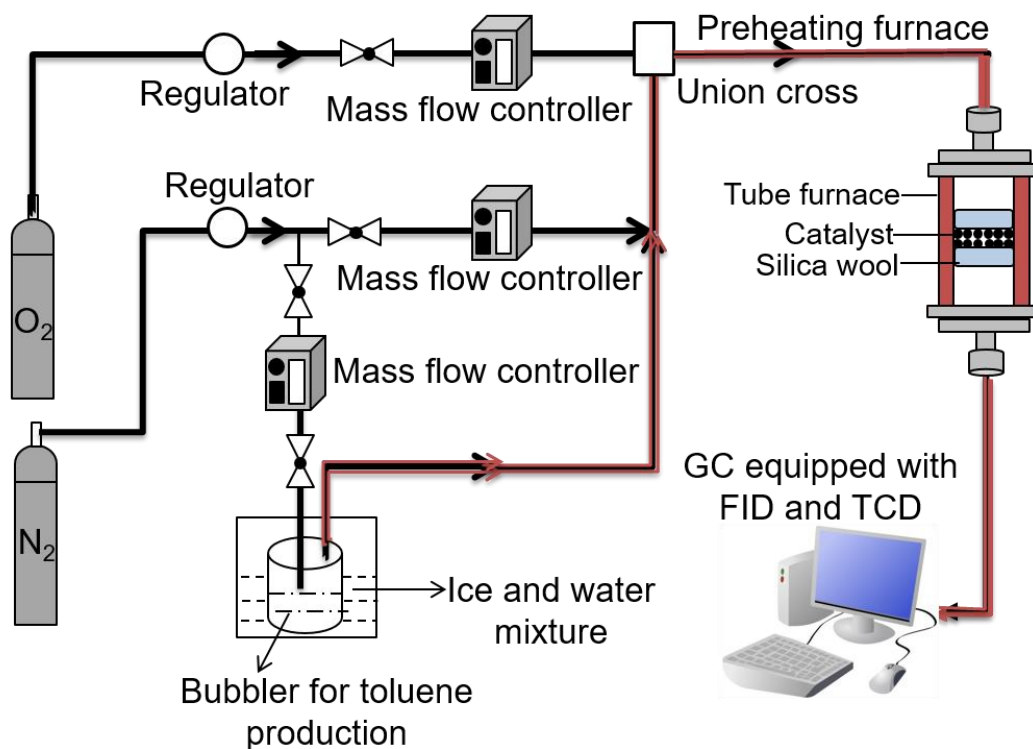


Fig. 1.2. Experimental performance of VOCs catalytic oxidation.

1.7 Objective of this study

As demonstrated above, both noble-metal-based catalysts and transition-metal-oxides-based catalysts are widely investigated and developed for the catalytic oxidation of VOCs, which could efficiently and environmentally remove VOCs at relatively low temperatures, and provide a promising way to protect our environment and all lives on the earth. However, noble-metal-based catalysts are restricted to large-scale applications, especially the industrial process, as a result of their high cost. In contrast, transition-metal-oxides based catalysts with low cost could perform similar catalytic activity as those of noble noble-metal-based catalysts. According to this, the objective of this study is focusing on the development of transition metal oxides-based catalysts. We used the facile preparation method of electrodeposition, and the time-saving and effective way, which could prepare active and stable mixed metal oxides catalysts with special porous structure for efficient VOC oxidation. Moreover, electrodeposition method provides a promising way to increase the utilization of high-cost metal oxide-based catalysts, and therefore reduce the cost in the practical process.

1.8 Scope of this dissertation

Chapter 1 reviews the classification and influence of volatile organic compounds (VOCs), different kinds of strategies and catalysts for VOCs removal, mechanisms of VOCs catalytic oxidation, deactivation/regeneration of catalysts, as well as the experimental device for catalytic oxidation of VOCs.

Chapter 2 presents the hetero-metal doped Co-based catalysts prepared by a unipolar pulse electro-deposition (UPED) electrodeposition method for low temperature combustion of toluene, the influence of different hetero-metal doping on the physiochemical properties and catalytic performance of pure $\text{Co}_3\text{O}_4/\text{NF}$ catalyst and the hetero-metal doped Co-based catalysts are investigated by scanning electron microscopy (SEM), X-ray diffraction (XRD), hydrogen

temperature-programmed reduction (H₂-TPR), oxygen temperature-programmed desorption (O₂-TPD), X-ray photoelectron spectroscopy (XPS) and fixed-bed system. Additionally, the catalyst stability is investigated in the presence and the absence of water vapor for long-term test.

Chapter 3 demonstrates a series of Ce modified Co-based (Co-Ce) mixed oxide catalysts are supported on the nickel foam (NF) using the same electrodeposition method and applied directly for the catalytic oxidation of a model VOC, i.e., toluene. The morphology and surface element composition of the prepared catalysts at different molar ratio of Co to Ce (Co/Ce) are investigated by SEM technique equipped with X-ray detector (EDX) analysis, which further analyzed by transmission electron microscopy (TEM) analysis at high resolution in nano-scale. Moreover, the redox properties and surface chemical composition and elemental valence states of the catalysts in this part are characterized by H₂-TPR, O₂-TPD and XPS. As stated above, the catalytic activity, stability and water vapor effect of the catalysts are evaluated on a fixed-bed system connected to the on-line gas chromatograph (Shimadzu-2014) equipped with FID as well as FTIR gas analyzer.

Chapter 4 focuses on a three-step electrochemical process is developed to prepare a three-dimensional (3D) structure Ag doped CeO₂ based catalysts, in which copper nanowires (CNWs) were generated on the surface of three-dimensional Cu foam (CF) by an electro-oxidation process at first and then, CeO₂ was uniformly coated on the CNWs by the UPED method and finally highly dispersed Ag nanoparticles were embedded on the surface of CeO₂ using a constant voltage electrodeposition method. The obtained Ag-CeO₂@CNWs/CF are applied for the catalytic oxidation of toluene. The physiochemical properties of the catalysts with different Ag loading amounts are investigated by XRD, SEM, TEM, H₂-TPR, O₂-TPD and NH₃-TPD and XPS techniques. The catalytic performances of the Ag-CeO₂@CNWs/CF catalysts were evaluated in a fixed bed reactor with a continuous gas flow containing about 1000 ppm toluene. Long-term stability of the optimum catalyst (80Ag-CeO₂@CNWs/CF) with the best performance is carried out in the presence and

absence of water vapor (5 vol%).

Chapter 5 introduces Mn-Co mixed oxides are deposited on the Cu nanowires, which are *in-situ* generated on the Cu foam (CF), by using novel UPED method and applied for the catalytic oxidation of toluene. The influence of Mn/Co molar ratio in the Mn-Co/CF catalyst on its physicochemical properties is investigated and characterized by SEM, TEM, XRD, H₂-TPR, O₂-TPD and XPS analyses. The catalytic performance is evaluated in a continuous flow fixed-bed reactor with a dilute toluene gas flow at the atmospheric pressure, and the catalytic stability was tested in the presence and absence of water vapor.

Chapter 6 summarizes all researches which present in this work, accompanied by outlooks for the future work in this field.

References

- [1] W.B. Li, J.X. Wang, H. Gong, Catalytic combustion of VOCs on non-noble metal catalysts, *Catalysis Today*. 148 (2009) 81-87.
- [2] Y. Liu, J. Deng, S. Xie, Z. Wang, H. Dai, Catalytic removal of volatile organic compounds using ordered porous transition metal oxide and supported noble metal catalysts, *Chinese Journal of Catalysis*. 37 (2016) 1193-1205.
- [3] J. Bedia, J. Rosas, J. Rodríguez-Mirasol, T. Cordero, Pd supported on mesoporous activated carbons with high oxidation resistance as catalysts for toluene oxidation, *Applied Catalysis B: Environmental*. 94 (2010) 8-18.
- [4] M. Zawadzki, J. Okal, Effect of Co and Fe substitution on catalytic VOCs removal on zinc aluminate, *Catalysis Today*. 257 (2015) 136-143.
- [5] A. Rokicińska, P. Natkański, B. Dudek, M. Drozdek, L. Lityńska-Dobrzyńska, P. Kuśtrowski, Co₃O₄-pillared montmorillonite catalysts synthesized by hydrogel-assisted route for total oxidation of toluene, *Applied Catalysis B: Environmental*. 195 (2016) 59-68.
- [6] Y. Chen, G. Tian, M. Zhou, Z. Huang, C. Lu, P. Hu, J. Gao, Z. Zhang, X. Tang, Catalytic control of typical particulate matters and volatile organic compounds emissions from simulated biomass burning, *Environmental science & technology*. 50 (2016) 5825-5831.
- [7] M.S. Kamal, S.A. Razzak, M.M. Hossain, Catalytic oxidation of volatile organic compounds (VOCs) – A review, *Atmospheric Environment*. 140 (2016) 117-134.
- [8] L.F. Liotta, Catalytic oxidation of volatile organic compounds on supported noble metals, *Applied Catalysis B Environmental*. 100 (2010) 403-412.
- [9] M. Drobek, A. Figoli, S. Santoro, N. Navascués, J. Motuzas, S. Simone, C. Algieri, N. Gaeta, L. Querze, A. Trotta, PVDF-MFI mixed matrix membranes as VOCs adsorbers, *Microporous & Mesoporous Materials*. 207 (2015) 126-133.
- [10] M. Duplančić, V. Tomašić, Z. Gomzi, Catalytic oxidation of toluene: comparative study over powder and monolithic manganese-nickel mixed oxide catalysts, *Environmental Technology*. (2017)

1.

- [11] M. Hodgson, H. Levin, P. Wolkoff, Volatile organic compounds and indoor air, *Journal of Allergy and Clinical Immunology*. 94 (1994) 296-303.
- [12] T. Choudhary, S. Banerjee, V. Choudhary, Catalysts for combustion of methane and lower alkanes, *Applied Catalysis A: General*. 234 (2002) 1-23.
- [13] S.C. Kim, W.G. Shim, Catalytic combustion of VOCs over a series of manganese oxide catalysts, *Applied Catalysis B: Environmental*. 98 (2010) 180-185.
- [14] J.-K. Chung, W. Yuan, G. Liu, J. Zheng, Investigation of bioactivation and toxicity of styrene in CYP2E1 transgenic cells, *Toxicology*. 226 (2006) 99-106.
- [15] H. Pan, J. Zhao, X. Zhang, Y. Yi, F. Liu, Q. Lin, Catalytic combustion of styrene over the binary mixture of manganese and copper based catalyst in the absence and presence of water vapor, *Kinetics and Catalysis*. 59 (2018) 296-303.
- [16] Z.M. De Pedro, L.M. Gómez-Sainero, E. González-Serrano, J.J. Rodríguez, Gas-phase hydrodechlorination of dichloromethane at low concentrations with palladium/carbon catalysts, *Industrial & engineering chemistry research*. 45 (2006) 7760-7766.
- [17] A.A. Meharg, D. Osborn, Dioxins released from chemical accidents, *Nature*. 375 (1995) 353-354.
- [18] T. Salthammer, S. Mentese, R. Marutzky, Formaldehyde in the indoor environment, *Chemical reviews*. 110 (2010) 2536-2572.
- [19] S. Bashkova, A. Bagreev, T.J. Bandosz, Effect of surface characteristics on adsorption of methyl mercaptan on activated carbons, *Industrial & engineering chemistry research*. 41 (2002) 4346-4352.
- [20] A. Kołodziej, J. Łojewska, Optimization of structured catalyst carriers for VOC combustion, *Catalysis Today*. 105 (2005) 378-384.
- [21] C. Yeom, S. Lee, H. Song, J. Lee, Vapor permeations of a series of VOCs/N₂ mixtures through PDMS membrane, *Journal of membrane Science*. 198 (2002) 129-143.
- [22] R. Shah, B. Thonon, D. Benforado, Opportunities for heat exchanger applications in

environmental systems, *Applied Thermal Engineering*. 20 (2000) 631-650.

[23] Y.-C. Chiang, P.-C. Chiang, C.-P. Huang, Effects of pore structure and temperature on VOC adsorption on activated carbon, *Carbon*. 39 (2001) 523-534.

[24] S. Santos, K. Jones, R. Abdul, J. Boswell, J. Paca, Treatment of wet process hardboard plant VOC emissions by a pilot scale biological system, *Biochemical engineering journal*. 37 (2007) 261-270.

[25] S. Wang, H. Ang, M.O. Tade, Volatile organic compounds in indoor environment and photocatalytic oxidation: state of the art, *Environment international*. 33 (2007) 694-705.

[26] H. Yu, K. Zhang, C. Rossi, Theoretical study on photocatalytic oxidation of VOCs using nano-TiO₂ photocatalyst, *Journal of Photochemistry and Photobiology A: Chemistry*. 188 (2007) 65-73.

[27] S.T. Oyama, P. Hunter, Control of volatile organic compound emissions: conventional and emerging technologies, Wiley-Interscience New York (2000).

[28] H. Einaga, A. Ogata, Benzene oxidation with ozone over supported manganese oxide catalysts: effect of catalyst support and reaction conditions, *Journal of hazardous materials*. 164 (2009) 1236-1241.

[29] Q.H. Trinh, Y.S. Mok, Environmental plasma-catalysis for the energy-efficient treatment of volatile organic compounds, *Korean Journal of Chemical Engineering*. 33 (2016) 735-748.

[30] R. Peng, S. Li, X. Sun, Q. Ren, L. Chen, M. Fu, J. Wu, D. Ye, Size effect of Pt nanoparticles on the catalytic oxidation of toluene over Pt/CeO₂ catalysts, *Applied Catalysis B: Environmental*. 220 (2018) 462-470.

[31] Q. Zhao, Y. Zheng, C. Song, Q. Liu, N. Ji, D. Ma, X. Lu, Novel monolithic catalysts derived from in-situ decoration of Co₃O₄ and hierarchical Co₃O₄@ MnO_x on Ni foam for VOC oxidation, *Applied Catalysis B: Environmental*. 265 (2020) 118552.

[32] W. Li, J. Wang, H. Gong, Catalytic combustion of VOCs on non-noble metal catalysts, *Catalysis Today*. 148 (2009) 81-87.

- [33] S. Balasubramanian, D.S. Viswanath, A Model for Catalytic Oxidation of Hydrocarbons in the Vapor Phase, *Industrial & Engineering Chemistry Fundamentals*. 14 (1975) 158-165.
- [34] G.I. Golodets, Heterogeneous catalytic reactions involving molecular oxygen, 15 (1983).
- [35] J.J. Spivey, Complete catalytic oxidation of volatile organics, *Ind.eng.chem.res.* 26 (1989) 2165--2180.
- [36] S. Minicò, S. Scirè, C. Crisafulli, Catalytic combustion of volatile organic compounds on gold/iron oxide catalysts, *Applied Catalysis B Environmental*. 28 (2000) 245-251.
- [37] N. Burgos, M.A. Paulis, M.M. Antxustegi, M. Montes, Deep oxidation of VOC mixtures with platinum supported on $\text{Al}_2\text{O}_3/\text{Al}$ monoliths, *Applied Catalysis B: Environmental*. 38 (2002) 251-258.
- [38] X. Chen, S. Cai, J. Chen, W. Xu, H. Jia, J. Chen, Catalytic combustion of toluene over mesoporous Cr_2O_3 -supported platinum catalysts prepared by in situ pyrolysis of MOFs, *Chemical Engineering Journal*. 334 (2018) 768-779.
- [39] Y.-F.Y. Yao, The oxidation of CO and hydrocarbons over noble metal catalysts, *Journal of Catalysis*. 87 (1984) 152-162.
- [40] K.S. Song, D. Klvana, J. Kirchnerova, Kinetics of propane combustion over $\text{La}_{0.66}\text{Sr}_{0.34}\text{Ni}_{0.3}\text{Co}_{0.7}\text{O}_3$ perovskite, *Applied Catalysis A: General*. 213 (2001) 113-121.
- [41] X. Feng, J. Guo, X. Wen, M. Xu, Y. Chu, S. Yuan, Enhancing performance of Co/CeO₂ catalyst by Sr doping for catalytic combustion of toluene, *Applied Surface Science*. 445 (2018) 145-153.
- [42] T. Masui, H. Imadzu, N. Matsuyama, N. Imanaka, Total oxidation of toluene on Pt/CeO₂-ZrO₂-Bi₂O₃/γ-Al₂O₃ catalysts prepared in the presence of polyvinyl pyrrolidone, *Journal of Hazardous Materials*. 176 (2010) 1106-1109.
- [43] S. Carabineiro, X. Chen, M. Konsolakis, A. Psarras, P. Tavares, J. Órfão, M.F.R. Pereira, J.L. Figueiredo, Catalytic oxidation of toluene on Ce-Co and La-Co mixed oxides synthesized by exotemplating and evaporation methods, *Catalysis Today*. 244 (2015) 161-171.
- [44] H. Pan, Y. Jian, C. Chen, C. He, Z. Hao, Z. Shen, H. Liu, Sphere-shaped Mn₃O₄ catalyst with remarkable low-temperature activity for methyl-ethyl-ketone combustion, *Environmental science &*

technology. 51 (2017) 6288-6297.

[45] G. Avgouropoulos, E. Oikonomopoulos, D. Kanistras, T. Ioannides, Complete oxidation of ethanol over alkali-promoted Pt/Al₂O₃ catalysts, *Applied Catalysis B: Environmental*. 65 (2006) 62-69.

[46] C. Zhang, H. He, K.I. Tanaka, Catalytic performance and mechanism of a Pt/TiO₂ catalyst for the oxidation of formaldehyde at room temperature, *Applied Catalysis B Environmental*. 65 (2006) 37-43.

[47] Z. Abdelouahab-Reddam, R. El Mail, F. Coloma, A. Sepúlveda-Escribano, Platinum supported on highly-dispersed ceria on activated carbon for the total oxidation of VOCs, *Applied Catalysis A: General*. 494 (2015) 87-94.

[48] G. Centi, Supported palladium catalysts in environmental catalytic technologies for gaseous emissions, *Journal of Molecular Catalysis A: Chemical*. 173 (2001) 287-312.

[49] K. Bendahou, L. Cherif, S. Siffert, H.L. Tidahy, H. Benaïssa, A. Aboukaïs, The effect of the use of lanthanum-doped mesoporous SBA-15 on the performance of Pt/SBA-15 and Pd/SBA-15 catalysts for total oxidation of toluene, *Applied Catalysis A General*. 351 (2008) 82-87.

[50] C. Wang, C. Tian, Y. Guo, Z. Zhang, W. Hua, W. Zhan, Y. Guo, L. Wang, G. Lu, Ruthenium oxides supported on heterostructured CoPO-MCF materials for catalytic oxidation of vinyl chloride emissions, *Journal of hazardous materials*. 342 (2018) 290-296.

[51] M. Lamallem, H. El Ayadi, C. Gennequin, R. Cousin, S. Siffert, F. Aïssi, A. Aboukaïs, Effect of the preparation method on Au/Ce-Ti-O catalysts activity for VOCs oxidation, *Catalysis Today*. 137 (2008) 367-372.

[52] K. Yang, Y. Liu, J. Deng, X. Zhao, J. Yang, Z. Han, Z. Hou, H. Dai, Three-dimensionally ordered mesoporous iron oxide-supported single-atom platinum: Highly active catalysts for benzene combustion, *Applied Catalysis B: Environmental*. 244 (2019) 650-659.

[53] M. Hosseini, S. Siffert, R. Cousin, A. Aboukaïs, Z. Hadj-Sadok, B.-L. Su, Total oxidation of VOCs on Pd and/or Au supported on TiO₂/ZrO₂ followed by “operando” DRIFT, *Comptes Rendus*

Chimie. 12 (2009) 654-659.

[54] T. Barakat, J.C. Rooke, H.L. Tidahy, M. Hosseini, R. Cousin, J.F. Lamonier, J.M. Giraudon, G. De Weireld, B.L. Su, S. Siffert, Noble-Metal-Based Catalysts Supported on Zeolites and Macro-Mesoporous Metal Oxide Supports for the Total Oxidation of Volatile Organic Compounds, *ChemSusChem*. 4 (2011) 1420-1430.

[55] H.S. Kim, T.W. Kim, H.L. Koh, S.H. Lee, B.R. Min, Complete benzene oxidation over Pt-Pd bimetal catalyst supported on γ -alumina: influence of Pt-Pd ratio on the catalytic activity, *Applied Catalysis A: General*. 280 (2005) 125-131.

[56] Y. Xia, L. Xia, Y. Liu, T. Yang, J. Deng, H. Dai, Concurrent catalytic removal of typical volatile organic compound mixtures over Au-Pd/ α -MnO₂ nanotubes, *Journal of Environmental Sciences*. 64 (2018) 276-288.

[57] M. Hosseini, S. Siffert, H.L. Tidahy, R. Cousin, J.F. Lamonier, A. Aboukais, A. Vantomme, M. Roussel, B.L. Su, Promotional effect of gold added to palladium supported on a new mesoporous TiO₂ for total oxidation of volatile organic compounds, *Catalysis Today*. 122 (2007) 391-396.

[58] L. Matějová, P. Topka, K. Jiráťová, O. Šolcová, Total oxidation of model volatile organic compounds over some commercial catalysts, *Applied Catalysis A General*. 443-444 (2012) 40-49.

[59] A.G.M.D. Silva, H.V. Fajardo, R. Balzer, L.F.D. Probst, A.S.P. Lovón, J.J. Lovón-Quintana, G.P. Valença, W.H. Schreine, P.A. Robles-Dutenhefner, Versatile and efficient catalysts for energy and environmental processes: Mesoporous silica containing Au, Pd and Au-Pd, *Journal of Power Sources*. 285 (2015) 460-468.

[60] Z. Chen, J. Li, P. Yang, Z. Cheng, J. Li, S. Zuo, Ce-modified mesoporous γ -Al₂O₃ supported Pd-Pt nanoparticle catalysts and their structure-function relationship in complete benzene oxidation, *Chemical Engineering Journal*. 356 (2019) 255-261.

[61] T. Barakat, J.C. Rooke, M. Franco, R. Cousin, J.F. Lamonier, J.M. Giraudon, B.L. Su, S. Siffert, Pd-and/or Au-Loaded Nb-and V-Doped Macro-Mesoporous TiO₂ Supports as Catalysts for the Total Oxidation of VOCs, *European Journal of Inorganic Chemistry*. 2012 (2012) 2812-2818.

- [62] K.E. Jeong, S.K. Ihm, Y.D. Jun, D.C. Kim, Low-temperature deactivation and oxidation state of Pd/ γ -Al₂O₃ catalysts for total oxidation of n-hexane, *Catalysis Today*. 93 (2004) 149-154.
- [63] J. Tsou, P. Magnoux, M. Guisnet, J. Orfao, J.L. Figueiredo, Catalytic oxidation of volatile organic compounds: Oxidation of methyl-isobutyl-ketone over Pt/zeolite catalysts, *Applied Catalysis B: Environmental*. 57 (2005) 117-123.
- [64] C. Cellier, S. Lambert, E.M. Gaigneaux, C. Poleunis, V. Ruaux, P. Eloy, C. Lahousse, P. Bertrand, J.-P. Pirard, P. Grange, Investigation of the preparation and activity of gold catalysts in the total oxidation of n-hexane, *Applied Catalysis B: Environmental*. 70 (2007) 406-416.
- [65] C. Gennequin, M. Lamallem, R. Cousin, S. Siffert, V. Idakiev, T. Tabakova, A. Aboukaïs, B. Su, Total oxidation of volatile organic compounds on Au/Ce–Ti–O and Au/Ce–Ti–Zr–O mesoporous catalysts, *Journal of materials science*. 44 (2009) 6654.
- [66] C. He, J. Li, P. Li, J. Cheng, Z. Hao, Z.-P. Xu, Comprehensive investigation of Pd/ZSM-5/MCM-48 composite catalysts with enhanced activity and stability for benzene oxidation, *Applied Catalysis B: Environmental*. 96 (2010) 466-475.
- [67] Z. Abbasi, M. Haghighi, E. Fatehifar, S. Saedy, Synthesis and physicochemical characterizations of nanostructured Pt/Al₂O₃–CeO₂ catalysts for total oxidation of VOCs, *Journal of hazardous materials*. 186 (2011) 1445-1454.
- [68] Q.-Y. Chen, N. Li, M.-F. Luo, J.-Q. Lu, Catalytic oxidation of dichloromethane over Pt/CeO₂–Al₂O₃ catalysts, *Applied Catalysis B: Environmental*. 127 (2012) 159-166.
- [69] S.S.T. Bastos, S.a.C. Carabineiro, J.J.M. Órfão, M.F.R. Pereira, J.J. Delgado, J.L. Figueiredo, Total oxidation of ethyl acetate, ethanol and toluene catalyzed by exotemplated manganese and cerium oxides loaded with gold, *Catalysis Today*. 180 (2012) 148-154.
- [70] J.C. Rooke, T. Barakat, M.F. Finol, P. Billefont, G.D. Weireld, Y. Li, R. Cousin, J.M. Giraudon, S. Siffert, J.F. Lamonier, Influence of hierarchically porous niobium doped TiO₂ supports in the total catalytic oxidation of model VOCs over noble metal nanoparticles, *Applied Catalysis B Environmental*. 142-143 (2013) 149-160.

- [71] Y. Liu, H. Dai, J. Deng, S. Xie, H. Yang, T. Wei, W. Han, J. Yang, G. Guo, Mesoporous Co_3O_4 -supported gold nanocatalysts: Highly active for the oxidation of carbon monoxide, benzene, toluene, and o-xylene, *Journal of Catalysis*. 309 (2014) 408-418.
- [72] T.K. Nevanperä, S. Ojala, N. Bion, F. Epron, R.L. Keiski, Catalytic oxidation of dimethyl disulfide (CH_3SSCH_3) over monometallic Au, Pt and Cu catalysts supported on $\gamma\text{-Al}_2\text{O}_3$, CeO_2 and $\text{CeO}_2\text{-Al}_2\text{O}_3$, *Applied Catalysis B: Environmental*. 182 (2016) 611-625.
- [73] W. Tang, Y. Deng, Y. Chen, Promoting effect of acid treatment on Pd-Ni/SBA-15 catalyst for complete oxidation of gaseous benzene, *Catalysis Communications*. 89 (2017) 86-90.
- [74] S. Xie, Y. Liu, J. Deng, J. Yang, X. Zhao, Z. Han, K. Zhang, Y. Wang, H. Arandian, H. Dai, Mesoporous CoO -supported palladium nanocatalysts with high performance for o-xylene combustion, *Catalysis Science & Technology*. 8 (2018) 806-816.
- [75] Y. Gu, S. Shao, W. Sun, H. Xia, X. Gao, Q. Dai, W. Zhan, X. Wang, The oxidation of chlorinated organic compounds over W-modified Pt/ CeO_2 catalysts, *Journal of Catalysis*. 380 (2019) 375-386.
- [76] D. Chen, J. Shi, H. Shen, High-dispersed catalysts of core-shell structured Au@SiO_2 for formaldehyde catalytic oxidation, *Chemical Engineering Journal*. 385 (2020) 123887.
- [77] K.-J. Kim, H.-G. Ahn, Complete oxidation of toluene over bimetallic Pt-Au catalysts supported on $\text{ZnO/Al}_2\text{O}_3$, *Applied Catalysis B: Environmental*. 91 (2009) 308-318.
- [78] T. Sreethawong, D. Sukjit, P. Ouraipryvan, J.W. Schwank, S. Chavadej, Oxidation of Oxygenated Volatile Organic Compound Over Monometallic and Bimetallic Ru-Au Catalysts, *Catalysis letters*. 138 (2010) 160-170.
- [79] P. Qiao, S. Xu, D. Zhang, R. Li, S. Zou, J. Liu, W. Yi, J. Li, J. Fan, Sub-10 nm Au-Pt-Pd alloy trimetallic nanoparticles with a high oxidation-resistant property as efficient and durable VOC oxidation catalysts, *Chemical Communications*. 50 (2014) 11713-11716.
- [80] S. Xie, J. Deng, S. Zang, H. Yang, G. Guo, H. Arandian, H. Dai, Au-Pd/3DOM Co_3O_4 : Highly active and stable nanocatalysts for toluene oxidation, *Journal of catalysis*. 322 (2015) 38-48.

- [81] Z. Wu, J. Deng, S. Xie, H. Yang, X. Zhao, K. Zhang, H. Lin, H. Dai, G. Guo, Mesoporous Cr₂O₃-supported Au–Pd nanoparticles: High-performance catalysts for the oxidation of toluene, *Microporous and Mesoporous Materials*. 224 (2016) 311-322.
- [82] X. Fu, Y. Liu, W. Yao, Z. Wu, One-step synthesis of bimetallic Pt-Pd/MCM-41 mesoporous materials with superior catalytic performance for toluene oxidation, *Catalysis Communications*. 83 (2016) 22-26.
- [83] H. Wang, W. Yang, P. Tian, J. Zhou, R. Tang, S. Wu, A highly active and anti-coking Pd-Pt/SiO₂ catalyst for catalytic combustion of toluene at low temperature, *Applied Catalysis A General*. 529 (2017) 60-67.
- [84] Y. Guo, S. Zhang, J. Zhu, L. Su, X. Xie, Z. Li, Effects of Pt on physicochemical properties over Pd based catalysts for methanol total oxidation, *Applied Surface Science*. 416 (2017) 358-364.
- [85] Y. Li, L. Xiao, F. Liu, Y. Dou, S. Liu, Y. Fan, G. Cheng, W. Song, J. Zhou, Core-shell structure Ag@Pd nanoparticles supported on layered MnO₂ substrate as toluene oxidation catalyst, *Journal of Nanoparticle Research*. 21 (2019).
- [86] M.-M. Wang, D. Chen, N.-J. Li, Q.-F. Xu, H. Li, J.-H. He, J.-M. Lu, Highly efficient catalysts of bimetallic Pt-Ru nanocrystals supported on ordered ZrO₂ nanotube for toluene oxidation, *ACS Applied Materials & Interfaces*. (2020).
- [87] V. Gaur, A. Sharma, N. Verma, Catalytic oxidation of toluene and m-xylene by activated carbon fiber impregnated with transition metals, *Carbon*. 43 (2005) 3041-3053.
- [88] K.H. Chuang, Z.S. Liu, Y.H. Chang, C.Y. Lu, M.Y. Wey, Study of SBA-15 supported catalysts for toluene and NO removal: the effect of promoters (Co, Ni, Mn, Ce), *Reaction Kinetics Mechanisms & Catalysis*. 99 (2010) 409-420.
- [89] D. Yu, Y. Liu, Z. Wu, Low-temperature catalytic oxidation of toluene over mesoporous MnO_x–CeO₂/TiO₂ prepared by sol–gel method, *Catalysis Communications*. 11 (2010) 788-791.
- [90] W. Ma, Q. Huang, Y. Xu, Y. Chen, S. Zhu, S. Shen, Catalytic combustion of toluene over Fe–Mn mixed oxides supported on cordierite, *Ceramics International*. 39 (2013) 277-281.

- [91] P. Yang, X. Xue, Z. Meng, R. Zhou, Enhanced catalytic activity and stability of Ce doping on Cr supported HZSM-5 catalysts for deep oxidation of chlorinated volatile organic compounds, *Chemical Engineering Journal*. 234 (2013) 203-210.
- [92] Y. Wang, Y. Xue, C. Zhao, D. Zhao, F. Liu, K. Wang, D.D. Dionysiou, Catalytic combustion of toluene with $\text{La}_{0.8}\text{Ce}_{0.2}\text{MnO}_3$ supported on CeO_2 with different morphologies, *Chemical Engineering Journal*. 300 (2016) 300-305.
- [93] A.L. Kustov, O.P. Tkachenko, L.M. Kustov, B.V. Romanovsky, Lanthanum cobaltite perovskite supported onto mesoporous zirconium dioxide: Nature of active sites of VOC oxidation, *Environment International*. 37 (2011) 1053-1056.
- [94] P. Doggali, Y. Teraoka, P. Mungse, I.K. Shah, S. Rayalu, N. Labhsetwar, Combustion of volatile organic compounds over Cu–Mn based mixed oxide type catalysts supported on mesoporous Al_2O_3 , TiO_2 and ZrO_2 , *Journal of Molecular Catalysis A: Chemical*. 358 (2012) 23-30.
- [95] S. Hosseini, A. Niaei, D. Salari, S. Nabavi, Nanocrystalline AMn_2O_4 (A= Co, Ni, Cu) spinels for remediation of volatile organic compounds—synthesis, characterization and catalytic performance, *Ceramics International*. 38 (2012) 1655-1661.
- [96] C. He, Y. Yu, C. Chen, L. Yue, N. Qiao, Q. Shen, J. Chen, Z. Hao, Facile preparation of 3D ordered mesoporous $\text{CuO}_x\text{--CeO}_2$ with notably enhanced efficiency for the low temperature oxidation of heteroatom-containing volatile organic compounds, *RSC Advances*. 3 (2013) 19639-19656.
- [97] Y. Deng, W. Tang, W. Li, Y. Chen, $\text{MnO}_2\text{-nanowire@NiO-nanosheet}$ core-shell hybrid nanostructure derived interfacile Effect for promoting catalytic oxidation activity, *Catalysis Today*. 308 (2018) 58-63.
- [98] Q. Li, T. Odoom-Wubah, Y. Zhou, R. Mulka, Y. Zheng, J. Huang, D. Sun, Q. Li, Coral-like CoMnO_x as a highly active catalyst for benzene catalytic oxidation, *Industrial & Engineering Chemistry Research*. 58 (2019) 2882-2890.
- [99] Y. Wang, H. Arandiyan, Y. Liu, Y. Liang, Y. Peng, S. Bartlett, H. Dai, S. Rostamnia, J. Li, Template-free Scalable Synthesis of Flower-like $\text{Co}_{3-x}\text{Mn}_x\text{O}_4$ Spinel Catalysts for Toluene Oxidation,

ChemCatChem. 10 (2018) 3429-3434.

[100] J. Gutiérrez-Ortiz, R. López-Fonseca, U. Aurrekoetxea, J. González-Velasco, Low-temperature deep oxidation of dichloromethane and trichloroethylene by H-ZSM-5-supported manganese oxide catalysts, *Journal of Catalysis*. 218 (2003) 148-154.

[101] M.A. Alvarez-Merino, M.F. Ribeiro, J.M. Silva, F. Carrasco-Marín, ., F.J. Maldonado-Hódar, Activated carbon and tungsten oxide supported on activated carbon catalysts for toluene catalytic combustion, *Environmental Science & Technology*. 38 (2004) 4664-4670.

[102] C.Y. Lu, M.Y. Wey, K.H. Chuang, Catalytic treating of gas pollutants over cobalt catalyst supported on porous carbons derived from rice husk and carbon nanotube, *Applied Catalysis B Environmental*. 90 (2009) 652-661.

[103] R. Ma, P. Hu, L. Jin, Y. Wang, J. Lu, M. Luo, Characterization of $\text{CrO}_x/\text{Al}_2\text{O}_3$ catalysts for dichloromethane oxidation, *Catalysis Today*. 175 (2011) 598-602.

[104] M. Wu, K.C. Ung, Q. Dai, X. Wang, Catalytic combustion of chlorinated VOCs over VO_x/TiO_2 catalysts, *Catalysis Communications*. 18 (2012) 72-75.

[105] X. Ma, Q. Sun, X. Feng, X. He, J. Guo, H. Sun, H. Cao, Catalytic oxidation of 1, 2-dichlorobenzene over $\text{CaCO}_3/\alpha\text{-Fe}_2\text{O}_3$ nanocomposite catalysts, *Applied Catalysis A: General*. 450 (2013) 143-151.

[106] S. Jiang, S. Song, Enhancing the performance of Co_3O_4 /CNTs for the catalytic combustion of toluene by tuning the surface structures of CNTs, *Applied Catalysis B Environmental*. 140-141 (2013) 1-8.

[107] M.G. Jeong, E.J. Park, B. Jeong, D.H. Kim, Y.D. Kim, Toluene combustion over NiO nanoparticles on mesoporous SiO_2 prepared by atomic layer deposition, *Chemical Engineering Journal*. 237 (2014) 62-69.

[108] H. Huang, Y. Gu, J. Zhao, X. Wang, Catalytic combustion of chlorobenzene over VO_x/CeO_2 catalysts, *Journal of Catalysis*. 326 (2015) 54-68.

[109] Q.-L. Wang, Q.-X. Huang, H.-F. Wu, S.-Y. Lu, H.-L. Wu, X.-D. Li, J.-H. Yan, Catalytic

decomposition of gaseous 1, 2-dichlorobenzene over $\text{CuO}_x/\text{TiO}_2$ and $\text{CuO}_x/\text{TiO}_2\text{-CNTs}$ catalysts: Mechanism and PCDD/Fs formation, *Chemosphere*. 144 (2016) 2343-2350.

[110] M. Konsolakis, S. Carabineiro, G. Marnellos, M. Asad, O. Soares, M. Pereira, J. Órfão, J. Figueiredo, Volatile organic compounds abatement over copper-based catalysts: Effect of support, *Inorganica Chimica Acta*. 455 (2017) 473-482.

[111] J. Su, W. Yao, Y. Liu, Z. Wu, The impact of CrO_x loading on reaction behaviors of dichloromethane (DCM) catalytic combustion over Cr-O/HZSM-5 catalysts, *Applied Surface Science*. 396 (2017) 1026-1033.

[112] Y. Qin, Z. Qu, C. Dong, Y. Wang, N. Huang, Highly catalytic activity of Mn/SBA-15 catalysts for toluene combustion improved by adjusting the morphology of supports, *Journal of Environmental Sciences*. (2018).

[113] X. Chen, S. Cai, E. Yu, J. Chen, H. Jia, $\text{MnO}_x/\text{Cr}_2\text{O}_3$ composites prepared by pyrolysis of Cr-MOF precursors containing in situ assembly of MnO_x as high stable catalyst for toluene oxidation, *Applied Surface Science*. 475 (2019) 312-324.

[114] Q. Zhao, Q. Liu, Y. Zheng, R. Han, C. Song, N. Ji, D. Ma, Enhanced catalytic performance for volatile organic compound oxidation over in-situ growth of MnO_x on Co_3O_4 nanowire, *Chemosphere*. 244 (2020) 125532.

[115] Y. Zeng, Y. Wang, F. Song, S. Zhang, Q. Zhong, The effect of CuO loading on different method prepared CeO_2 catalyst for toluene oxidation, *Science of The Total Environment*. 712 (2020) 135635.

[116] A.Z. Abdullah, M.Z.A. Bakar, S. Bhatia, Combustion of chlorinated volatile organic compounds (VOCs) using bimetallic chromium-copper supported on modified H-ZSM-5 catalyst, *Journal of Hazardous Materials*. 129 (2006) 39-49.

[117] W.B. Li, M. Zhuang, T.C. Xiao, M.L.H. Green, MCM-41 supported Cu-Mn catalysts for catalytic oxidation of toluene at low temperatures, *Journal of Physical Chemistry B*. 110 (2006) 21568.

[118] M. Alifanti, M. Florea, V.I. Pârvulescu, Ceria-based oxides as supports for LaCoO_3 perovskite;

catalysts for total oxidation of VOC, *Applied Catalysis B: Environmental*. 70 (2007) 400-405.

[119] J. Deng, L. Zhang, H. Dai, C.-T. Au, In situ hydrothermally synthesized mesoporous LaCoO₃/SBA-15 catalysts: High activity for the complete oxidation of toluene and ethyl acetate, *Applied Catalysis A: General*. 352 (2009) 43-49.

[120] J. Belkouch, A. Ould-Dris, B. Taouk, Removal of hazardous chlorinated VOCs over Mn–Cu mixed oxide based catalyst, *Journal of hazardous materials*. 169 (2009) 758-765.

[121] Q. Huang, S. Zuo, R. Zhou, Catalytic performance of pillared interlayered clays (PILCs) supported CrCe catalysts for deep oxidation of nitrogen-containing VOCs, *Applied Catalysis B Environmental*. 95 (2010) 327-334.

[122] S.M. Saqer, D.I. Kondarides, X.E. Verykios, Catalytic oxidation of toluene over binary mixtures of copper, manganese and cerium oxides supported on γ -Al₂O₃, *Applied Catalysis B: Environmental*. 103 (2011) 275-286.

[123] Q. Huang, Y. Xiaokang, L. Bing, C. Yingwen, Z. Shemin, S. Shubao, Study on catalytic combustion of benzene over cerium based catalyst supported on cordierite, *Journal of Rare Earths*. 31 (2013) 124-129.

[124] C.K. Sang, Y.K. Park, J.W. Nah, Property of a highly active bimetallic catalyst based on a supported manganese oxide for the complete oxidation of toluene, *Powder Technology*. 266 (2014) 292-298.

[125] A. Carrillo, J. Carriazo, Cu and Co oxides supported on halloysite for the total oxidation of toluene, *Applied Catalysis B: Environmental*. 164 (2015) 443-452.

[126] J. Li, S. Zuo, C. Qi, Preparation and high performance of rare earth modified Co/USY for benzene catalytic combustion, *Catalysis Communications*. 91 (2017) 30-33.

[127] W. Li, H. Liu, X. Ma, S. Mo, S. Li, Y. Chen, Fabrication of silica supported Mn–Ce benzene oxidation catalyst by a simple and environment-friendly oxalate approach, *Journal of Porous Materials*. 25 (2018) 107-117.

[128] S. Todorova, J. Blin, A. Naydenov, B. Lebeau, H. Kolev, P. Gaudin, A. Dotzeva, R. Velinova,

D. Filkova, I. Ivanova, $\text{Co}_3\text{O}_4\text{-MnO}_x$ oxides supported on SBA-15 for CO and VOCs oxidation, *Catalysis Today*. (2019).

[129] T. Xue, R. Li, Y. Gao, Q. Wang, Iron mesh-supported vertically aligned Co-Fe layered double oxide as a novel monolithic catalyst for catalytic oxidation of toluene, *Chemical Engineering Journal*. 384 (2020) 123284.

[130] A.K. Sinha, K. Suzuki, Three-Dimensional Mesoporous Chromium Oxide: A Highly Efficient Material for the Elimination of Volatile Organic Compounds, *Angewandte Chemie International Edition*. 44 (2005) 271-273.

[131] M.R. Morales, B.P. Barbero, L.E. Cadús, Total oxidation of ethanol and propane over Mn-Cu mixed oxide catalysts, *Applied Catalysis B: Environmental*. 67 (2006) 229-236.

[132] D. Das, K. Parida, Mn (III) oxide pillared titanium phosphate (TiP) for catalytic deep oxidation of VOCs, *Applied Catalysis A: General*. 324 (2007) 1-8.

[133] C. Hu, Q. Zhu, Z. Jiang, Y. Zhang, Y. Wang, Preparation and formation mechanism of mesoporous CuO-CeO_2 mixed oxides with excellent catalytic performance for removal of VOCs, *Microporous & Mesoporous Materials*. 113 (2008) 427-434.

[134] X. Yunsheng, D. Hongxing, J. Haiyan, D. Jiguang, H. Hong, A. Chak Tong, Mesoporous chromia with ordered three-dimensional structures for the complete oxidation of toluene and ethyl acetate, *Environmental Science & Technology*. 43 (2009) 8355-8360.

[135] B. Puertolas, B. Solsona, S. Agouram, R. Murillo, A.M. Mastral, A. Aranda, S.H. Taylor, T. Garcia, The catalytic performance of mesoporous cerium oxides prepared through a nanocasting route for the total oxidation of naphthalene, *Applied Catalysis B: Environmental*. 93 (2010) 395-405.

[136] V. Santos, M. Pereira, J. Órfão, J. Figueiredo, The role of lattice oxygen on the activity of manganese oxides towards the oxidation of volatile organic compounds, *Applied Catalysis B: Environmental*. 99 (2010) 353-363.

[137] Y. Xia, H. Dai, H. Jiang, L. Zhang, J. Deng, Y. Liu, Three-dimensionally ordered and wormhole-like mesoporous iron oxide catalysts highly active for the oxidation of acetone and

methanol, Journal of hazardous materials. 186 (2011) 84-91.

[138] J. Li, P. Zhao, S. Liu, SnO_x–MnO_x–TiO₂ catalysts with high resistance to chlorine poisoning for low-temperature chlorobenzene oxidation, Applied Catalysis A: General. 482 (2014) 363-369.

[139] Y. Peng, S. Yang, Z. Shi, Z. Meng, R. Zhou, Deep oxidation of chlorinated VOCs over CeO₂-based transition metal mixed oxide catalysts, Applied Catalysis B Environmental. 162 (2015) 227-235.

[140] A. Tang, L. Hu, X. Yang, Y. Jia, Y. Zhang, Promoting effect of the addition of Ce and Fe on manganese oxide catalyst for 1, 2-dichlorobenzene catalytic combustion, Catalysis Communications. 82 (2016) 41-45.

[141] S. Xie, Y. Liu, J. Deng, J. Yang, X. Zhao, Z. Han, K. Zhang, H. Dai, Insights into the active sites of ordered mesoporous cobalt oxide catalysts for the total oxidation of o-xylene, Journal of Catalysis. 352 (2017) 282-292.

[142] J. Chen, X. Chen, W. Xu, Z. Xu, H. Jia, J. Chen, Homogeneous introduction of CeO_y into MnO_x-based catalyst for oxidation of aromatic VOCs, Applied Catalysis B: Environmental. 224 (2018) 825-835.

[143] X. Ma, J. Wen, H. Guo, G. Ren, Facile template fabrication of Fe-Mn mixed oxides with hollow microsphere structure for efficient and stable catalytic oxidation of 1, 2-dichlorobenzene, Chemical Engineering Journal. 382 (2020) 122940.

[144] C.H. Bartholomew, Mechanisms of catalyst deactivation, Applied Catalysis A: General. 212 (2001) 17-60.

[145] W. Cui, S. Li, D. Wang, Y. Deng, Y. Chen, High reactivity and sintering resistance of CH₄ oxidation over modified Pd/Al₂O₃, Catalysis Communications. 119 (2019) 86-90.

[146] P. Gelin, L. Urfels, M. Primet, E. Tena, Complete oxidation of methane at low temperature over Pt and Pd catalysts for the abatement of lean-burn natural gas fuelled vehicles emissions: influence of water and sulphur containing compounds, Catalysis Today. 83 (2003) 45-57.

[147] S. Cao, X. Fei, Y. Wen, Z. Sun, H. Wang, Z. Wu, Bimodal mesoporous TiO₂ supported Pt, Pd

and Ru catalysts and their catalytic performance and deactivation mechanism for catalytic combustion of Dichloromethane (CH_2Cl_2), *Applied Catalysis A: General*. 550 (2018) 20-27.

[148] M. Ma, H. Huang, C. Chen, Q. Zhu, L. Yue, R. Albilali, C. He, Highly active SBA-15-confined Pd catalyst with short rod-like micro-mesoporous hybrid nanostructure for n-butylamine low-temperature destruction, *Molecular Catalysis*. 455 (2018) 192-203.

[149] B. Darif, S. Ojala, L. Pirault-Roy, M. Bensitel, R. Brahmi, R.L. Keiski, Study on the catalytic oxidation of DMDS over Pt-Cu catalysts supported on Al_2O_3 , AlSi_{20} and SiO_2 , *Applied Catalysis B: Environmental*. 181 (2016) 24-33.

[150] X. Chen, X. Chen, E. Yu, S. Cai, H. Jia, J. Chen, P. Liang, In situ pyrolysis of Ce-MOF to prepare CeO_2 catalyst with obviously improved catalytic performance for toluene combustion, *Chemical Engineering Journal*. (2018).

[151] P. Yang, Z. Shi, S. Yang, R. Zhou, High catalytic performances of $\text{CeO}_2\text{-CrO}_x$ catalysts for chlorinated VOCs elimination, *Chemical Engineering Science*. 126 (2015) 361-369.

[152] N. Hafezkhiaani, S. Fathi, B. Shokri, S.I. Hosseini, A novel method for decoking of Pt-Sn/ Al_2O_3 in the naphtha reforming process using RF and pin-to-plate DBD plasma systems, *Applied Catalysis A: General*. 493 (2015) 8-16.

CHAPTER 2 Stable hetero-metal doped Co-based catalysts prepared by electrodeposition method for low temperature combustion of toluene

2.1 Introduction

The removal of volatile organic compounds (VOCs) has been become more and more important in recent years since they have harmful effects on human health and our living environment, especially the secondary pollution of ozone and photochemical smog resulted from them [1, 2]. Emissions of VOCs are mainly from human activities of industrial production processes (e.g., painting, materials building and waste treating) and transportation [3, 4]. Over the last decades, numbers of techniques including incineration, condensation, adsorption, absorption, biological degradation, direct combustion and catalytic combustion have already been investigated and applied for the removal of VOCs [5, 6], in which the catalytic combustion is the most effective and environmental way since it can completely convert VOCs into harmless substances of CO_2 and H_2O at a temperature below $500\text{ }^\circ\text{C}$ [7, 8]. The commonly used catalysts for VOC combustion are noble metal (e.g., Pt, Pd, Au, Rh) based catalysts and transition metal oxides (e.g., Co_3O_4 , MnO_2 , CeO_2 , and CuO) based catalysts [9, 10]. However, the cost using noble metal-based catalysts is too high although they have excellent catalytic performance. Thus, more researches are concentrated to design novel high-performance catalysts with low cost for the VOC combustion, in which transition metal oxides based catalysts are paid special attention due to their low cost, high thermal stability, excellent anti-poisoning capability and flexible structures [10].

Among transition metal oxides, cobalt-based ones have been reported to have high activities towards combustions of various kinds of VOCs. For instances, Ren *et al.* [11] developed three-dimensional (3D) hierarchical Co_3O_4 nanocatalysts with different kinds of crystal planes by using the hydrothermal method, and found that the catalysts with cubes-stacked Co_3O_4 microsphere

exhibited higher catalytic activity for toluene combustion than those Co_3O_4 catalysts with plates-, needles- and sheets-stacked structures. Herein, the exposed active phase of (111) crystal planes, the high specific surface area and the highly defective structure with abundant surface adsorbed oxygen species and surface Co^{3+} species played important roles for the enhancement of Co_3O_4 activity. Dissanayake *et al.* [12] prepared a mesoporous Co_3O_4 catalyst by an inverse micelle method for the catalytic combustion of 2-propanol, which performed impressive catalytic performance and excellent stability as a result of its superior physiochemical properties, i.e. the low temperature reducibility, large pore volume, high amounts of $\text{Co}^{3+}/\text{Co}^{2+}$ and surface active oxygen species. Consequently, the structure of cobalt oxide could significantly influence the catalytic combustion performance.

Generally, the catalytic activity of single metal oxide could be improved by doping hetero-metal since the valance state and the lattice oxygen mobility can be modified by the introduced hetero-metal [13-15]. It is reported that the catalytic activity of cobalt oxides were effectively enhanced by modifying with other metals such as manganese (Mn) [16], copper (Cu) [17], cerium (Ce) [18], iron (Fe) [19], and zirconium (Zr) [20]. On the other hand, the modification method could also affect the catalyst performance. For instance, Wu *et al.* [21] prepared lanthanum-cobalt (La-Co) composite oxides by a co-precipitation method, and found that the doped La enhanced the low temperature reducibility by generation of more active species of Co^{3+} and oxygen species on the catalyst surface, which finally promoted the catalytic activity and stability for the combustion of toluene at a temperature as low as 225 °C. Meanwhile, Mei *et al.* [22] developed $\text{Co}_3\text{O}_4/\text{CeO}_2$ - Co_3O_4 catalyst with hierarchical porous structure by using carbon sphere as the hard template and applied for the combustion of CH_2Br_2 , which is generally difficult to be combusted at low temperatures. It is found that the hierarchical porous structure and high specific surface area were favorable to the adsorption of CH_2Br_2 molecules and then the adsorbed CH_2Br_2 molecules were further oxidized on the rich active sites of this hierarchical catalyst, which resulted in a low conversion temperature of T_{90} at around 321 °C (T_{90} : the temperature for 90% conversion of CH_2Br_2) with excellent stability. As a result, catalyst with improved catalytic performance can be designed by doping hetero-metals,

especially the widely used MnO_x , CuO_x and NiO based composites have already been investigated and proved to be active to the catalytic combustion of VOCs.

In the present work, in order to improve the catalytic performance of Co-based catalysts, the cobalt oxide catalysts with various hetero-metal dopings (Ni, Mn, and Cu) were prepared by a facile electrodeposition method, and applied for the catalytic combustion of toluene. The physiochemical properties of the obtained catalysts were characterized by SEM, XRD, H_2 -TPR, O_2 -TPD and XPS techniques. The catalytic performances of the prepared catalysts were evaluated on a fixed bed reactor at atmospheric condition with 950 ppm toluene in the reaction gas flow. Moreover, the long-term stability test was carried out over the optimum catalyst in the presence and absence of water vapor. It is expected to find an effective catalyst for the combustion of VOCs.

2.2 Experimental

2.2.1 Chemicals and Materials

Hydrochloric acid (HCl), cobalt, nickel, manganese, iron and copper nitrate hydrates, i.e., $\text{Co}(\text{NO}_3)_2 \cdot 6\text{H}_2\text{O}$, $\text{Ni}(\text{NO}_3)_2 \cdot 6\text{H}_2\text{O}$, $\text{Mn}(\text{NO}_3)_2 \cdot 6\text{H}_2\text{O}$, and $\text{Cu}(\text{NO}_3)_2 \cdot 3\text{H}_2\text{O}$ (Wako, Japan), were used without any further treatment. Nickel foam (NF, thickness: 1.5 mm, bulk density: 0.23 g/cm^3 ; number of pores per inch: 110) was provided by MTI, Japan, and used as the catalyst support. It was cut into small pieces ($1.5 \text{ cm} \times 1.5 \text{ cm}$), and pretreated with the assistance of ultrasound in 1 M HCl solution and distilled water (H_2O) for 15 min successively and then, the cleaned NF was washed completely and sealed in water prior to use.

2.2.2 Catalyst preparation

Based on the preliminary experiments, 100 mL of 0.1 M $\text{Co}(\text{NO}_3)_2 \cdot 6\text{H}_2\text{O}$ solutions mixed with 0.01 M $\text{Ni}(\text{NO}_3)_2 \cdot 6\text{H}_2\text{O}$, 0.01 M $\text{Mn}(\text{NO}_3)_2 \cdot 6\text{H}_2\text{O}$, and 0.01 M $\text{Cu}(\text{NO}_3)_2 \cdot 3\text{H}_2\text{O}$ respectively at a molar ratio of 10:1 were prepared for the UPED of hetero-metal doped Co-based catalysts on NF. Herein, the UPED was performed with a constant potential of -1.0 V, on/off time of 1.0 s, and pulse cycles of 500 also based on the preliminary experiments. Herein, the pretreated NF, Ag/AgCl/saturated KCl electrode and platinum wire (ALS, Japan) were used as the working,

reference and counter electrodes, respectively. Subsequently, the obtained samples were washed with distilled water for several times, vacuum-dried at 80 °C for overnight, and finally calcined in a muffle furnace at 350 °C for 2 h with a 5 °C/min heating rate. The prepared catalysts are denoted as 10Co-Ni/NF, 10Co-Mn/NF and 10Co-Cu/NF, respectively. For comparison, the pure catalyst of Co₃O₄/NF was also prepared.

2.2.3 Characterizations

The morphologies and surface elemental compositions of the prepared catalysts were analyzed on a scanning electron microscopy (SEM) (Hitachi SU8010, Japan) accompanied by X-ray spectrometry (EDS) (Horiba EMAX). Crystalline structures were analyzed by an X-ray diffraction (XRD, Rigaku Smartlab, Japan) with a Cu-K α radiation ($\lambda=0.15418$ nm) in a range of 10°-90° with a scanning speed of 10° min⁻¹. The surface chemical composition and elemental valence states of catalyst were further investigated by an X-ray photoelectron spectroscopy (XPS) with an ESCALab220i-XL electron spectrometer (VG, Scientific ESCALab250i-XL unit, UK), in which the C 1s peak was fixed at the binding energy of 284.6 eV. Hydrogen temperature-programmed reduction (H₂-TPR) was carried out on a BELCAT catalyst analyzer with a thermal conductivity detection (TCD). In each procedure, 100 mg of catalyst was loaded into a U-shape tube, which was pretreated firstly at 300 °C for 30 min with a He flow (50 cm³/min) and cooled down to room temperature (RT). Thereafter, the temperature was raised from RT to 900 °C with a 10 °C/min heating rate under a gas flow of 5 vol% H₂/Ar (50 cm³/min). For oxygen temperature-programmed desorption (O₂-TPD), 100 mg of each sample was pretreated at 300 °C with a He flow (50 cm³/min) for 1 h in order to remove the surface water, after cooling down to RT, the sample was treated by a O₂ flow (50 cm³/min) and purged by a He flow (50 cm³/min) for 1 h, respectively, finally, the sample was heated from RT to 900 °C with a heating rate of 10 °C/min.

2.2.4 Catalytic performance test

The catalytic performance of the prepared catalyst for the combustion of toluene was conducted in a fixed bed operated in a continuous flow of oxygen (O₂, 20 vol%) with nitrogen (N₂, 80 vol%) as

the balance gas at the atmospheric condition. Briefly, the prepared catalyst was cut into the particles with a size < 3 mm at first. Then, 0.1 g of catalyst mixed with 0.3 g of silicon carbide (100 mesh) was transferred into a Pyrex reaction tube (i.d.=10 mm) with the quartz wools packing at both ends of the catalyst bed. For each of reaction, the catalyst was pretreated in a nitrogen flow at 100 °C for 1.5 h. Subsequently, the catalytic performance was tested in the set temperature range of 150~300 °C for the combustion of toluene with a concentration of around 950 ppm in the gas flow. Herein, based on the preliminary experiments, the total gas flow rate was kept at 50 cm³/min with a weight hourly space velocity (WHSV) of 30,000 mL·g⁻¹·h⁻¹. A thermocouple was inserted into the catalyst layer to test the reaction temperature. The inlet and outlet concentrations of toluene were analyzed by an on-line gas chromatograph (Shimadzu-2014) equipped with a flame ionization detector (FID) detector, and meanwhile, the gas samples were also analyzed by a Fourier Transform Infrared Spectroscopy (FTIR, Horiba, FG-120).

Toluene conversion and CO₂ selectivity were calculated as follows:

$$\text{Conversion} = \frac{C_{\text{Inlet}} - C_{\text{Outlet}}}{C_{\text{Inlet}}} \times 100\% \quad (2.1)$$

$$\text{CO}_2 \text{ selectivity} = \frac{n_{\text{CO}_2}}{7n_{\text{consumed toluene}}} \times 100\% \quad (2.2)$$

where, C_{Inlet} is the inlet concentration of toluene, C_{Outlet} the outlet concentration of toluene. n_{CO_2} and $n_{\text{consumed toluene}}$ molar numbers of the produced CO₂ in the off gas and the consumed toluene during the reaction, respectively. In this work, the carbon balances of all experiments were closed with errors lower than 5%.

The stability on stream test for the optimum catalyst was also performed. The reaction temperature was set at T=270 °C with a WHSV=30,000 mL·g⁻¹·h⁻¹, and water vapor contents were set at 5 and 10 vol%, respectively for different moisture endurance tests.

2.3. Results and discussion

2.3.1 Morphology, surface composition and crystal phase

Fig. 2.1 shows SEM images of the prepared hetero-metal doped Co-based catalysts. It can be

observed that the pure catalyst of $\text{Co}_3\text{O}_4/\text{NF}$ in **Fig. 2.1a** had a nanosheet structure on the surface of NF. Obviously, the morphology of hetero-metal doped catalyst (**Fig. 2.1(b-d)**) was significantly influenced by hetero-metal type. For Co-Ni/NF catalyst, the nanosheet structure became denser when compared with pure one. However, some large clusters were formed on the surfaces of Co-Mn/NF and Co-Cu/NF catalysts. Moreover, the real doping amounts of hetero-metal on the surfaces of catalysts were also different. As summarized in **Table 2.1**, the content of Cu element on Co-Cu/NF catalyst was extremely higher than other element, in which the value was reached up to 47.6 wt%. For comparison, Co-0.05Ni/NF and Co-0.05Mn/NF catalysts were prepared by mixing 0.1 M $\text{Co}(\text{NO}_3)_2 \cdot 6\text{H}_2\text{O}$ with 0.05 M $\text{Ni}(\text{NO}_3)_2 \cdot 6\text{H}_2\text{O}$ and 0.05 M $\text{Mn}(\text{NO}_3)_2 \cdot 6\text{H}_2\text{O}$, respectively, the corresponding results were displayed in **Fig. 2.1(e and f)**. It can be observed that dense nanosheet structures with large exposed nickel surface formed on these two catalysts, the content of Ni and Mn elements were increased to 30.9 and 9.5 wt%, respectively.

Table 2.1 Hetero-metal contents on the prepared catalyst surfaces.

Sample	Ni (wt %)	Mn (wt %)	Cu (wt %)
Co-Ni/NF	19.4	-	-
Co-Mn/NF	-	0.5	-
Co-Cu/NF	-	-	47.6
Co-0.05Ni/NF	30.9	-	-
Co-0.05Mn/NF	-	9.5	-

(The weight percentages (wt %) of Ni, Mn and Cu were obtained from the EDX analysis results).

XRD patterns of the prepared hetero-metal doped Co-based catalysts are shown in **Fig. 2.2**. In terms of pure $\text{Co}_3\text{O}_4/\text{NF}$ catalyst, the weak characteristic diffraction peaks at 2θ of 37.6° , 59.9° and 65.8° assigned to the crystal planes of (311), (511) and (440) of Co_3O_4 , respectively (JCDs-42-1467). For hetero-metal doping catalysts, except for the Co-Cu/NF catalyst, only diffraction peaks of Co_3O_4 were detected in the corresponding XRD patterns. It is possible that these metals were well dispersed

on the catalysts with small particle sizes and low concentrations. In comparison, in the XRD pattern of Co-Cu/NF catalyst, strong diffraction peaks corresponding to Cu, Cu₂O, and CuO were observed since the Cu species was doped on the catalysts with a high content as confirmed by the EDX analysis (**Table 2.1**), which also led to the weak Co₃O₄ diffraction peaks observed. Herein, it also indicated that Cu should be much easier to deposit on the NF than other metals during the UPED process.

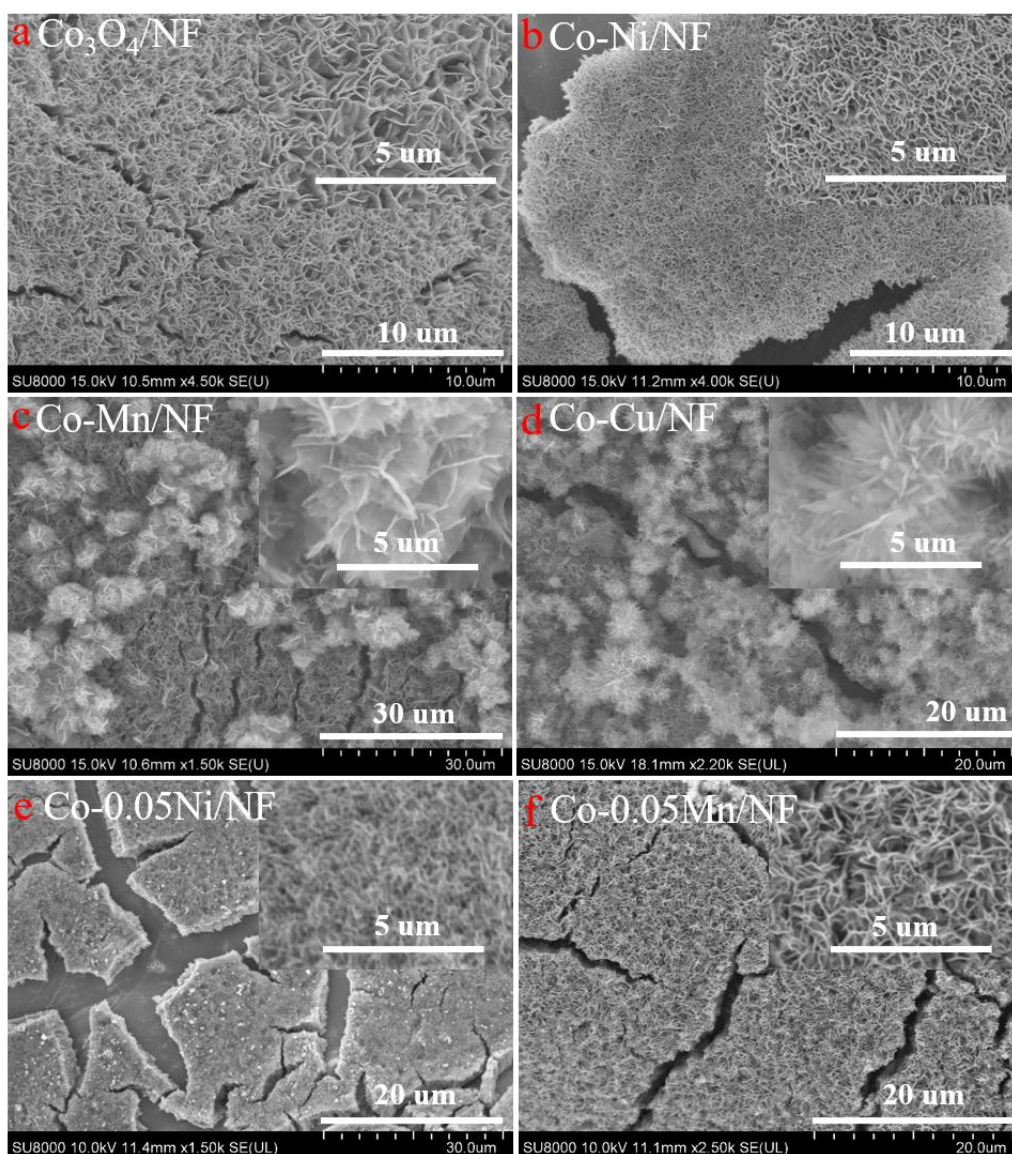


Fig. 2.1. SEM images of the prepared hetero-metal doped Co-based catalysts with different metals.

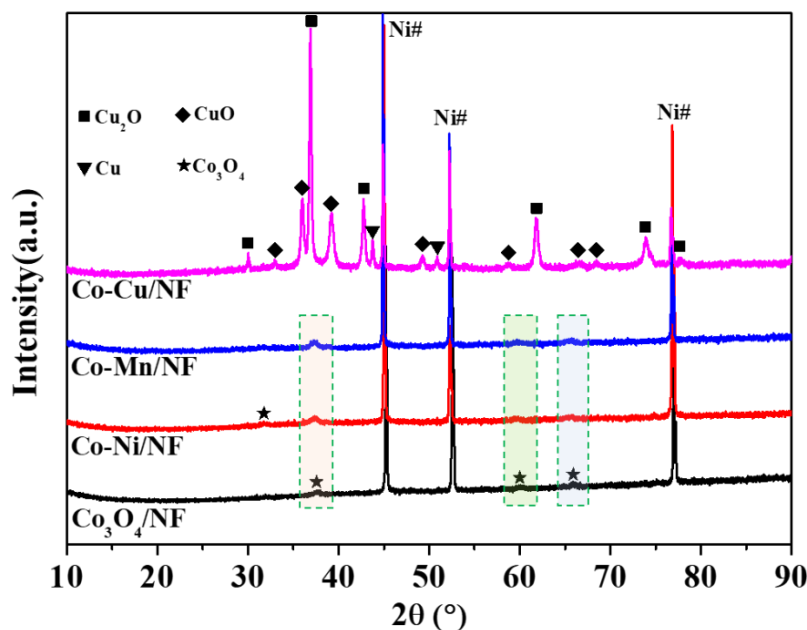


Fig. 2.2. XRD patterns of the prepared hetero-metal doped Co-based catalysts.

2.3.2 Redox properties

The reducibility of the hetero-metal doped Co-based catalysts was investigated by hydrogen temperature-programmed reduction (H_2 -TPR) analysis, and the corresponding results are shown in **Fig. 2.3**. For the pure Co_3O_4/NF catalyst, two main reduction peaks in the temperature range of 150–450 °C appeared. The one peak located at 272 °C was assigned to the reduction of Co_3O_4 to CoO whereas the other one at a higher temperature of 337 °C was contributed by the reduction of CoO to Co [23, 24]. For the hetero-metal doping catalysts, the $Co-Ni/NF$ catalyst showed the similar reduction process as the pure Co_3O_4/NF , however, the reduction peak for the $Co-Ni/NF$ catalyst slightly shifted to the left side with a lower temperature range, indicating that the doping of Ni improved the reducibility of this catalyst. In comparison, $Co-Mn/NF$ and $Co-Cu/NF$ catalysts showed complex reduction profiles, this should be resulted from the multiple oxidation states and different chemical environments of Mn and Cu combining with the Co . One can see that the beginning of reduction temperature was much lower than that of the pure Co_3O_4/NF for $Co-Mn/NF$ and $Co-Cu/NF$ catalysts, implying that both Mn and Cu dopings enhanced the reducibility of multiple compositions within the catalysts, which could be favorable for the low temperature reduction of catalyst,

improving the catalytic performance of these catalysts [25].

As indicated in **Table 2.2**, the H₂-consumption at low temperature for these Co-based catalysts was decreased in the sequence of Co-Mn/NF > Co-Cu/NF > Co-Ni/NF > Co₃O₄/NF. However, it should be noted that the Co-Cu/NF catalyst exhibited a lower initial reduction temperature than the Co-Mn/NF catalyst, which might be favorable for the generation of the more easily reducible species. It was proved that low-temperature reducibility is related to the surface active oxygen species, it will benefit the catalytic activity of VOCs combustion [26].

In general, oxygen species in the catalysts is extremely important for the catalytic combustion of VOCs. The type and mobility of oxygen species of the prepared Co-based catalysts were determined by oxygen temperature-programmed desorption (O₂-TPD) analysis. As shown in **Fig. 2.4**, the desorption peaks in O₂-TPD profiles can be divided into three regions: the first one at the low temperature below 300 °C was assigned to the surface oxygen species of weakly chemisorbed oxygen of O_{sur} (O₂⁻, O₂²⁻, or O⁻), the second one located at the middle temperature range of 300 ~600 °C was contributed by the superficial lattice oxygen species of O_{lat,α} (O²⁻) derived from the lattice defects, and the last one concentrated at the high temperature above 600 °C was related to the lattice oxygen species of O_{lat,β} from the bulk metal oxides, respectively [27, 28]. It is obvious that the intensities of lattice oxygen desorption peaks at middle and high temperature ranges for the Co-based catalysts significantly increased after the doping of hetero-metals, demonstrating that the hetero-metal doping promoted the generation of lattice oxygen species, especially, it is confirmed by the fact that the intensities of O_{lat,α} for Co-Ni/NF, Co-Mn/NF and Co-Cu/NF catalysts significantly increased when compared with the pure Co₃O₄/NF catalysts, indicating that Ni, Mn and Cu dopings were more effective for the formation of lattice defects, which could generate more oxygen vacancies and facilitate the oxygen mobility [29]. As the H₂-TPR result stated above, the improved low-temperature reducibility of mixed metal based catalysts also might be contributed to the increased lattice oxygen species, which promoted more active oxygen species could transfer more

easily from bulk to the catalyst surface. Consequently, hetero-metal doping promoted the generation of both surface and lattice active oxygen species at low temperatures. Moreover, it is well known that surface oxygen species and lattice oxygen species at low temperatures are more important for the catalytic combustion of VOCs because they could be continuously substituted by the oxygen from gas phase under Mars-van Krevelen (MVK) mechanism [30]. Consequently, the increased oxygen species at low temperature could enhance the oxygen mobility and finally improve the catalytic performance of Co-based catalysts in this work.

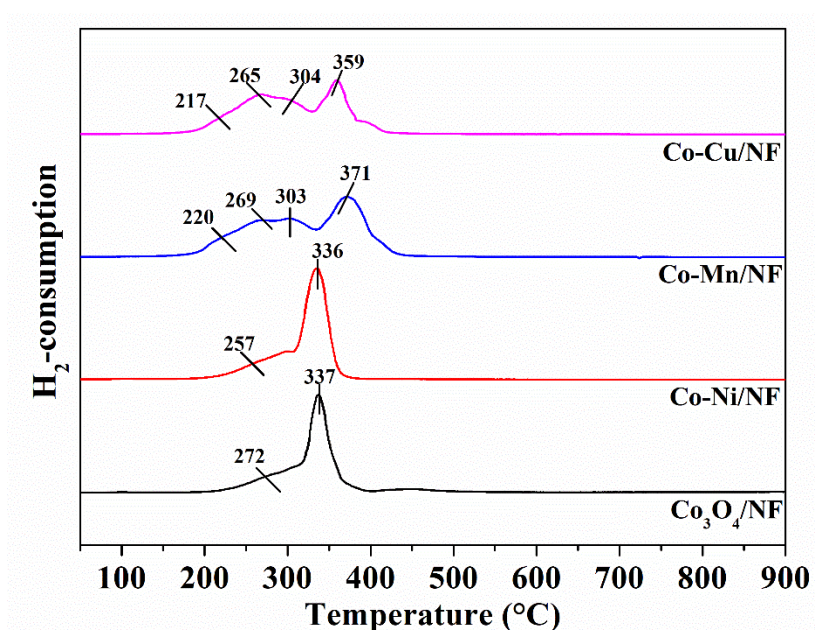


Fig. 2.3. H₂-TPR profiles of the prepared Co-based catalysts.

Table 2.2 Hydrogen consumptions of the prepared Co-based catalysts in H₂-TPR analyses.

Sample	Reduction T ₁ /°C	H ₂ -consumption (mmol/g)	Reduction T ₂ /°C	H ₂ -consumption (mmol/g)
Co ₃ O ₄ /NF	272	0.281	337	0.592
Co-Ni/NF	257	0.288	336	0.664
Co-Mn/NF	< 303	0.760	371	0.621
Co-Cu/NF	< 304	0.635	359	0.372

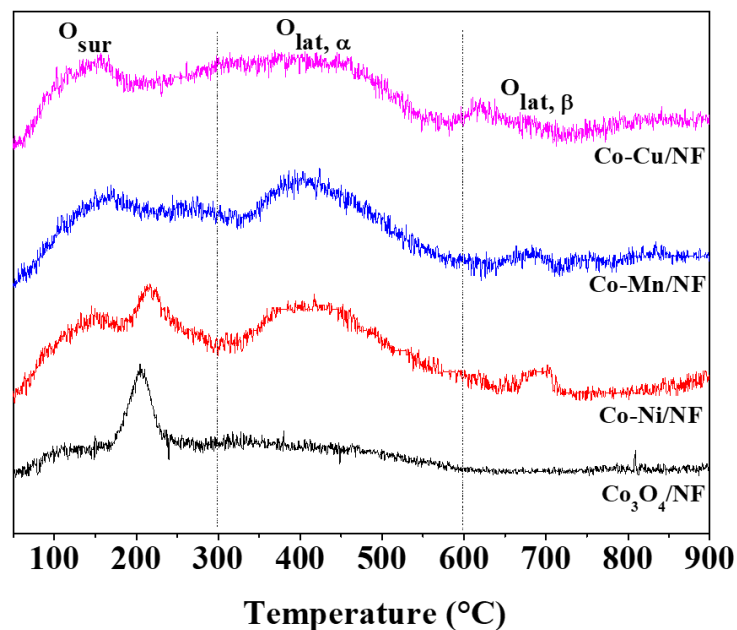


Fig. 2.4. O₂-TPD profiles of the prepared Co-based catalysts.

2.3.3 Surface composition and metal oxidation state

The chemical valence states and the surface compositions of the prepared Co-based catalysts were determined by the XPS analyses, the related results are shown in **Fig. 2.5** and **Table 2.3**. **Fig. 2.5a (1)** shows the Ni 2p XPS spectrum, in which the peaks concentrated at 856.1 eV and 873.1 eV were related to Ni 2p_{3/2} and Ni 2p_{1/2}, respectively [31, 32]. Herein, the Ni 2p_{3/2} spectrum can be further deconvoluted into the peaks corresponding to Ni²⁺ (854.7 eV) and Ni³⁺ (861.6 eV), indicating that the coexistence of two valences of nickel oxides within the catalyst. Meanwhile, Mn 2p XPS spectrum for the Co-Mn/NF catalyst was not so clear, which should be resulted from the low loading of Mn element (**Table 2.1**). However, as shown in **Fig. 2.5a (2)**, three peaks can be divided from Mn 2p_{2/3} XPS spectrum with the binding energies of 643.3, 641.7 and 640.8 eV assigning to the surface Mn⁴⁺, Mn³⁺ and Mn²⁺, respectively[33], which revealed the existence of Mn₃O₄ in the Co-Mn/NF catalyst. It is well known that the presence of polyvalent states in manganese oxides is favorable for the oxygen mobility within the redox couples of Mn⁴⁺/Mn³⁺ and Mn⁴⁺/Mn²⁺, and thereby improving the catalytic performance during the catalytic combustion of VOCs [34]. For the Cu 2p_{3/2} XPS spectrum of the obtained Co-Cu/NF catalyst (**Fig. 2.5a (3)**), which can be fitted into two peaks, one

at binding energy of 932.5 eV related to the chemical valence state of Cu^{2+} , whereas the other one focused at 934.7 eV was contributed to Cu^+ , demonstrating that Cu species also had multivalent properties as the elements of Ni and Mn [35].

Fig. 2.5b shows the XPS spectra of Co 2p for all the prepared catalysts, which can be divided into Co 2p_{3/2} and Co 2p_{1/2}, respectively [12]. The peaks located at 779.9 and 794.9 eV were assigned to the surface active species of Co^{3+} , whereas the peaks concentrated at 781.6 and 796.4 eV were corresponding to the surface Co^{2+} with the shake-up satellites [36]. The molar ratios of $\text{Co}^{3+}/\text{Co}^{2+}$ are summarized in **Table 2.3**. It can be seen that the hetero-metal doping significantly enhanced the generation of surface Co^{3+} , which might be caused by the interaction of Co with Ni, Mn, or Cu. Moreover, the redox $\text{Co}^{3+}/\text{Co}^{2+}$ couple could enhance the transformation of electrons, and especially the surface Co^{3+} should be conducive to the improvement of the catalytic combustion of VOCs [37].

Fig. 2.5c depicts the O 1s XPS spectra for all the prepared Co-based catalysts, in which the broad and asymmetrical peaks can be divided into three components at the ranges of 529.5-530.0, 530.3-531.0 and 531.7-532.0 eV, which corresponded to the surface lattice oxygen of O^{2-} (O_{lat}), surface absorbed oxygen of O_2^- , O^- or O_2^{2-} (O_{sur}) and the absorbed OH groups or molecular water (O_{ads}), respectively [38, 39]. As summarized in **Table 2.3**, it is worth noting that $\text{O}_{\text{sur}}/\text{O}_{\text{lat}}$ ratios for all hetero-metal doped catalysts were higher than that of pure $\text{Co}_3\text{O}_4/\text{NF}$ catalyst, suggesting that the metal doping was beneficial to the generation of surface oxygen species. Combining with the O_2 -TPD analysis results, it can be concluded that hetero-metal doping could enhance the formations of both surface oxygen species and lattice oxygen species. It is important that surface and lattice oxygen species are related to the oxygen vacancies, by which the involved oxygen species will be more active to the catalytic combustion of VOCs [17].

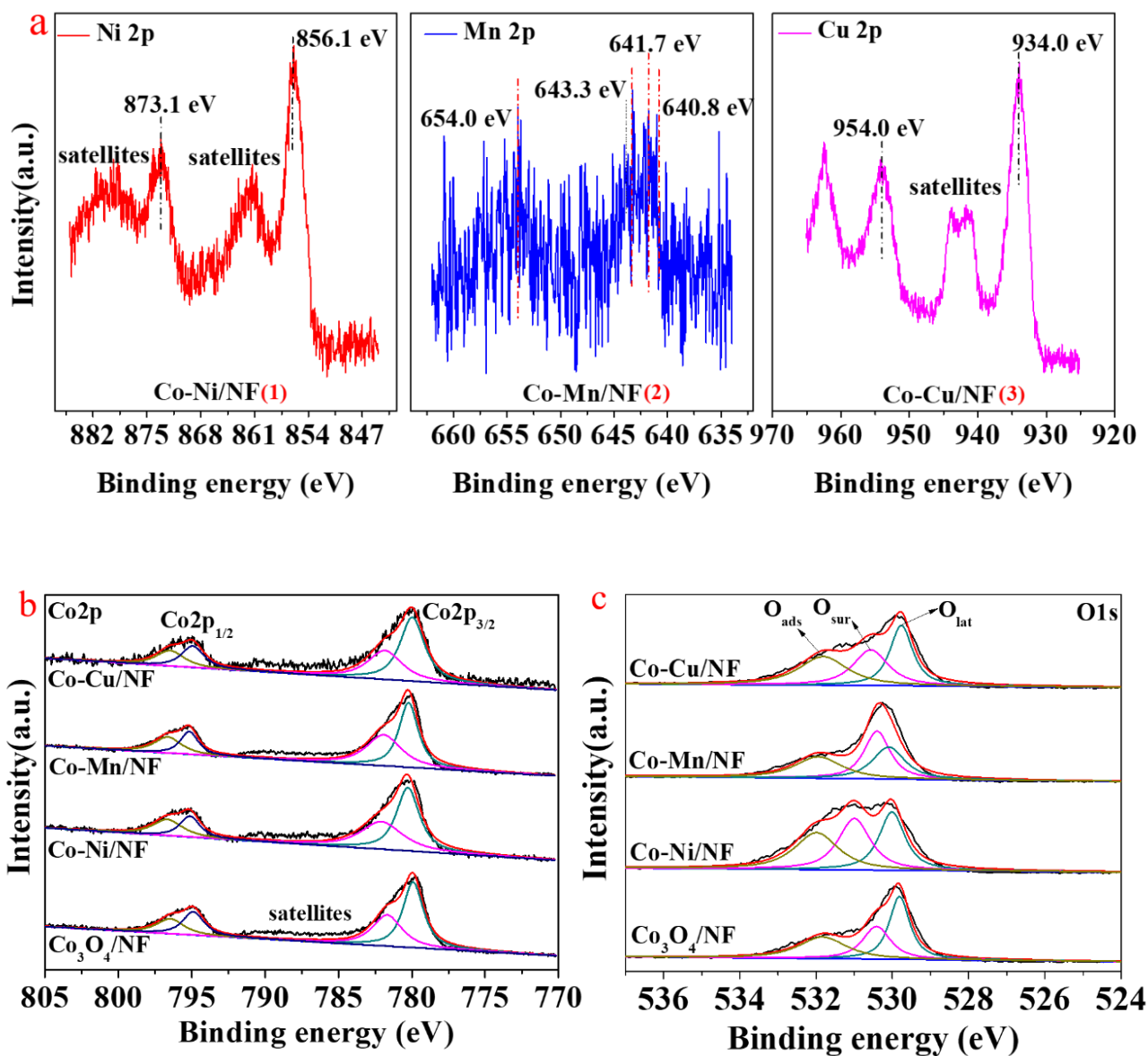


Fig. 2.5. XPS spectra of Ni 2p, Mn 2p and Cu 2p (a), Co 2p (b) and O 1s (c) for pure Co₃O₄/NF, hetero-metal doping catalysts of Co-Ni/NF, Co-Mn/NF, and Co-Cu/NF.

Table 2.3 Surface elemental compositions and valence states of Co-based catalysts based on XPS analysis.

Catalysts	Area ratio of O 1s	Area ratio of Co 2p
	O _{sur} /O _{latt}	Co ³⁺ /Co ²⁺
Co ₃ O ₄ /NF	0.79	1.14
Co-Ni/NF	1.02	1.33
Co-Mn/NF	0.99	1.35
Co-Cu/NF	0.91	1.43

2.3.4 Catalytic performance

The evaluation of catalytic performance was conducted under the conditions of toluene concentration = 950 ppm in a mixed gas of N₂ (80 vol%) and O₂ (20 vol%) as the reaction gas with a WHSV = 30,000 mL·g⁻¹·h⁻¹. The reaction temperature was set in the range of 150-300 °C, and the temperatures of conversions of 10% (T₁₀), 50% (T₅₀) and 90% (T₉₀) were used for comparison. The obtained results are shown in **Fig. 2.6** and summarized in **Table 2.4**. For the pure Co₃O₄/NF catalyst (**Fig. 2.6a**), it can be seen that the toluene conversion increased gradually with the increase in the reaction temperature, and finally completely converted into CO₂ and H₂O at 270 °C. However, after the hetero-metal doping, the catalytic activity was significantly improved, and the temperature of conversion decreased in the order of Co-Cu/NF > Co-Ni/NF > Co-Mn/NF, demonstrating that Cu doping improved the catalytic activity at the greatest extent with the lowest conversion temperatures of T₁₀=222 °C, T₅₀=242 °C and T₉₀=248 °C, respectively. For comparison, the catalytic activity of Co-0.05Ni/NF and Co-0.05Mn/NF catalysts with high content of Ni and Mn elements were also evaluated, details in **Fig. 2.6b** and **Table 2.4** suggesting that catalytic activity of these two catalysts was not improved when the amount of the doped Ni and Mn elements increased. As it depicted in **Fig. 2.1(e and f)**, the nanosheet structure of Co-0.05Ni/NF and Co-0.05Mn/NF catalysts became denser accompanied by large area of inactive NF surface exposed, which might be the reason for their decreased catalytic activity when compared with Co-Ni/NF and Co-Mn/NF catalysts. Consequently, the catalytic activity of metal doped Co-based catalysts was closely related to the catalyst structure, and catalysts possessed porous nanosheet structure was more favorable to the catalytic combustion of toluene.

Generally, the catalytic activity for VOCs combustion over transition metal oxide catalysts is dependent on the catalyst reducibility, surface active oxygen species and the state of the metal ions. As discussed above, the H₂-TPR and O₂-TPD analysis results indicated that the hetero-metal doping enhanced the low temperature reducibility and promoted the generation of lattice oxygen which related to oxygen defects, it was favorable to the oxygen mobility, and especially, the Co-Cu/NF

catalyst exhibited the best reducibility at low temperature. Additionally, the XPS results shown in **Fig. 2.5a** also demonstrated that the doping metals of Ni, Mn, and Cu possessed multivalence, which facilitated the electron transfer within the redox couples, leading to the formation of high content Co^{3+} . Consequently, the concentration ratio of $\text{Co}^{3+}/\text{Co}^{2+}$ was as high as 1.43 in the Co-Cu/NF catalyst, as listed in **Table 2.3**. As such, the best catalytic activity achieved over Co-Cu/NF catalyst should be contributed by its low-temperature reducibility, increased active species of surface and lattice oxygen, and high content of Co^{3+} species.

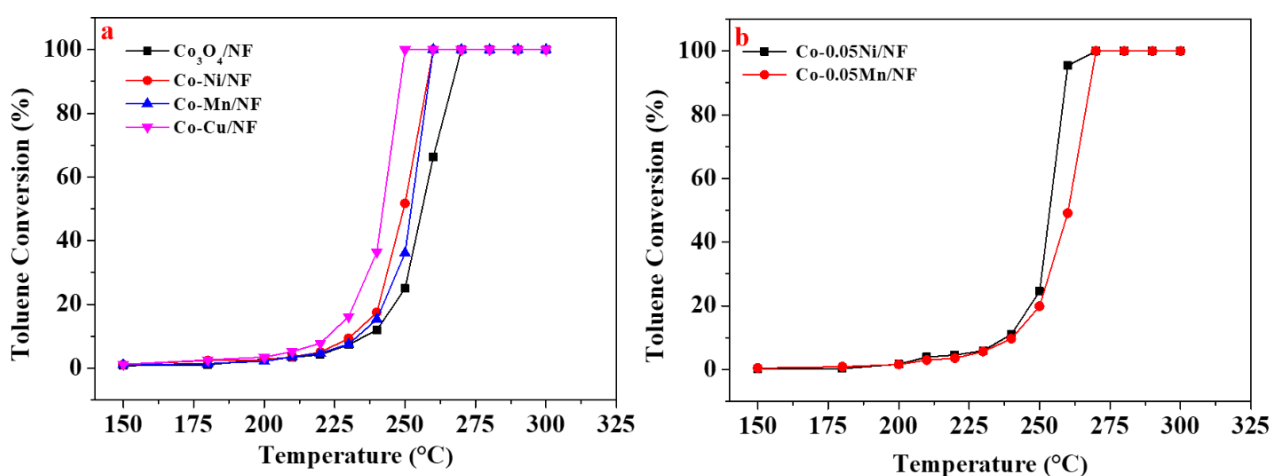


Fig. 2.6. Catalytic performances of the prepared Co-based catalysts for catalytic combustion of toluene.

Literatures reported by Feng *et al.* [29] and Santos *et al.* [41] proved that toluene catalytic combustion follows the Mars and van Krevelen (MVK) mechanism, in which lattice oxygen species play an important role in the catalytic reaction. It was found that lattice oxygen species closely connect with metal ions has the properties of nucleophilicity, which could activate the adsorbed VOCs molecules, immediately, the consumed oxide species replenished by the generated active oxygen species which transferred from the gas phase oxygen through the existed oxygen vacancies, and the pollutant toluene molecules could be finally selectively oxidized into harmless substances of CO_2 and H_2O by the surface oxygen active species. As a result, the enrichment of both surface and lattice oxygen species were conducive to the catalytic combustion of VOCs, as it stated above,

hetero-metal doping increased the amount of active oxygen species at low temperatures, resulting in the enhanced catalytic activity of the mixed metal oxides based catalysts for toluene combustion.

Table 2.4 Performance test results for the prepared Co-based catalysts for the catalytic combustion of toluene.

Catalyst	Toluene conversion (°C)			Ideal CO ₂ concentration (V ^a _{CO2} /V _{N2} , %)	Actual CO ₂ concentration (V ^b _{CO2} /V _{N2} , %)	Error (%)
	T ₁₀	T ₅₀	T ₉₀			
Co ₃ O ₄ /NF	235	255	267	0.786	0.770	2.1
Co-Ni/NF	229	249	257	0.780	0.804	3.1
Co-Mn/NF	233	252	258	0.806	0.845	4.6
Co-Cu/NF	222	242	248	0.779	0.760	2.5
Co-0.05Ni/NF	238	253	259	0.734	0.727	0.9
Co-0.05Mn/NF	240	260	267	0.845	0.810	4.1

V^a_{CO2}, the flow rate of the ideal produced CO₂;

V^b_{CO2}, the flow rate of the actual produced CO₂;

V_{N2}, the flow rate of N₂ as balance gas for reaction.

2.3.5 Long-term stability test on stream

The stability test was conducted for the optimum catalyst of Co-Cu/NF, in which the moisture effect on the long-term combustion performance was also investigated. As displayed in **Fig. 2.7**, the toluene conversion maintained at 100% before introducing water vapor, but decreased to ~80% when 5 vol% water vapor was introduced, which was contributed by the competition contacting between toluene and water molecules at the active sites of the catalyst [40]. Continuously, when the water vapor content was increased to 10 vol%, the toluene conversion further decreased to 60%. Thus, the high content of water vapor should play a significant role in the decrease of toluene conversion. However, as soon as the water vapor introduction was stopped, the toluene conversion recovered to 100%, demonstrating that this catalyst possessed good renewability and high moisture endurance ability. Additionally, the selectivity of CO₂ during the long-term catalytic combustion process always maintained at around 100%, demonstrating that the Co-Cu/NF catalyst was highly selective for CO₂

in the catalytic combustion of toluene. Therefore, it can be concluded that the Co-Cu/NF catalyst had excellent catalytic stability and high CO₂ selectivity in the presence and absence of water vapor.

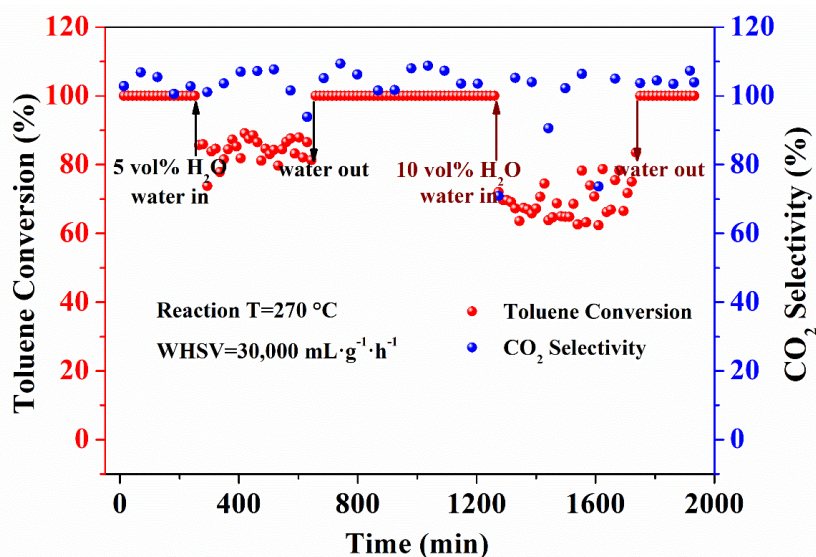


Fig. 2.7. Long-term stability test in the absence and presence of water vapor for the catalytic combustion of toluene.

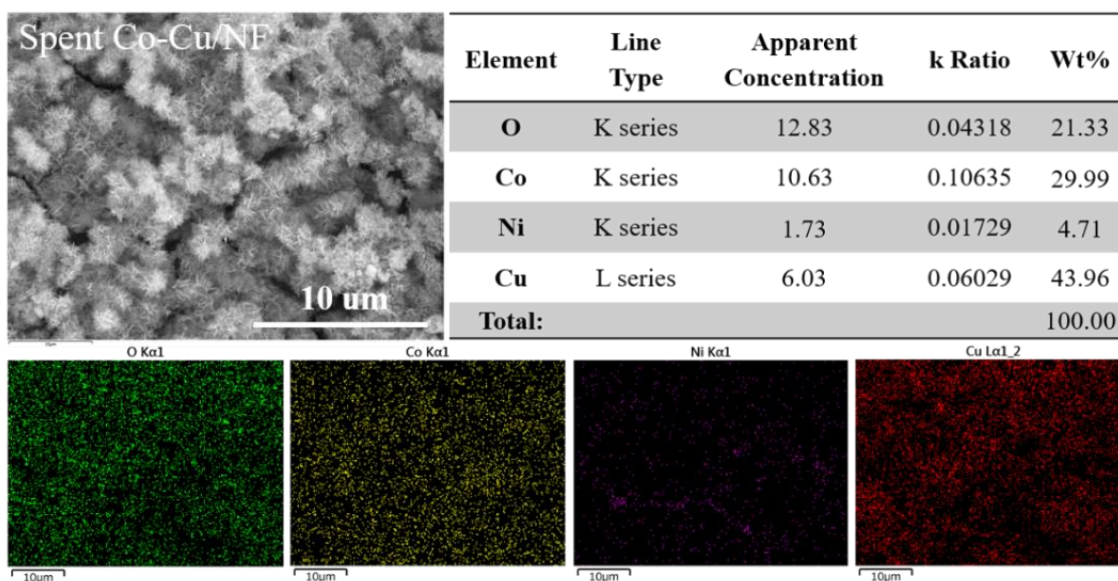


Fig. 2.8. Surface elemental compositions of the spent Co-Cu/NF catalyst after the long-term stability test (The weight percent of wt % for O, Co, Ni and Cu were taken by EDX analysis).

Fig. 2.8 shows the SEM image and surface elemental composition of the spent Co-Cu/NF catalyst after the long-term stability test. It can be seen that the catalyst maintained its morphology when compared with the fresh one (**Fig. 2.1d**), and also there was no obvious change in the surface

elemental composition, implying that the good stability of Co-Cu/NF should be contributed by its stable physiochemical properties. It is expected that this kind of catalyst could be an alternative catalyst for the catalytic combustion of VOCs in a practical process.

2.4 Conclusions

In summary, a series of Co-based catalysts with various hetero-metal (Ni, Mn, and Cu) dopings were prepared by an electrodeposition method, which showed high activity and stability to the catalytic combustion of toluene. The morphology of the hetero-metal doped cobalt oxide was significantly influenced by the type of hetero-metal doped, resulting in the contents of the metal elements on the Co-based catalysts were different, and increase in Ni and Mn elements content made a negative influence on the catalyst structure. H₂-TPR analysis results indicated that the hetero-metal doping enhanced the low-temperature reducibility, which is favorable to the catalytic oxidation of toluene. Meanwhile, O₂-TPD analysis results proved that the hetero-metal doping resulted in the formation of lattice defects, which could generate oxygen vacancies and facilitate oxygen mobility. For the catalytic combustion of toluene, the Co-Cu/NF catalyst exhibited the highest catalytic activity with the lowest toluene conversion temperature of T₉₀ at 248 °C, which should be contributed by its low-temperature reducibility, increased surface and lattice oxygen species, and high content of active Co³⁺ species promoted by the interaction of the mixed metal oxides. Additionally, increase in Ni and Mn elements led to denser nanosheet formed on the catalysts of Co-0.05Ni/NF and Co-0.05Mn/NF and decreased their catalytic performance, therefore the catalytic activity of Co-based catalysts was closely related to the catalyst structure. During the long-term stability test, the optimum catalyst of Co-Cu/NF also performed excellent catalytic stability and high selectivity to CO₂ in the presence and absence of water vapour for the catalytic combustion of toluene. It is expected that this Co-Cu/NF catalyst could be an alternative catalyst for the catalytic combustion of VOCs in the practical application.

References

- [1] J. Lelieveld, T. Butler, J. Crowley, T. Dillon, H. Fischer, L. Ganzeveld, H. Harder, M. Lawrence, M. Martinez, D. Taraborrelli, Atmospheric oxidation capacity sustained by a tropical forest, *Nature*. 452 (2008) 737-740.
- [2] M.S. Kamal, S.A. Razzak, M.M. Hossain, Catalytic oxidation of volatile organic compounds (VOCs) – A review, *Atmospheric Environment*. 140 (2016) 117-134.
- [3] R. Atkinson, Atmospheric chemistry of VOCs and NO_x, *Atmospheric Environment*. 34 (2000) 2063-2101.
- [4] Z. G. Zhang, Process, reactor and catalyst design: Towards application of direct conversion of methane to aromatics under nonoxidative conditions, *Carbon Resources Conversions*. 2 (2019) 157-174.
- [5] H. B. Huang, Y. Xu, Q. Y. Feng, D.Y. Leung, Low temperature catalytic oxidation of volatile organic compounds: a review, *Catalysis Science & Technology*. 5 (2015) 2649-2669.
- [6] Y. C. Chiang, P. C. Chiang, C. P. Huang, Effects of pore structure and temperature on VOC adsorption on activated carbon, *Carbon*. 39 (2001) 523-534.
- [7] K. Everaert, J. Baeyens, Catalytic combustion of volatile organic compounds, *Journal of Hazardous Materials*. 109 (2004) 113-139.
- [8] L.F. Liotta, Catalytic oxidation of volatile organic compounds on supported noble metals, *Applied Catalysis B-Environmental*. 100 (2010) 403-412.
- [9] W. B. Li, J. H. Wang, H. Gong, Catalytic combustion of VOCs on non-noble metal catalysts, *Catalysis Today*. 148 (2009) 81-87.
- [10] P.M. Kouotou, Z. Y. Tian, H. Vieker, A. Beyer, A. Götzhäuser, K. Kohse-Höinghaus, Selective synthesis of α -Fe₂O₃ thin films and effect of the deposition temperature and lattice oxygen on the catalytic combustion of propene, *Journal of Materials Chemistry A*. 1 (2013) 10495-10504.
- [11] Q. Ren, S. Mo, R. Peng, Z. Feng, M. Zhang, L. Chen, M. Fu, J. Wu, D. Ye, Controllable synthesis of 3D hierarchical Co₃O₄ nanocatalysts with various morphologies for the catalytic

oxidation of toluene, *Journal of Materials Chemistry A*. 6 (2018) 498-509.

[12] S. Dissanayake, N. Wasalathanthri, A.S. Amin, J. He, S. Poges, D. Rathnayake, S.L. Suib, Mesoporous Co_3O_4 catalysts for VOC elimination: Oxidation of 2-propanol, *Applied Catalysis A-General*. 590 (2020) 117366.

[13] J. Hou, Y. Li, M. Mao, X. Zhao, Y. Yue, The effect of Ce ion substituted OMS-2 nanostructure in catalytic activity for benzene oxidation, *Nanoscale*. 6 (2014) 15048-15058.

[14] L. Li, J. Luo, Y. Liu, F. Jing, D. Su, W. Chu, Self-propagated flaming synthesis of highly active layered $\text{CuO}-\delta\text{-MnO}_2$ hybrid composites for catalytic total oxidation of toluene pollutant, *ACS Applied Materials & Interfaces*. 9 (2017) 21798-21808.

[15] Y. Deng, W. Tang, W. Li, Y. Chen, MnO_2 -nanowire@NiO-nanosheet core-shell hybrid nanostructure derived interfacile Effect for promoting catalytic oxidation activity, *Catalysis Today*. 308 (2018) 58-63.

[16] Y. Huang, K. Ye, H. Li, W. Fan, F. Zhao, Y. Zhang, H. Ji, A highly durable catalyst based on $\text{Co}_x\text{Mn}_{3-x}\text{O}_4$ nanosheets for low-temperature formaldehyde oxidation, *Nano Research*. 9 (2016) 3881-3892.

[17] S. Li, H. Wang, W. Li, X. Wu, W. Tang, Y. Chen, Effect of Cu substitution on promoted benzene oxidation over porous CuCo-based catalysts derived from layered double hydroxide with resistance of water vapor, *Applied Catalysis B-Environmental*. 166 (2015) 260-269.

[18] C. Wang, C. Zhang, W. Hua, Y. Guo, G. Lu, S. Gil, A. Giroir-Fendler, Catalytic oxidation of vinyl chloride emissions over Co-Ce composite oxide catalysts, *Chemical Engineering Journal*. 315 (2017) 392-402.

[19] J. Carpentier, J.-F. Lamonier, S. Siffert, H. Laversin, A. Aboukais, Preparation and characterization of Co-Fe-Cu mixed oxides via hydrotalcite-like precursors for toluene catalytic oxidation, *Studies in Surface Science and Catalysis*. 142 (2002) 1197-1204.

[20] Z. Pu, Y. Liu, H. Zhou, W. Huang, Y. Zheng, X. Li, Catalytic combustion of lean methane at low temperature over ZrO_2 -modified Co_3O_4 catalysts, *Applied Surface Science*. 422 (2017) 85-93.

- [21] M. Wu, S. Chen, A. Soomro, S. Ma, M. Zhu, X. Hua, W. Xiang, Investigation of synergistic effects and high performance of La-Co composite oxides for toluene catalytic oxidation at low temperature, *Environmental Science and Pollution Research*. 26 (2019) 12123-12135.
- [22] J. Mei, J. Xie, Y. Sun, Z. Qu, N. Yan, Design of $\text{Co}_3\text{O}_4/\text{CeO}_2\text{--Co}_3\text{O}_4$ hierarchical binary oxides for the catalytic oxidation of dibromomethane, *Journal of Industrial and Engineering Chemistry*. 73 (2019) 134-141.
- [23] S. Todorova, H. Kolev, J.P. Holgado, G. Kadinov, C. Bonev, R. Pereñíguez, A. Caballero, Complete n -hexane oxidation over supported Mn–Co catalysts, *Applied Catalysis B-Environmental*. 94 (2010) 46-54.
- [24] Z. Zhu, G. Lu, Z. Zhang, Y. Guo, Y. Guo, Y. Wang, Highly Active and Stable $\text{Co}_3\text{O}_4/\text{ZSM-5}$ Catalyst for Propane Oxidation: Effect of the Preparation Method, *ACS Catalysis*. 3 (2013) 1154–1164.
- [25] X. Yang, X. Yu, M. Lin, X. Ma, M. Ge, Enhancement effect of acid treatment on Mn_2O_3 catalyst for toluene oxidation, *Catalysis Today*. 327 (2019) 254-261.
- [26] X. Chen, S. Cai, J. Chen, W. Xu, H. Jia, J. Chen, Catalytic combustion of toluene over mesoporous Cr_2O_3 -supported platinum catalysts prepared by in situ pyrolysis of MOFs, *Chemical Engineering Journal*. 334 (2018) 768-779.
- [27] Q. Meng, W. Wang, X. Weng, Y. Liu, H. Wang, Z. Wu, Active oxygen species in $\text{La}_{n+1}\text{Ni}_n\text{O}_{3n+1}$ layered perovskites for catalytic oxidation of toluene and methane, *The Journal of Physical Chemistry C*. 120 (2016) 3259-3266.
- [28] W.Y. Hernández, D. Lopez-Gonzalez, S. Ntais, C. Zhao, A. Boréave, P. Vernoux, Silver-modified manganite and ferrite perovskites for catalyzed gasoline particulate filters, *Applied Catalysis B-Environmental*. 226 (2018) 202-212.
- [29] X. Feng, J. Guo, X. Wen, M. Xu, Y. Chu, S. Yuan, Enhancing performance of Co/CeO_2 catalyst by Sr doping for catalytic combustion of toluene, *Applied Surface Science*. 445 (2018) 145-153.
- [30] Z. Hou, J. Feng, T. Lin, H. Zhang, X. Zhou, Y. Chen, The performance of manganese-based

catalysts with $\text{Ce}_{0.65}\text{Zr}_{0.35}\text{O}_2$ as support for catalytic oxidation of toluene, *Applied Surface Science*. 434 (2018) 82-90.

[31] X. Zhang, R. You, D. Li, T. Cao, W. Huang, Reaction sensitivity of ceria morphology effect on Ni/CeO_2 catalysis in propane oxidation reactions, *ACS Applied Materials & Interfaces*. 9 (2017) 35897-35907.

[32] X. Zhang, S.D. House, Y. Tang, L. Nguyen, Y. Li, A.A. Opalade, J.C. Yang, Z. Sun, F.F. Tao, Complete oxidation of methane on NiO nanoclusters supported on CeO_2 nanorods through synergistic effect, *ACS Sustainable Chemistry & Engineering*. 6 (2018) 6467-6477.

[33] Z. Q. Zou, M. Meng, Y. Q. Zha, Surfactant-assisted synthesis, characterizations, and catalytic oxidation mechanisms of the mesoporous $\text{MnOx}-\text{CeO}_2$ and $\text{Pd}/\text{MnOx}-\text{CeO}_2$ catalysts used for CO and C_3H_8 oxidation, *The Journal of Physical Chemistry C*. 114 (2009) 468-477.

[34] Y. Wang, S. Xie, J. Deng, S. Deng, H. Wang, H. Yan, H. Dai, Morphologically controlled synthesis of porous spherical and cubic LaMnO_3 with high activity for the catalytic removal of toluene, *ACS Applied Materials & Interfaces*. 6 (2014) 17394-17401.

[35] J. H. Zhuang, B. Lu, F. N. Gu, Z. Y. Zhong, F. B. Su, Ordered mesoporous $\text{Cu}-\text{Ca}-\text{Zr}$: A superior catalyst for direct synthesis of methyl formate from syngas, *Carbon Resources Conversions*. 1 (2018) 174-182.

[36] L.F. Liotta, G.D. Carlo, G. Pantaleo, A.M. Venezia, G. Deganello, $\text{Co}_3\text{O}_4/\text{CeO}_2$ composite oxides for methane emissions abatement: Relationship between $\text{Co}_3\text{O}_4-\text{CeO}_2$ interaction and catalytic activity, *Applied Catalysis B-Environmental*. 66 (2006) 217-227.

[37] C. Ma, Z. Mu, J. Li, Y. Jin, J. Cheng, G. Lu, Z. Hao, S. Qiao, Mesoporous Co_3O_4 and $\text{Au}/\text{Co}_3\text{O}_4$ with high catalytic activities for oxidation of trace ethylene, *Journal of the American Chemical Society*. 132 (2010) 2608-2613.

[38] K. Ji, H. Dai, J. Deng, L. Song, B. Gao, Y. Wang, X. Li, Three-dimensionally ordered macroporous $\text{Eu}_{0.6}\text{Sr}_{0.4}\text{FeO}_3$ supported cobalt oxides: Highly active nanocatalysts for the combustion of toluene, *Applied Catalysis B-Environmental*. 129 (2013) 539-548.

- [39] W. Tang, J. Li, X. Wu, Y. Chen, Limited nanospace for growth of Ni–Mn composite oxide nanocrystals with enhanced catalytic activity for deep oxidation of benzene, *Catalysis Today*. 258 (2015) 148-155.
- [40] S. Xie, H. Dai, J. Deng, Y. Liu, H. Yang, Y. Jiang, W. Tan, A. Ao, G. Guo, Au/3DOM Co_3O_4 : highly active nanocatalysts for the oxidation of carbon monoxide and toluene, *Nanoscale*. 5 (2013) 11207-11219.
- [41] V. Santos, M. Pereira, J. Órfão, J. Figueiredo, The role of lattice oxygen on the activity of manganese oxides towards the oxidation of volatile organic compounds, *Applied Catalysis B-Environmental*. 99 (2010) 353-363.

CHAPTER 3 Catalytic oxidation of volatile organic compound over Ce modified Co-based mixed oxide catalysts synthesized by electrodeposition method

3.1 Introduction

Volatile organic compounds (VOCs) mainly include halogenated compounds (e.g., chloroform, chlorobenzene, and trichloroethylene), aldehydes (e.g., formaldehyde), aromatic compounds (e.g., toluene and benzene), polycyclic aromatic hydrocarbons (e.g., naphthalene, phenanthrene and pyrene), alcohols (e.g., ethyl alcohol) and ketones (e.g., ethyl isobutyl ketone) [1]. They are harmful to the environment and the human health since they are not only toxic but also can be the precursors of ozone/photochemical smog [2-4]. The main sources of VOCs are from human activities, such as the utilization of vehicle transportation, solvents, building materials, decorative materials, fiber materials, office supplies and so on [5, 6]. Accordingly, pollution caused by VOCs has become a severe issue, and VOCs removal has already aroused widespread concern [7].

For decades, various kinds of technologies including adsorption, absorption, bio-degradation, membrane separation, thermal incineration and combustion, pyrolysis, photocatalytic oxidation have been applied to remove VOCs [8-9]. Among all these approaches, catalytic oxidation is the most effective and environmentally-friendly method, by which VOCs can be transferred into harmless substances of CO_2 and H_2O at a relatively low temperature [10]. To date, two groups of catalysts, i.e., noble-metal-based catalysts and transition-metal-oxide-based catalysts, have been widely developed for the catalytic oxidation of VOCs [11]. However, the former ones are restricted to the large-scale applications due to their high cost. In contrast, the latter ones exhibit similar or only a little lower catalytic performance, but they have lower cost. It is found that single-transition-metal oxide catalysts always have relatively lower activity for VOCs oxidation [11, 12]. To solve this problem, mixed transition metal oxide catalysts have been extensively synthesized and applied [13-15]. For example, incorporation of Ce species into Co oxides could modify the redox properties and the

chemical states of the Co-Ce mixed oxide catalysts since cobalt oxide can provide active mobile oxygen while cerium oxide has high oxygen storage and releasing capacity with redox properties (couples of $\text{Ce}^{4+}/\text{Ce}^{3+}$), which could provide more active oxygen for the oxidation reactions, and as such, their synergistic effect could enhance the catalytic activity in VOCs oxidation [16-20].

It is well known that the catalyst preparation method and the structure of the catalyst have great influence on the catalytic performance. Compared with the conventional preparation methods such as impregnation, hydrothermal synthesis, co-precipitation and template-assisted methods [14-20], the electrodeposition method is not only a simple and time-saving preparation method, but also a way which can control the size, density and composition of the final catalyst [21-23]. In addition, the electrodeposition conditions can be controllably modulated by changing deposition mode, time, current density and potential [22]. Consequently, it can be applied to prepare various catalysts. Moreover, for VOCs oxidation catalysts, when the conventional preparation methods are applied, the obtained catalysts have to be coated on some porous supports by an additional process such as wash-coating and spray coating. However, if the catalyst can be directly coated on the porous supports such as nickel foam (NF), the catalysts can be directly applied in a practical process. This may simplify catalyst preparation and reduce the total catalyst preparation cost.

In the present study, a series of Ce modified Co-based (Co-Ce) mixed oxide catalysts were supported on the NF using a unipolar pulse electro-deposition (UPED) method and applied directly for the catalytic oxidation of a model VOC, i.e., toluene for the first time. Physicochemical properties of the prepared Co-Ce/NF catalysts were obtained by scanning electron microscope (SEM) with an energy dispersive X-ray (EDX) detector, Transmission electron microscopy (TEM), X-ray diffraction (XRD), hydrogen temperature-programmed reduction (H_2 -TPR), oxygen temperature-programmed desorption (O_2 -TPD) and X-ray photoelectron spectroscopy (XPS). The catalytic performances for removing toluene were evaluated in a fixed bed at varying temperatures. As a result, it was found that 10Co-Ce/NF catalyst prepared with an initial molar ratio of Co/Ce at 10 in the solution achieved the best catalytic performance with a complete conversion temperature at

268 °C and CO₂ selectivity of 100%. The effect of steam on the catalytic stability was also evaluated.

3.2 Experimental

3.2.1 Chemicals and Materials

Hydrochloric acid (HCl), ethanol, cobalt and cerium nitrate hydrates (Co (NO₃)₂·6H₂O and Ce(NO₃)₃·6H₂O were purchased from Wako, Japan) and used without any further treatment. Nickel foam (NF, thickness: 1.5 mm, bulk density: 0.23 g/cm³; number of pores per inch: 110) was provided by MTI, Japan, and used as the catalyst support. It was cut into small pieces (1.5 cm×1.5 cm), and then successively treated in 1 M HCl and absolute ethanol for 15 min with the assistance of ultrasound. Finally, the cleaned NF was washed completely and sealed in ethanol solution prior to use.

3.2.2 Preparation of catalysts

Mixed solutions of Co (NO₃)₂·6H₂O and Ce(NO₃)₃·6H₂O with molar ratios of Co to Ce (Co/Ce) of 15:1, 10:1, and 5:1 were prepared, and the corresponding solution concentration ratios were 0.15 M:0.01M, 0.10 M:0.01M and 0.05 M:0.01M, respectively, and 100 mL of each solution was used as the electrolyte in each electrodeposition process. Platinum wire (ALS, Japan), Ag/AgCl/saturated KCl electrode (ALS, Japan) and the cleaned NF substrate were used as the counter electrode, reference electrode and working electrode, respectively. Based on the preliminary experiments, the electrodeposition was performed at room temperature using the UPED method at a constant potential of -1.0 V, pulse durations of on-time and off-time of 1.0 s, and pulse cycles of 500 in this study [23]. The obtained sample was thoroughly rinsed with distilled water, vacuum-dried at 100 °C overnight, and finally calcined at 350 °C in a muffle furnace for 2 h with a heating a rate of 5 °C/min. As such, the obtained Co-Ce mixed oxide coated NF samples were labeled as 15Co-Ce/NF, 10Co-Ce/NF and 5Co-Ce/NF, respectively. For comparison, pure Co₃O₄ coated NF (Co₃O₄/NF) was also prepared using the same method with the initial solution of 0.10 M Co (NO₃)₂·6H₂O. The loading amounts of the metal oxides on NF were summarized in **Table 3.1**, in which the loading amounts (weight percentage, wt%) of Co-Ce oxides on NF support were increased from 3.36 to 5.69 wt% with the

gradual rising of Co/Ce molar ratio from 5:1 to 15:1. In addition, for the 10Co-Ce/NF catalysts prepared at the pulse cycles of 1000 and 1500, the loading amounts were around 9.38 and 11.38 wt%, respectively.

Table 3.1 Loading amounts of catalysts on NF.

Sample	Pulse cycles	Loading amount (wt%)
5Co-Ce/NF	500	3.36
10Co-Ce/NF	500	5.27
15Co-Ce/NF	500	5.69
Co ₃ O ₄ /NF	500	4.19
10Co-Ce/NF	1000	9.34
10Co-Ce/NF	1500	11.38

The weight percentage (wt%) of loaded metal oxides.

3.2.3 Characterizations

Morphology was observed on a scanning electron microscopy (SEM) (Hitachi SU8010, Japan), and meanwhile, the surface elemental compositions of the corresponding catalyst on NF was quantified by X-ray spectrometry (EDX) (Horiba EMAX). Crystalline structure was analyzed by XRD (Rigaku Smartlab, Japan) with Cu-K α radiation ($\lambda=0.15418$ nm) in a range of 10°-90° with a scanning speed of 2° min⁻¹. Transmission electron microscopy (TEM) analysis was performed using a JEM-2100F TEM JEOL operating at 200 kV. X-ray photoelectron spectroscopy (XPS, Thermo-Scientific ESCALab250i) equipped with Al-K α radiation (K α =1486.6 eV) was used to analyze the surface chemical composition and elemental valence states, in which the C1s peak was fixed at the binding energy of 284.6 eV. Hydrogen temperature-programmed reduction (H₂-TPR) and oxygen temperature-programmed desorption (O₂-TPD) were carried out on a BELCAT catalyst analyzer with a thermal conductivity detector (TCD). In each procedure, 50 mg catalyst was loaded into a U-shaped tube, which was pretreated firstly at 300 °C for 30 min with a He flow (50 cm³/min) and cooled down to room temperature (RT). Thereafter, the temperature was raised from RT to 900 °C with a heating rate of 10 °C/min under a gas flow of 5 vol% H₂/Ar (50 cm³/min). For O₂-TPD

analysis, 100 mg of sample was pretreated with He flow ($50 \text{ cm}^3/\text{min}$) for 1 h in order to remove surface water. After cooling down to RT, the sample was treated by O_2 flow ($50 \text{ cm}^3/\text{min}$) and purged by He flow ($50 \text{ cm}^3/\text{min}$) for 1 h, successively. Finally, the sample was heated from RT to 900°C at a rate of $10^\circ\text{C}/\text{min}$ for the analysis.

3.2.4 Catalytic activity test

Performance of the prepared catalysts in the toluene oxidation was carried out in a fixed bed operated in a continuous flow at atmospheric pressure. Briefly, the prepared catalyst was cut into pieces with a size of smaller than $3 \times 3 \text{ mm}^2$ at first. 0.1 g of catalyst and 0.3 g of silica sand (40~60 mesh) were mixed and transferred into a Pyrex reaction tube (i.d.=10 mm) with quartz wools packed at both ends of the catalyst bed. Before the reaction, the catalysts were pretreated in a nitrogen flow at 100°C for 1.5 h. Subsequently, in a testing temperature range of $160\text{--}370^\circ\text{C}$, the performance of catalysts was evaluated in a stream of mixed gas of a toluene (900 ppm), oxygen (O_2 , 20 vol%), nitrogen (N_2 , 80 vol% as balance), and the total flow rate was maintained at $50 \text{ cm}^3/\text{min}$ (at the standard temperature and pressure). For the best catalyst, its performances at different weight hourly space velocities (WHSVs) and different gaseous hourly space velocities (GHSVs) were also evaluated, in which different WHSVs with the different catalyst weights of 50 (WHSV= $60,000 \text{ mL g}^{-1} \text{ h}^{-1}$) and 150 mg (WHSV= $20,000 \text{ mL g}^{-1} \text{ h}^{-1}$), respectively, were used. Meanwhile, the experiments at different GHSVs by fixing the catalyst weight to 100 mg and increasing the total flow rate to 100 (GHSV= $60,000 \text{ mL g}^{-1} \text{ h}^{-1}$) and 140 mL (WGHSV= $84,000 \text{ mL g}^{-1} \text{ h}^{-1}$) respectively were also carried out. In addition, the water resistance performance of the best catalyst was examined by adding 5.0 vol% of water vapor to the above described gas mixture by passing the feed stream through a saturated water bubbler. The inlet and outlet concentrations of toluene were analyzed by an on-line gas chromatograph (Shimadzu-2014) equipped with a flame ionization detector (FID), and meanwhile, the reaction products were also analyzed by a FTIR gas analyzer (Horiba, FG-120). Toluene conversion and CO_2 selectivity were calculated by Eqs. (3.1) and (3.2), respectively:

$$X_{\text{Conversion}} = \frac{C_{\text{Inlet}} - C_{\text{Outlet}}}{C_{\text{Inlet}}} \times 100\% \quad (3.1)$$

$$\text{CO}_2 \text{ selectivity} = \frac{C_{\text{CO}_2}}{7(C_{\text{Inlet}} - C_{\text{Outlet}})} \times 100\% \quad (3.2)$$

where C_{Inlet} and C_{Outlet} are concentrations of toluene at the inlet and outlet of the reactor, respectively; C_{CO_2} is the concentration of the produced CO_2 in the off gas tested by FTIR online. In this work, the carbon balances of all experiments were closed with errors lower than 5%.

3.3 Results and discussion

3.3.1 SEM analysis

Fig. 3.1 shows SEM images of the prepared various catalysts. It can be seen that the electrodeposited pure Co_3O_4 had a dense nanosheet structure (**Fig. 3.1(a)**). With the incorporation of Ce in the catalysts, the thickness of the sheet of the obtained Co-Ce mixed oxide became thinner (**Figs.(b)-(d)**). EDX analysis results (**Table 3.2**) indicate that the best coverage of NF by the mixed oxide was achieved in the case of 10Co-Ce/NF (**Fig. (c)**) since the detected amount of Ni element on it was the lowest. However, as more Ce species was added, uneven clusters were formed with serious aggregation, and some areas of NF were not covered by the catalysts (**Fig. (d)**). EDX analysis results (**Table 3.2**) also indicate that the amount of Ni detected by EDX increased as the Co/Ce molar ratio was decreased below 10:1, and 5Co-Ce/NF showed a much higher relative weight percentage (wt %) of nickel element on the surface. It can be concluded that the morphology of the Co-Ce mixed oxide catalyst was significantly influenced by the composition of initial solution, and in the case of 10Co-Ce/NF, the best coverage property was obtained among the all prepared catalyst in this study. As shown in **Table 3.2**, the relative amount of Co increased with the increasing of molar ratio of Co/Ce in the initial preparation solution, and in contrast, the content of Ce become lower. Additionally, Co/Ce molar ratio tested by XPS also had a similar trend as the EDX analysis results.

SEM image of the surface and EDX analysis results of the spent 10Co-Ce/NF catalyst for the catalytic oxidation of toluene are depicted in **Fig. 3.2**. After a long-term reaction, the morphology of the catalyst remained almost the same as the fresh one, meanwhile, as summarized in **Table 3.2**, the

molar ratios of Co/Ce from the EDX and XPS analyses did not change significantly when compared with the fresh one, suggesting that the obtained Co-Ce/NF catalyst performed excellent structure stability, which in turn led to the stable activity during the oxidation process.

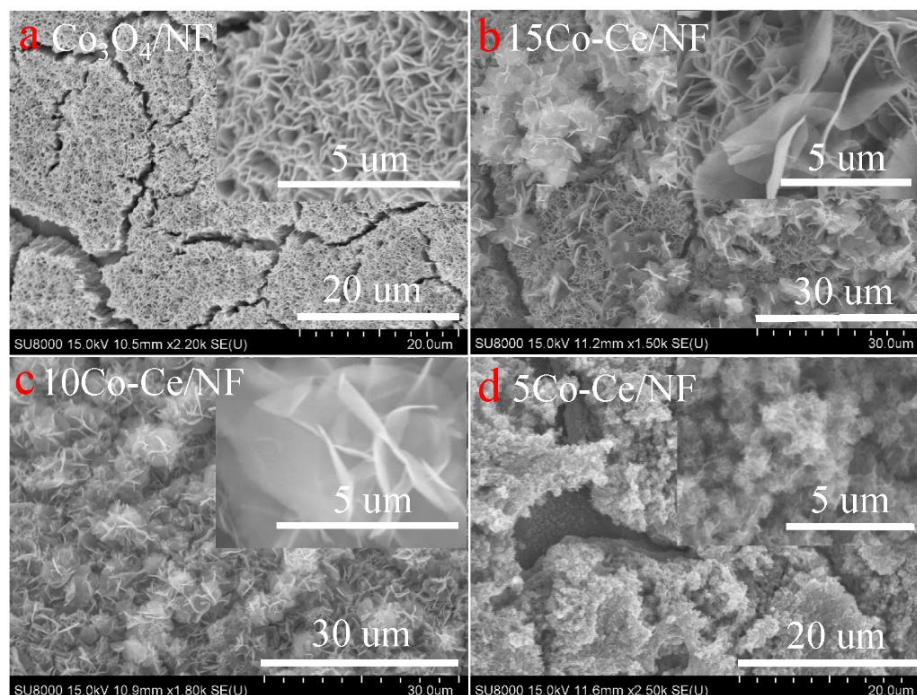


Fig. 3.1. SEM images of the surfaces of various Co-Ce/NF catalysts (Insets: the enlarged ones).

Table 3.2 Elemental compositions on the surfaces of Co-Ce/NF catalysts prepared with different initial molar ratios of Co/Ce.

Sample	Molar ratio of Co/Ce in initial solution	O (wt %)	Co (wt %)	Ce (wt %)	Ni (wt %)	Molar ratio of Co/Ce ^a	Molar ratio of Co/Ce ^b
5Co-Ce/NF	5:1	15.7	54.8	12.2	17.4	10.7:1	3.9:1
10Co-Ce/NF	10:1	36.7	57.1	5.1	1.1	26.6:1	14.7:1
15Co-Ce/NF	15:1	12.6	80.7	3.3	3.5	58.1:1	40.6:1
Co ₃ O ₄ /NF	-	28.9	66.8	-	4.3	-	-
Spent 10Co-Ce/NF	10:1	30.3	53.8	8.0	7.8	16.0:1	8.2:1

The weight percent (wt%) of O, Co, Ce and Ni are taken by EDX analyses;

^a data taken by EDX analyses;

^b data taken by XPS analyses.

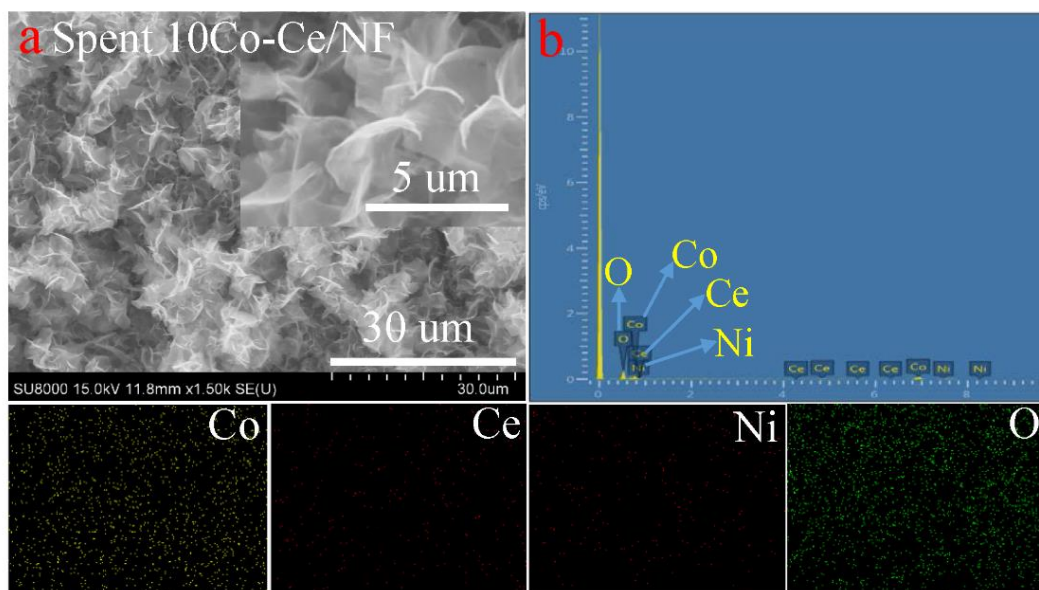


Fig. 3.2. SEM image (a) and EDX analysis (b) of the spent 10Co-Ce/NF catalysts (Inset: the enlarged image).

3.3.2 XRD analysis

Fig. 3.3 shows XRD patterns of the prepared catalysts. For pure cobalt oxide supported catalyst of $\text{Co}_3\text{O}_4/\text{NF}$, four specific diffraction peaks observed at 31.76° , 37.37° , 59.81° and 65.41° of 2θ were attributed to characteristic facets of (220), (311), (511) and (440) of Co_3O_4 crystal (JCDs-42-1467). With the decrease in the molar ratio of Co/Ce, the diffraction peaks related to Co_3O_4 became weak. The peaks corresponding to Ce species were not identified in the XRD patterns for all the samples. However, its doping improved the distribution of the deposited metal oxide species. It can be seen that the widths of the Co_3O_4 diffraction peaks in Co-Ce/NF catalysts were smaller than those of the pure $\text{Co}_3\text{O}_4/\text{NF}$ catalyst, and those intensities got weaker with the decreasing of Co/Ce molar ratio in the initial solution from 15/1 to 5/1. These results reveal that the incorporation of Ce was beneficial to improve the distribution of Co species on NF. Additionally, no finding of diffraction peaks related to Ce species could be caused by its low contents (shown in **Table 3.2**).

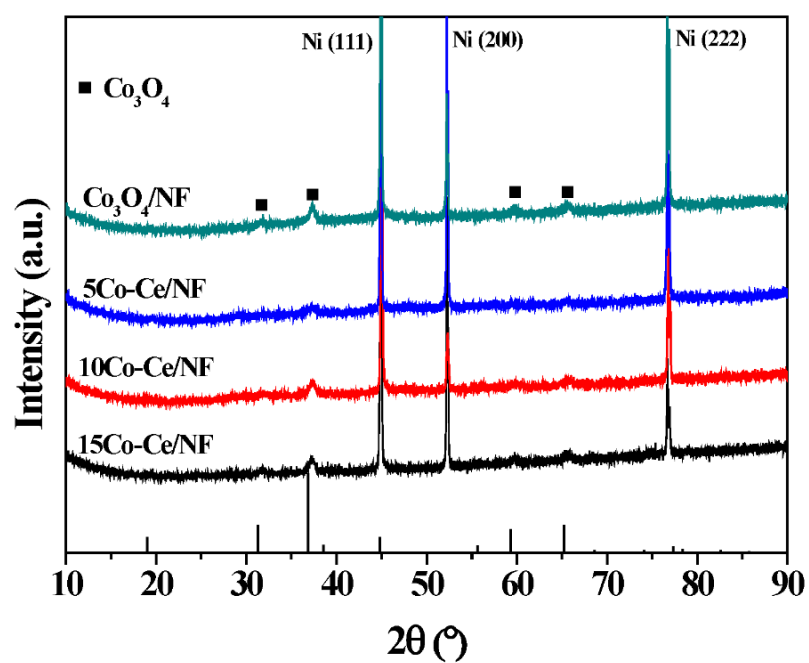
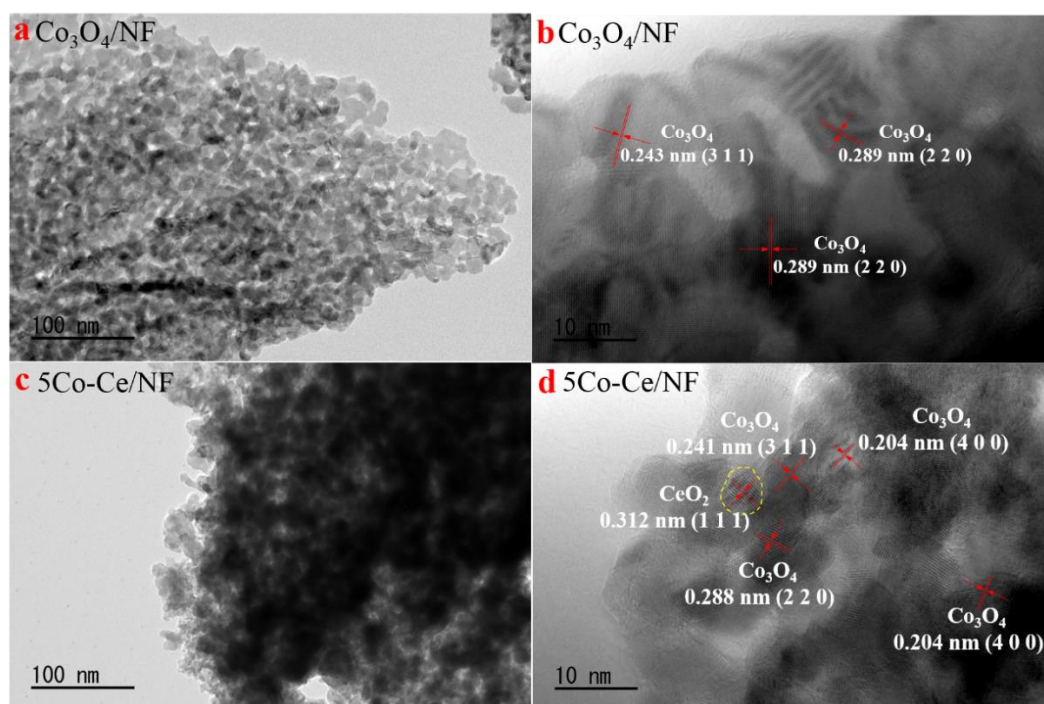


Fig. 3.3. XRD patterns of as-prepared Co-Ce/NF catalysts.



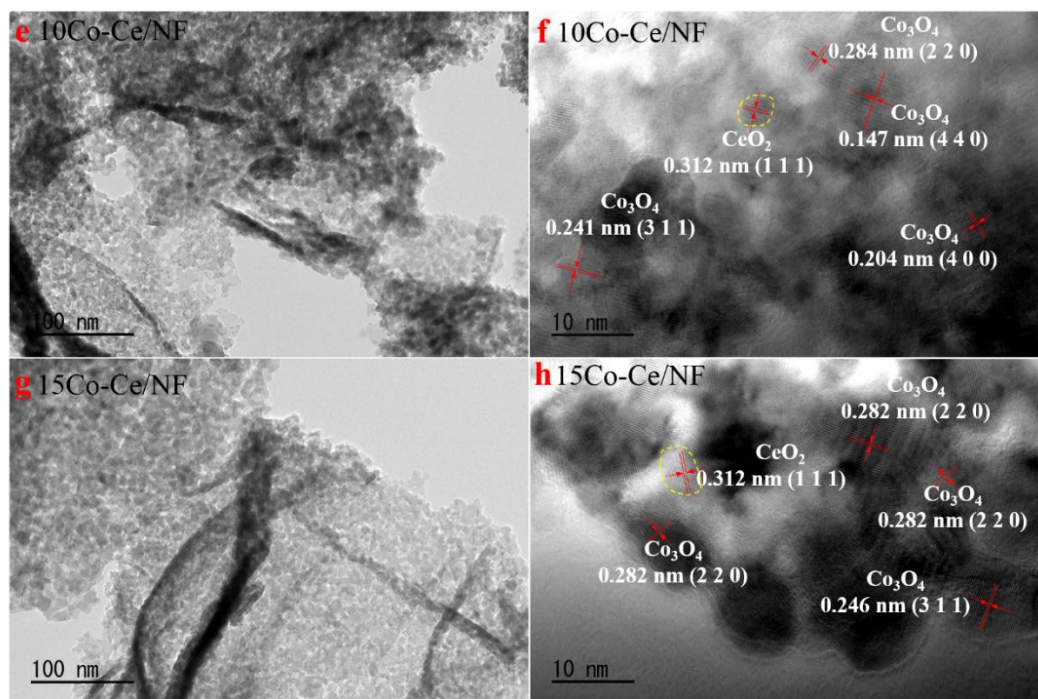


Fig. 3.4. TEM and HRTEM images of $\text{Co}_3\text{O}_4/\text{NF}$ catalyst (a, b), $5\text{Co-Ce}/\text{NF}$ catalyst(c, d), $10\text{Co-Ce}/\text{NF}$ catalyst (e, f) and $15\text{Co-Ce}/\text{NF}$ catalyst (g, h).

3.3.3 TEM analysis

Fig. 3.4 shows TEM and HRTEM images of $\text{Co}_3\text{O}_4/\text{NF}$ (a, b), $5\text{Co-Ce}/\text{NF}$ (c, d), $10\text{Co-Ce}/\text{NF}$ (e, f) and $15\text{Co-Ce}/\text{NF}$ catalysts (g, h). The well-defined crystalline structures with the fringe spacings of 0.243 and 0.289 nm assignable to the (311) and (220) lattice planes of Co_3O_4 phase respectively were observed on the HRTEM images for all the catalysts, which were corresponding well to the fact that Co_3O_4 was detected by the XRD analysis. In the HRTEM images of $5\text{Co-Ce}/\text{NF}$, $10\text{Co-Ce}/\text{NF}$ and $15\text{Co-Ce}/\text{NF}$ ((**Fig. 3.4 (d), (f) and (h)**)), two kinds of lattice fringes, i.e., one with the spacing of 0.204 nm corresponding to the (400) crystal plane of Co_3O_4 phase and the other one with 0.312 nm related to the (111) crystal plane of CeO_2 , were additionally observed. An interplanar spacing of 0.147 nm corresponding to the (440) lattice plane of Co_3O_4 phase was also found in **Fig. 3.4 (f)** for $10\text{Co-Ce}/\text{NF}$. The observation of the (111) plane of CeO_2 suggests that most of Ce species were existing as the crystalline CeO_2 . The diameter of these observed crystallites were approximately 5 nm for both Co_3O_4 and CeO_2 in $\text{Co-Ce}/\text{NF}$ catalysts, indicating that nanosized metal oxide particles were successfully deposited on NF substrate by using the current electrodeposition method.

Moreover, the intimate contact between Co_3O_4 and CeO_2 crystals was observed especially in **Fig. 3.4 (d)**, which is important for realizing synergetic effects on improving the catalytic activity. Therefore, it is concluded that the electrodeposition method applied in this work is not only facile but also appropriate to produce nanosized mixed metal oxide catalysts with intimate contacts.

3.3.4 H_2 -TPR analysis

H_2 -TPR analyses were performed for all Co-Ce/NF samples in order to investigate their reducibility and the obtained profiles are shown in **Fig. 3.5**. It is demonstrating that all samples showed the reduction peaks in the temperature range of 200-500 °C, corresponding to a two-step reduction process, in which both Co and Ce species can be reduced [24, 25]. For pure Co_3O_4 profile, the first reduction peak at low temperature range of 150-315 °C should be attributed to the reduction of Co^{3+} to Co^{2+} while the second shoulder peak at a relatively higher temperature range around 315-450 °C can be assigned to the reduction of Co^{2+} to Co, respectively [26]. The TPR profiles of all Co-Ce/NF samples were similar to that of pure Co_3O_4 , but their reduction peaks shifted to lower temperatures after doping Ce, indicating that Ce doping improved the reducibility of the supported Co-Ce mixed metal oxides. This result is consistent with the reported in the literature [27]. Notably, a flat peak was observed at high temperature around 445.5 °C only for 5Co-Ce/NF. It is probably assigned to the reduction of Ce^{4+} to Ce^{3+} . Observation of this peak separately from the reduction peaks of Co species suggests that some of Ce species deposited separately from Co species on this catalyst. This might be the reason why 5Co-Ce/NF exhibited poor catalytic activity as described below. Nevertheless, one can see that narrow overlapping peaks appeared at high temperature range of 300-500 °C in the H_2 -TPR profiles for 15Co-Ce/NF and 10Co-Ce/NF samples, which might be resulted from the reduction of different valence states of Co-Ce mixed metal oxides [28]. Furthermore, the reduction peaks located at 349.8 and 355.6 °C corresponding to Ce species in these two catalysts shifted to lower temperature direction when compared with 5Co-Ce/NF catalyst, indicating that the reducibility of Ce species in the catalysts was also improved by the closely contacted Co species during the reduction process. As indicated above, the intimate contact between

Co_3O_4 and CeO_2 displayed in the TEM images could be the main reason for the improved reducibility on the Co-Ce/NF catalysts.

In addition, the XRD results also demonstrated that Ce doping enhanced the distribution of Co species on NF, which is also associated with the better reducibility of the catalysts since the smaller particles of metal oxides are more easily reduced [29]. Furthermore, it should be noted that the initial reduction peaks of Co-Ce/NF catalysts not only shifted to lower temperatures, but also became wider, suggesting that more surface adsorbed oxygen species were generated on the catalysts by the incorporation of Ce [30]. In particular, compared with the pure Co_3O_4 /NF and other Co-Ce/NF catalysts, for the 10Co-Ce/NF, the first reduction peak appeared at the lowest temperature of 287.8 °C with the largest reduction peak area corresponding to the H_2 -consumption (**Table 3.3**), indicating that the largest amount of reducible species were generated by the doping of cerium in this case. Additionally, comparing with other catalysts, the experimental amount of H_2 -consumption for the 10Co-Ce/NF catalyst was only a little higher than the theoretical amount, indicating that the Co species within the 10Co-Ce/NF catalyst was easier to be reduced [25]. Moreover, with the incorporation of Ce, the reduction peak area (at around 336 °C) corresponding to the second reduction peak also increased for the Co-Ce/NF catalysts. However, as over doping of Ce (e.g., 5Co-Ce/NF) resulted in the decrease of the intensity of this peak. Therefore, only a suitable Ce doping amount can produce more easily reducible species. He *et al.* reported that low-temperature reducibility should be favorable to the good catalytic oxidation since it means that oxygen species in the catalyst can be more easily activated or migrate to the catalyst surface [31]. As such, in this study, the 10Co-Ce/NF catalyst could have higher activity for the VOCs oxidation.

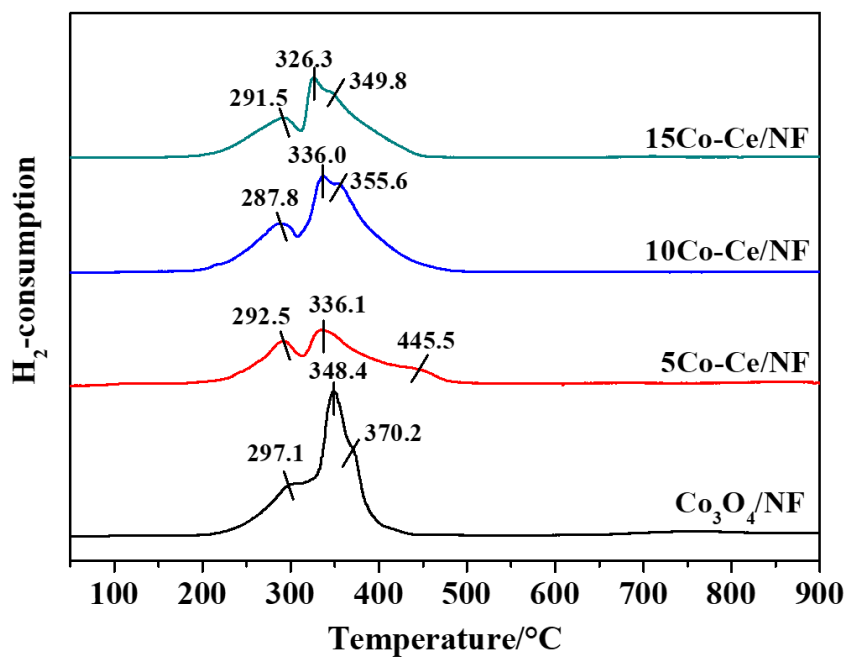


Fig. 3.5. H₂-TPR profiles of Co-Ce/NF catalysts.

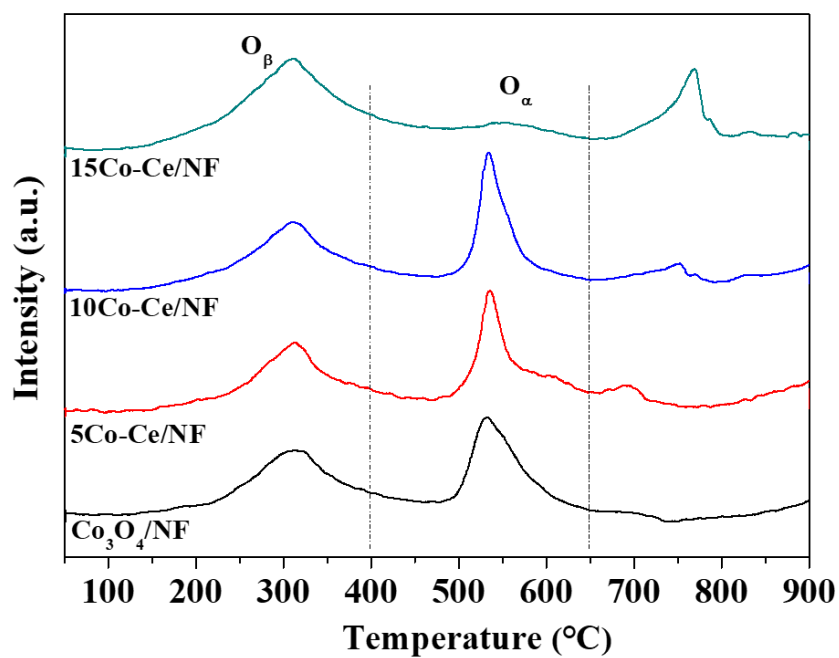


Fig. 3.6. O₂-TPD profiles of Co-Ce/NF catalysts.

Table 3.3 Hydrogen consumption and O₂ desorption of Co-Ce/NF catalysts.

Sample	T ₁ /°C	H ₂ -uptake (mmol/g)	T ₂ /°C	H ₂ -uptake (mmol/g)	Experimental H ₂ -uptake (mmol/g)	Theoretical H ₂ -uptake (mmol/g) ^a	O _β desorption (mmol/g)	O _α desorption (mmol/g)
5Co-Ce/NF	292.5	0.152	> 336.1	0.285	0.437	0.522	0.056	0.064
10Co-Ce/NF	287.8	0.276	> 336.0	0.620	0.896	0.854	0.086	0.073
15Co-Ce/NF	291.5	0.223	> 326.3	0.449	0.682	0.928	0.072	0.008
Co ₃ O ₄ /NF	297.1	0.229	> 348.4	0.704	0.633	0.695	0.048	0.045

^a, Theoretical H₂-uptake based on the consumption of Co₃O₄ in the catalysts.

Table 3.4 Surface elemental compositions of Co-Ce/NF catalysts.

Catalyst	Area ratio of Co 2p	Area ratio of O 1s	Area ratio of Ce 3d
	Co ³⁺ /Co ²⁺	O _{sur} /O _{latt}	Ce ³⁺ /(Ce ³⁺ +Ce ⁴⁺)
5Co-Ce/NF	1.296	0.649	0.255
10Co-Ce/NF	1.517	0.796	0.342
15Co-Ce/NF	1.325	0.702	0.338
Co ₃ O ₄ /NF	1.385	0.796	-
Spent 10Co-Ce/NF	1.350	0.682	0.362

3.3.5 O₂-TPD analysis

The type and mobility of oxygen species over the prepared catalysts were investigated by O₂-TPD. In **Fig. 3.6**, the profiles can be separated into three regions: the peaks located at low temperatures (<400 °C) were assigned to the desorption of the surface adsorbed oxygen species (O_β), the peaks concentrated at medium temperatures (400~650 °C) can be contributed to the evolution of surface/subsurface lattice oxygen (O_α) and the peaks at high temperatures (> 650 °C) correspond to the desorption of bulk lattice oxygen from the Co-Ce mixed oxides, respectively [32]. For the O₂-TPD profiles of the prepared Co-Ce/NF catalysts, it can be seen that the intensity of peaks corresponding to O_β increased with the increasing of Co/Ce molar ratio in the initial solution from 5:1 to 15:1. As summarized in **Table 3.3**, the amount of O_β followed the increased order of Co₃O₄/NF < 5Co-Ce/NF < 15Co-Ce/NF < 10Co-Ce/NF. Therefore, the 10Co-Ce/NF catalyst had the maximum amount of surface adsorbed oxygen species at low temperature range. It reveals that Ce doping improved the generation of surface oxygen species at low temperatures, which is consistent with the H₂-TPR result. Notably, the amount of surface adsorbed oxygen species is related to the oxygen vacancies, and as a result, more oxygen vacancies were generated on the catalysts by doping Ce [33]. Additionally, it can be seen from **Fig. 3.6** that the obvious peaks related to the lattice oxygen species of O_α at middle temperature range were observed for Co₃O₄/NF, 5Co-Ce/NF and 10Co-Ce/NF catalysts. Meanwhile, for the 15Co-Ce/NF catalyst, the intensity of this peak was significantly decreased with the increase of another peak intensity at high temperatures (> 650 °C) contributable to the desorption of bulk lattice oxygen species. It is reported that the lattice oxygen species derived from the lattice defects are benefit to generate oxygen vacancies and improve the oxygen mobility of the catalysts [34]. As such, more oxygen vacancies generated by lattice oxygen species at relatively low temperature range for the 10Co-Ce/NF catalyst should be helpful to enhance its reducibility. As stated above, the H₂-TPR result for the 10Co-Ce/NF catalyst also exhibited the best reducibility among all the prepared samples, which might also contribute to the increased lattice oxygen species, promoting the active oxygen species easily transferred from the bulk to the surface.

As shown in **Table 3.3**, the amounts of O_a for the 5Co-Ce/NF and 10Co-Ce/NF catalysts were 0.064 and 0.073 mmol/g, respectively, which were higher than that of Co_3O_4 /NF catalyst. Therefore, Ce doping enhanced the formation of both surface oxygen species and lattice oxygen species at relatively low temperature since the Ce species possesses excellent ability to store and release oxygen. Additionally, it is reported that active oxygen species could be efficiently transferred from gas-phase oxygen through the existed oxygen vacancies and participate in the reaction, and finally lead to the good catalytic activity during the VOCs oxidation [35].

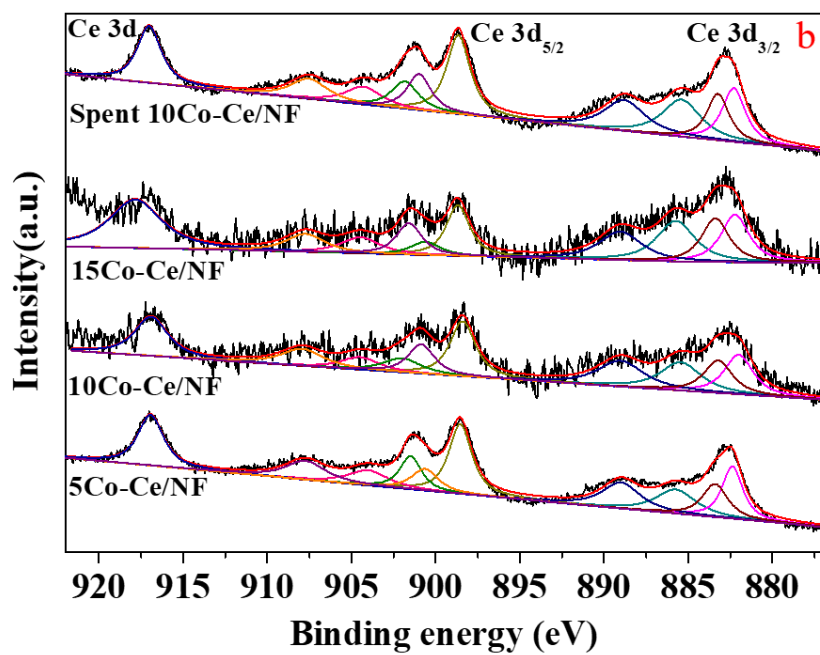
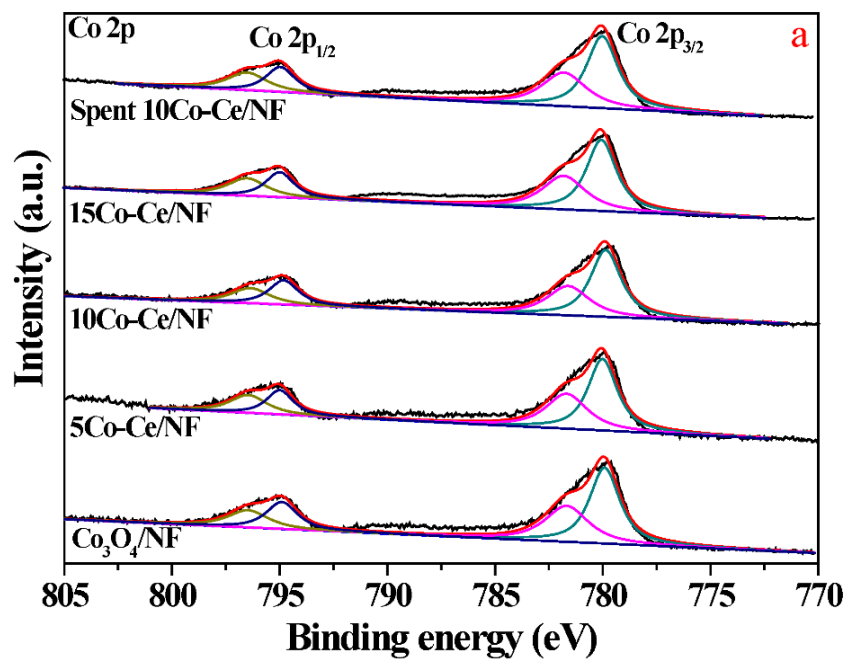
3.3.6 XPS analysis

Surface chemical compositions and elemental valence states of the prepared catalysts were determined by XPS analyses. The results related to Co 2p, O 1s and Ce 3d are shown in **Fig. 3.7**, and the corresponding calculated results are summarized in **Table 3.4**. For Co 2p XPS spectrum (**Fig. 3.7a**), it can be fitted by two components of Co 2p_{3/2} and Co 2p_{1/2} [36]. Herein, the principal peak in Co 2p_{3/2} spectrum centered at around 780.0 eV is ascribed to the surface Co^{3+} while that at the binding energy of 781.7 eV belongs to the surface Co^{2+} [29]. Meanwhile, the peaks in the Co 2p_{1/2} spectrum at the binding energies of 794.9 eV and 796.5 can be also assigned to Co^{3+} and Co^{2+} , respectively. As summarized in **Table 3.4**, the molar ratio of Co^{3+}/Co^{2+} increased in the sequence of 5Co-Ce/NF < 15Co-Ce/NF < Co_3O_4 /NF < 10Co-Ce/NF. It is reported that the exposed surface Co^{3+} should be the active species, which can improve the catalytic oxidation performance [37,38]. Therefore, the high Co^{3+}/Co^{2+} molar ratio in the 10Co-Ce/NF catalyst could perform higher catalytic activity than others.

In the Ce 3d spectra of all prepared samples (**Fig. 3.7b**), the peaks at the binding energies of 883.4, 888.9, 898.5, 900.6, 907.7 and 916.9 eV are attributed to Ce^{4+} while the other four at 882.3, 885.7, 901.4 and 904.0 eV are assigned to Ce^{3+} [39]. It indicates that the main chemical valence of Ce species for the Co-Ce mixed oxides in this study was Ce^{4+} , which is consistent with the results reported by Ma *et al.* [40]. It is reported that Ce^{3+} could be regarded as the representative of oxygen vacancies in CeO_2 , which is benefit for the catalytic oxidation of VOCs [41,42]. Therefore, as

demonstrated by H₂-TPR and O₂-TPD results, the Ce doping promoted the formation of oxygen vacancies, resulting in more amount of surface and lattice oxygen species generated on Co-Ce/NF catalysts at relatively low temperature, which played an important role in the improved reducibility and oxygen mobility of the catalyst. Consequently, the existence of the redox couples of Ce⁴⁺/Ce³⁺ should be beneficial to the oxygen storage and release, and therefore enhancing the catalytic oxidation performance in this study [27]. Besides, when compared with the pure Co₃O₄/NF sample, the relative content of Co³⁺ active species in the 10Co-Ce/NF catalyst also increased after the Ce doping, indicating that Ce species promoted more Co³⁺ active species formed. The data summarized in **Table 3.4** illustrate that the relative area ratio of Ce³⁺/(Ce³⁺+Ce⁴⁺) in the spent 10Co-Ce/NF catalyst was only slightly higher than that in the fresh one. Meanwhile, from the SEM images shown in **Figs. 3.1c** and **3.2**, one can also see that no obvious change occurred on the Co-Ce/NF catalyst after a long-time oxidation process, indicating the good stability of the catalyst.

Fig. 3.7c displays the asymmetrical O 1s spectra, in which the peak at the low binding energy of about 529.8 eV can be assigned to the lattice oxygen O²⁻ (O_{lat}) in the fresh catalyst, the resolved peak centered at the medium binding energy in the range of 529.8-530.4 eV is contributed by hydroxyl oxygen in OH⁻, and that at the high binding energy of 531.6 eV corresponds to the surface adsorption oxygen species O₂⁻, O⁻ or O₂²⁻ (O_{sur}) [43,44]. As summarized in **Table 3.4**, the ratio of surface oxygen to lattice oxygen on the 10Co-Ce/NF catalyst was the highest. Meanwhile, as indicated by H₂-TPR results, the 10Co-Ce/NF catalyst had the best reducibility among all the catalysts. That is to say, more surface oxygen species should be beneficial to the reducibility of the catalyst. Moreover, it is reported that the oxygen species of both O_{sur} and O_{lat} are conducive to the catalytic oxidation reaction [45]. Thus, rich in the active oxygen species of Co-Ce/NF catalyst could improve the catalytic performance as confirmed below.



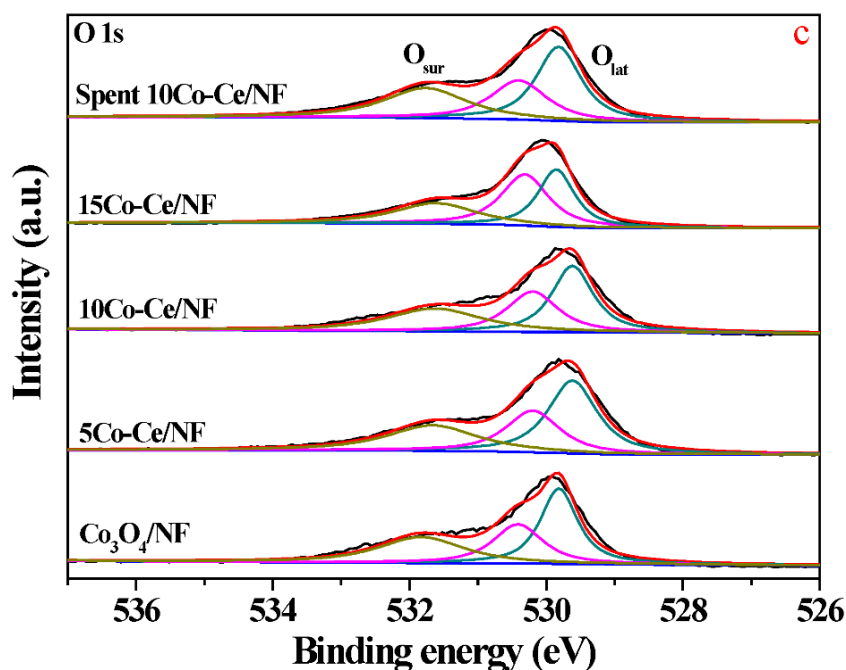


Fig. 3.7. XPS spectra of Co-Ce/NF catalysts: Co 2p (a), Ce 3d (b) and O 1s (c).

3.3.7 Catalytic activity

The catalytic activities of NF and Co-Ce/NF catalysts for the catalytic oxidation of toluene were evaluated in a conventional fixed bed reactor with a testing temperature range of 160-370 °C. **Fig. 3.8** displays the catalytic activity of NF substrate, and toluene was completely converted into CO₂ and H₂O until temperature was increased to 420 °C. Curves in **Fig. 3.9a** show the catalytic activity of the supported catalysts, indicating that the toluene conversion over the pure Co₃O₄/NF catalyst was increased with the increasing of temperature. Herein, toluene was started to be converted at 253 °C and completely oxidized at 296 °C. For comparison, for the mixed metal oxide catalyst of 10Co-Ce/NF, the complete oxidation temperature decreased to 268 °C. Moreover, the selectivity towards CO₂ was quite close to 100%, and the error between the actual and ideal CO₂ concentrations was only 0.4% (**Table 3.5**). Herein, the lower oxidation temperature represents the better catalytic performance. Thus, it can be concluded that the catalytic performance was improved by Ce doping since it enhanced the low-temperature reducibility, and simultaneously increased the amount of active oxygen species and Co³⁺ active species, which was confirmed by H₂-TPR, O₂-TPD and XPS results as indicated above. Moreover, as reported in the literatures [46, 47], cerium has high oxygen

storage and releasing capability, and the presence of the $\text{Ce}^{4+}/\text{Ce}^{3+}$ redox couples in the catalysts is favorable to the oxidation reaction. It can be clearly seen in **Fig. 3.9a** that all Co-Ce/NF catalysts underwent a similar reaction process, and the complete conversion temperature for toluene was obtained at a temperature below 300 °C, which was much lower than that of NF (**Fig. 3.8**), and the catalytic activity followed the order of $\text{Co}_3\text{O}_4/\text{NF} < 5\text{Co-Ce/NF} < 15\text{Co-Ce/NF} < 10\text{Co-Ce/NF}$. Therefore, in terms of toluene conversion, the most active catalyst was the 10Co-Ce/NF, which was consistent with its properties as indicated above. Moreover, as shown in **Fig. 3.9b**, the CO_2 selectivity of the prepared catalysts also showed the same increasing trend during the reaction process. Consequently, the 10Co-Ce/NF showed the optimum catalytic performance in the toluene catalytic oxidation with $T_{10\%}$, $T_{50\%}$, and $T_{100\%}$ values at 237, 259 and 268 °C (**Table 3.5**), respectively. Additionally, FT-IR analyses revealed that only CO_2 and H_2O were produced during the whole reaction process for each catalyst, indicating that toluene could be completely oxidized into harmless substances of CO_2 and H_2O over the Co-Ce/NF catalysts.

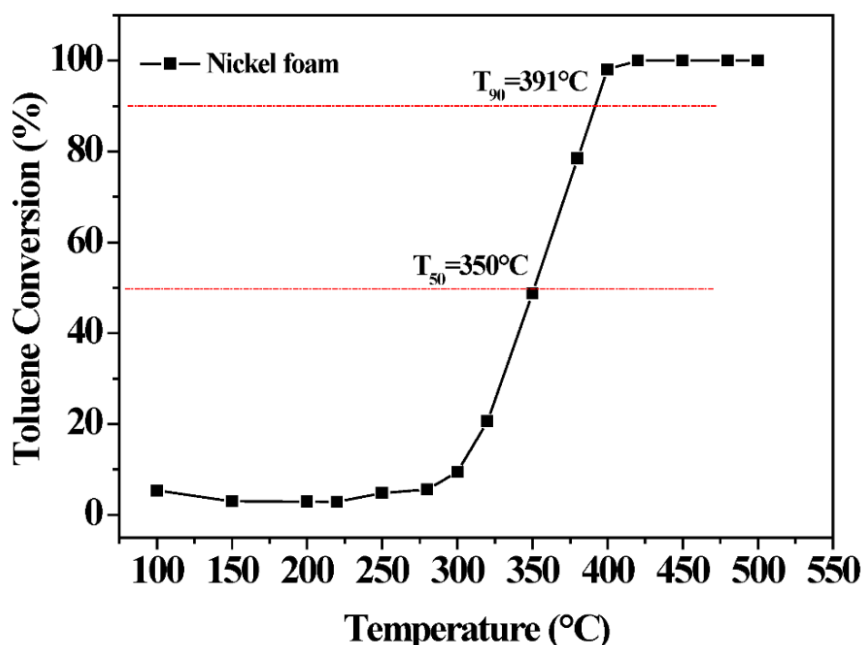


Fig. 3.8. Catalytic activity of nickel foam for the catalytic oxidation of toluene.

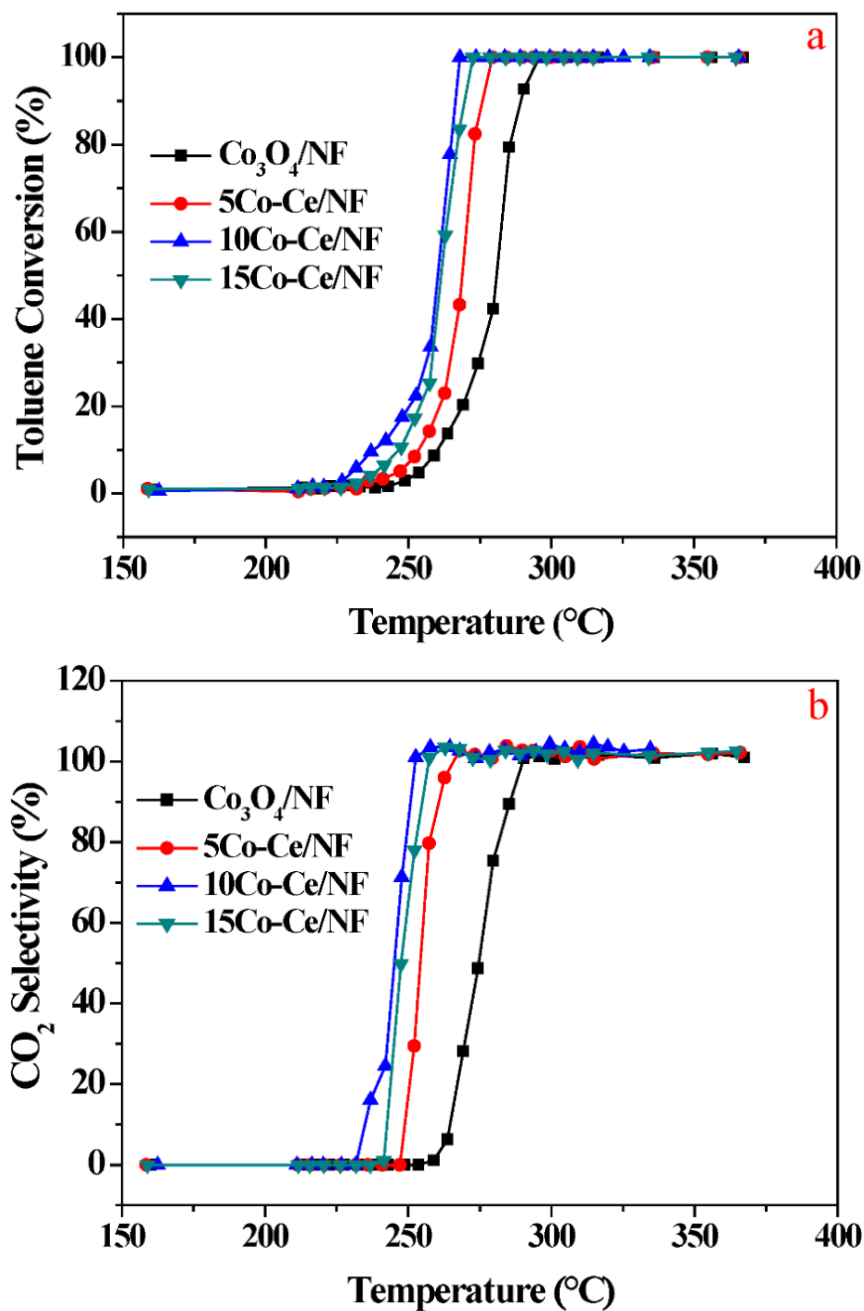


Fig. 3.9. Performances of Co-Ce/NF catalysts for the catalytic oxidation of toluene: (a) Toluene conversion; (b) CO_2 selectivity.

As indicated above, the 10Co-Ce mixed oxide on the NF possessed a uniform nanosheet structure with well elemental distribution, the intimate contact between Co_3O_4 and CeO_2 crystals, improved low-temperature reducibility and oxygen mobility, and increased surface and lattice oxygen species at low temperatures, which are conducive to the catalytic oxidation of toluene. Meanwhile, XPS results confirmed that the Ce doping promoted the generation of oxygen vacancies and Co^{3+} active

species, especially the $\text{Ce}^{4+}/\text{Ce}^{3+}$ redox couples on the 10Co-Ce/NF catalyst with the strongest ability to store and release oxygen. Consequently, the 10Co-Ce/NF catalyst achieved the best catalytic performance in the toluene catalytic oxidation among all catalysts.

Co-based catalysts for VOCs oxidation have already been widely investigated and reported. **Table 3.6** compares the performance of 10Co-Ce/NF catalyst with those reported powder-type catalysts [14] and supported Co-Ce mixed oxide catalysts [18] for the catalytic oxidation of toluene. One can see that the electrodeposited catalyst of 10Co-Ce/NF performed comparable catalytic activity as those of powder-type ones. Although some reported supported catalysts such as $\text{Co}_3\text{O}_4\text{-CeO}_2/\text{Silica-pillared clay}$ [18] also showed much better performance, the present 10Co-Ce/NF catalyst prepared by a time-saving method of electrodeposition in this work. It is more important that the nanosheet structured Co-Ce mixed metal oxide of 10Co-Ce/NF catalyst with low loading amount of 5.27 wt% was uniformly coated on NF support, and the high utilization of Co and Ce active species made this kind of catalyst have relatively low cost and could be used in a practical process. In other words, the time-saving method of electrodeposition provides a promising way to prepare highly active transition metal based catalysts for efficient VOC oxidation.

Table 3.5 Results of catalytic oxidation of toluene over Co-Ce/NF catalysts.

Catalyst	Toluene conversion ($^{\circ}\text{C}$)			Ideal CO_2 concentration ($V^{\text{a}}_{\text{CO}_2}/V_{\text{N}_2}$, %)	Actual CO_2 concentration ($V^{\text{b}}_{\text{CO}_2}/V_{\text{N}_2}$, %)	Error (%)
	$T_{10\%}$	$T_{50\%}$	$T_{100\%}$			
$\text{Co}_3\text{O}_4/\text{NF}$	260	281	296	0.786	0.770	2.1
5Co-Ce/NF	253	268	279	0.748	0.779	4.1
10Co-Ce/NF	237	259	268	0.751	0.754	0.4
15Co-Ce/NF	247	261	272	0.742	0.773	4.2

$V^{\text{a}}_{\text{CO}_2}$, the flow rate of the ideal produced CO_2 ;

$V^{\text{b}}_{\text{CO}_2}$, the flow rate of the actual produced CO_2 ;

V_{N_2} , the flow rate of N_2 as balance gas for reaction.

Table 3.6 Comparison of common Co-Ce mixed oxide catalysts for toluene catalytic oxidation reported in the literature with this work.

Catalyst	Toluene concentration	Toluene conversion (°C)		References
		T _{50%}	T _{100%}	
Co-Ce CX Co/Ce=2/1	Toluene ~266 ppmV	246	261	[14]
Co-Ce CXN Co/Ce=2/1	Toluene 1000 ppm	241	251	[14]
Co-Ce EM Co/Ce=2/1	Toluene 1000 ppm	253	265	[14]
Co ₃ O ₄ -CeO ₂ /Silica-pillared clay Co/Ce=5/1 Loading amount=15 wt%	Toluene 1000 ppm	141	~200	[18]
Co-Ce/NF with nanosheet structure Co/Ce=10/1	Toluene 900 ppm	259	268	This work

The metal ratios in the table are molar ratios; CX and CXN represent using two kinds of carbon xerogels as the templates for the catalyst preparations; EM represents the evaporation method; EX represents the exotemplating method.

3.3.8 Effect of supported Co-Ce loading amount, WHSV and GHSV

The effect of metal oxides loading amount was investigated by using the optimum catalyst of 10Co-Ce/NF prepared with different pulse cycles. As shown in **Fig. 3.10**, the toluene conversion temperatures of T_{50%} and T_{100%} over the 10Co-Ce/NF catalysts with loading amounts of 9.34 and 11.38 wt% were little higher than those with the lower loading amounts, indicating that over-loading of Co-Ce mixed oxides was not favorable for the catalytic oxidation of toluene in this work. It can be seen from **Fig. 3.11** that serious aggregation occurred on the catalyst surface, there were large metal oxides clusters formed on the surface of NF support (**Fig. 3.11 (a, b, c)**) and some of them even crashed into un-uniform bulks (**Fig. 3.11 (d, e, f)**). The high loading amounts of metal oxides might block the macropores of NF support and hinder the transmission of the involved molecules during the reaction process, and therefore led to the decrease in the catalytic activity.

In addition, the weight hourly space velocity (WHSV) and gaseous hourly space velocity (GHSV) also play an important role in the catalytic oxidation of toluene. For the effect of WHSV, it can be obviously observed in **Fig. 3.12a** that the catalytic performance was influenced by the decreasing of WHSV from 60,000 to 20,000 mL g⁻¹ h⁻¹, where the toluene complete conversion temperature increased approximately 10 °C. Similar results were also obtained for the effect of GHSV. As displayed **Fig. 3.12b**, high GHSV also needed higher conversion temperature for toluene complete conversion. Therefore, either high WHSV or high GHSV made a negative influence on the catalytic oxidation of toluene in this work, however, it should be noted that the effects were not so obvious.

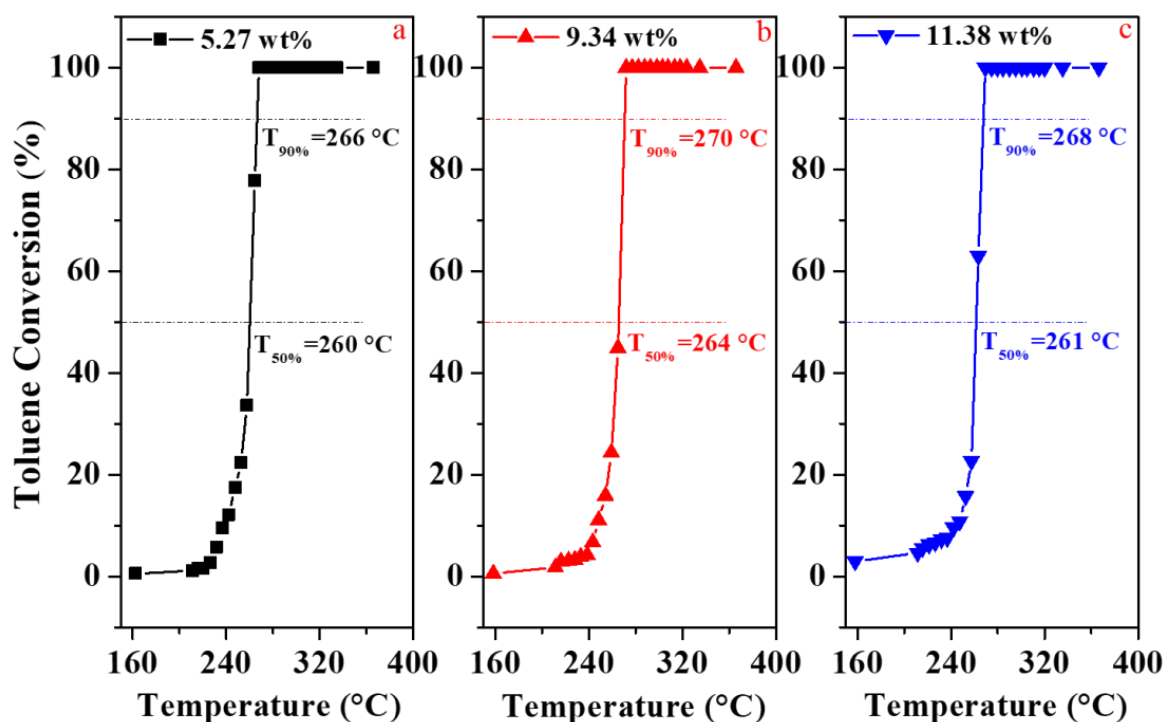


Fig. 3.10. Catalytic performance of 10Co-Ce/NF catalyst with different loading amounts prepared by different pulse cycles for the catalytic oxidation of toluene: (a) 500 cycles, (b) 1000 cycles and (c) 1500 cycles.

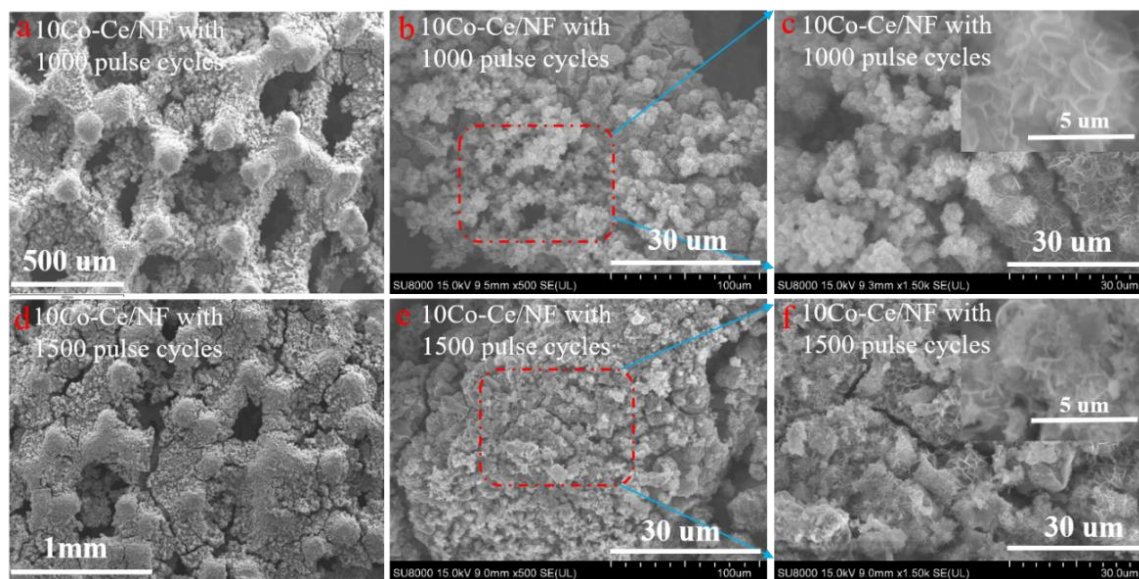


Fig. 3.11. SEM images of 10Co-Ce/NF catalysts prepared by different pulse cycles; (a, b) 1000 cycles and (c, d) 1500 cycles.

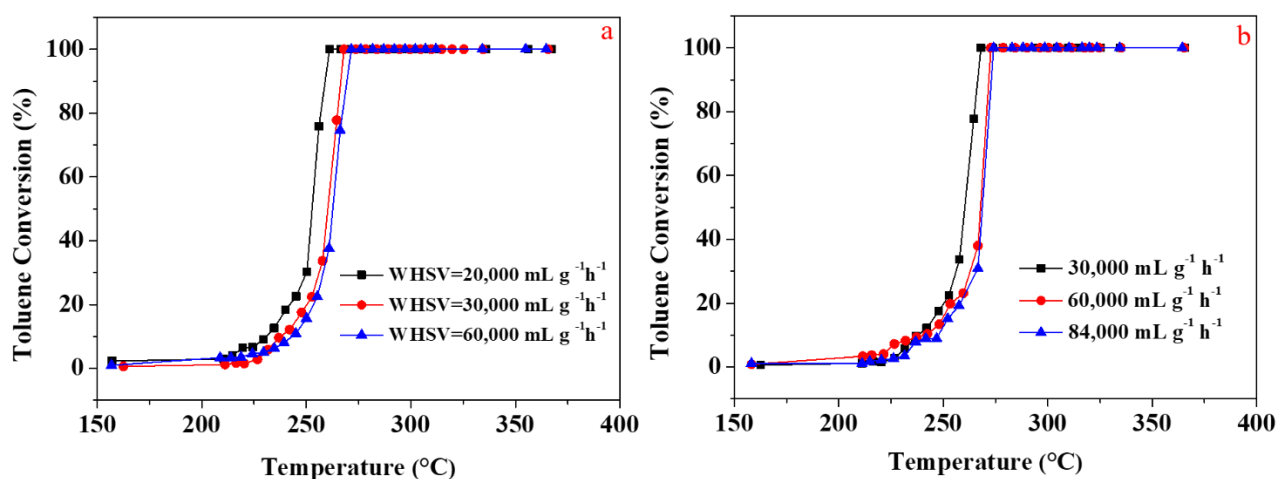


Fig. 3.12. Effects of WHSV (a) and GHSV (b) on the catalytic oxidation of toluene over 10Co-Ce/NF catalyst.

3.3.9 Effect of water in long-term stability evaluation

Generally, VOCs emissions from industry always contains water. Thus, the effect of water vapor on the toluene catalytic oxidation was also investigated. As shown in **Fig. 3.13**, there was no significant change in the catalytic performance of 10Co-Ce/NF catalyst after three rounds of the catalytic oxidation on-stream, indicating that the catalyst possessed excellent stability and reusability for the toluene catalytic oxidation in this work. Long-term on-stream stability test was conducted at a

temperature of 262 °C for more than 1500 min with a period of water vapor introduction. As shown in **Fig. 3.14**, the toluene conversion temperature maintained at 100% in the first 320 min, then, as the water vapor was introduced on the way for a period of 480 min, the conversion was decreased from 100% to 96%. Importantly, the toluene conversion was recovered to 100% after the stopping of the water vapor introduction. It indicates that the 10Co-Ce/NF catalyst did not suffer from the deactivation in the presence of water vapor. This result is coincided with the results from **Figs. 4.13** and **4.15**. Additionally, no other by-products other than CO₂ and H₂O were generated during the whole catalytic oxidation process. Therefore, it can be concluded that the 10Co-Ce/NF catalyst had superior water resistance and stability, which could be applied in practical processes.

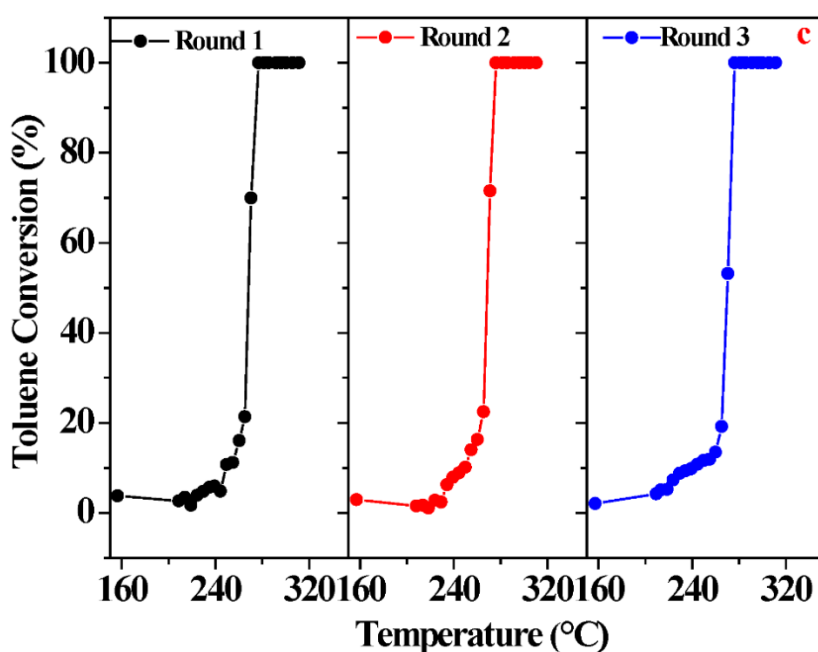


Fig. 3.13. Recycled catalytic performances of 10Co-Ce/NF catalyst on-stream for catalytic oxidation of toluene (WHSV = 30,000 mL·g⁻¹·h⁻¹, toluene concentration = 900 ppm, water vapor content = 5.0 vol%).

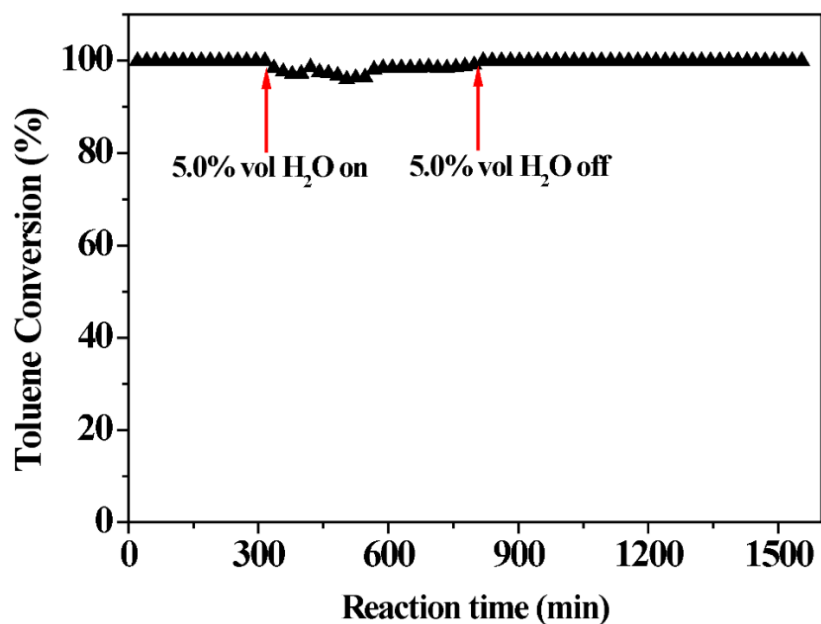


Fig. 3.14. Long time evaluation on-stream of toluene catalytic oxidation over 10Co-Ce/NF catalyst (WHSV=30,000 mL g⁻¹ h⁻¹, toluene concentration = 900 ppm, reaction temperature = 262 °C, reaction time = 1660 min).

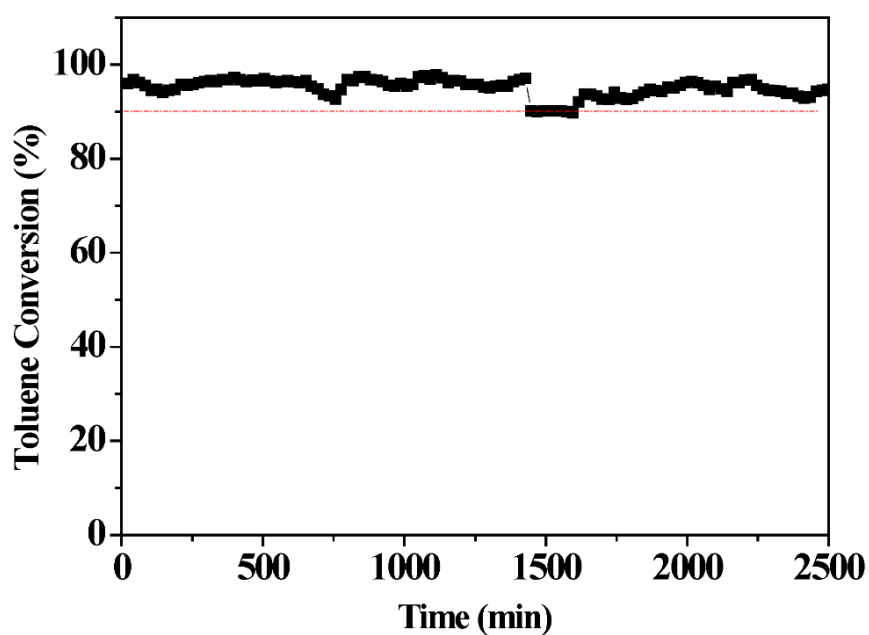


Fig. 3.15. Long-term evaluation of toluene catalytic oxidation on 10Co-Ce/NF catalyst (WHSV=30,000 mL·g⁻¹·h⁻¹, toluene concentration = 900 ppm, reaction temperature was set at 250 °C in order to maintain the conversion >90%, reaction time =2500 min).

3. 4. Conclusions

In summary, Co-Ce/NF catalysts with different Co/Ce molar ratios were prepared by the UPED method and successfully applied for the catalytic oxidation of toluene. It is found that toluene was completely combusted over these catalysts at a temperature of below 300 °C with only CO₂ and H₂O produced. The morphology of Co-Ce/NF catalyst was significantly influenced by the Co/Ce molar ratio in the initial solution for electrodeposition. When the initial molar ratio of Co/Ce was 10, the Co-Ce mixed oxide with a well nanosheet structure was uniformly deposited on the NF support. The XRD and TEM results confirmed that the incorporation of Ce improved the distribution of Co oxide particles on the NF. The intimate contact between Co₃O₄ and CeO₂ particles was found by HRTEM, which is important for realizing synergistic effects on improving catalytic activity. Moreover, as analyzed by H₂-TPR, O₂-TPD and XPS, the 10Co-Ce/NF catalyst had the excellent reducibility, rich surface and lattice active oxygen species at low temperatures, high content of Co³⁺ active species with high oxygen vacancies and Ce⁴⁺/Ce³⁺ redox couples in the catalyst, which were favorable to the catalytic oxidation of toluene. As a result, the 10Co-Ce/NF achieved the optimum catalytic performance with a complete conversion temperature of 268 °C. Recycled catalytic performance test and long-term evaluation on-stream results indicated that the 10Co-Ce/NF possessed superior water resistance and stability in the catalytic oxidation of toluene, and no obvious change occurred in the morphology and the active species of the spent catalyst when compared with the fresh one. Consequently, such an electrodeposition method should be a facile and effective way to prepare mixed metal oxides catalysts with special porous structure for efficient VOC oxidation.

References

- [1] M.S. Kamal, S.A. Razzak, M.M. Hossain, Catalytic oxidation of volatile organic compounds (VOCs) – A review, *Atmospheric Environment*. 140 (2016) 117-134.
- [2] A. Altshuller, Natural volatile organic substances and their effect on air quality in the United States, *Atmospheric Environment*. 17 (1983) 2131-2165.
- [3] R. Atkinson, Atmospheric chemistry of VOCs and NO_x, *Atmospheric Environment*. 34 (2000) 2063-2101.
- [4] R. Peng, X. Sun, S. Li, L. Chen, M. Fu, J. Wu, D. Ye, Shape effect of Pt/CeO₂ catalysts on the catalytic oxidation of toluene, *Chemical Engineering Journal*. 306 (2016) 1234-1246.
- [5] Y. Liu, J. Deng, S. Xie, Z. Wang, H. Dai, Catalytic removal of volatile organic compounds using ordered porous transition metal oxide and supported noble metal catalysts, *Chinese Journal of Catalysis*. 37 (2016) 1193-1205.
- [6] G. Zhou, H. Lan, T. Gao, H. Xie, Influence of Ce/Cu ratio on the performance of ordered mesoporous CeCu composite oxide catalysts, *Chemical Engineering Journal*. 246 (2014) 53-63.
- [7] X. Chen, X. Chen, E. Yu, S. Cai, H. Jia, J. Chen, P. Liang, In situ pyrolysis of Ce-MOF to prepare CeO₂ catalyst with obviously improved catalytic performance for toluene combustion, *Chemical Engineering Journal*. 334 (2018) 469-479.
- [8] C. He, F. Zhang, L. Yue, X. Shang, J. Chen, Z. Hao, Nanometric palladium confined in mesoporous silica as efficient catalysts for toluene oxidation at low temperature, *Applied Catalysis B-Environmental*. 111 (2012) 46-57.
- [9] A. Giroirfendler, A. Baylet, L. Retailleau, A. Boreave, G.Z. Lu, Y. Guo, Y.L. Guo, C.H. Zhang, LaMnO₃ perovskite oxides prepared by different methods for catalytic oxidation of toluene, *Applied Catalysis B-Environmental*. 148-149 (2014) 490-498.
- [10] X. Chen, S. Cai, J. Chen, W. Xu, H. Jia, J. Chen, Catalytic combustion of toluene over mesoporous Cr₂O₃-supported platinum catalysts prepared by in situ pyrolysis of MOFs, *Chemical Engineering Journal*. 334 (2018) 768-779.

- [11] C.S. Heneghan, G.J. Hutchings, S.H. Taylor, The destruction of volatile organic compounds by heterogeneous catalytic oxidation, *Catalysis*. 17 (2004) 105-151.
- [12] S.S.T. Bastos, J.J.M. Órfão, M.M.A. Freitas, M.F.R. Pereira, J.L. Figueiredo, Manganese oxide catalysts synthesized by exotemplating for the total oxidation of ethanol, *Applied Catalysis B-Environmental*. 93 (2009) 30-37.
- [13] W. B. Li, M. Zhuang, T. C. Xiao, M. L. Green, MCM-41 supported Cu-Mn catalysts for catalytic oxidation of toluene at low temperatures, *The Journal of Physical Chemistry B*. 110 (2006) 21568-21571.
- [14] S. Carabineiro, X. Chen, M. Konsolakis, A. Psarras, P. Tavares, J. Órfão, M. Pereira, J.L. Figueiredo, Catalytic oxidation of toluene on Ce-Co and La-Co mixed oxides synthesized by exotemplating and evaporation methods, *Catalysis Today*. 244 (2015) 161-171.
- [15] Z. Qu, K. Gao, Q. Fu, Y. Qin, Low-temperature catalytic oxidation of toluene over nanocrystal-like Mn-Co oxides prepared by two-step hydrothermal method, *Catalysis Communications*. 52 (2014) 31-35.
- [16] L. F. Liotta, M. Ousmane, G. Di Carlo, G. Pantaleo, G. Deganello, A. Boreave, A. Giroir-Fendler, Catalytic removal of toluene over $\text{Co}_3\text{O}_4\text{-CeO}_2$ mixed oxide catalysts: Comparison with $\text{Pt/Al}_2\text{O}_3$, *Catalysis Letters*. 127(2009)270-276.
- [17] C. Ma, Z. Mu, C. He, P. Li, J. Li, Z. Hao, Catalytic oxidation of benzene over nanostructured porous $\text{Co}_3\text{O}_4\text{-CeO}_2$ composite catalysts, *Journal of Environmental Sciences*. 23(12)(201)2078-2086.
- [18] Z. Cheng, Z. Chen, J. Li, S. Zuo, P. Yang, Mesoporous silica-pillared clays supported nanosized $\text{Co}_3\text{O}_4\text{-CeO}_2$ for catalytic combustion of toluene, *Applied Surface Science*. 459 (2018) 32-39.
- [19] S. Zhang, S. Liu, X. Zhu, Y. Yang, W. Hu, H. Zhao, R. Qu, C. Zheng, X. Gao, Low temperature catalytic oxidation of propane over cobalt-cerium spinel oxides catalysts, *Applied Surface Science*. 479 (2019) 1132-1140.
- [20] X. Chen, S. A. C. Carabineiro, S. S. T. Bastos, P. B. Tavares, J. J. M. Orfao, M. F. R. Pereira, J. L. Figueiredo, Catalytic oxidation of ethyl acetate on cerium-containing mixed oxides, *Applied*

Catalysis A-General. 472(2014)101-112.

[21] S. Woo, I. Kim, J.K. Lee, S. Bong, J. Lee, H. Kim, Preparation of cost-effective Pt-Co electrodes by pulse electrodeposition for PEMFC electrocatalysts, *Electrochimica Acta*. 56 (2011) 3036-3041.

[22] K.H. Choi, H.S. Kim, T.H. Lee, Electrode fabrication for proton exchange membrane fuel cells by pulse electrodeposition, *Journal of Power Sources*. 75 (1998) 230-235.

[23] X. Li, X. Du, X. Ma, Z. Wang, X. Hao, A. Abudula, A. Yoshida, G. Guan, CuO nanowire@Co₃O₄ ultrathin nanosheet core-shell arrays: an effective catalyst for oxygen evolution reaction, *Electrochimica Acta*. 250 (2017) 77-83

[24] Z. Sihaib, F. Puleo, J.M. Garcia-Vargas, L. Retailleau, C. Descorme, L.F. Liotta, J.L. Valverde, S. Gil, A. Giroir-Fendler, Manganese oxide-based catalysts for toluene oxidation, *Applied Catalysis B-Environmental*. 209 (2017) 689-700.

[25] M. Konsolakis, S. Carabineiro, G. Marnellos, M. Asad, O. Soares, M. Pereira, J. Órfão, J. Figueiredo, Effect of cobalt loading on the solid state properties and ethyl acetate oxidation performance of cobalt-cerium mixed oxides, *Journal of Colloid Interface Science*. 496 (2017) 141-149.

[26] Z. Zhu, G. Lu, Z. Zhang, Y. Guo, Y. Guo, Y. Wang, Highly active and stable Co₃O₄/ZSM-5 catalyst for propane oxidation: Effect of the preparation method, *ACS Catalysis*. 3 (2013) 1154-1164.

[27] N. Jiang, Y. Zhao, C. Qiu, K. Shang, N. Lu, J. Li, Y. Wu, Y. Zhang, Enhanced catalytic performance of CoO_x-CeO₂ for synergetic degradation of toluene in multistage sliding plasma system through response surface methodology (RSM), *Applied Catalysis B-Environmental*. 259 (2019) 118061.

[28] W. Tang, X. Wu, S. Li, W. Li, Y. Chen, Porous Mn-Co mixed oxide nanorod as a novel catalyst with enhanced catalytic activity for removal of VOCs, *Catalysis Communications*. 56 (2014) 134-138.

[29] C. Wang, C. Zhang, W. C. Hua, Y. Guo, G. Lu, S. Gil, A. Giroir-Fendler, Catalytic oxidation of

vinyl chloride emissions over Co-Ce composite oxide catalysts, *Chemical Engineering Journal*. 315 (2017) 392-402.

[30] L. Zhao, Z. Zhang, Y. Li, X. Leng, T. Zhang, F. Yuan, X. Niu, Y. Zhu, Synthesis of Ce_aMnO_x hollow microsphere with hierarchical structure and its excellent catalytic performance for toluene combustion, *Applied Catalysis B-Environmental*. 245 (2019) 502-512.

[31] C.He, Y. Yu, Y. Lin, N. Qiao, J. Li, Q. Shen, W. Yu, J. Chen, Z. Hao, Low-temperature removal of toluene and propanal over highly active mesoporous CuCeO_x catalysts synthesized via a simple self-precipitation protocol, *Applied Catalysis B-Environmental*. 147 (2014) 156-166.

[32] L. Yu, G. Diao, F. Ye, M. Sun, J. Zhou, Y. Li, Y. Liu, Promoting effect of Ce in Ce/OMS-2 catalyst for catalytic combustion of dimethyl ether, *Catalysis Letters*. 141 (2011) 111-119.

[33] M.H. Castaño, R. Molina, S. Moreno, Cooperative effect of the Co-Mn mixed oxides for the catalytic oxidation of VOCs: Influence of the synthesis method, *Applied Catalysis A-General*. 492 (2015) 48-59.

[34] X. Feng, J. Guo, X. Wen, M. Xu, Y. Chu, S. Yuan, Enhancing performance of Co/ CeO_2 catalyst by Sr doping for catalytic combustion of toluene, *Applied Surface Science*. 445 (2018) 145-153.

[35] S. Mo, Q. Zhang, J. Li, Y. Sun, Q. Ren, S. Zou, Q. Zhang, J. Lu, M. Fu, D. Mo, J. Wu, H. Huang, D. Ye, Highly efficient mesoporous MnO_2 catalysts for the total toluene oxidation: oxygen-vacancy defect engineering and involved intermediates using in situ DRIFTS. *Applied Catalysis B-Environmental*. 264 (2020) 118464.

[36] Y. Luo, Y. Zheng, J. Zuo, X. Feng, X. Wang, T. Zhang, K. Zhang, L. Jiang, Insights into the high performance of Mn-Co oxides derived from metal-organic frameworks for total toluene oxidation, *Journal of Hazardous Materials*. 349 (2018) 119-127.

[37] X. Xie, Y. Li, Z. Liu, M. Haruta, W. Shen, Low-temperature oxidation of CO catalysed by Co_3O_4 nanorods, *Nature*. 458 (2009) 746-749.

[38] W. Zhao, Y. Zhang, X. Wu, Y. Zhan, X. Wang, C. Au, L. Jiang, Synthesis of Co-Mn oxides with double-shelled nanocages for low-temperature toluene combustion, *Catalysis Science & Technology*.

8 (2018) 4494-4502.

[39] J. Kan, L. Deng, B. Li, Q. Huang, S. Zhu, S. Shen, Y. Chen, Performance of co-doped Mn-Ce catalysts supported on cordierite for low concentration chlorobenzene oxidation, *Applied Catalysis A-General*. 530 (2017) 21-29.

[40] X. Ma, X. Feng, X. He, H. Guo, L. Lv, J. Guo, H. Cao, T. Zhou, Mesoporous CuO/CeO₂ bimetal oxides: One-pot synthesis, characterization and their application in catalytic destruction of 1,2-dichlorobenzene, *Microporous & Mesoporous Materials*. 158 (2012) 214-218.

[41] R. Peng, S. Li, X. Sun, Q. Ren, L. Chen, M. Fu, J. Wu, D. Ye, Size effect of Pt nanoparticles on the catalytic oxidation of toluene over Pt/CeO₂ catalysts, *Applied Catalysis B-Environmental*. 220 (2018) 462-470.

[42] S. Mo, S. Li, W. Li, J. Li, J. Chen, Y. Chen, Excellent low temperature performance for total benzene oxidation over mesoporous CoMnAl composited oxides from hydrotalcites, *Journal of Materials Chemistry A*. 4 (2016) 8113-8122.

[43] L. Qi, Q. Yu, Y. Dai, C. Tang, L. Liu, H. Zhang, F. Gao, L. Dong, Y. Chen, Influence of cerium precursors on the structure and reducibility of mesoporous CuO-CeO₂ catalysts for CO oxidation, *Applied Catalysis B-Environmental*. 119-120 (2012) 308-320.

[44] L. Jiang, H. Zhu, R. Razzaq, M. Zhu, C. Li, Z. Li, Effect of zirconium addition on the structure and properties of CuO/CeO₂ catalysts for high-temperature water-gas shift in an IGCC system, *International Journal of Hydrogen Energy*. 37 (2012) 15914-15924.

[45] W. Tang, X. Wu, D. Li, Z. Wang, G. Liu, H. Liu, Y. Chen, Oxalate route for promoting activity of manganese oxide catalysts in total VOCs' oxidation: Effect of calcination temperature and preparation method, *Journal of Materials Chemistry A*. 2 (2014) 2544-2554.

[46] C. He, Y. Yu, J. Shi, Q. Shen, J. Chen, H. Liu, Mesoporous Cu-Mn-Ce-O composites with homogeneous bulk composition for chlorobenzene removal: Catalytic performance and microactivation course, *Materials Chemistry and Physics*. 157 (2015) 87-100.

[47] S. Cao, H. Wang, F. Yu, M. Shi, S. Chen, X. Weng, Y. Liu, Z. Wu, Catalyst performance and

mechanism of catalytic combustion of dichloromethane (CH_2Cl_2) over Ce doped TiO_2 , Journal of Colloid Interface and Science. 463 (2016) 233-241.

CHAPTER 4 Highly dispersed Ag nanoparticles embedded on the surface of CeO₂/CF nanowires derived from three-dimensional structured Cu foam for toluene catalytic oxidation

4.1 Introduction

Volatile organic compounds (VOCs) are harmful to the environment and human health since they have toxic nature and could result in the formation of photochemical smog and ozone pollution [1, 2]. VOCs are mainly derived from human activities such as transportation and industrial processes [3]. Currently, various strategies have already been investigated and applied for the removal of VOCs [4, 5]. Among them, the catalytic oxidation is one of the most efficient and environmentally friendly pathways to convert VOCs into harmless substances of water (H₂O), carbon dioxide (CO₂) and other less harmful chemicals [6, 7]. The key issue for this method is to design and prepare catalysts with high performance at low operating temperatures. Two kinds of catalysts, i.e., noble metal (e.g., Pt, Pd or Au) based catalysts and transition metal oxide (e.g., MnO₂, CuO or Co₃O₄) based catalysts, are generally applied for the catalytic oxidation of VOCs [8-10]. The former ones always have much higher activity than the latter ones but have high cost. The catalyst preparation method and the selection of catalyst support could affect the catalytic performances of transition metal oxide based catalysts [11].

To date, various materials such as zeolites [12], SBA-15 [13] and metal oxide [14, 15] have been used as the supports of VOC oxidation catalysts. Among them, cerium oxide (CeO₂) is always applied as either catalyst or catalyst support. Especially, the rich oxygen vacancies and excellent redox property of the cerium oxide make it have high catalytic performance [16, 17]. The conventional methods to prepare CeO₂ based catalysts include co-deposition [18], heating reflux aging [19] and hydrothermal method [20]. Recently, it is found the electrodeposition method is a

time-saving and simple preparation process with the ability to control the catalyst size, density, and composition [21]. Moreover, the obtained catalysts could be applied directly in a practical process. To improve the performance of CeO₂ based catalysts, it has been proved that doping other metal on it could enhance activity of CeO₂. For example, Peng *et al.* [22] doped Pt on CeO₂ by a glycol reduction method and used for the catalytic oxidation of toluene. It is found that the physiochemical properties of the obtained Pt/CeO₂ catalysts mainly depended on the Pt particle size, and the exposed Pt atom and oxygen vacancies on CeO₂ were active sites for the reaction. Consequently, the best catalytic activity was achieved at a toluene conversion temperature (T₉₀, 90% conversion) as low as 143 °C. Meanwhile, Guo *et al.* [23] prepared Pd/kit-CeO₂ (CeO₂ made from KIT-6 template) catalysts using a biogenic method, which possessed a high concentration of Pd⁰ metal, a large amount of oxygen adsorption species, good low-temperature reducibility, and strong interactions between Pd NPs and kit-CeO₂ support, and therefore leading to the benzene conversion temperature of T₉₀ significantly decreased from 260 to 187 °C when compared with that of the kit-CeO₂ support.

As a less expensive metal element than other noble metals, Ag was also used to dope cerium oxide for the catalytic oxidation of VOCs. For instances, Mikheeva *et al.* [24] fabricated Ag-CeO₂/SBA-15 catalysts for the catalytic oxidation of methanol. It is found that the doping of Ag on the CeO₂/SBA-15 effectively enhanced the activity due to the synergetic function of the active oxidative species of Ag and ceria on the Ag-CeO₂ interface. Qin *et al.* [20] doped Ag on CeO₂ with three different morphologies as the catalyst support to develop Ag/CeO₂ catalysts for the catalytic oxidation of ethyl acetate, and found that the catalyst with CeO₂ nanocubes (CeO₂-c) morphology displayed higher catalytic activity than the catalysts shaped with nanorods CeO₂ (CeO₂-r) and nano-octahedra CeO₂ (CeO₂-o) since the CeO₂-c had higher content of active Ag⁰ and Ce³⁺ species, more surface active oxygen and better reducibility.

In this work, a three-step electrochemical process was developed to prepare a three-dimensional (3D) structure Ag doped CeO₂ based catalysts, in which copper nanowires (CNWs) were generated on the surface of three-dimensional Cu foam (CF) by an electro-oxidization process at first and then,

CeO₂ was uniformly coated on the CNWs by a unipolar pulse electro-deposition (UPED) method and finally highly dispersed Ag nanoparticles were embedded on the surface of CeO₂ using a constant voltage electrodeposition method. The obtained Ag-CeO₂@CNWs/CF was applied for the catalytic oxidation of toluene. The physiochemical properties of the catalysts with different Ag loading amounts were characterized by XRD, SEM, TEM, H₂-TPR, O₂-TPD and NH₃-TPD and XPS techniques. The catalytic performances of the Ag-CeO₂@CNWs/CF catalysts were evaluated in a fixed bed reactor with a continuous gas flow containing about 1000 ppm toluene. Long-term stability of the catalyst (80Ag-CeO₂@CNWs/CF) with the best performance was carried out in the presence and absence of water vapor (5 vol%).

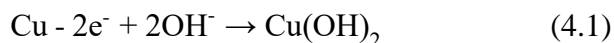
4.2 Experimental

4.2.1 Chemicals and Materials

Hydrochloric acid (HCl, Wako, Japan), cerium and silver nitrate hydrates (Ce(NO₃)₃·6H₂O and AgNO₃, Wako, Japan) were used without any further treatment. Cu foam (CF, thickness: 1.6 mm, surface density: 350 g/cm²; number of pores per inch: ≥98%) was provided by Fujian, China, and used as the catalyst support. It was cut into small pieces (2.0 cm×2.0 cm), then pretreated with the assistance of ultrasound in 1 M HCl solution and distilled water (H₂O) for 10 min successively. Finally, the cleaned CF was washed completely and sealed in water prior to use.

4.2.2 Catalyst preparation

Pretreatment of CF support: Electro-oxidization was performed to generate Cu nanowires (CNWs) on the surface of CF. Herein, the CF (2.0 cm×2.0 cm) was put into 60 mL of KOH solution and oxidized by using the galvanostatic method with an applied current of 80 mA for 1200 s, by which the reaction as(Eq. (4.1)) occurred. After the electro-oxidation, Cu foam was washed with distilled water and dried. As indicated by the SEM image (**Fig. 4.1a**), homogeneous nanowire arrays were formed on the surface of Cu foam.



Preparation of catalysts: Firstly, based on the preliminary experimental results, $\text{Ce}(\text{OH})_3/\text{CF}$ was electrodeposited on the surfaces of Cu nanowires by using a unipolar pulse electro-deposition (UPED) method under the following conditions: a constant potential of -1.0 V, on/off time of 1.0/1.0 s, and pulse cycles of 1000. The oxidized substrate of CF with the Cu nanowires, platinum wire (ALS, Japan) and Ag/AgCl/saturated KCl electrode (ALS, Japan) were used as the working, counter and reference electrodes, respectively. The molar concentration of $\text{Ce}(\text{NO}_3)_3 \cdot 6\text{H}_2\text{O}$ was 0.05 mol/L, and the total solution volume was 100 mL during the UPED process. The obtained samples were thoroughly washed with distilled water and dried at 60 °C for 2 h. Subsequently, electrodeposition of Ag species on the above $\text{Ce}(\text{OH})_3$ coated CNWs on the CF was performed by using a constant voltage electrodeposition method with an applied potential of -0.6 V for 40 s, 60 s, 80 s and 100 s, separately. The achieved samples were washed with distilled water, vacuum-dried at 80 °C for overnight, and calcined at 350 °C in a muffle furnace for 2 h with a heating rate of 5 °C/min. As such, the obtained samples are donated based on the electrodeposition time as 40Ag-CeO₂@CNWs/CF, 60Ag-CeO₂@CNWs/CF, 80Ag-CeO₂@CNWs/CF and 100Ag-CeO₂@CNWs/CF, respectively. For comparison, the catalyst was prepared by a wet impregnation method, which is named as 3.7wt%Ag-CeO₂@CNWs/CF.

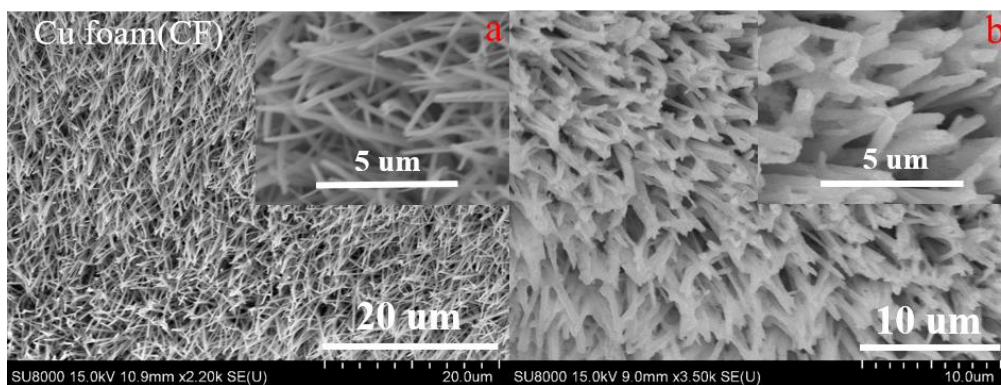


Fig. 4.1. SEM images of (a) Cu nanowires on Cu foam (CF) and (b) CeO₂@CNWs/CF catalyst (Insets: the enlarged images).

4.2.3 Characterizations

Morphology and elemental composition of the prepared catalysts were investigated by a scanning

electron microscopy (SEM, SU8010, Hitachi, Japan) with an energy dispersive X-ray detector (EDX, Horiba Scientific). Herein, a small piece of Ag-CeO₂@CNWs attached on the test plate was used for the EDX analysis, and the weight percentage (wt%) of each detected element was obtained from the “Map Sum Spectrum”. The nanostructures were observed by a transmission electron microscope (TEM, JEM-2100F, JEOL) operating at 200 kV. Crystalline structure of the catalyst was determined by an X-ray diffractor (XRD, Rigaku Smartlab, Japan) with the Cu-K α radiation ($\lambda=0.15418$ nm) in a 2θ range of 10° - 90° with a scanning speed of $10^\circ \text{ min}^{-1}$. The surface chemical compositions and elemental valence states of all catalysts were analyzed by X-ray photoelectron spectroscopy (XPS) with an ESCALab220i-XL electron spectrometer (VG, Scientific ESCALab250i-XL unit, UK), in which the C 1s peak was fixed at the binding energy of 284.7 eV. For the quantitative XPS analysis, the atomic percentages related to the detected elements (O1s, Cu 2p, Ag 3d and Ce 3d) were transferred into weight percentages in order to compare with the results tested by EDX analysis.

The redox properties of catalysts were evaluated by hydrogen temperature-programmed reduction (H₂-TPR) and oxygen temperature-programmed desorption (O₂-TPD) analyses carried on a BELCAT catalyst analyzer with a thermal conductivity detector (TCD). Briefly, 60 mg of each sample was loaded into a U-shaped tube, and then pretreated in a He gas flow (50 cm³/min) from room temperature (RT) to 300 °C with a heating rate of 10 °C/min and held at 300 °C for 30 min. After cooled down, the sample was exposed to a 50 cm³/min gas flow of 5% H₂-Ar (v/v) mixture and heated from RT to 900 °C at a heating rate of 10 °C/min. For O₂-TPD analysis, 150 mg of sample was pretreated in a He gas flow (50 cm³/min) for 1 h in order to remove the surface water at first. After cooling down to RT, the sample was treated by an O₂ gas flow (50 cm³/min) and then purged by a He gas flow (50 cm³/min) for 1 h. Finally, the sample was heated from RT to 900 °C with a heating rate of 10 °C/min. For ammonia temperature-programmed desorption (NH₃-TPD) analysis, 100 mg of each sample was pretreated by a He gas flow (50 cm³/min) at 300 °C for 1 h, purged with 5% NH₃/He for 1h after cooled down to RT, subsequently, NH₃ desorption started from 100 to 600 °C with a 10 °C/min heating rate in He gas atmosphere.

4.2.4 Catalytic activity test

Performances of the Ag-CeO₂@CNWs/CF catalysts prepared with different electrodeposition periods were evaluated for toluene catalytic oxidation in a continuous flowing fixed-bed reactor at the atmospheric pressure. In each test, the catalyst coated CNWs/CF was cut into a size of < 3 mm in advance, 100 mg of catalyst and 300 mg of quartz sand (40~60 mesh) were mixed and transferred to a Pyrex tube reactor (i.d.=10 mm) with quartz wool to seal both ends of the catalyst bed. The catalyst bed was pretreated in the nitrogen atmosphere at 100 °C for 1.5 h at first and then, the reaction was conducted in tested temperature range of 150~320 °C. Based on the preliminary experiments, the total flow rate with the toluene concentration of around 978 ppm in the atmosphere of oxygen (O₂, 20 vol%)-nitrogen (N₂, 80 vol%) mixed gas flow (50 cm³/min) with a weight hourly space velocity (WHSV) of 30,000 mL g⁻¹ h⁻¹. Herein, the gaseous toluene was carried by N₂ gas flow from a bubbler filled with toluene in an ice-water mixing bath. Long-term water resistance performance was examined by adding 5.0 vol% of water vapor to the above described gas mixture by passing the feed stream through a saturated water bubbler. During the reaction, the inlet and outlet concentrations of toluene were analyzed on-line by a gas chromatograph (Shimadzu-2014), which was equipped with a flame ionization detector (FID), and simultaneously, the outgoing products from the reactor were also analyzed on a FTIR gas analyzer (Horiba, FG-120).

Toluene conversion and CO₂ selectivity were calculated from Eqs. (4.2) and (4.3):

$$X_{\text{Conversion}} = \frac{C_{\text{Inlet}} - C_{\text{Outlet}}}{C_{\text{Inlet}}} \times 100\% \quad (4.2)$$

$$\text{CO}_2 \text{ selectivity} = \frac{C_{\text{CO}_2}}{7(C_{\text{Inlet}} - C_{\text{Outlet}})} \times 100\% \quad (4.3)$$

where, C_{Inlet} and C_{Outlet} are the inlet and outlet concentrations of toluene, respectively. C_{CO₂} is the concentration of the produced CO₂ in the off gas during the reaction. In this work, only carbon dioxide was produced in the gas phase, the carbon balances of all reactions were closed with errors lower than 5.0 %.

4.3 Results and discussion

4.3.1 XRD analysis and SEM/TEM characterizations

Fig. 4.2 shows the XRD patterns of the as-prepared catalysts prepared with the electrodeposition time varied from 40 to 100 s, in which 2θ peaks located at 44.20° , 51.26° and 74.88° are well matched with those characteristic peaks of the Cu metal (PDF#04-0836) from CF support and the diffraction peaks corresponding to CuO and Cu₂O were also obviously observed, indicating that multivalent Cu species existing in the catalysts. The peaks at $2\theta = 29.37^\circ$, 33.87° , 48.29° and 57.28° were the characteristic peaks of cerium oxide (CeO₂), which are assigned to the crystal planes of (111), (200), (220) and (311) (PDF# 34-0394080-1541), respectively. Especially, it is worth noting that the diffraction peaks corresponding to Ag (PDF#04-0836) were too weak to be observed for the 40Ag-CeO₂@CNWs/CF catalyst, but the intensity increased gradually with the increase in the electrodeposition time from 40 to 100 s. Herein, it is possible that Ag particles on the Ag-CeO₂@CNWs/CF catalyst prepared with short electrodeposition time might be too small and well dispersed on the CeO₂@CNWs/CF.

As shown in **Fig. 4.1**, the surface of Cu nanowire (**Fig. 4.1a**) became rough after supporting CeO₂ on it (**Fig. 4.1b**). One can see that CeO₂ was uniformly coated on the CNWs so that the diameter of NWs increased to some extent. **Fig. 4.3** (a~d) shows the SEM images of Ag-CeO₂@CNWs/CF prepared with the electrodeposition time varied from 40 to 100 s for Ag loading, in which no obvious morphology changes were observed since the Ag loading amount on the catalyst surface was only increased gradually from 2.7 to 5.6 wt% based on the EDX analysis results, which is much lower than those of the main contents of cerium and copper. As such, the weak diffraction peaks related to Ag in the XRD patterns (**Fig. 4.2**) should be also contributed to these low loading amounts. Moreover, XPS analyses also confirmed the Ag percentages on the surfaces of the catalysts (**Table 4.1**). Comparing the weight percentages (wt%) of Ag element obtained from EDX and XPS results, it can be found that the value from the former were only a little higher than that of the latter, which should be contributed to the difference of the instruments.

However, one can see that the results obtained from the two instruments showed the same increase trend for Ag weight percentage with the increase in the electrodeposition time. Additionally, **Fig. 4.4** shows the morphology of the spent 80Ag-CeO₂@CNWs/CF, in which the catalyst with the best performance was as described in the sections 3.5 and 3.6. One can see that the catalyst maintained its original morphology after the long-term reaction, indicating its structure stability.

Fig. 4.5a shows TEM image (low magnification) of the single CNW without CeO₂ coating, which possessed a diameter less than 150 nm. After CeO₂ coating, the diameter of CeO₂@CNWs increased to more than 500 nm (**Fig. 4.5 (b-f)**), demonstrating that cerium species can be easily deposited on the surface of CNWs on CF by the electrodeposition method. **Fig. 4.6a** shows HRTEM image of 40Ag-CeO₂@CNWs/CF, in which four types of lattice fringes were observed. The three well-defined crystalline structures with fringe spacings of 0.14, 0.20 and 0.23 nm were attributed to the (220), (222) and (111) lattice planes of Ag phase, respectively, whereas the other one with the fringe spacing of 0.32 nm was assigned to the (111) crystal plane of CeO₂ phase. In particular, Ag nanoparticles with diameters less than 10 nm were found to be highly dispersed on the surface of CeO₂, indicating that the electrodeposition method is a good way to dope nanoparticles on the catalysts. Thus, the weak diffraction peaks in the XRD patterns (**Fig. 4.2**) should be also due to the well dispersion of Ag nanoparticles. Furthermore, the interfaces between Ag and CeO₂ phases were observed in the TEM images, indicating the well embedding of Ag nanoparticles on the surface of CeO₂. As shown in **Fig. 4.6(b-d)**, both CeO₂ and Ag lattice planes were also observed on other Ag-CeO₂@CNWs/CF samples. Herein, it should be noted that Ag nanoparticles with three different crystal phases existed in the prepared Ag-CeO₂@CNWs/CF samples, which should provide the active sites for the VOC oxidation as described in the sections 3.5 and 3.6. In addition, the Ag nanoparticle size also significantly increased with the increase in the electrodeposition time for Ag, which is also in agreement with the XRD analysis results (**Fig. 4.2**).

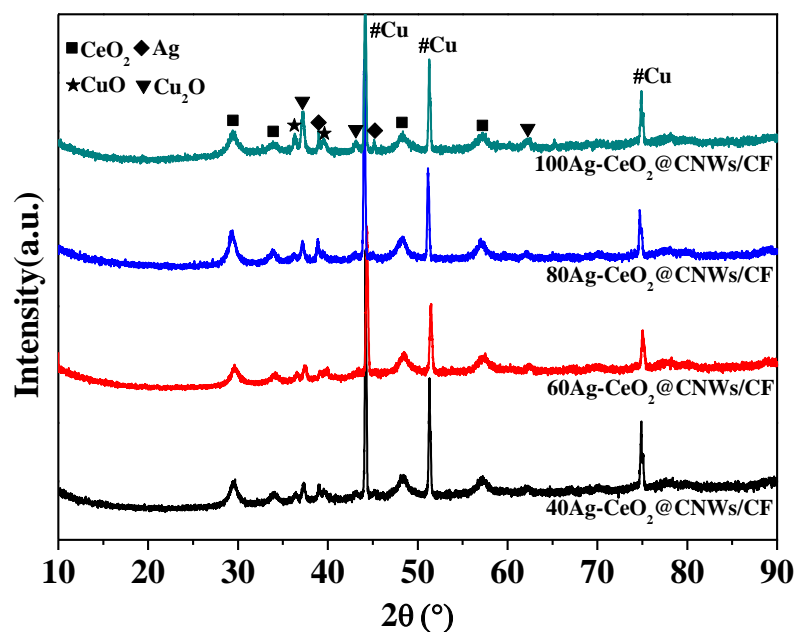


Fig. 4.2. XRD patterns of Ag-CeO₂@CNWs/CF catalysts prepared with the electrodeposition time varied from 40 to 100 s for Ag loading.

Table 4.1 Surface elemental compositions of Ag-CeO₂@CNWs/CF catalysts prepared with the electrodeposition time varied from 40 to 100 s for Ag loading.

Sample	O (wt%) ^a	Cu (wt%) ^a	Ce (wt%) ^a	Ag (wt%) ^a	Ag (wt%) ^b
40Ag-CeO ₂ @CNWs/CF	20.9	18.2	58.2	2.7	1.5
60Ag-CeO ₂ @CNWs/CF	21.3	15.0	60.1	3.6	3.5
80Ag-CeO ₂ @CNWs/CF	18.6	16.2	61.1	4.1	3.7
100Ag-CeO ₂ @CNWs/CF	19.7	19.9	54.8	5.6	3.0

The weight percentages (wt%) of O, Cu, Ce and Ag were taken by

^a, EDX analysis;

^b, XPS analysis.

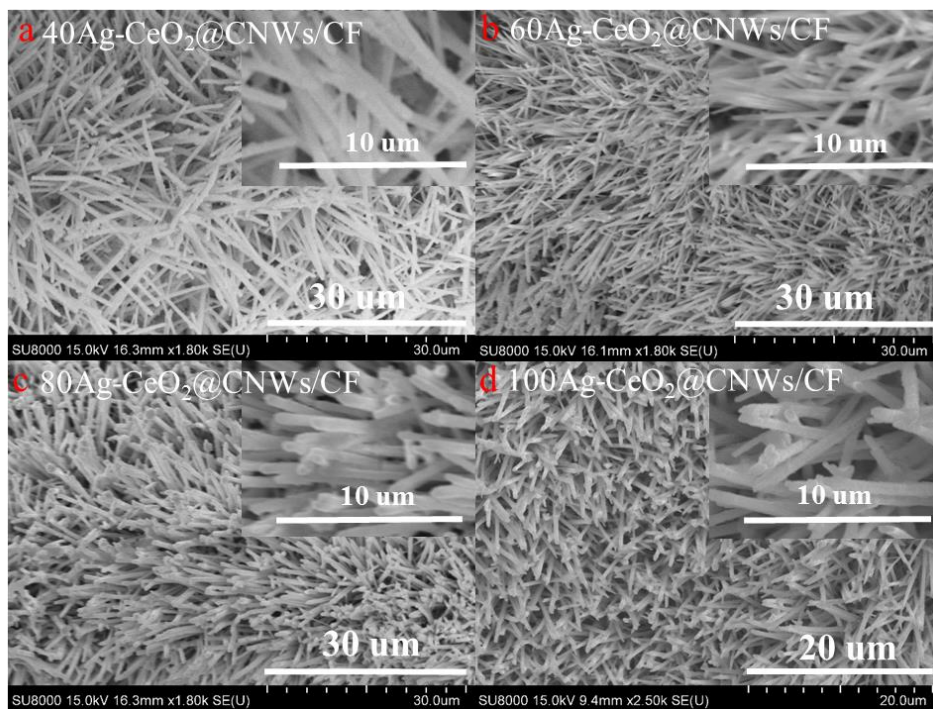


Fig. 4.3. SEM images of the prepared Ag-CeO₂@CNWs/CF catalysts (Insets: the enlarged images).

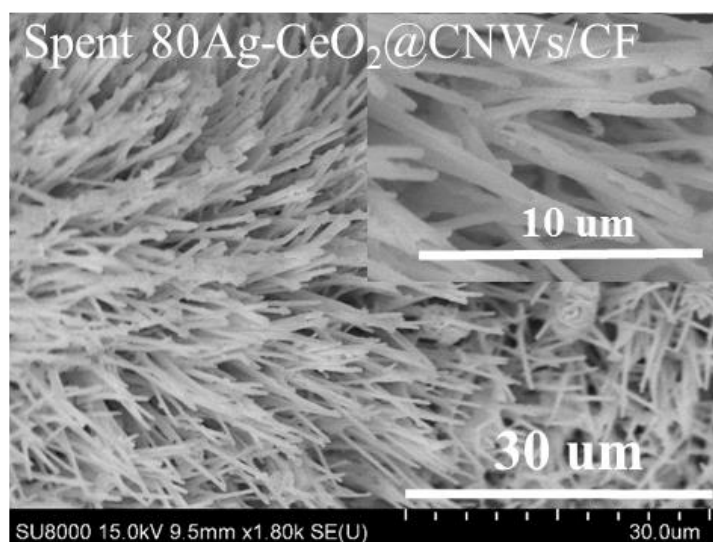


Fig. 4.4. SEM image of the spent 80Ag-CeO₂@CNWs/CF catalyst (Inset: the enlarged image).

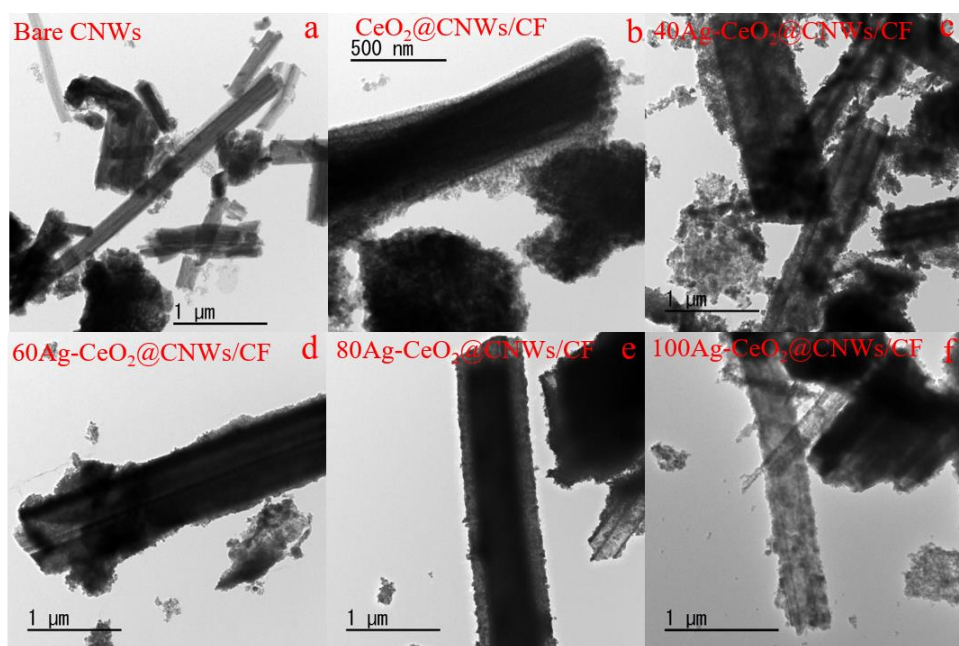


Fig. 4.5. TEM images of (a) bare single CNWs, (b) CeO_2 @CNWs and (c-f) Ag- CeO_2 @CNWs catalysts.

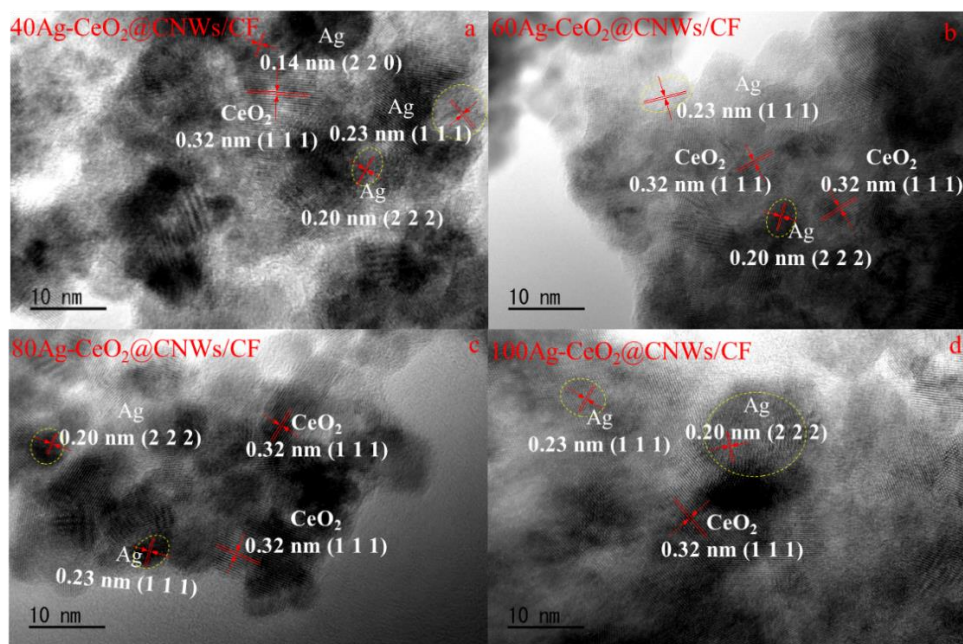


Fig. 4.6. HRTEM images of the prepared Ag- CeO_2 @CNWs/CF catalysts.

4.3.2 Redox performance

Fig. 4.7 shows the H_2 -TPR profiles of the prepared Ag- CeO_2 @CNWs/CF catalysts, which corresponding H_2 consumptions are summarized in **Table 4.2**. Generally, the reduction performance of CeO_2 includes three regions, i.e., a low temperature range of 100-400 °C for the surface oxygen

reduction, a middle temperature range of 400-600 °C for the subsurface oxygen reduction and a high temperature range of 600-900 °C for the bulk oxygen reduction [25, 26]. Herein, for the 40Ag-CeO₂@CNWs/CF catalyst, the asymmetrical peak was located at 294.2 °C is assigned to the reduction of the surface oxygen. Other Ag-CeO₂@CNWs/CF catalysts also displayed the similar reduction behavior. Notably, the asymmetrical peak at the low temperature range gradually shifted to the lower temperature direction with the increase in the electrodeposition time for Ag until 80 s, which assigned to the spillover of hydrogen from Ag to CeO₂ [27]. However, further increasing of the electrodeposition time (e.g., 100 s electrodeposition) decreased the reducibility. As a result, the 100Ag-CeO₂@CNWs/CF catalyst exhibited a higher reduction temperature of 294.3 °C, which might be caused by the high loading of Ag species. Herein, the high loading of Ag could hinder the mobility of oxygen species over the catalyst surface [27], and thus increased the reduction temperature. Consequently, in this study, the optimum electrodeposition time was 80 s, and the obtained 80Ag-CeO₂@CNWs/CF catalyst possessed the lowest reduction temperature of 263 °C, the value is much lower than that of 40Ag-CeO₂@CNWs/CF catalyst, indicating that the supporting of Ag nanoparticles with proper loading on the CeO₂ could significantly promote the reducibility of the catalyst, which is benefit for the formation of active surface oxygen for the catalytic oxidation of toluene [28, 29]. In addition, as summarized in **Table 4.2**, with the increase in the electrodeposition time for Ag loading, H₂-uptake amount (H₂ consumption) during the reduction of Ag-CeO₂@CNWs/CF catalyst at the low temperature range decreased at first and then increased, which might contributed by the coverage extent of the loading Ag nanoparticles on the surface of CeO₂ due to the preventing of the partial reduction of CeO₂. It is consistent with TEM measurement, where Ag nanoparticles were highly dispersed on CeO₂ surface. Obviously, with the increasing of electrodeposition time for Ag, the increase of H₂-uptake amount over the obtained 80Ag-CeO₂@CNWs/CF catalyst appeared again but the amount was slightly less than that of 100Ag-CeO₂@CNWs/CF. Thus, as indicated in the section 3.5, the 80Ag-CeO₂@CNWs/CF catalyst exhibited the highest activity among the prepared catalysts due to its good low temperature

reducibility.

Table 4.2 Hydrogen consumption and oxygen desorption of various Ag-CeO₂@CNWs/CF catalysts for H₂-TPR and O₂-TPD analyses.

Sample	Reduction T ₁ /°C	H ₂ -uptake (mmol/g)	O ₂ desorption T ₂ /°C	O _{ads} desorption (mmol/g)
40Ag-CeO ₂ @CNWs/CF	294.2	6.852	208.8	0.141
60Ag-CeO ₂ @CNWs/CF	275.9	5.827	207.4	0.156
80Ag-CeO ₂ @CNWs/CF	263.0	5.923	202.0	0.159
100Ag-CeO ₂ @CNWs/CF	294.3	6.055	210.2	0.156

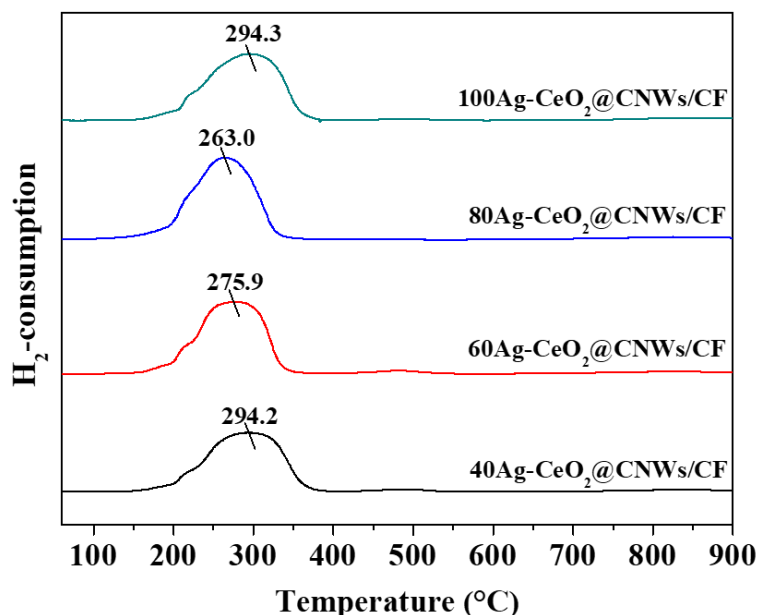


Fig. 4.7. H₂-TPR profiles of the prepared Ag-CeO₂@CNWs/CF catalysts with different Ag loading amounts.

Fig. 4.8 shows O₂-TPD profiles of various Ag-CeO₂@CNWs/CF catalysts, in which three regions were divided, i.e., the peaks at a low temperature range below 350 °C can be ascribed to the desorption of chemisorbed surface oxygen, the peaks concentrated at a medium temperature range of 350-600 °C are attributed to the desorption of surface lattice oxygen and the peaks located at a high temperature range of above 600 °C are assigned to the desorption of bulk lattice oxygen, respectively [30, 31]. In general, with the increase in temperature, oxygen species could undergo the following

transition process, i.e., $\text{O}_2(\text{ads}) \rightarrow \text{O}_2^-(\text{ads}) \rightarrow \text{O}^-(\text{ads}) \rightarrow \text{O}^{2-}(\text{lat})$. Herein, $\text{O}_2(\text{ads})$ is the physically adsorbed oxygen, $\text{O}_2^-(\text{ads})$ is the adsorbed molecular oxygen, $\text{O}^-(\text{ads})$ is surface adsorbed chemical oxygen and $\text{O}^{2-}(\text{lat})$ is the lattice oxygen, respectively [32, 33]. In **Fig. 4.8**, it is obvious that the possible oxygen species in the Ag-CeO₂@CNWs/CF catalysts mainly related to the low and high temperature regions. Thus, the oxygen species corresponding to the low temperature range should be related to the desorption of chemisorbed surface oxygen (O_2^- , O^-) bound to oxygen vacancies whereas the oxygen species corresponding to the high temperature range should be attributed to the desorption of lattice oxygen (O^{2-}) from CeO₂.

As summarized in **Table 4.2**, the O₂ desorption temperature decreased with the increase in the Ag loading amount at first until that for 80Ag-CeO₂@CNWs/CF, and then increased with the further increase of the Ag loading amount (e.g., 100Ag-CeO₂@CNWs/CF). Meanwhile, the amount of oxygen species (O_{ads}) at the low temperature range increased gradually with the increase of Ag loading amount until that for 80Ag-CeO₂@CNWs/CF and then decreased, implying that the suitable Ag loading could promote the generation of the oxygen vacancies, which could improve the catalytic activity for VOC oxidation[34]. These results are almost consistent with the H₂-TPR analysis results. Thus, the suitable Ag loading amount could enhance the formation of the more active oxygen species on the catalysts related to the low-temperature oxidation and simultaneously improve the low-temperature reducibility. In this study, among the prepared catalysts, 80Ag-CeO₂@CNWs/CF was confirmed to have the largest amount of active oxygen species and the best reducibility at low temperature range, which also showed the best activity in the catalytic oxidation of toluene as indicated in the sections 3.5 and 3.6.

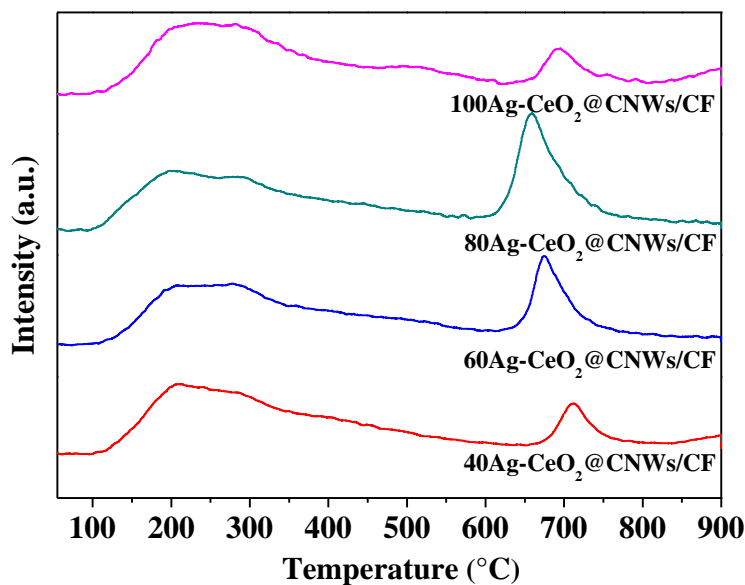


Fig. 4.8. O₂-TPD profiles of the prepared Ag-CeO₂@CNWs/CF catalysts.

4.3.3 XPS analysis

Surface composition and local atomic environments of the prepared catalysts were further analyzed by an X-ray photoelectron spectroscopy (XPS) instrument. **Fig. 4.9** shows XPS spectra of Ce 3d, Ag 3d and O 1s for all prepared Ag-CeO₂@CNWs/CF catalysts, whose detail quantitative analysis results are summarized in **Table 4.3**. Herein, can be deconvoluted into Ce 3d_{5/2} and Ce 3d_{3/2}, respectively. As shown in **Fig. 4.9a**, four peaks located at 882.2 eV (U), 885.4 eV (U₁), 901.2 eV (U₂) and 902.9 eV (U₃) are assigned to Ce³⁺ species whereas the other six peaks at 883.3 eV (I), 888.8 eV (I₁), 889.4 eV (I₂), 900.6 eV (I₃), 907.5 eV (I₄) and 916.7 eV (I₅) are contributed by Ce⁴⁺ species, respectively[35, 36]. One can see that the main chemical valence of Ce species was Ce⁴⁺, but Ce³⁺ and Ce⁴⁺ species coexisted within the catalyst. As shown in **Table 4.3**, the concentration ratio of Ce³⁺/(Ce³⁺+Ce⁴⁺) in Ag-CeO₂@CNWs/CF catalysts increased gradually with the increasing of Ag loading amount and it reached the maximum value when the electrodeposition time for Ag was 80 s, demonstrating that the presence of Ag nanoparticles promoted the formation of active Ce³⁺ species. As proved by other researchers [25], Ce³⁺ could induce the formation of oxygen vacancies over ceria surface and therefore improve the catalytic activity. Thus, the formation of high concentration of Ce³⁺ over the present catalyst surface could be also beneficial for the catalytic oxidation of VOCs.

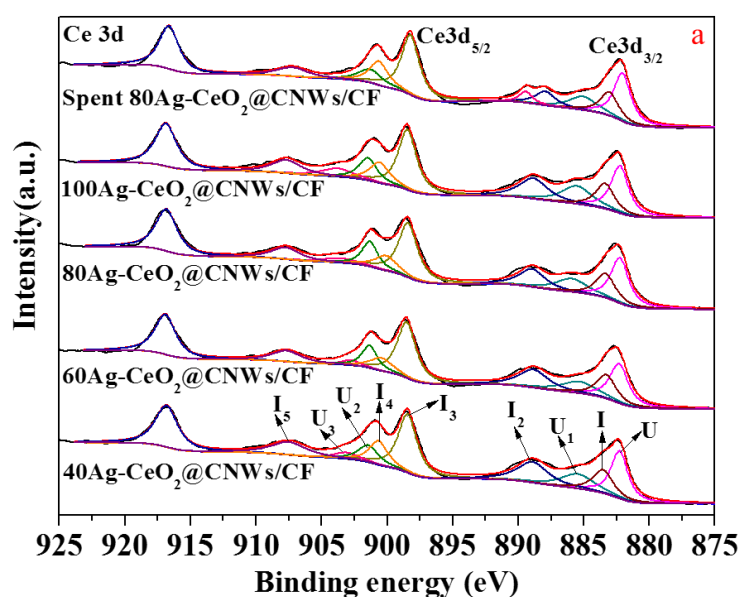
Fig. 4.9b shows the XPS spectra of Ag 3d. Herein, the bonding energies of Ag 3d_{5/2} assigned to the metallic Ag nanoparticles (Ag⁰) [37, 38] for the Ag-CeO₂@CNWs/CF catalysts prepared by the electrodeposition time varied from 40 to 100 s were 368.4, 368.0, 368.2 and 368.2 eV, respectively. Meanwhile, the bonding energies in the range of 367.6-367.8 eV corresponded to the oxidation state of Ag species (Ag₂O). Thus, both Ag⁰ and Ag₂O were found to be existed on the catalyst surface, which could be resulted from the electron transfer between Ag and CeO₂ as $\text{Ag}^+ + \text{Ce}^{3+} \rightarrow \text{Ag}^0 + \text{Ce}^{4+}$, indicating that the formation of Ce³⁺ species should have great relationship with the active species of Ag⁰. Such a phenomenon as that between noble metal (Ag, Au, Pd or Pt) and metal oxide (MnO₂, CeO₂) was also reported by Li *et al.* [39] and Yang *et al.* [40]. Additionally, in **Table 4.3**, the first decrease in the concentration ratio of Ce³⁺/(Ce³⁺ + Ce⁴⁺) could be resulted from the consumption of Ag⁺ ions to form more Ce⁴⁺ ions. Thereafter, the increase of this ratio might be due to the increase in Ag loading amount. In addition, it is worth noting that the observed negative shift in the Ag 3d_{5/2} spectra indicated the more cationic property of Ag species [41]. These results are consistent with the conclusion from Ce 3d spectra, further confirmed that Ag species loading promoted the formation of Ce³⁺ active species. Therefore, it can be concluded that there was a strong interaction between Ag species and CeO₂, which will finally affect the catalytic performance as indicated in the sections 3.5 and 3.6.

Fig. 4.9c displays the asymmetrical O 1s spectra, which can be fitted into three peaks: the peak at the low binding energy range of 529.1-529.5 eV corresponding to the lattice oxygen O²⁻ (O_{lat}), the peak located at the middle binding energy range of 530.1-530.9 eV attributing to the surface adsorbed oxygen of O₂⁻, O⁻ or O₂²⁻ (O_{sur}) and the peak centered at the high binding energy over 531.4 eV are ascribing to the hydroxyl groups and/or carbonate species, respectively[42, 43]. As indicated in **Table 4.3**, lattice oxygen species should be the main oxygen species, and the concentration ratios of O_{sur}/O_{lat} over Ag-CeO₂@CNWs/CF catalysts prepared with the electrodeposition time varied from 40 to 100 s for Ag loading were 0.408, 0.440, 0.519 and 0.448, respectively. Such a change trend is consistent with those of Ce³⁺/(Ce³⁺ + Ce⁴⁺). Moreover, it should be noted that the spent

80Ag-CeO₂@CNWs/CF catalyst after long-term test (as indicated in the section 3.6) showed the similar values as those of the fresh catalyst, indicating its stable chemical stability during the oxidation process. It has been proved that the surface active oxygen is favorable to enhance the catalytic activity of VOCs oxidation [40]. Thus, in this study, the highest content of surface oxygen species for the 80Ag-CeO₂@CNWs/CF catalyst should be play an important role in its excellent catalytic performance for the oxidation of toluene as indicated in the sections 3.5 and 3.6.

Table 4.3 Surface element compositions and valence states of Ag-CeO₂/CF catalysts tested by XPS technique.

Catalysts	Area ratio of Ce 3d	Area ratio of O 1s
	Ce ³⁺ /(Ce ³⁺ +Ce ⁴⁺)	O _{sur} /O _{latt}
40Ag-CeO ₂ @CNWs/CF	0.306	0.408
60Ag-CeO ₂ @CNWs/CF	0.312	0.440
80Ag-CeO ₂ @CNWs/CF	0.336	0.519
100Ag-CeO ₂ @CNWs/CF	0.345	0.448
Spent 80Ag-CeO ₂ @CNWs/CF	0.333	0.481



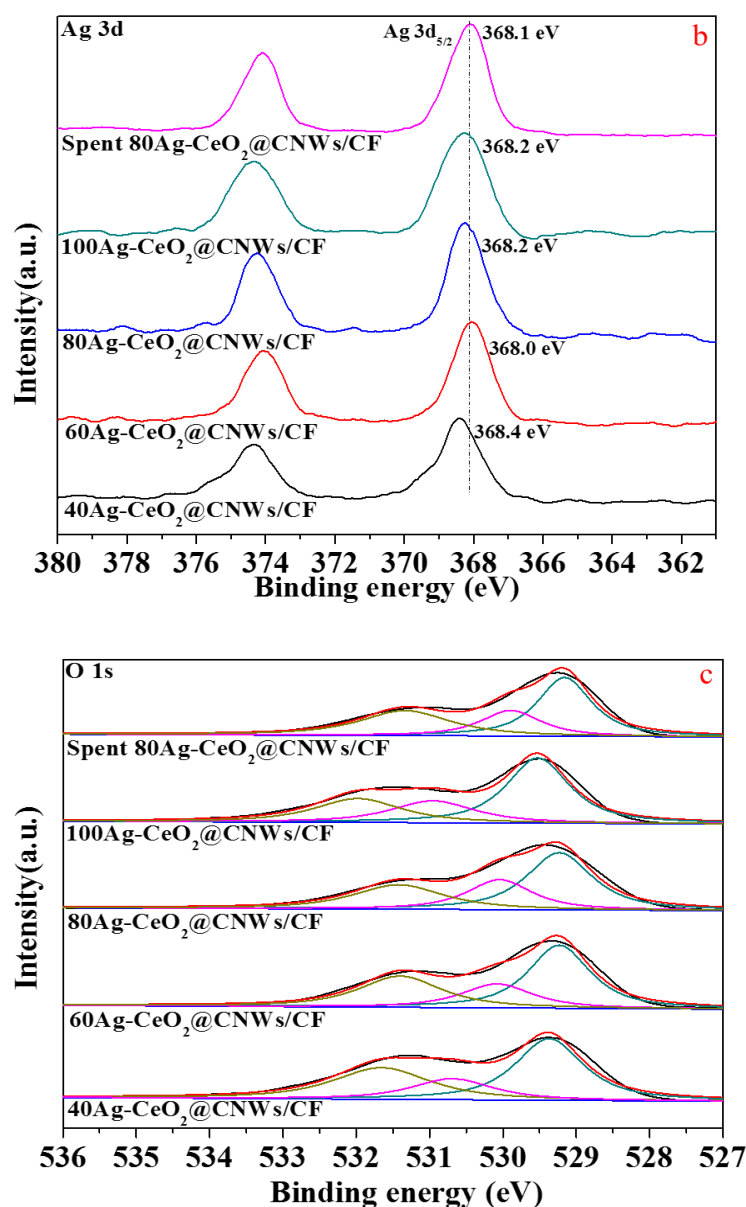


Fig. 4.9. XPS profiles of Ce 3d, Ag 3d and O 1s of the prepared Ag-CeO₂@CNWs/CF catalysts.

4.3.4 Surface acidity

The surface acidity of the Ag-CeO₂@CNWs/CF catalyst was investigated by NH₃-TPD measurement, and the results are displayed in **Fig. 4.10**. One can see that all samples exhibited two desorption peaks in the temperature range of 150-550 °C, indicating that both Lewis acid sites and Brønsted acid sites existed on the surface of Ag-CeO₂@CNWs/CF catalysts [44]. Notably, there was a significant change in the profiles when the electrodeposition time for Ag during the catalyst preparation was increased to 60 s, and the intensity of desorption peak corresponding to the Lewis

acid site increased when the electrodeposition time for Ag was increased to 80 and 100 s, indicating that more weak acid sites were formed on the catalyst surface. Therefore, the increase in Ag loading amount influenced the distribution of acid sites on the catalyst, which might also affect the performance for the catalytic oxidation of VOCs as reported by de Rivas *et al.* [45] and Piumetti *et al.* [46].

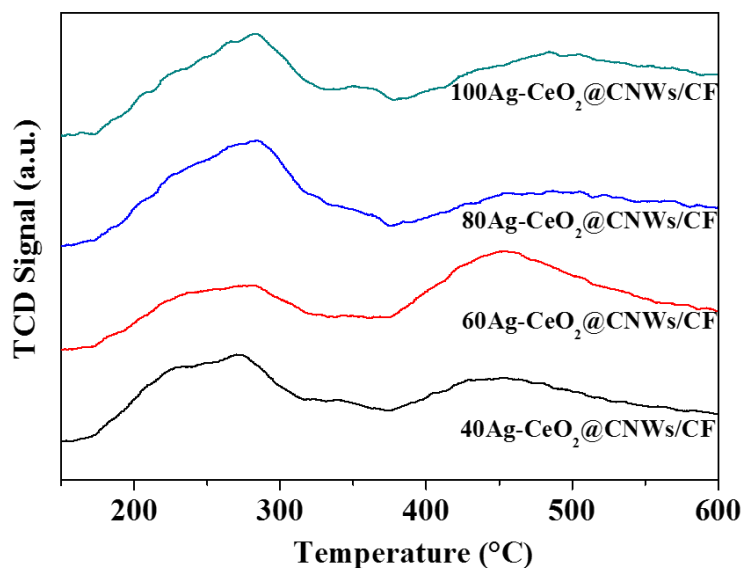


Fig. 4.10. NH₃-TPD profiles of the prepared Ag-CeO₂@CNWs/CF catalysts.

4.3.5 Catalytic performance

Catalytic performances of Ag-CeO₂@CNWs/CF catalysts with different Ag loading amounts for the catalytic oxidation of toluene was evaluated in a traditional fixed bed reactor with a testing temperature range of 150-320 °C, in which the temperatures of T₁₀, T₅₀, and T₉₀ corresponding to the toluene conversions of 10%, 50%, 90%, respectively were used, and the results are shown in **Fig. 4.11** and summarized in **Table 4.4**. As shown in **Fig. 4.11a**, the toluene conversion increased gradually with the increasing of reaction temperature, it can be clearly seen that the conversion temperature of toluene (T₉₀) decreased significantly as the following order: 40 Ag-CeO₂@CNWs/CF > 60 Ag-CeO₂@CNWs/CF > 80 Ag-CeO₂@CNWs/CF, in which the T₉₀ decreased around 33°C when the electrodeposition time increased from 40 to 80s, consequently, the catalytic performance of Ag-CeO₂@CNWs catalysts was significantly improved by the highly dispersed Ag nanoparticles.

However, with the further increase in the Ag loading amount (e.g., for 100Ag-CeO₂@CNWs/CF), T₉₀ was increased. As a result, the 80Ag-CeO₂@CNWs/CF catalyst performed the best catalytic activity, which possessed the lowest T₁₀, T₅₀ and T₉₀ of 222, 240 and 256 °C, respectively for the toluene catalytic oxidation (**Table 5.4**). Additionally, for comparison, the catalytic performance of 3.7wt%Ag-CeO₂@CNWs/CF (Here, the 3.7wt%Ag loading amount was the same as that in 80Ag-CeO₂@CNWs/CF) catalyst prepared using the wet impregnation method was also investigated and the corresponding results are shown in **Fig. 4.12**. Obviously, higher T₅₀ and T₉₀ values of 258 and 270 °C were obtained, respectively, for this catalyst. As shown in **Fig. 4.13**, 3.7wt%Ag-CeO₂@CNWs/CF had a random structure with uneven Ag particle distribution. Thus, the electrodeposition method using in this study should be a promising way to prepare high-performance VOC oxidation catalysts.

The selectivity of CO₂ over 80Ag-CeO₂@CNWs/CF catalyst for the catalytic oxidation of toluene was displayed in **Fig. 4.14**, which showed the similar increased trend as the toluene conversion depicted in **Fig. 4.11a** when the set reaction temperature varied from 150 to 320 °C. The process of toluene catalytic oxidation is the commonly benzoate route, which involves the formation of intermediate products derived from toluene and ended with the formation of CO₂ [47]. As it reported by Luo *et al.* [48] and Chen *et al.* [49] that byproducts such as benzaldehyde, benzoic acid, or maleic anhydride were produced at a relatively low temperature with incomplete toluene oxidation when toluene catalytic oxidation occurred over MOF (metal organic frameworks)-Mn1Co1 catalyst and Pt@M-Cr₂O₃ (Pt-loaded mesoporous Cr₂O₃) catalyst. Consequently, the selectivity of CO₂ in **Fig. 4.14** was lower than 100% at the low temperature range might be caused by the production of byproducts within the liquid phase, while it maintained around 100% at relatively high temperatures as a result of the complete conversion of toluene.

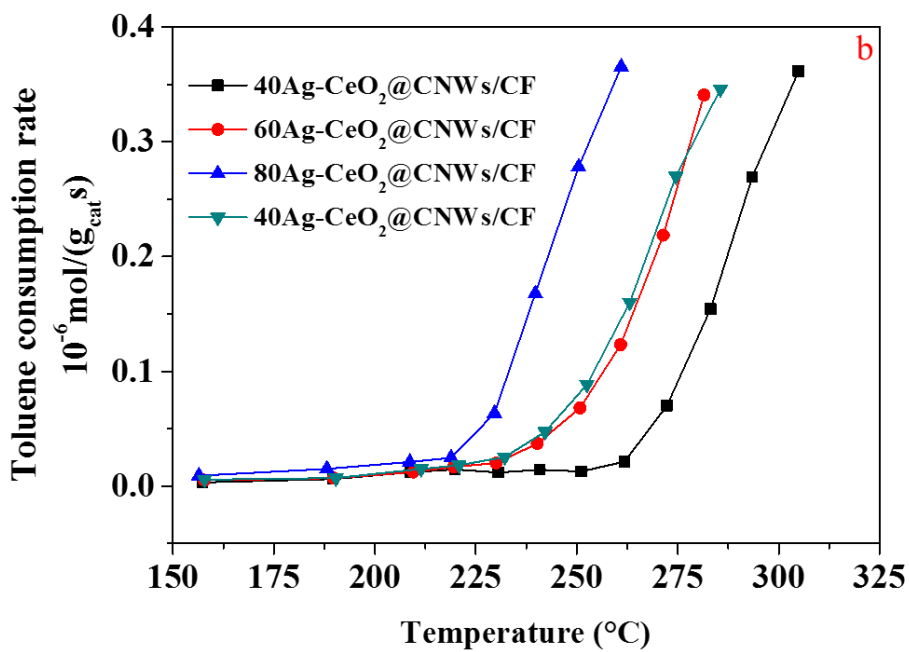
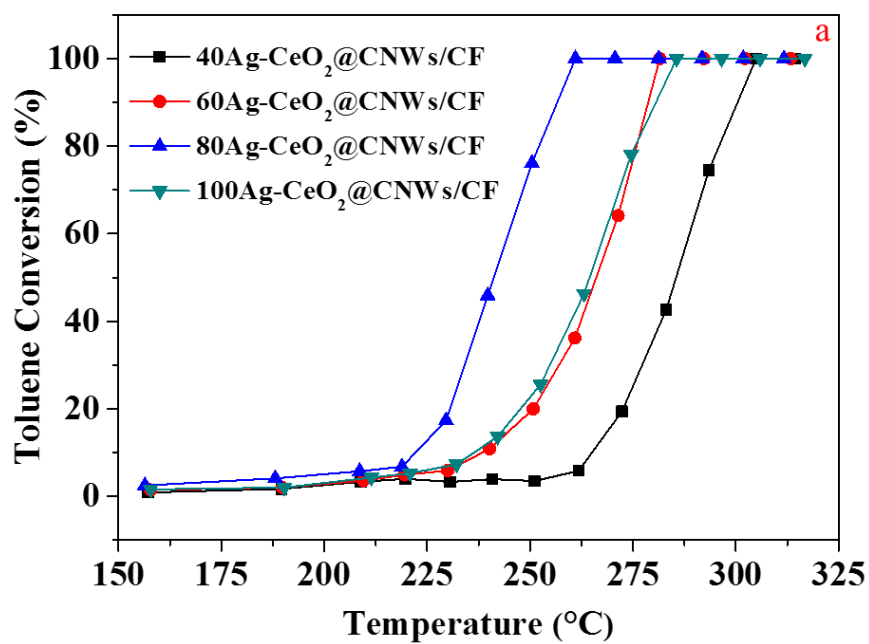
Fig. 4.11b shows the toluene consumption rate over the prepared catalysts. It can be seen that the toluene consumption rate over 80Ag-CeO₂@CNWs/CF was around 6.33×10^{-8} mol/(g_{cat} s)) at 229 °C, which was the highest value among all the prepared Ag-CeO₂@CNWs/CF catalysts. Based on the

kinetics studies, the catalytic oxidation of toluene should obey the first-order kinetics mechanism under the excess oxygen atmosphere with the following equation [49]:

$$r = -kc = [-A \exp(-\frac{E_a}{RT})]c \quad (4.4)$$

where r , k , c , A and E_a are the reaction rate ($\mu\text{mol}/(\text{g s})$), rate constant (s^{-1}), toluene concentration (mol), pre-exponential factor and apparent activation energy (kJ/mol), respectively. Herein, the Arrhenius plots for catalytic oxidation of toluene was obtained with the toluene conversion less than 20% since the phase change or material migration could be avoided in this condition. As shown in **Fig. 4.11c** and **Table 4.4**, the E_a value over Ag-CeO₂@CNWs/CF catalysts decreased in the order of 40Ag-CeO₂@CNWs/CF > 100Ag-CeO₂@CNWs/CF > 60Ag-CeO₂@CNWs/CF > 80Ag-CeO₂@CNWs/CF. As a result, the 80Ag-CeO₂@CNWs/CF catalyst possessed the lowest E_a of 29.66 (kJ/mol) and performed the best catalytic activity in the catalytic oxidation of toluene.

As stated above, the catalytic performance is always related to the physiochemical properties of the catalyst. Herein, from the SEM and HRTEM characterizations, the CeO₂ was uniformly coated on the CNWs of CF, and thereafter, the Ag nanoparticles with three different active crystal planes were highly dispersed on the surface of CeO₂. As indicated above, the redox property of the catalyst was greatly enhanced. Especially, the low-temperature reducibility was effectively improved and the amounts of oxygen vacancies and active Ce³⁺ species were significantly increased by the loading of Ag species using the electrodeposition method. As a result, when the electrodeposition time was 80 s, namely, the 80Ag-CeO₂@CNWs/CF catalyst exhibited the highest catalytic activity due to its good reducibility, high concentration surface oxygen species and the optimum Ag loading amount with nanoparticle size as well as highly dispersion.



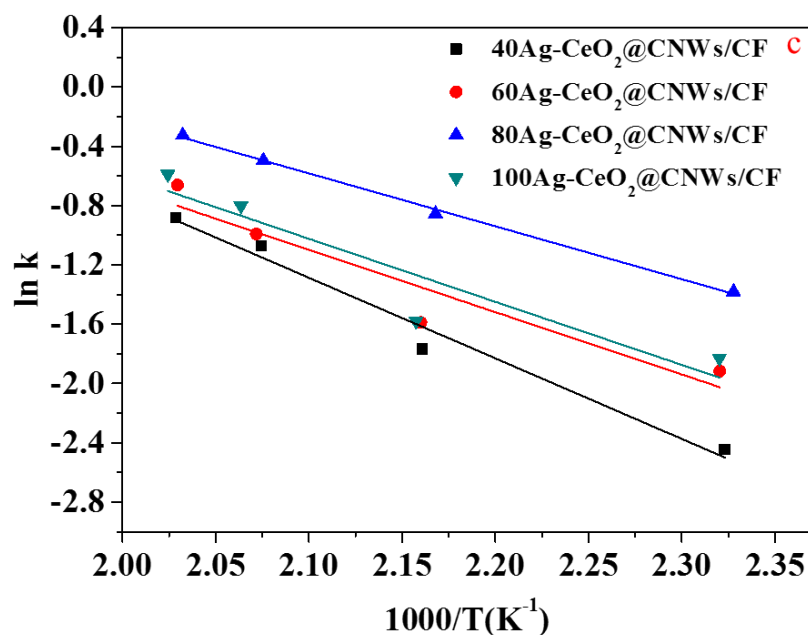


Fig. 4.11. (a) Toluene conversion, (b) toluene consumption rate per gram of catalyst and (c) Arrhenius plots of the prepared Ag-CeO₂@CNWs/CF catalysts for catalytic oxidation of toluene.

Table 4.4 Summary of the results on the catalytic oxidation of toluene over the prepared Ag-CeO₂@CNWs/CF catalysts.

Sample	Toluene conversion (°C)			Ideal CO ₂ concentration (V ^a _{CO2} /V _{N2} , %)	Actual CO ₂ concentration (V ^b _{CO2} /V _{N2} , %)	Ea(kJ/mol)
	T ₁₀	T ₅₀	T ₉₀			
40Ag-CeO ₂ @CNWs/CF	250	277	289	0.745	0.747	45.19
60Ag-CeO ₂ @CNWs/CF	238	266	278	0.758	0.789	34.95
80Ag-CeO ₂ @CNWs/CF	222	240	256	0.804	0.827	29.66
100Ag-CeO ₂ @CNWs/CF	236	264	280	0.793	0.809	35.37

V^a_{CO2}, the flow rate of the ideal produced CO₂;

V^b_{CO2}, the flow rate of the actual produced CO₂;

V_{N2}, the flow rate of N₂ as balance gas for reaction.

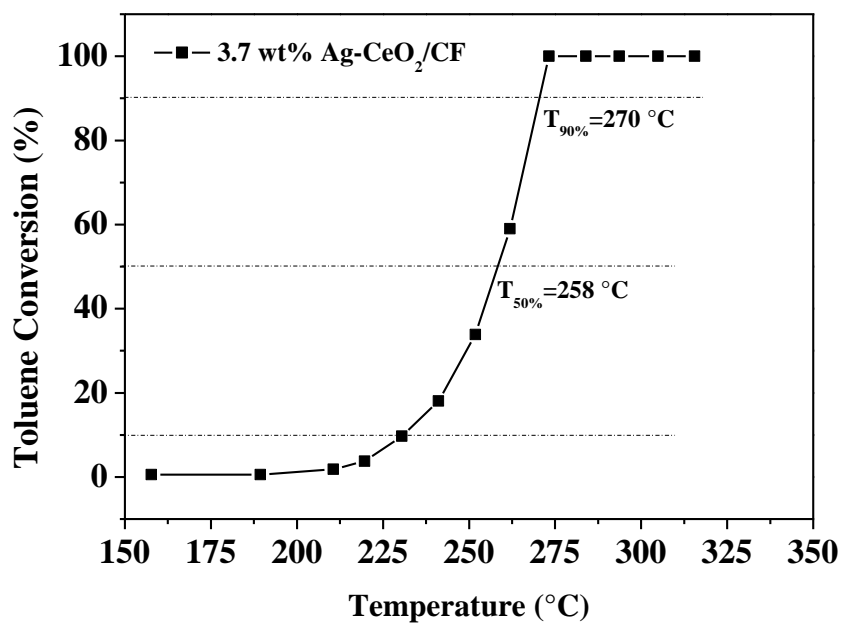


Fig. 4.12. Catalytic activity of 3.7wt% Ag-CeO₂@CNWs/CF catalyst prepared by a wet impregnation method for catalytic oxidation of toluene.

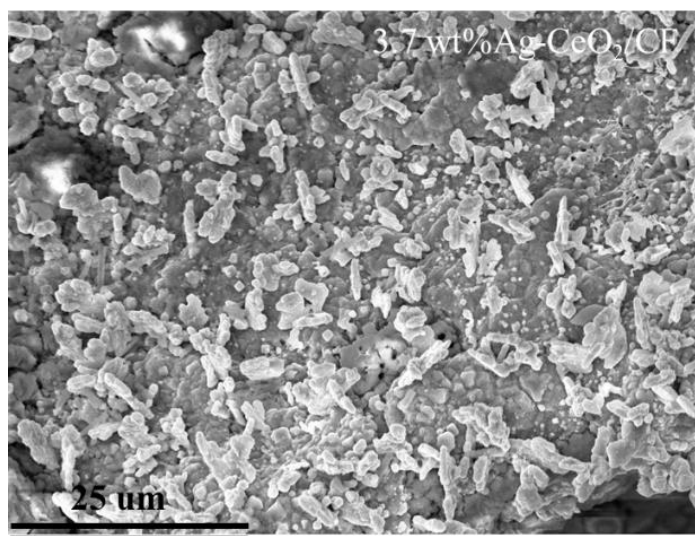


Fig. 4.13. SEM image of 3.7wt% Ag-CeO₂@CNWs/CF catalyst prepared by a wet impregnation method.

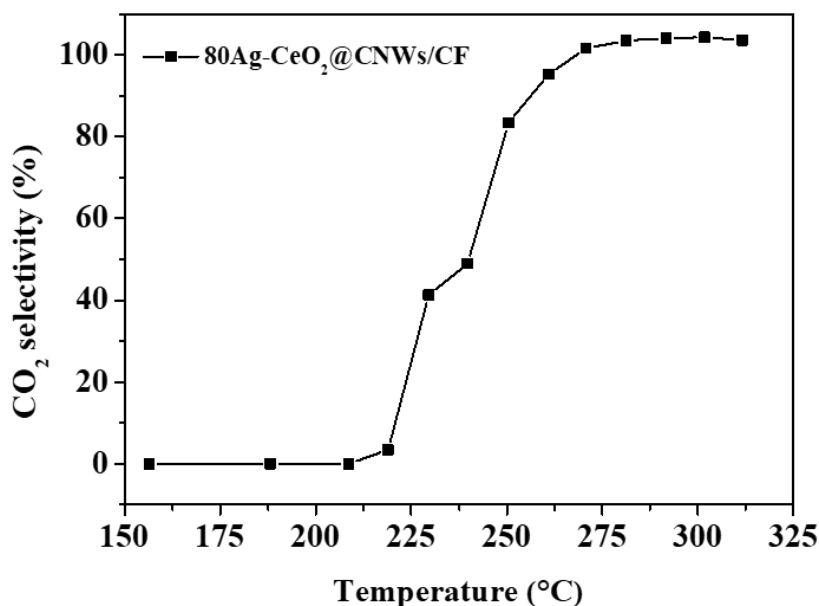


Fig. 4.14. CO₂ selectivity of 80Ag-CeO₂@CNWs/CF for the catalytic oxidation of toluene.

4.3.6 Stability

The stability of 80Ag-CeO₂@CNWs/CF catalyst was further evaluated in the absence and presence of water vapor. As shown in **Fig. 4.15**, the toluene conversion maintained at 100 % in the first 1113 min period. Then, as 5 vol% water vapor was introduced into the reactor together with the gas flow, the conversion was slightly decreased to 90% but almost retained at this value until the water vapor introduction was cut off. Herein, the decrease of toluene conversion should be resulted from the competition between toluene and water molecules contacting with the active sites of the catalysts. However, as the introduction of water vapor was stopped, the catalytic activity was also recovered so that the toluene conversion returned to the original level of 100%. Importantly, it is observed that the catalytic activity for the toluene conversion always maintained in a certain value with or without water vapor introduction, indicating that the 80Ag-CeO₂@CNWs/CF catalyst possessed excellent stability and water resistance ability. Moreover, the stability of this catalyst with a lower toluene conversion in the absence of water vapor was also tested. As shown in **Fig. 4.16**, there was no significant decrease in the toluene conversion during the long-term test in the absence of water. Furthermore, as discussed in the above, combining the XPS analysis results of Ce 3d and O1s, the values of $\text{Ce}^{3+}/(\text{Ce}^{3+} + \text{Ce}^{4+})$ and $\text{O}_{\text{sur}}/\text{O}_{\text{lat}}$ on the spent 80Ag-CeO₂@CNWs/CF catalyst, it is

also found that they were maintained almost unchanged with compared with the fresh one (**Table 4.3**). Therefore, the 80Ag-CeO₂@CNWs/CF should be a promising catalyst for the catalytic oxidation of VOCs.

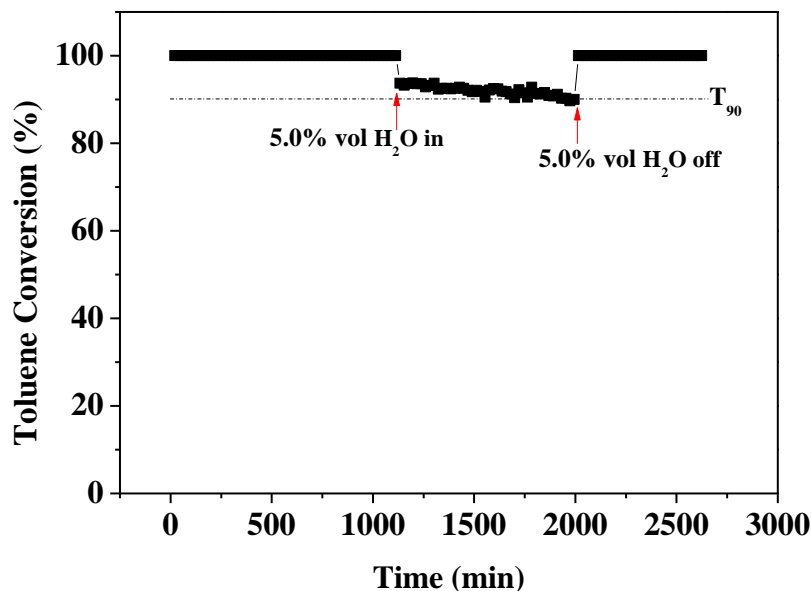


Fig. 4.15. Long-term on-stream evaluation of 80Ag-CeO₂@CNWs/CF catalyst for the catalytic oxidation of toluene in the presence and absence of water vapor (Reaction conditions: toluene concentration = 961 ppm, WHSV=30,000 mL g⁻¹ h⁻¹, reaction temperature=280 °C, reaction time=2625 min).

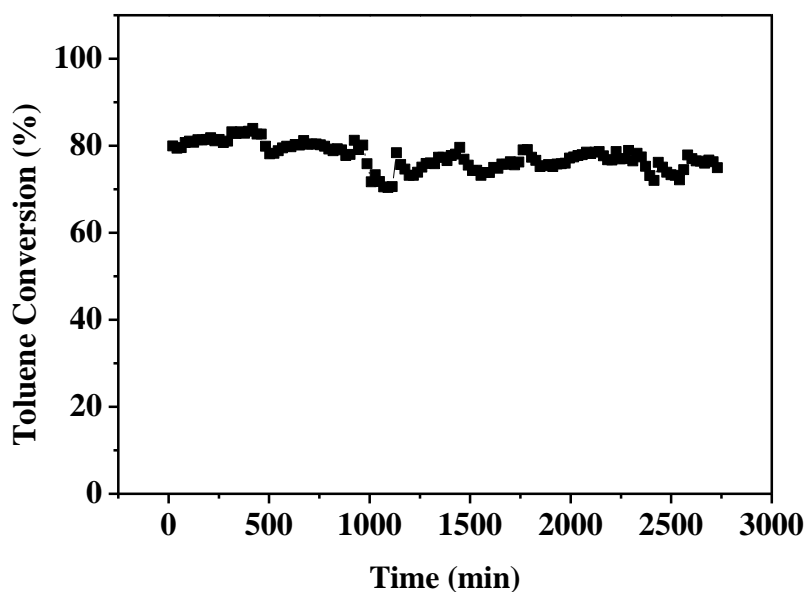


Fig. 4.16. Stability test of 80Ag-CeO₂@CNWs/CF catalyst for the catalytic oxidation of toluene in the

absence of water vapor with a lower toluene conversion (Reaction conditions: toluene concentration = 961 ppm, WHSV=30,000 mL g⁻¹ h⁻¹, reaction temperature = 257 °C, reaction time=2730 min).

4.4 Conclusions

In summary, Ag-CeO₂@CNWs/CF catalysts with highly dispersed Ag nanoparticles were successfully prepared by a three-step electrochemical process, which showed high activity and stability for the catalytic oxidation of toluene. It is found that CeO₂ can be uniformly coated along with the Cu nanowires (CNWs) on Cu foam, and then the active Ag nanoparticles with different active crystal planes can be further highly dispersed on the CeO₂ surface by using the electrodeposition method. The suitable Ag loading amount effectively enhanced the low-temperature reducibility, the generation of oxygen vacancies, and distribution of surface acid sites, which are favorable to the catalytic oxidation of toluene. When the electrodeposition time for the Ag loading was 80 s, the obtained 80Ag-CeO₂@CNWs/CF catalyst exhibited the high concentration ratios of Ce³⁺/ (Ce³⁺ +Ce⁴⁺) and O_{sur}/O_{latt} of 0.336 and 0.519, respectively. As a result, the 80Ag-CeO₂@CNWs/CF achieved the best catalytic activity with the T₁₀, T₅₀ and T₉₀ of toluene conversions at 222, 240 and 256 °C, respectively, which were much lower than those of 3.7wt%Ag-CeO₂@CNWs/CF catalyst prepared by a general wet impregnation method. Long-term stability tests in the presence and absence of water vapor further indicated that the 80Ag-CeO₂@CNWs/CF catalyst had good stability and water resistance ability during the catalytic oxidation of VOCs. It is expected that the present electrodeposition method could be a promising way to prepare high-performance catalysts for the catalytic oxidation of VOCs.

References

- [1] M. Ma, H. Huang, C. Chen, Q. Zhu, L. Yue, R. Albilali, C. He, Highly active SBA-15-confined Pd catalyst with short rod-like micro-mesoporous hybrid nanostructure for n-butylamine low-temperature destruction, *Molecular Catalysis*. 455 (2018) 192-203.
- [2] X. Wang, L. Ran, Y. Dai, Y. Lu, Q. Dai, Removal of Cl adsorbed on Mn-Ce-La solid solution catalysts during CVOC combustion, *Journal of Colloid Interface Science*. 426 (2014) 324-332.
- [3] L. Deng, Y. Ding, B. Duan, Y. Chen, P. Li, S. Zhu, S. Shen, Catalytic deep combustion characteristics of benzene over cobalt doped Mn-Ce solid solution catalysts at lower temperatures, *Molecular Catalysis*. 446 (2018) 72-80.
- [4] J. Kujawa, S. Cerneaux, W. Kujawski, Removal of hazardous volatile organic compounds from water by vacuum pervaporation with hydrophobic ceramic membranes, *Journal of Membrane Science*. 474 (2015) 11-19.
- [5] M.S. Kamal, S.A. Razzak, M.M. Hossain, Catalytic oxidation of volatile organic compounds (VOCs)-A review, *Atmospheric Environment*. 140 (2016) 117-134.
- [6] T. Odoom-Wubah, Q. Li, Q. Wang, M.Z.R. Usha, J. Huang, Q. Li, Template-free synthesis of carbon self-doped ZnO superstructures as efficient support for ultra fine Pd nanoparticles and their catalytic activity towards benzene oxidation, *Molecular Catalysis*. 469 (2019) 118-130.
- [7] A.S. Poyraz, S. Biswas, H.C. Genuino, S. Dharmarathna, C.H. Kuo, S.L. Suib, Bimodification of mesoporous silicon oxide by coupled “In situ oxidation at the interface and ion exchange” and its catalytic activity in the gas-phase toluene oxidation, *ChemCatChem*. 5 (2013) 920-930.
- [8] S. Irusta, M. Pina, M. Menéndez, J. Santamaria, Catalytic combustion of volatile organic compounds over La-based perovskites, *Journal of Catalysis*. 179 (1998) 400-412.
- [9] J.-M. Giraudon, A. Elhachimi, F. Wyrwalski, S. Siffert, A. Aboukais, J.-F. Lamonier, G. Leclercq, Studies of the activation process over Pd perovskite-type oxides used for catalytic oxidation of toluene, *Applied Catalysis B-Environmental*. 75 (2007) 157-166.
- [10] C. He, Y. Yu, C. Chen, L. Yue, N. Qiao, Q. Shen, J. Chen, Z. Hao, Facile preparation of 3D

ordered mesoporous $\text{CuO}_x\text{-CeO}_2$ with notably enhanced efficiency for the low temperature oxidation of heteroatom-containing volatile organic compounds, *RSC Advances*. 3 (2013) 19639-19656.

[11] H. Huang, Y. Xu, Q. Feng, D.Y. Leung, Low temperature catalytic oxidation of volatile organic compounds: a review, *Catalysis Science & Technology*. 5 (2015) 2649-2669.

[12] J.-H. Park, B. Kim, C.-H. Shin, G. Seo, S.H. Kim, S.B. Hong, Methane combustion over Pd catalysts loaded on medium and large pore zeolites, *Topics in Catalysis*. 52 (2009) 27-34.

[13] J. Bassil, A. AlBarazi, P. Da Costa, M. Boutros, Catalytic combustion of methane over mesoporous silica supported palladium, *Catalysis Today* 176 (2011) 36-40.

[14] T. Masui, H. Imadzu, N. Matsuyama, N. Imanaka, Total oxidation of toluene on $\text{Pt/CeO}_2\text{-ZrO}_2\text{-Bi}_2\text{O}_3/\gamma\text{-Al}_2\text{O}_3$ catalysts prepared in the presence of polyvinyl pyrrolidone, *Journal of Hazardous Materials*. 176 (2010) 1106-1109.

[15] J.-H. Park, J.H. Cho, Y.J. Kim, E.S. Kim, H.S. Han, C.-H. Shin, Hydrothermal stability of Pd/ZrO_2 catalysts for high temperature methane combustion, *Applied Catalysis B-Environmental*. 160 (2014) 135-143.

[16] M. Cargnello, V.V. Doan-Nguyen, T.R. Gordon, R.E. Diaz, E.A. Stach, R.J. Gorte, P. Fornasiero, C.B. Murray, Control of metal nanocrystal size reveals metal-support interface role for ceria catalysts, *Science*. 341 (2013) 771-773.

[17] M. Hoffmann, S. Kreft, G. Georgi, G. Fulda, M.-M. Pohl, D. Seeburg, C. Berger-Karin, E.V. Kondratenko, S. Wohlrab, Improved catalytic methane combustion of Pd/CeO_2 catalysts via porous glass integration, *Applied Catalysis B-Environmental*. 179 (2015) 313-320.

[18] S. Aouad, E. Abi-Aad, A. Aboukaïs, Simultaneous oxidation of carbon black and volatile organic compounds over Ru/CeO_2 catalysts, *Applied Catalysis B-Environmental: Environ*. 88 (2009) 249-256.

[19] L. Jinwei, L. Weibin, Effect of preparation method on the catalytic activity of Au/CeO_2 for VOCs oxidation, *Journal of Rare Earths* 28 (2010) 547-551.

[20] Y. Qin, X. Liu, T. Zhu, T. Zhu, Catalytic oxidation of ethyl acetate over silver catalysts

- supported on CeO₂ with different morphologies, *Materials Chemistry and Physics*. 229 (2019) 32-38.
- [21] S. Woo, I. Kim, J.K. Lee, S. Bong, J. Lee, H. Kim, Preparation of cost-effective Pt-Co electrodes by pulse electrodeposition for PEMFC electrocatalysts, *Electrochimica Acta* 56 (2011) 3036-3041.
- [22] R. Peng, S. Li, X. Sun, Q. Ren, L. Chen, M. Fu, J. Wu, D. Ye, Size effect of Pt nanoparticles on the catalytic oxidation of toluene over Pt/CeO₂ catalysts, *Applied Catalysis B-Environmental*. 220 (2018) 462-470.
- [23] Y. Guo, Y. Gao, X. Li, G. Zhuang, K. Wang, Y. Zheng, D. Sun, J. Huang, Q. Li, Catalytic benzene oxidation by biogenic Pd nanoparticles over 3D-ordered mesoporous CeO₂, *Chemical Engineering Journal*. 362 (2019) 41-52.
- [24] N. Mikheeva, V. Zaikovskii, G. Mamontov, The effect of Ag and CeO₂ distribution on SBA-15 surface on the activity of Ag-CeO₂/SBA-15 catalysts in CO and methanol oxidation, *Journal of Sol-gel Science and Technology*. 92 (2019) 398-407.
- [25] J.M. López, A.L. Gilbank, T. García, B. Solsona, S. Agouram, L. Torrente-Murciano, The prevalence of surface oxygen vacancies over the mobility of bulk oxygen in nanostructured ceria for the total toluene oxidation, *Applied Catalysis B-Environmental*. 174 (2015) 403-412.
- [26] X. Wu, H. Yu, D. Weng, S. Liu, J. Fan, Synergistic effect between MnO and CeO₂ in the physical mixture: Electronic interaction and NO oxidation activity, *Journal of Rare Earths*. 31 (2013) 1141-1147.
- [27] Z. Fu, L. Liu, Y. Song, Q. Ye, S. Cheng, T. Kang, H. Dai, Catalytic oxidation of carbon monoxide, toluene, and ethyl acetate over the xPd/OMS-2 catalysts: Effect of Pd loading, *Frontiers of Chemical Science and Engineering*. 11 (2017) 185-196.
- [28] F. Hu, J. Chen, S. Zhao, K. Li, W. Si, H. Song, J. Li, Toluene catalytic combustion over copper modified Mn_{0.5}Ce_{0.5}O_x solid solution sponge-like structures, *Applied Catalysis A-General*. 540 (2017) 57-67.
- [29] D. Li, W. Li, Y. Deng, X. Wu, N. Han, Y. Chen, Effective Ti doping of δ -MnO₂ via anion route

for highly active catalytic combustion of benzene, *The Journal of Physical Chemistry C*. 120 (2016) 10275-10282.

[30] Z. Ye, J.-M. Giraudon, N. Nuns, P. Simon, N. De Geyter, R. Morent, J.-F. Lamonier, Influence of the preparation method on the activity of copper-manganese oxides for toluene total oxidation, *Applied Catalysis B-Environmental*. 223 (2018) 154-166.

[31] Z. Hu, S. Qiu, Y. You, Y. Guo, Y. Guo, L. Wang, W. Zhan, G. Lu, Hydrothermal synthesis of NiCeO_x nanosheets and its application to the total oxidation of propane, *Applied Catalysis B-Environmental*. 225 (2018) 110-120.

[32] P. Li, C. He, J. Cheng, C.Y. Ma, B.J. Dou, Z.P. Hao, Catalytic oxidation of toluene over $\text{Pd/Co}_3\text{AlO}$ catalysts derived from hydrotalcite-like compounds: Effects of preparation methods, *Applied Catalysis B-Environmental*. 101 (2011) 570-579.

[33] X. Chen, X. Chen, E. Yu, S. Cai, H. Jia, J. Chen, P. Liang, In situ pyrolysis of Ce-MOF to prepare CeO_2 catalyst with obviously improved catalytic performance for toluene combustion, *Chemical Engineering Journal*. 344 (2018) 469-479.

[34] Y. Huang, K. Ye, H. Li, W. Fan, F. Zhao, Y. Zhang, H. Ji, A highly durable catalyst based on $\text{Co}_x\text{Mn}_{3-x}\text{O}_4$ nanosheets for low-temperature formaldehyde oxidation, *Nano Research*. 9 (2016) 3881-3892.

[35] R. Peng, X. Sun, S. Li, L. Chen, M. Fu, J. Wu, D. Ye, Shape effect of Pt/CeO_2 catalysts on the catalytic oxidation of toluene, *Chemical Engineering Journal*. 306 (2016) 1234-1246.

[36] M. Romeo, K. Bak, J. El Fallah, F. Le Normand, L. Hilaire, XPS study of the reduction of cerium dioxide, *Surface and Interface Analysis*. 20 (1993) 508-512.

[37] P. Citrin, G. Wertheim, Y. Baer, Surface-atom X-ray photoemission from clean metals: Cu, Ag, and Au, *Physical Review B*. 27 (1983) 3160.

[38] B. Xin, L. Jing, Z. Ren, B. Wang, H. Fu, Effects of simultaneously doped and deposited Ag on the photocatalytic activity and surface states of TiO_2 , *The Journal of Physical Chemistry B*. 109 (2005) 2805-2809.

- [39] J. Li, Z. Qu, Y. Qin, H. Wang, Effect of MnO₂ morphology on the catalytic oxidation of toluene over Ag/MnO₂ catalysts, *Applied Surface Science*. 385 (2016) 234-240.
- [40] H. Yang, J. Deng, Y. Liu, S. Xie, Z. Wu, H. Dai, Preparation and catalytic performance of Ag, Au, Pd or Pt nanoparticles supported on 3DOM CeO₂-Al₂O₃ for toluene oxidation, *Journal of Molecular Catalysis: Chemical A*. 414 (2016) 9-18.
- [41] Y. Wang, J.-M. Zheng, K. Fan, W.-L. Dai, One-pot solvent-free synthesis of sodium benzoate from the oxidation of benzyl alcohol over novel efficient AuAg/TiO₂ catalysts, *Green Chemistry*. 13 (2011) 1644-1647.
- [42] K. Jiráťová, J. Mikulová, J. Klempa, T. Grygar, Z. Bastl, F. Kovanda, Modification of Co-Mn-Al mixed oxide with potassium and its effect on deep oxidation of VOC, *Applied Catalysis A-General*. 361 (2009) 106-116.
- [43] S. Xie, J. Deng, S. Zang, H. Yang, G. Guo, H. Arandian, H. Dai, Au-Pd/3DOM Co₃O₄: Highly active and stable nanocatalysts for toluene oxidation, *Journal of Catalysis*. 322 (2015) 38-48.
- [44] G. Gao, J.-W. Shi, C. Liu, C. Gao, Z. Fan, C. Niu, Mn/CeO₂ catalysts for SCR of NO_x with NH₃: comparative study on the effect of supports on low-temperature catalytic activity, *Applied Surface Science*. 411 (2017) 338-346.
- [45] B. de Rivas, R. López-Fonseca, C. Jiménez-González, J.I. Gutiérrez-Ortiz, Synthesis, characterisation and catalytic performance of nanocrystalline Co₃O₄ for gas-phase chlorinated VOC abatement, *Journal of Catalysis*. 281 (2011) 88-97.
- [46] M. Piumetti, D. Fino, N. Russo, Mesoporous manganese oxides prepared by solution combustion synthesis as catalysts for the total oxidation of VOCs, *Applied Catalysis B-Environmental*. 163 (2015) 277-287.
- [47] K. Li, J. Chen, B. Bai, S. Zhao, F. Hu, J. Li, Bridging the reaction route of toluene total oxidation and the structure of ordered mesoporous Co₃O₄: the roles of surface sodium and adsorbed oxygen, *Catalysis Today*. 297 (2017) 173-181.
- [48] Y. Luo, Y. Zheng, J. Zuo, X. Feng, X. Wang, T. Zhang, K. Zhang, L. Jiang, Insights into the high

performance of Mn-Co oxides derived from metalorganic frameworks for total toluene oxidation, *Journal of Hazardous Materials*. 349 (2018) 119-127.

[49] X. Chen, S. Cai, J. Chen, W. Xu, H. Jia, J. Chen, Catalytic combustion of toluene over mesoporous Cr₂O₃-supported platinum catalysts prepared by in situ pyrolysis of MOFs. *Chemical Engineering Journal*. 334 (2018) 768-779.

CHAPTER 5 Mn-Co oxide decorated on Cu nanowires as efficient catalysts for catalytic oxidation of toluene

5.1 Introduction

Emission of volatile organic compounds (VOCs) to the atmosphere from human activities could cause photochemical smog and threaten our health and environment [1-3]. Accordingly, it is necessary to avoid the emission of VOCs from the sources of the industrial activities. Nowadays, various techniques have been developed to remove VOCs. Among them, catalytic oxidation is considered one of the most effective and economical ways, in which VOCs can be completely converted into harmless substances of CO₂ and H₂O at relatively low temperatures [4-6]. Generally, two types of catalysts, i.e., noble metal based catalysts and transition metal oxide based catalysts, are applied [7], and the latter is more attractive and widely used than the former as a result of the low cost and comparable catalytic activity as the former [8, 9].

Manganese oxides (e.g., MnO₂, Mn₂O₃, Mn₃O₄) have been extensively investigated as the promising catalysts for the catalytic oxidation of VOCs [10-12]. It is found that the morphology of manganese oxide could affect its activity. Hence, various morphologies such as wire, rod, tube and flower-like manganese oxides have been controllably synthesized using different ways including hydrothermal, impregnation, solvothermal, and electrodeposition methods [13-16]. For instance, Cheng *et al.* prepared α -MnO₂ catalysts with the special structures of nanorod, nanowire and microsphere by the widely used hydrothermal synthesis method with different synthesis temperatures and reaction times, and used for the catalytic combustion of dimethyl ether [17]. It is found that the α -MnO₂ with a nanorod shape presented better catalytic performance than other shapes. Meanwhile, manganese oxide can be combined with other oxides to enhance its activity. For instance, Zhang *et al.* confined MnO₂ nanoparticles into TiO₂ nanotubes by the vacuum-assisted impregnation method [18], and found that the confinement effect of TiO₂ nanotube enhanced the formation and migration of the active oxygen species, and therefore improved the catalytic performance of the prepared catalyst in

the catalytic oxidation of butane. In addition, doping foreign elements on the manganese oxide could also improve its catalytic performance. For instance, Zhao *et al.* prepared Co-Mn catalysts with double-shelled nanocages by a template-engaged strategy for the combustion of toluene, and found that the mixed metal oxides of Co-Mn performed better catalytic activity than that of single metal oxide of Co_3O_4 , which was contributed by the improved oxygen mobility, low-temperature toluene desorption and active Co^{3+} sites of the catalysts[19]. It is similar to the result reported by Li *et al* [20]. To date, in addition to Mn-Co, many other mixed metal oxides such as Cu-Ce, Ni-Ce, Ce-Mn and Mn-Cr are also widely applied as efficient catalysts due to their high activity for the catalytic oxidation of VOCs [21-24].

Besides, catalyst support could play an important role in the improvement of the catalytic performance [25, 26]. For instance, Huang *et al.* fabricated $\text{Co}_x\text{Mn}_{3-x}\text{O}_4$ nanosheets on carbon textile support, which showed excellent catalytic activity and stability for the complete oxidation of HCHO to CO_2 at a temperature as low as 100 °C [16]. Li *et al.* supported the Mn-Ce mixed oxides on silica spheres and applied for the deep oxidation of benzene [27]. The optimum catalyst achieved T_{90} (90% conversion) at 216 °C due to its large surface area, well dispersion of active sites, low reducibility and rich surface active species. Especially, the silica spheres provided *in-situ* sites for the decomposition of Mn-Ce precursor, therefore improved the distribution of active components. Thus, the selection of catalyst support is extremely crucial for the design of effective catalysts.

In this study, Mn-Co mixed oxides were deposited on the Cu nanowires, which were *in-situ* generated on the Cu foam (CF), by using a unipolar pulse electro-deposition (UPED) method and applied for the catalytic oxidation of toluene. The influence of Mn/Co molar ratio in the Mn-Co/CF catalyst on its physicochemical properties was investigated and characterized by scanning electron microscopy (SEM), transmission electron microscopy (TEM), X-ray diffraction (XRD), hydrogen temperature-programmed reduction (H_2 -TPR), oxygen temperature-programmed desorption (O_2 -TPD) and X-ray photoelectron spectroscopy (XPS) analyses. The catalytic performance was evaluated in a continuous flow fixed-bed reactor with a dilute toluene gas flow at the atmospheric

pressure, and the catalytic stability was tested in the presence and absence of water vapor. It is expected to obtain a catalyst which can work at a low temperature for complete removal of VOC from the emission gas.

5.2 Experimental

5.2.1 Chemicals and Materials

Hydrochloric acid (HCl), manganese and cobalt nitrate hydrates ($\text{Mn}(\text{NO}_3)_2 \cdot 6\text{H}_2\text{O}$ and $\text{Co}(\text{NO}_3)_2 \cdot 6\text{H}_2\text{O}$, Wako, Japan) were used without any further treatment. Cu foam (CF, thickness: 1.6 mm, bulk density: 0.45 g/cm^3 ; number of pores per inch: 90) was provided by MTI, Japan, and used as the catalyst support after the generation of Cu nanowires on the surface. It was cut into small pieces ($1.5 \text{ cm} \times 1.5 \text{ cm}$), then successively treated in 1 M HCl solution and distilled water (H_2O) for 10 min with the assistance of ultrasound. Finally, the cleaned CF was washed completely and sealed in water prior to use.

To generate Cu nanowires on the surface of CF, it was electro-oxidized as following: CF ($1.5 \text{ cm} \times 1.5 \text{ cm}$) was put into 50 mL of KOH solution and oxidized by using the galvanostatic method with an applied current of 40 mA for 1200 s, by which the reaction as Eq. (5.1) occurred. After the electro-oxidation, Cu foam was washed with distilled water and dried. As shown in **Fig. 5.1**, homogeneous nanowire arrays were formed on the surface of Cu foam.

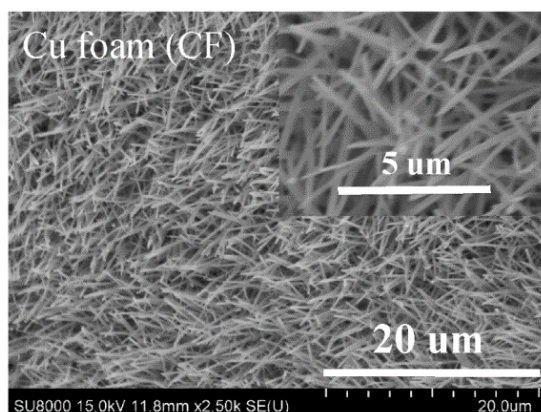
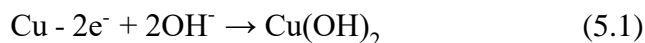


Fig. 5.1. SEM images of Cu foam (CF) possesses nanowires after electro-oxidation.

5.2.2 Electrodeposition of Mn-Co mixed metal oxides

Mn-Co mixed metal oxides with different Mn/Co molar ratios were separately electrodeposited on the Cu nanowires of the CF at room temperature by using the unipolar pulse electro-deposition (UPED) method at a constant potential of -1.0 V, on/off time of 1.0 s, and pulse cycles of 1000. Platinum wire (ALS, Japan), Ag/AgCl/saturated KCl electrode (ALS, Japan) and the oxidized substrate of CF with the Cu nanowires were used as the counter, reference and working electrodes, respectively. The molar concentration ratios of Mn (NO₃)₂·6H₂O and Co (NO₃)₃·6H₂O were 0.10M:0.01M, 0.05M:0.01M, 0.01M:0.01M (corresponding to the Mn/Co molar ratios of 10:1, 5:1 and 1:1), respectively. The total solution volume of each sample was 100 mL. The obtained samples were thoroughly washed with distilled water, vacuum-dried at 100 °C for overnight, and calcined at 350 °C in a muffle furnace for 2 h with a heating rate of 5 °C/min. Finally, the achieved Mn-Co mixed metal oxide covered on the Cu nanowires of CF are designated as 0.10Mn-0.01Co/CF, 0.05Mn-0.01Co/CF and 0.01Mn-0.01Co/CF, respectively. Single metal based catalysts of 0.01Co/CF and 0.10Mn/CF were prepared using the same method with pure solutions of 0.01 M Co(NO₃)₂·6H₂O and 0.10 Mn(NO₃)₂·6H₂O, respectively. For comparison, bare Cu foam with nanowires and 0.10Mn-0.01Co/NF catalyst prepared by using nickel foam (NF) support were also prepared.

5.2.3 Characterizations

Morphology and elemental distribution were obtained on a scanning electron microscopy (SEM, SU8010, Hitachi, Japan) with an energy dispersive X-ray detector (EDS, Horiba Scientific) and the nanostructures were observed by a transmission electron microscope (TEM, JEM-2100F, JEOL) operating at 200 kV. Crystalline structure of the catalyst was analyzed by X-ray diffraction (XRD, Rigaku Smartlab, Japan) with Cu-K α radiation ($\lambda=0.15418$ nm) in a range of 10°- 90° with a 2° min⁻¹ scanning speed. The surface chemical compositions and elemental valence states of all prepared samples were analyzed by X-ray photoelectron spectroscopy (XPS) with an ESCALab220i-XL electron spectrometer (VG, Scientific ESCALab250i-XL unit, UK), in which the C1s peak was fixed at the binding energy of 284.7 eV.

Hydrogen temperature-programmed reduction (H₂-TPR) and oxygen temperature-programmed desorption (O₂-TPD) analyses were performed on a BELCAT catalyst analyzer with a thermal conductivity detector (TCD). Briefly, 50 mg of each sample was loaded into a U-shaped tube, then treated in a He flow (50 cm³/min) from room temperature to 300 °C and held at 300 °C for 30 min. After being cooled down, the pretreated sample was exposed to a 50 cm³/min flow of 5% H₂-Ar (v/v) mixture and heated from room temperature to 900 °C with a heating rate of 10 °C/min. For O₂-TPD experiment, 100 mg of sample was pretreated in a He flow (50 cm³/min) for 1 h in order to remove the surface water at first. After cooling down to RT, the sample was treated by a O₂ flow (50 cm³/min) and then purged by a He flow (50 cm³/min) for 1 h. Finally, the sample was heated from RT to 900 °C at a rate of 10 °C/min.

5.2.4 Catalytic activity test

Catalytic oxidation of toluene was performed on the continuous flow fixed-bed reactor at the atmospheric pressure. In a typical test, the catalyst coated CF was cut into a size of < 3 mm in advance, 100 mg of catalyst and 300 mg of quartz sand (40~60 mesh) were mixed and transferred to a Pyrex reaction tube (i.d.=10 mm) with quartz wool packed at both ends of the catalyst bed. The catalyst bed was pretreated in the nitrogen atmosphere at 100 °C for 1.5 h at first and then, the reaction was conducted in the set temperature range of 150~300 °C. Based on the preliminary experiments, the total flow rate with the toluene concentration of around 978 ppm in the atmosphere of oxygen (O₂, 20 vol%)-nitrogen (N₂, 80 vol%) maintained at 50 cm³/min with a weight hourly space velocity (WHSV) of 30,000 mL g⁻¹ h⁻¹. Herein, the gaseous toluene was introduced by N₂ from a bubbler filled with toluene at a temperature of 0 °C. Long-term water resistance performance was examined by adding 5.0 vol% of water vapor to the above described gas mixture by passing the feed stream through a saturated water bubbler. During the reaction, the inlet and outlet concentrations of toluene were analyzed on-line by a gas chromatograph (Shimadzu-2014), which was equipped with a flame ionization detector (FID), simultaneously, the outgoing products from the reactor were also analyzed on a FTIR gas analyzer (Horiba, FG-120).

Toluene conversion and CO₂ selectivity were calculated from Eqs. (5.2) and (5.3):

$$X_{\text{Conversion}} = \frac{C_{\text{Inlet}} - C_{\text{Outlet}}}{C_{\text{Inlet}}} \times 100\% \quad (5.2)$$

$$\text{CO}_2 \text{ selectivity} = \frac{C_{\text{CO}_2}}{7(C_{\text{Inlet}} - C_{\text{Outlet}})} \times 100\% \quad (5.3)$$

where, C_{Inlet} and C_{Outlet} are the inlet and outlet concentrations of toluene, respectively. n_{CO_2} and $n_{\text{inlet toluene}}$ are molar numbers of the produced CO₂ in the off gas and the introduced toluene during the reaction, respectively. In this work, the carbon balances of all reactions were closed with errors lower than 5.0 %.

Turnover frequency (TOF) was calculated as following (Eq. (5.4)):

$$\text{TOF} = \frac{(C_{\text{Inlet}} - C_{\text{Outlet}})v/22400}{m_{\text{cat}} Y_{\text{Mn}}/M_{\text{Mn}}} \quad (5.4)$$

where v is the total gas flow rate for the reactor (50 cm³/min); m_{cat} is the catalyst weight; Y_{Mn} is the Mn loading content tested by XPS technique and M_{Mn} is the atomic weight of Mn (54.938g mol⁻¹). For calculating TOF, the reaction temperatures (222 and 232 °C) at which the conversion of toluene was lower than 25% were selected.

5.3. Results and discussion

5.3.1 SEM analysis

Fig. 5.2 shows surface SEM images of the prepared Mn-Co mixed metal oxides supported catalysts. It can be seen that Co species were grown on the surfaces and among the nanowires so that the whole surface became dense for the sample of 0.01Co/CF (**Fig. 5.2a**). In comparison, for the 0.10Mn/CF catalyst, Mn species were grown along with each nanowire and the coated nanowires were also uniformly distributed on the CF (**Fig. 5.2b**). **Figs. 5.2(c-e)** show the mixed metal oxides supported catalysts of 0.01Mn-0.01Co/CF, 0.05Mn-0.01Co/CF and 0.10Mn-0.01Co/CF. The morphology was slightly changed with the increase in the molar ratio of Mn/Co from 1:1 to 10:1 in the initial electrodeposition solution. Especially, for the morphology of 0.01Mn-0.01Co/CF, which was different from those of the other two, the Mn-Co mixed metal species grew on the nanowires with nanosheet structures and the spaces among the nanowires were full of materials. In comparison,

the morphologies of 0.05Mn-0.01Co/CF and 0.10Mn-0.01Co/CF catalyst were similar to that of 0.10Mn/CF catalyst, in which the metal oxide species coated on the nanowires more uniformly and the spaces among the nanowires were maintained, which could provide more spaces for the dispersion of reactants and gas products. In addition, **Fig. 5.2f** shows the morphology of the spent 0.10Mn-0.01Co/CF catalyst after a long-term evaluation. No obvious change was observed between the fresh and the spent ones, indicating that mixed metal oxides supported on the nanowires of CF were stable during the oxidation process. However, SEM images in **Fig. 5.3** display that serious aggregation occurs over 0.15Mn-0.01Co/CF catalyst when Mn/Co molar ratio is as high as 15:1, which may make an adverse effect on the catalytic activity of this catalyst.

The elemental compositions on the surfaces of all prepared Mn-Co/CF catalysts were determined by EDX analyses, and the results are listed in **Table 5.1**. Obviously, there was no obvious change on the content of O, Mn, Co and Cu elements for the spent 0.10Mn-0.01Co/CF catalyst when compared with the fresh one. It can be predicted that the present Mn-Co mixed metal oxide coated catalysts may perform excellent stability in the compositions in the catalytic oxidation of toluene.

Table 5.1 Surface elemental compositions of Mn-Co/CF catalysts prepared with different initial molar ratios of Mn/Co in the electrodeposition solutions.

Sample	Initial molar ratio of Mn/Co	O (wt%)	Mn (wt%)	Co (wt%)	Cu (wt%)
0.01Co/CF	-	25.1	-	31.3	43.6
0.10Mn/CF	-	16.8	71.5	-	11.6
0.01Mn-0.01Co /CF	1:1	32.9	15.9	12.1	39.1
0.05Mn-0.01Co /CF	5:1	28.6	25.7	18.3	27.4
0.10Mn-0.01Co /CF	10:1	31.4	37.2	12.5	18.9
Spent 0.10Mn-0.01Co /CF	10:1	30.4	45.2	11.8	12.7

The weight percentage (wt%) of O, Mn, Co and Cu were taken by EDX analyses.

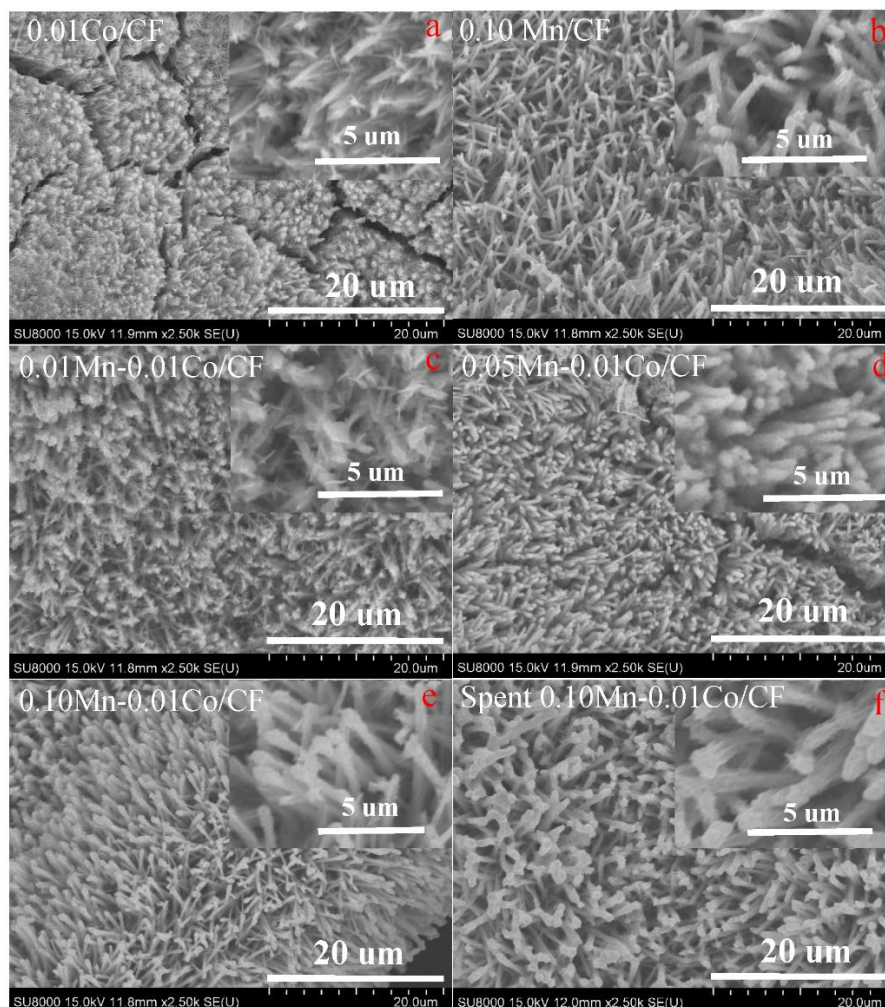


Fig. 5.2. SEM images of various Mn-Co/CF catalysts (Insets: the enlarged images).

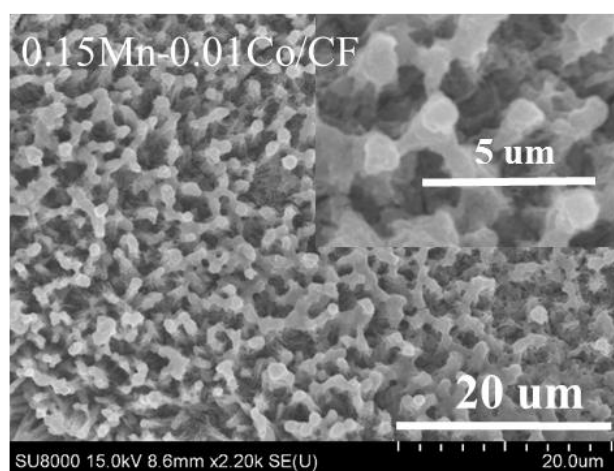


Fig. 5.3. SEM images of 0.15Mn-0.01Co/CF catalyst.

5.3.2 TEM analysis

Fig. 5.4 shows the nanostructures of pure 0.01Co/CF and 0.10Mn/CF catalysts. For the 0.01Co/CF catalyst, the well-defined crystalline structures were observed with the fringe spacings of 0.203, 0.243, 0.284 and 0.446 nm, which are attributed to the (400), (311), (220) and (111) lattice planes of Co_3O_4 phase, respectively (**Fig. 5.4 (a)** and **(c)**). Meanwhile, for the 0.10Mn/CF catalyst, three types of lattice fringes were observed. The two with the spacings of 0.241 and 0.311 nm are assigned to the (211) and (110) crystal planes of MnO_2 phase, but the other with the spacing of 0.491 nm corresponds to the (101) crystal plane of Mn_3O_4 phase (**Figs. 5.4 (b)** and **(d)**).

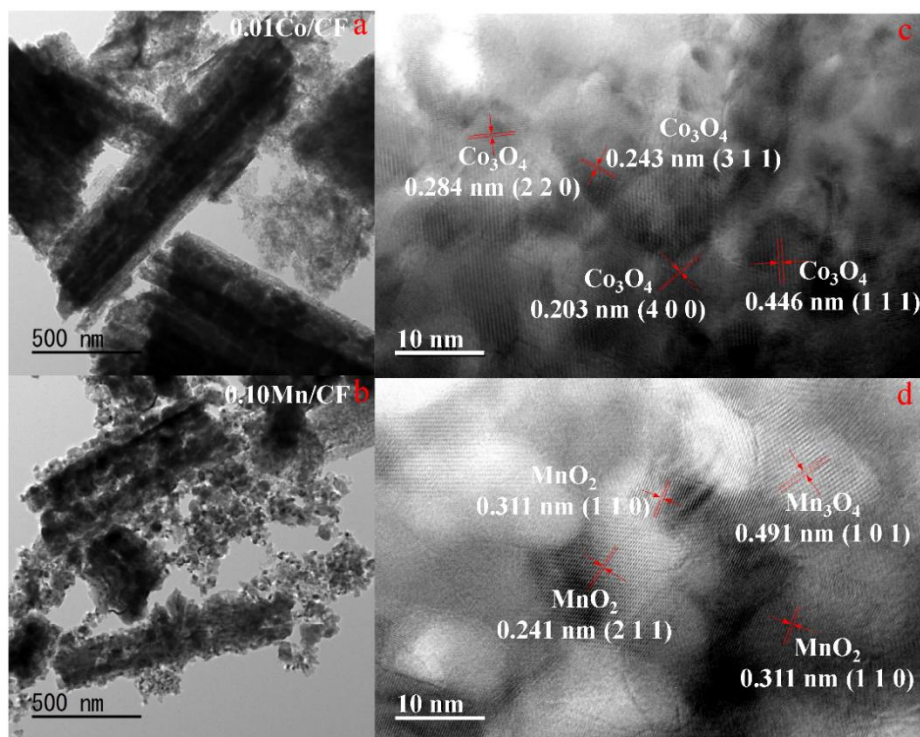


Fig. 5.4. TEM images of single 0.01Co/CF (a) and 0.10Mn/CF (b) catalysts and the corresponding HRTEM images (c, d).

Fig. 5.5 shows TEM and HRTEM images of the obtained Mn-Co/CF catalysts. The nanocrystals of both the manganese and cobalt oxides were observed in all images. As indicated in **Fig. 5.5a**, the Cu nanowire was surrounded by the nanosheets of 0.01Mn-0.01Co/CF catalyst, which is consistent with the SEM image (**Fig. 5.2c**). With the increase in the Mn/Co molar ratio, Mn-Co mixed oxides seemed to be coated on the nanowire more homogeneously (**Figs. 5.5b** and **6.5c**) and meanwhile

more Mn lattice fringes were observed, which is consistence with the results as shown in **Table 5.1**. It should be noted that two Mn oxidation states, i.e., MnO₂, Mn₃O₄, and only one Co oxidation state of Co₃O₄ were observed in the HRTEM images, which are agreement with the following XRD and XPS analyses. Moreover, the intimate contact between manganese and cobalt oxides crystals was observed in some places (**Figs. 5.5e** and **6.5f**), which could play the synergetic effects to improve the catalytic activity. Therefore, it is concluded that the electrodeposition method applied in this work is not only facile but also appropriate to produce nanosized mixed metal oxide catalysts with intimate contacts.

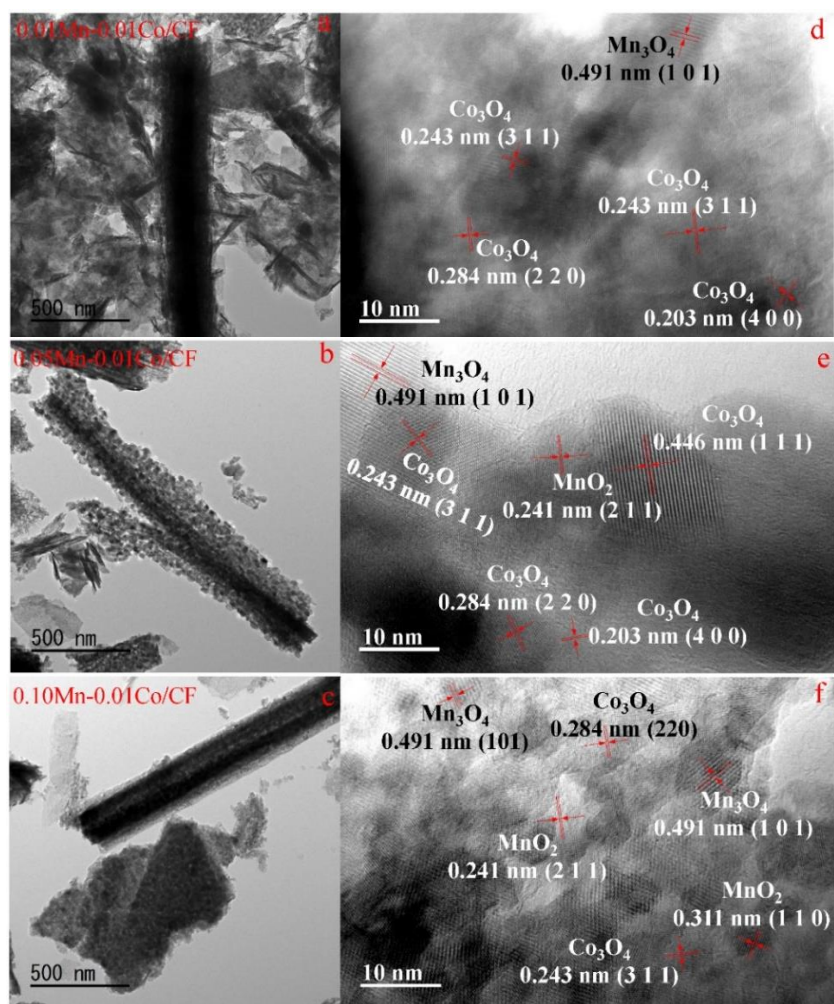


Fig. 5.5. TEM images of 0.01Mn-0.01Co/CF (a), 0.05Mn-0.01Co/CF (b) and 0.10Mn-0.01Co/CF (c) catalysts and (d, e, f) are the corresponding HRTEM images of (a, b, c).

5.3.3 XRD analysis

Fig. 5.6 shows XRD patterns of all prepared Mn-Co/CF catalysts, in which the strong peaks at 2 θ

= 43.73°, 50.80° and 74.57° are well indexed to the Cu metal (PDF#04-0836). For the pure 0.01Co/CF catalyst, the diffraction peaks located at 19.28°, 31.51°, 45.02°, 49.07°, 55.99°, 59.62°, 65.52°, 77.67° can be assigned to the (111), (220), (400), (331), (422), (511), (440) and (533) crystal planes of Co₃O₄ (PDF#43-1003), respectively. For the 0.10Mn/CF catalyst, the diffraction peaks centered at 18.47°, 29.42°, 31.41°, 32.84°, 38.68°, 58.89°, 60.31°, and 65.31° are indexed to (101), (112), (200), (103), (004), (321), (224), and (400) crystal planes of pristine Mn₃O₄ (PDF#24-0734), respectively. Furthermore, 0.10Mn/CF catalyst with high content of Mn element (**Table 5.1**) exhibited weaker diffraction peaks when compared with 0.01Co/CF catalyst, indicating that Mn species possesses better dispersion than Co species.

For the various Mn-Co/CF catalysts, the diffraction peaks corresponding to Co₃O₄ and Mn₃O₄ were obviously observed, and the intensities of main peaks corresponding to Mn₃O₄ slightly increased with the increase in the Mn/Co molar ratio. These results also revealed that Mn and Co species can be well deposited on the nanowires of Cu foam at the same time during the electrodeposition process. Meanwhile, the diffraction peaks (near $2\theta = 58.89^\circ$ and 60.31°) corresponding to Mn₃O₄ slightly shifted to the right, which could be resulted from the insertion of Co elements in its structure. In addition, the Mn₃O₄ diffraction peaks expanded a little due to the coordination of Mn and Co ions [19]. Besides, copper species of Cu, Cu₂O and CuO belonged to the catalyst support of Cu foam were also observed, especially the diffraction peaks of Cu and Cu₂O were very sharp. It is worth noting that MnO₂ diffraction peaks were not found in the XRD patterns but it was confirmed by the TEM observation (**Figs. 5.5(d-f)**). It is possible that the MnO₂ nanocrystals were well dispersed in the catalysts so that the related diffraction peaks were too weak to be observed. Furthermore, diffraction peaks corresponding to Mn and Co species over Mn-Co/CF catalysts located at 2θ around 18-20 degree are too weak to be observed, which might be contributed by their low content or well dispersion.

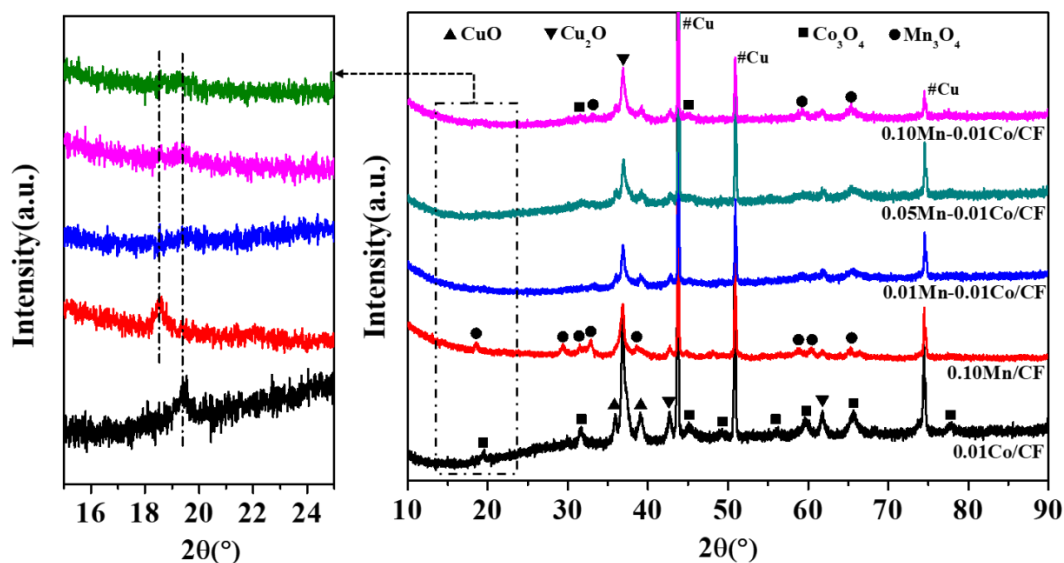


Fig. 5.6. XRD patterns of 0.01Co/CF, 0.01Mn/CF and three Mn-Co/CF catalysts.

5.3.4 H₂-TPR analysis

Fig. 5.7a shows H₂-TPR analysis results for the prepared catalysts. It can be seen that the pure 0.01Co/CF catalyst displayed two separated reduction peaks at the temperature range of 100~400 °C. Herein, one centered at a relatively low temperature of 267.3 °C is assigned to the reduction of Co³⁺ to Co²⁺ whereas the other one located at 330.4 °C is ascribed to the reduction of Co²⁺ to Co, indicating that cobalt oxides suffered a stepwise reduction process [28]. For the pure 0.10Mn/CF catalyst, two H₂ consumption peaks at 243.3 °C and 275.1 °C were observed, which corresponded to the reduction processes of Mn⁴⁺ to Mn³⁺ and Mn³⁺ to Mn²⁺, respectively [29]. Compared the two pure samples of 0.01Co/CF and 0.10Mn/CF (**Table 5.2**), the reduction temperature of the former (267.3 °C) was much higher than that of the latter (235.2 °C), indicating that Mn species were more easily reduced than Co species. Herein, Mn species were well dispersed over CF nanowires while Co species aggregated cover the catalyst surface and became dense, as a result, the dispersed Mn species were more easily reduced and exhibited lower reduction temperature.

For the Mn-Co/CF catalysts, the intensity of the asymmetrical peak increased gradually and the peak became broaden with the increase in Mn/Co molar ratio, indicating that more surface oxygen species can be provided [30], which is benefit for the oxidation. Additionally, the reduction peaks

shifted to the lower temperature when compared with the pure 0.01Co/CF catalyst, which should be ascribed to the well dispersion of the mixed metal oxides as stated above. However, compared with the pure 0.10Mn/CF catalyst, the reduction peaks of Mn-Co/CF catalysts were slightly shifted to higher temperatures even though they possess the well dispersion when compared with 0.10Mn/CF catalyst. Consequently, it might be contributed by the strong interaction between Mn and Co.

For Mn-Co/CF catalysts, the amount of H₂-consumption at the lower temperature range was increased from 1.911 to 2.690 mmol/g with the increase of Mn/Co molar ratio and the 0.10Mn-0.01Co/CF catalyst exhibited the maximum total H₂-consumption. It is worth noting that the value of H₂-consumption at the relatively low temperature for the single 0.01Co/CF catalyst was as high as 5.743 mmol/g, which might make a significant influence on the catalytic activity. It is reported that the low temperature reducibility is related to the active species of surface oxygen, and consequently, the higher concentration of H₂-consumption at low temperature will be more benefit for the catalytic activity [31]. Herein, the addition of a small amount of Co within Mn-based catalysts (e.g., 0.10Mn-0.01Co/CF) also increased the amount of H₂-consumption at the lower temperature, which should be favorable to the oxidation of toluene.

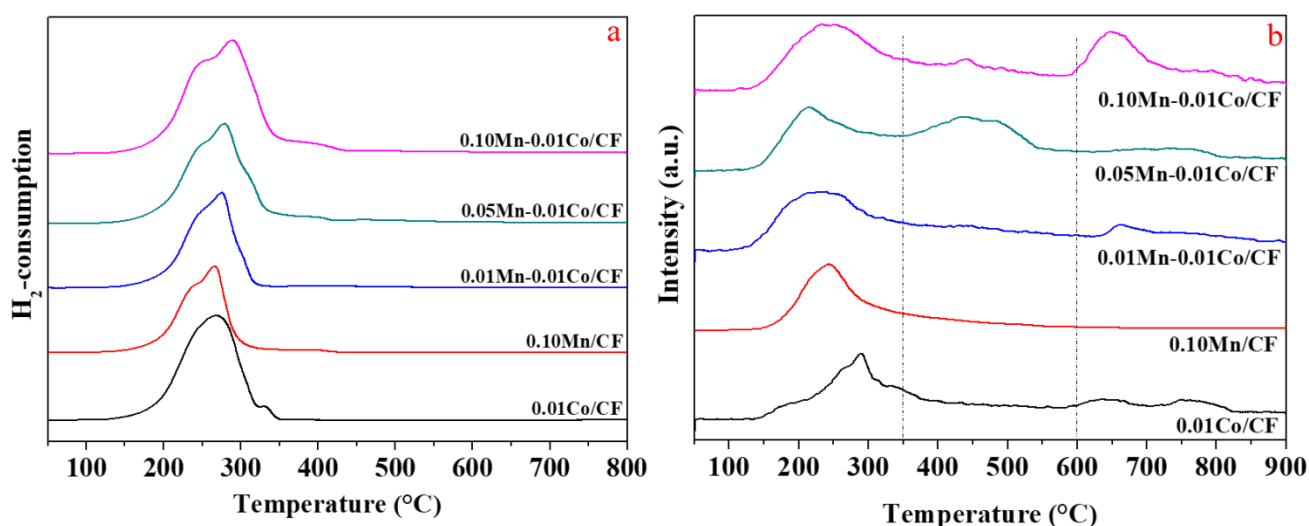


Fig. 5.7. H₂-TPR (a) and O₂-TPD (b) profiles of the prepared catalysts.

Table 5.2 Hydrogen consumption of Mn-Co/CF catalysts for H₂-TPR analysis

Sample	T ₁ /°C	H ₂ -uptake (mmol/g)	T ₂ /°C	H ₂ -uptake (mmol/g)	Total H ₂ -uptake (mmol/g)	O _{ads} desorption (mmol/g)
0.01Co/CF	267.3	5.743	330.4	0.191	5.934	0.053
0.10Mn/CF	235.2	2.540	266.1	2.638	5.178	0.063
0.01Mn-0.01Co /CF	244.7	1.911	274.7	2.544	4.455	0.060
0.05Mn-0.01Co /CF	244.1	2.335	286.5	3.072	5.407	0.064
0.10Mn-0.01Co /CF	244.3	2.690	288.6	3.911	6.601	0.074

5.3.5 O₂-TPD analysis

The type and mobility of oxygen species in the prepared catalysts were investigated by O₂-TPD. Generally, the adsorbed oxygen species could have the following transition route O₂(ads)→O₂⁻(ads)→O⁻(ads)→O²⁻(lat). It demonstrates that the oxygen species of the physically absorbed (O₂, ads) and the chemically adsorbed (O₂⁻, ads, and O⁻, ads) more easily migrate to the catalyst surface than the oxygen species from the lattice (O²⁻, lat) [32]. The obtained profiles of O₂-TPD are shown in **Fig. 5.7b**. The peaks located at the low temperature range (< 350 °C) are contributed to the desorption of the surface chemical oxygen (O_β) whereas the peaks centered at the medium temperature range (350-600 °C) are derived from desorption of the surface lattice oxygen ((O_α) and the peaks at the high temperature range (>600 °C) are assigned to the desorption of bulk lattice oxygen, respectively [33, 34]. It is obvious that the amounts of the surface absorbed oxygen species (O_β) on the Mn-Co/CF catalysts were higher than those of the pure samples of 0.01Co/CF and 0.10 Mn/CF, and the amount increased with the increasing of the Mn/Co molar ratio from 1:1 to 10:1 (**Table 5.2**), indicating that more active surface oxygen species were generated in the Mn-Co mixed oxides. It is consistent with the H₂-TPR results, implying that interaction between Mn and Co metal oxides should be favorable for the generation of active surface oxygen, and therefore influence their catalytic performance in the toluene catalytic oxidation.

5.3.6 XPS analysis

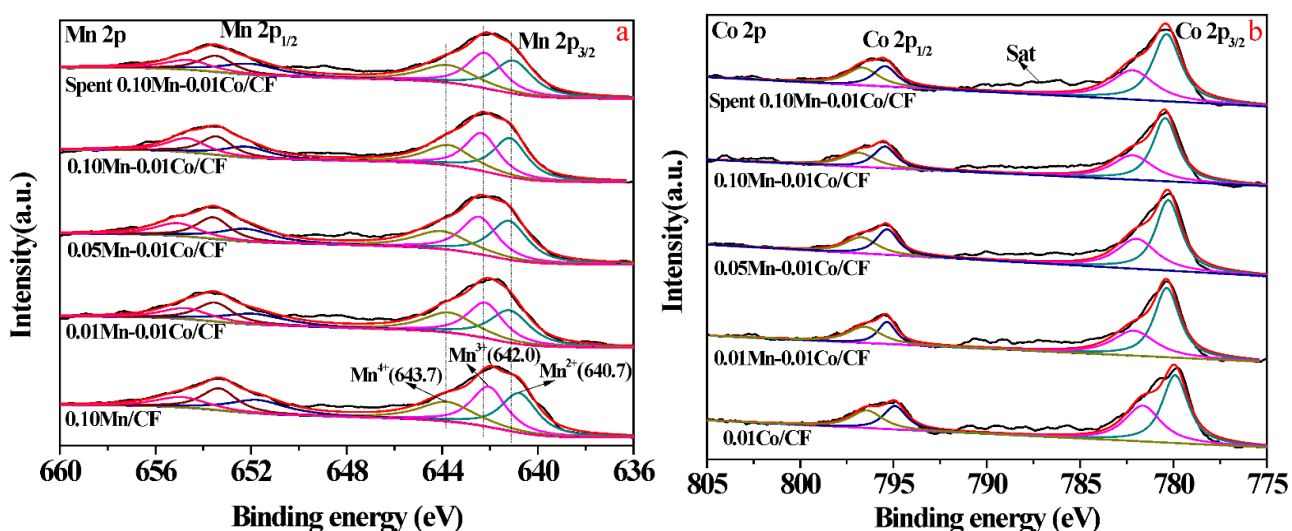
The surface compositions and valence states of the prepared Mn-Co/CF catalysts were also investigated by XPS technique and the corresponding spectra are shown in **Fig. 5.8**. The high-resolution Mn 2p spectra of all catalysts can be characterized by two main regions of Mn 2p_{1/2} and Mn 2p_{3/2} (**Fig. 5.8a**), and specifically, three main peaks located at 640.7 eV, 642.0 eV and 643.7 eV are contributed by Mn²⁺, Mn³⁺ and Mn⁴⁺, respectively[9, 35]. As summarized in **Table 5.3**, the peak area ratio of surface Mn⁴⁺/Mn³⁺ increased gradually with the increase in Mn/Co molar ratio. It is observed that 0.10Mn-0.01Co/CF with the addition of a little amount of Co exhibited a slightly higher surface Mn⁴⁺/Mn³⁺ ratio than the single 0.10Mn/CF catalyst, indicating that Co addition improved the formation of the surface Mn⁴⁺ species. Additionally, the binding energy of Mn 2p_{3/2} in the Mn-Co/CF catalysts increased when compared with the single 0.10Mn/CF catalyst, which might be caused by the interaction between Mn and Co oxides [36]. It is consistent with the results reported by Xiang *et al.* [37], in which they found that metal mixing could cause the energy shift.

Fig. 5.8b displays the XPS spectra of Co 2p of all the prepared catalysts and the spent catalysts. All Co 2p spectra showed two main peaks centered at 775-790 eV and 790-800 eV ranges, which are assigned to Co 2p_{3/2} and Co 2p_{1/2}[9]. The surface species of Co³⁺ at the binding energies of 780.3 eV while Co²⁺ accompanied by shake-up satellite centered at 782.1 eV, whereas they located at the binding energies of 795.3 eV and 796.5 eV, respectively, in the Co 2p_{3/2} spectrum. As summarized in **Table 5.3**, it is noteworthy that the ratios of Co³⁺/Co²⁺ were 1.25, 1.33, 1.38, 1.40, and 1.29 for the 0.01Co/CF, 0.01Mn-0.01Co/CF, 0.05Mn-0.01Co/CF, 0.10Mn-0.01Co/CF and the spent 0.10Mn-0.01Co/CF, respectively, revealing that the increase in Mn content should be benefit for the formation of the active species of Co³⁺ on the surface [38]. Thus, Mn and Co species promoted each other in the generation of active species within the Mn-Co/CF catalysts. Meanwhile, the peak area ratio of Co³⁺/Co²⁺ in the 0.10Mn-0.01Co/CF catalyst was the highest among all the catalysts. Moreover, for the spent 0.10Mn-0.01Co/CF catalyst, the peak area ratio of Co³⁺/Co²⁺ only decreased slightly after a long-term catalytic oxidation process, indicating that the Mn-Co/CF catalyst

possessed excellent stability during the reaction process.

Fig. 5.8c presents the XPS spectra of O 1s, which were fitted into three peaks. The low binding energy peak at 529.6-529.8 eV is attributed to the lattice oxygen (O_{lat}), and the other two peaks at the binding energies of 530.1-531.0 eV and 531.6-531.9 eV are assigned to the surface absorbed oxygen of O_2^- , O^- or O_2^{2-} (O_{sur}) and the hydroxyl groups and/or carbonate species, respectively [39, 40]. As summarized in **Table 5.3**, the peak area ratio of O_{sur}/O_{lat} increased gradually with the increasing of the molar ratio of Mn/Co from 1:1 to 10:1, and this value reached the maximum when the molar ratio was 10 in the initial electrodeposition solution.

From the above XPS results, the synergistic interaction between Mn and Co oxides enhanced the generation of active species of surface Mn^{4+} , Co^{3+} and O_{sur} for the improvement of the catalytic activity [38, 41, 42]. Additionally, the peak area ratio of Mn^{4+}/Mn^{3+} showed a linear relationship with that of Co^{3+}/Co^{2+} as shown in **Fig. 5.8d**, and the increase trend was the same as that of the amount of H_2 -consumption for the Mn-Co/CF catalysts (**Table 5.3**). Especially, 0.10Mn-0.01Co/CF achieved the maximum peak area ratios of Mn^{4+}/Mn^{3+} , Co^{3+}/Co^{2+} , and O_{sur}/O_{lat} among all the catalysts, indicating that it should have superior catalytic activity in the catalytic oxidation of toluene as indicated below.



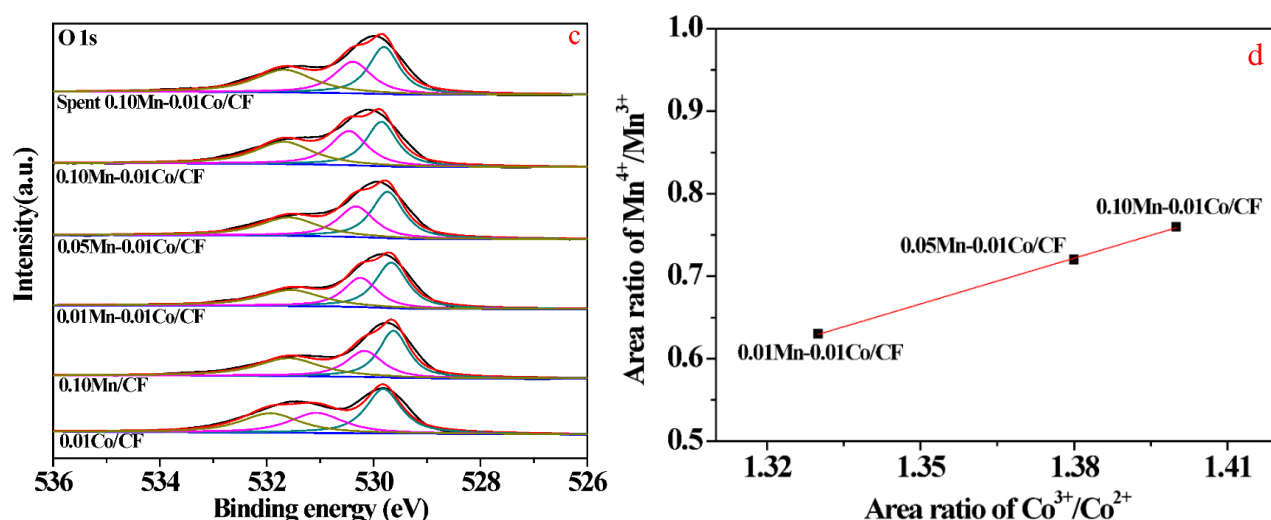


Fig. 5.8. XPS profiles of Mn 2p (a), Co 2p (b), O 1s (c) of 0.01Co/CF, 0.10Mn/CF and Mn-Co/CF catalysts and linear relationship between $\text{Mn}^{4+}/\text{Mn}^{3+}$ and $\text{Co}^{3+}/\text{Co}^{2+}$ tested by XPS (d).

Table 5.3 Surface element compositions and valence states of Mn-Co/CF catalysts.

Sample	Area ratio of Mn 2p	Area ratio of Co 2p	Area ratio of O 1s
	$\text{Mn}^{4+}/\text{Mn}^{3+}$	$\text{Co}^{3+}/\text{Co}^{2+}$	$\text{O}_{\text{sur}}/\text{O}_{\text{lat}}$
0.01Co/CF	-	1.25	0.74
0.10Mn/CF	0.75	-	0.82
0.01Mn-0.01Co /CF	0.63	1.33	0.67
0.05Mn-0.01Co /CF	0.74	1.38	0.72
0.10Mn-0.01Co /CF	0.76	1.40	0.93
Spent 0.01Mn-0.01Co /CF	0.71	1.29	0.92

5.3.7 Catalytic activity

Catalytic performances of the 0.01Co/CF, 0.10Mn/CF and Mn-Co/CF catalysts for the catalytic oxidation of toluene were evaluated on a continuous flow fixed-bed reactor system. Herein, the toluene conversions in a reaction temperature range of 160~320 °C were measured, and the catalytic activities of all catalysts were compared based on the values of $T_{10\%}$, $T_{50\%}$, and $T_{90\%}$, which correspond to 10%, 50%, 90% conversions, respectively. Result in **Fig. 5.9** showing that less than 20% of toluene was converted into CO_2 and H_2O over bare CF possesses nanowires during the reaction process, implying that bare CF was not active to the catalytic oxidation of toluene even though it possesses high content of Cu (**Table 5.1**), and hence most of Cu is inactive species within the CF

support. However, the catalytic performance was significantly improved after supporting mixed metal oxides of Mn and Co, and the obtained results are shown in **Fig. 5.9a** and summarized in **Table 5.4**. For the single 0.01Co/CF catalyst it can be seen that the toluene conversion was less than 5% at a temperature below 220 °C, and then increased gradually with the increase in the reaction temperature, the complete conversion temperature was around 273 °C. Meanwhile, the single 0.10Mn/CF catalyst also underwent a similar reaction process, and especially the total toluene conversion temperature (274 °C) was very similar as that of the single 0.01Co/CF catalyst.

For the mixed metal catalysts of Mn-Co/CF, the order of the catalytic activity was 0.10Mn-0.01Co/CF > 0.05Mn-0.01Co/CF > 0.01Mn-0.01Co/CF. Especially, the conversion temperatures of $T_{50\%}$ and $T_{90\%}$ over the 0.10Mn-0.01Co/CF catalyst was as low as 243 and 251 °C, respectively, which were much lower than those of the single metal based catalysts of 0.01Co/CF ($T_{50\%}=249$, $T_{90\%}=260$) and 0.10Mn/CF ($T_{50\%}=256$, $T_{90\%}=270$). The two values were also lower than that of 0.15Mn-0.01Co/CF catalyst as it depicted in **Table 5.4**, the decrease in 0.15Mn-0.01Co/CF catalyst might be mainly caused by the serious aggregation of Mn and Co species obtained at high concentration ratio of 15:1(**Fig. 5.3**). Consequently, these results revealed that the catalytic performance can be improved by mixing Mn and Co species in the composite oxide with a proper molar ratio, and in this study, the 0.10Mn-0.01Co/CF catalyst performed the best catalytic performance for the catalytic oxidation of toluene among all the prepared catalysts. Additionally, as shown in **Fig. 5.9b**, the CO₂ selectivity also increased gradually with the reaction temperature, which reached the maximum value when the toluene conversion was 100%, and herein all errors between the actual and ideal CO₂ concentrations were less than 5.0 %. Meanwhile, FT-IR online analyses indicated that only CO₂ and H₂O were produced during the reaction process for all samples, and no other by-products existed during the catalytic oxidation of toluene.

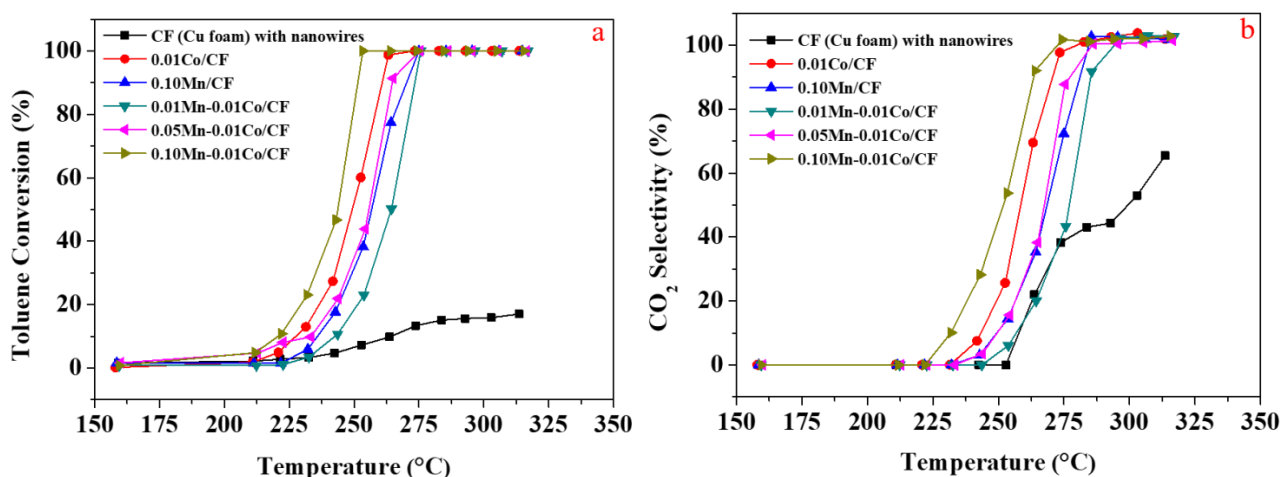


Fig. 5.9. Catalytic performances of Mn-Co/CF catalysts for the toluene oxidation: (a) Toluene conversion and (b) CO₂ selectivity.

Table 5.4 Results of catalytic oxidation of toluene over Mn-Co/CF catalysts.

Sample	Toluene conversion (°C)			Ideal CO ₂ concentration (V ^a _{CO2} /V _{N2} , %)	Actual CO ₂ concentration (V ^b _{CO2} /V _{N2} , %)	Error (%)
	T _{10%}	T _{50%}	T _{90%}			
0.01Co/CF	227	249	260	0.826	0.846	2.4
0.10Mn/CF	235	256	270	0.853	0.864	1.3
0.01Mn-0.01Co/CF	243	264	273	0.942	0.950	0.8
0.05Mn-0.01Co/CF	233	255	264	0.937	0.942	0.5
0.10Mn-0.01Co/CF	220	243	251	0.834	0.851	2.0
0.15 Mn-0.01Co/CF	226	257	268	0.843	0.837	0.7

V^a_{CO2}, the flow rate of the ideal produced CO₂;

V^b_{CO2}, the flow rate of the actual produced CO₂;

V_{N2}, the flow rate of N₂ as balance gas for reaction.

Catalyst support is an important factor for the catalytic reaction. Therefore, the effect of the catalyst support for the catalytic oxidation of toluene was also studied in this work. For the catalyst of 0.10Mn-0.01Co/CF catalyst whose Cu foam support did not pretreated by electro-deposition method before supporting mixed metal oxides, from **Fig. 5.10a** it can be seen that toluene conversion

temperatures of $T_{50\%}$ and $T_{90\%}$ were 262 and 276 °C, respectively. The two values are little lower than that of the 0.10Mn-0.01Co/NF catalyst prepared by nickel foam (NF) support (**Fig. 5.10b**), which contributed by the similar three-dimensional structures of CF and NF, as well as the analogous morphologies of the supported Mn and Co species with large clusters in **Fig. 5.11 (a)** and **(b)**. Obviously, CF support has advantages over NF support in this work, especially the CF support possesses nanowires, which can provide special loading locations for active species, and therefore enhanced the dispersion of them. H_2 -TPR results further proved that the low-temperature reducibility of the catalyst was assigned to the well dispersion and the synergistic interaction between Mn and Co oxides. Consequently, 0.10Mn-0.01Co/CF catalysts possessing nanowires exhibited the best catalytic performance with the lowest toluene conversion temperature among all the prepared catalysts, indicating such a kind of catalyst exhibited good catalytic performance in the catalytic oxidation of toluene. The reason is that the best catalyst of 0.10Mn-0.01Co/CF possesses superior physiochemical properties of well dispersion, high amounts of active species of Mn^{4+} , Co^{3+} and surface oxygen (listed in **Table 5.3**). Consequently, it can be concluded that the mixed metal oxides based catalysts with excellent catalyst support performed better catalytic performance than single metal oxide based catalysts in this work.

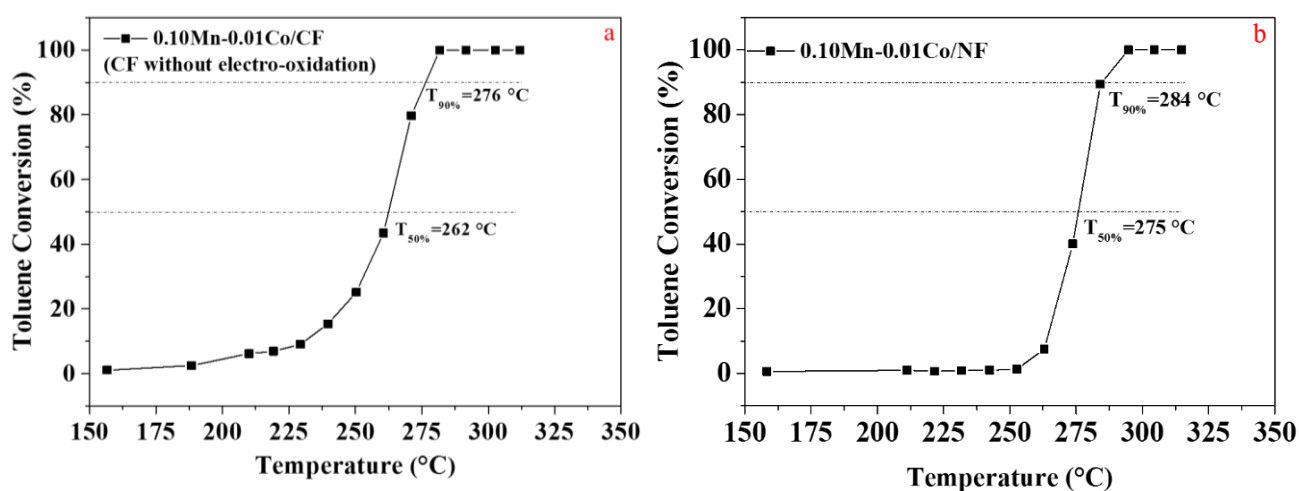


Fig. 5.10. Catalytic performances of 0.10Mn-0.01Co/CF catalyst (CF without electro-oxidation) (a), 0.10Mn-0.01Co/NF catalyst was prepared by using nickel foam (NF) support (b).

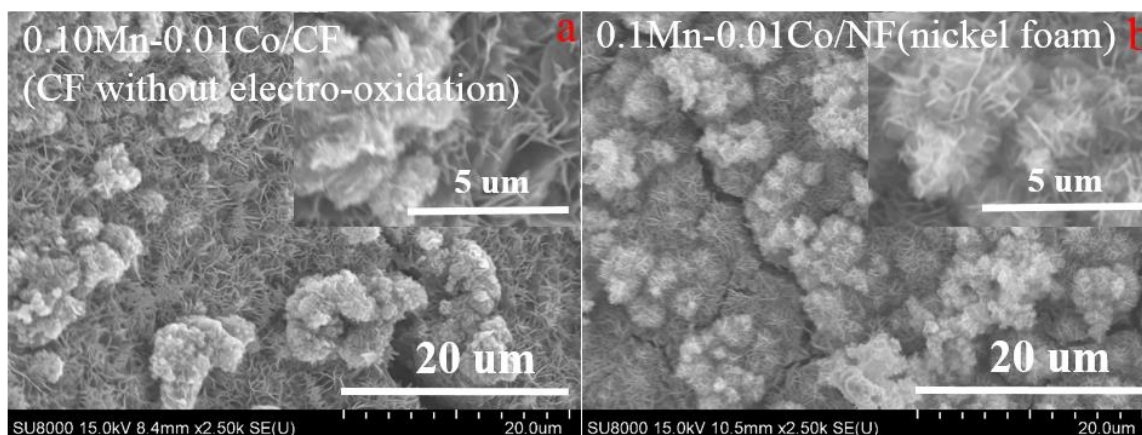


Fig. 5.11. SEM images of (a) 0.10Mn-0.01Co/CF catalyst (CF without electro-oxidation) and (b) 0.10Mn-0.01Co/ NF (nickel foam) catalyst was prepared by using NF support.

Turnover frequencies (TOFs) based on the amount of Mn species of the prepared catalysts at 222 and 232 °C were calculated and shown in **Fig. 5.12**, the TOF value of Mn-Co/CF catalysts was increased gradually with the increased Mn/Co molar ratio from 1:1 to 10:1 in the initial electrodeposition solution, and the 0.10Mn-0.01Co/CF had the highest TOF ($9.13 \times 10^{-4} \text{ min}^{-1}$) among all the catalysts, it is consistent with the catalytic performance as shown in **Fig. 5.9**, indicating that it is the most active material for the catalytic oxidation of toluene in this work.

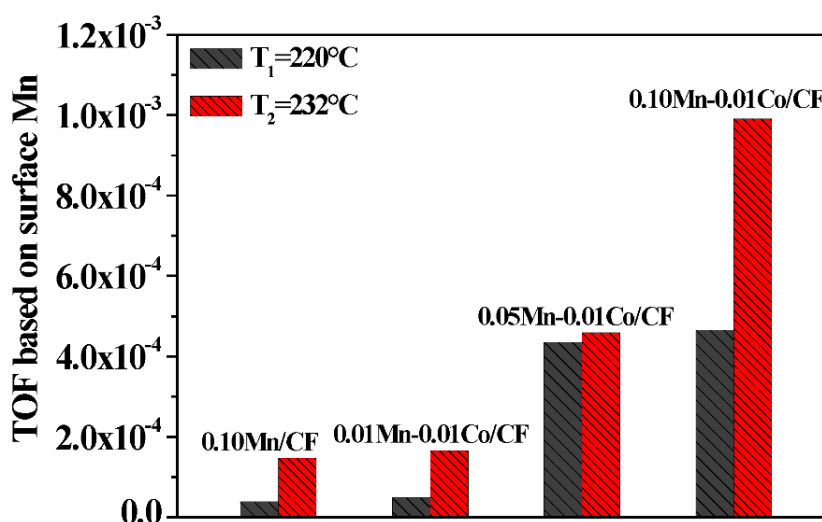


Fig. 5.12. TOFs based on the surface Mn species of the prepared catalysts at 222 °C and 232 °C.

5.3.8 Long-term on-stream stability test

The water effect is considered to be an important parameter for the catalytic oxidation of toluene because VOCs always exist in the industrial exhaust gas together with water vapor. Herein, the effect of water vapor on the performance of the 0.10Mn-0.01Co/CF catalyst was investigated and the obtained result is shown in **Fig. 5.13**. It can be seen that the toluene conversion maintained 100% at the first 365 min in the absence of water vapor and then, after introducing water vapor in the oxidation system for a period of 950 min the toluene conversion gradually decreased to 82%. However, the conversion was recovered to 100% soon after stopping water vapor supply. Herein, since the set temperature was fixed, the decrease in toluene conversion could be due to the local temperature decreasing, and simultaneously, the competition adsorptions of water and toluene molecules on the active sites of 0.10Mn-0.01Co/CF catalyst could also decrease the conversion of toluene. However, the catalyst did not suffer from the deactivation in the presence of water vapor.

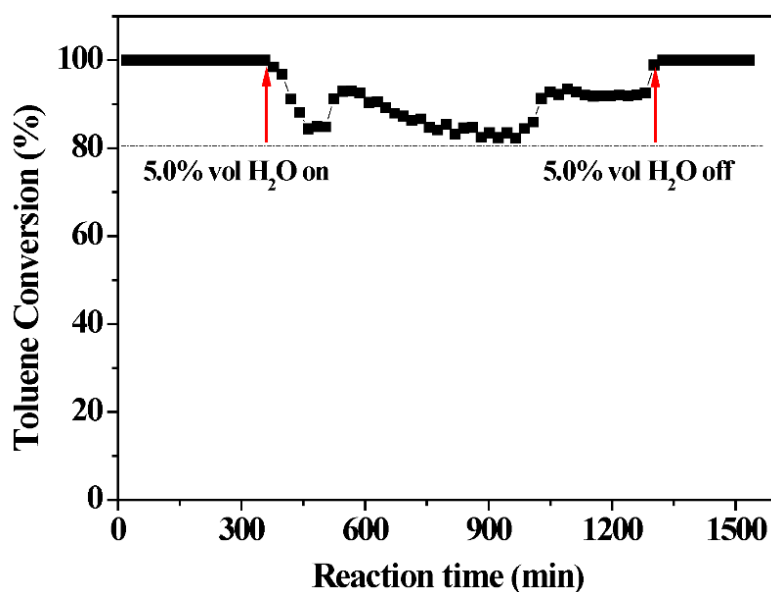


Fig. 5.13. Long-term on-stream evaluation of 0.10Mn-0.01Co/CF catalyst for the catalytic oxidation of toluene in the presence of water vapor (Reaction conditions: toluene concentration = 978 ppm, WHSV=30,000 mL g⁻¹ h⁻¹, reaction temperature=261 °C, reaction time=1500 min).

Long-term evaluation of the 0.10Mn-0.01Co/CF catalyst in the absence of water vapor was also

conducted under the conditions of reaction temperature = 237 °C, WHSV = 30,000 mL g⁻¹ h⁻¹ and toluene concentration = 978 ppm. As shown in **Fig. 5.14**, the toluene conversion maintained at 42% during the whole reaction process. The results from the FT-IR gas analyzer revealed that only CO₂ and H₂O were produced. As indicated by **Figs. 5.2e** and **6.2f**, the structure of 0.10Mn-0.01Co/CF catalyst before and after the stability test maintained almost unchanged. Meanwhile, the active species of Mn⁴⁺, Co³⁺ and O_{sur} also have no obvious change (**Table 5.3**). Combined with the result from **Fig. 5.14**, it can be concluded that the mixed metal catalysts of Mn-Co/CF synthesized by electrodeposition method were highly active and stable in the catalytic oxidation of toluene with or without water vapor. In addition, it is considered that the Cu nanowires formed on the CF provided advantages for the dispersion of the active species of Mn and Co, and therefore enhanced the catalytic performance of the catalyst.

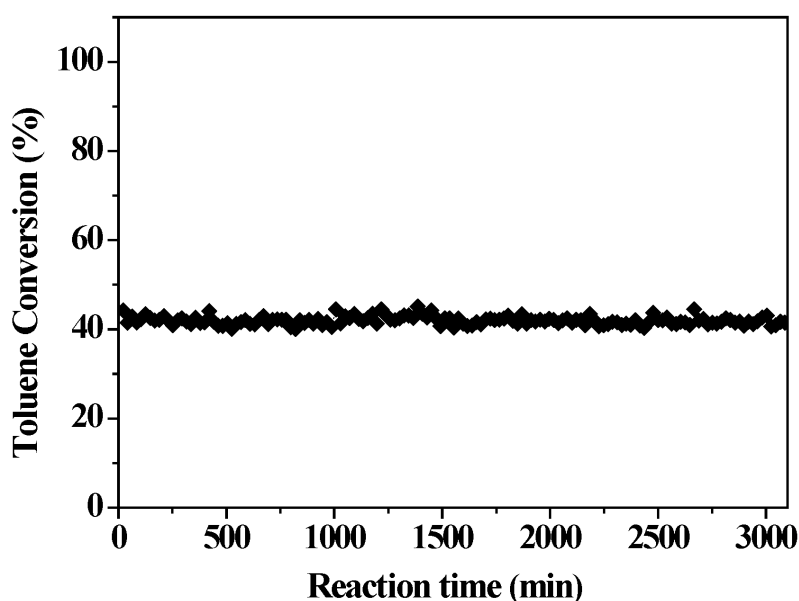


Fig. 5.14. Long-term evaluation of 0.10Mn-0.01Co/CF catalyst for the catalytic oxidation of toluene in the absence of water vapor (Reaction conditions: toluene concentration = 978 ppm, WHSV=30,000 mL g⁻¹ h⁻¹, reaction temperature = 237 °C, reaction time=3100 min).

5.4. Conclusions

In summary, highly active Mn-Co/CF catalysts with Mn-Co-oxide@Cu-nanowire array structure were prepared by the UPED method followed with calcination and used for the catalytic oxidation of

toluene. The Mn-Co oxide composite were uniformly coated on the Cu nanowires generated on the CF, and the nanowires provided advantages for the dispersion of the active species of Mn and Co, and the well-dispersed Mn and Co oxides and intimate contact of their nanocrystals exerted synergistic effect on the performance of final catalysts and therefore enhanced the catalytic performance of the catalyst. H₂-TPR, O₂-TPD and XPS analysis results indicated that the value of H₂-consumption (related to the low temperature reducibility), Mn⁴⁺/Mn³⁺, Co³⁺/Co²⁺, and O_{sur}/O_{lat} ratios of the Mn-Co/CF catalyst increased gradually with the increasing of Mn/Co molar ratio, and the related maximum values were achieved when the Mn/Co molar ratio was 10:1 in the initial solution for electrodeposition. As a result, the 0.10Mn-0.01Co/CF catalyst achieved the best catalytic activity with the complete toluene conversion to CO₂ and H₂O at a temperature as low as 253 °C. More importantly, the 0.10Mn-0.01Co/CF catalyst displayed excellent stability even in the presence of water vapor.

References

- [1] R. Atkinson, Atmospheric chemistry of VOCs and NO_x, *Atmospheric Environment*. 34(2000) 2063-2101.
- [2] A. Hellman, S. Klacar, H. Grönbeck, Low temperature CO oxidation over supported ultrathin MgO films, *Journal of the American Chemical Society*. 131 (2009) 16636-16637.
- [3] Y. Liu, J. Deng, S. Xie, Z. Wang, H. Dai, Catalytic removal of volatile organic compounds using ordered porous transition metal oxide and supported noble metal catalysts, *Chinese Journal of Catalysis*. 37 (2016) 1193-1205.
- [4] E.M. Cordi, J.L. Falconer, Oxidation of Volatile Organic Compounds on Al₂O₃, Pd/Al₂O₃, and PdO/Al₂O₃ Catalysts, *Journal of Catalysis*. 162 (1996) 104-117.
- [5] Y. Wu, S. Li, Y. Cao, S. Xing, Z. Ma, Y. Gao, Facile synthesis of mesoporous α -MnO₂ nanorod with three-dimensional frameworks and its enhanced catalytic activity for VOCs removal, *Materials Letters*. 97 (2013) 1-3.
- [6] M.S. Kamal, S.A. Razzak, M.M. Hossain, Catalytic oxidation of volatile organic compounds (VOCs) – A review, *Atmospheric Environment*. 140 (2016) 117-134.
- [7] G. Li, C. Zhang, Z. Wang, H. Huang, H. Peng, X. Li, Fabrication of mesoporous Co₃O₄ oxides by acid treatment and their catalytic performances for toluene oxidation, *Applied Catalysis A-General*. 550 (2018) 67-76.
- [8] C. Hu, Q. Zhu, Z. Jiang, Y. Zhang, Y. Wang, Preparation and formation mechanism of mesoporous CuO–CeO₂ mixed oxides with excellent catalytic performance for removal of VOCs, *Microporous & mesoporous materials*. 113 (2008) 427-434.
- [9] H. Chen, Y. Yan, Y. Shao, H. Zhang, Catalytic activity and stability of porous Co–Cu–Mn mixed oxide modified microfibrillar-structured ZSM-5 membrane/PSSF catalyst for VOCs oxidation, *RSC Advances*. 4 (2014) 55202-55209.
- [10] C. Lahousse, A. Bernier, P. Grange, B. Delmon, P. Papaefthimiou, T. Ioannides, X. Verykios, Evaluation of γ -MnO₂ as a VOC removal catalyst: comparison with a noble metal catalyst, *Journal of*

Catalysis. 178 (1998) 214-225.

[11] M. Baldi, E. Finocchio, F. Milella, G. Busca, Catalytic combustion of C3 hydrocarbons and oxygenates over Mn_3O_4 , Applied Catalysis B-Environmental. 16 (1998) 43-51.

[12] X. Weng, Y. Long, W. Wang, M. Shao, Z. Wu, Structural effect and reaction mechanism of MnO_2 catalysts in the catalytic oxidation of chlorinated aromatics, Chinese Journal of Catalysis. 40 (2019) 638-646.

[13] X. Zhang, X. Lv, F. Bi, G. Lu, Y. Wang, Highly efficient Mn_2O_3 catalysts derived from Mn-MOFs for toluene oxidation: The influence of MOFs precursors, Molecular Catalysis. (2019) 110701.

[14] N. Huang, Z. Qu, C. Dong, Y. Qin, X. Duan, Superior performance of α @ β - MnO_2 for the toluene oxidation: Active interface and oxygen vacancy, Applied Catalysis A-General. 560 (2018) 195-205.

[15] H. Pan, Y. Jian, C. Chen, C. He, Z. Hao, Z. Shen, H. Liu, Sphere-shaped Mn_3O_4 catalyst with remarkable low-temperature activity for methyl–ethyl–ketone combustion, Environmental Science & Technology. 51 (2017) 6288-6297.

[16] Y. Huang, K. Ye, H. Li, W. Fan, F. Zhao, Y. Zhang, H. Ji, A highly durable catalyst based on $\text{Co}_x\text{Mn}_{3-x}\text{O}_4$ nanosheets for low-temperature formaldehyde oxidation, Nano Research. 9 (2016) 3881-3892.

[17] G. Cheng, L. Yu, B. He, M. Sun, B. Zhang, W. Ye, B. Lan, Catalytic combustion of dimethyl ether over α - MnO_2 nanostructures with different morphologies, Applied Surface Science. 409 (2017) 223-231.

[18] S. Zhang, W. Luo, X. Yang, T. Lv, Y. Huang, K. Dong, X. Li, MnO_2 Nanoparticles Confined in TiO_2 Nanotubes for Catalytic Combustion of Butane, ChemistrySelect. 2 (2017) 4557-4560.

[19] W. Zhao, Y. Zhang, X. Wu, Y. Zhan, X. Wang, C.-T. Au, L. Jiang, Synthesis of Co–Mn oxides with double-shelled nanocages for low-temperature toluene combustion, Catalysis Science & Technology. 8 (2018) 4494-4502.

- [20] Q. Li, T. Odoom-Wubah, Y. Zhou, R. Mulka, Y. Zheng, J. Huang, D. Sun, Q. Li, Coral-like CoMnOx as a highly active catalyst for benzene catalytic oxidation, *Industrial & Engineering Chemistry Research*.58 (2019) 2882-2890.
- [21] D. Delimaris, T. Ioannides, VOC oxidation over CuO–CeO₂ catalysts prepared by a combustion method, *Applied Catalysis B-Environmental*. 89 (2009) 295-302.
- [22] B. Solsona, T. Garcia, E. Aylón, A.M. Dejoz, I. Vázquez, S. Agouram, T.E. Davies, S.H. Taylor, Promoting the activity and selectivity of high surface area Ni–Ce–O mixed oxides by gold deposition for VOC catalytic combustion, *Chemical Engineering Journal*. 175 (2011) 271-278.
- [23] Y. Wang, W. Deng, Y. Wang, L. Guo, T. Ishihara, A comparative study of the catalytic oxidation of chlorobenzene and toluene over Ce-Mn oxides, *Molecular Catalysis*. 459 (2018) 61-70.
- [24] X. Chen, S. Cai, E. Yu, J. Chen, H. Jia, MnOx/Cr₂O₃ composites prepared by pyrolysis of Cr-MOF precursors containing in situ assembly of MnOx as high stable catalyst for toluene oxidation, *Applied Surface Science*. 475 (2019) 312-324.
- [25] S.M. Maliyekkal, K.P. Lisha, T. Pradeep, A novel cellulose–manganese oxide hybrid material by in situ soft chemical synthesis and its application for the removal of Pb (II) from water, *Journal of Hazardous Materials*. 181 (2010) 986-995.
- [26] V. Subramanian, H. Zhu, B. Wei, Alcohol-assisted room temperature synthesis of different nanostructured manganese oxides and their pseudocapacitance properties in neutral electrolyte, *Chemical physics letters*. 453 (2008) 242-249.
- [27] W. Li, H. Liu, X. Ma, S. Mo, S. Li, Y. Chen, Fabrication of silica supported Mn–Ce benzene oxidation catalyst by a simple and environment-friendly oxalate approach, *Journal of Porous Materials*. 25 (2018) 107-117.
- [28] S. Mo, S. Li, J. Li, Y. Deng, S. Peng, J. Chen, Y. Chen, Rich surface Co (III) ions-enhanced Co nanocatalyst benzene/toluene oxidation performance derived from Co^{II} Co^{III} layered double hydroxide, *Nanoscale*. 8 (2016) 15763-15773.
- [29] X. Jiang, W. Xu, S. Lai, X. Chen, Integral structured Co–Mn composite oxides grown on

interconnected Ni foam for catalytic toluene oxidation, RSC Advances. 9 (2019) 6533-6541.

[30] L. Zhao, Z. Zhang, Y. Li, X. Leng, T. Zhang, F. Yuan, X. Niu, Y. Zhu, Synthesis of Ce_aMnO_x hollow microsphere with hierarchical structure and its excellent catalytic performance for toluene combustion, Applied Catalysis B-Environmental. 245 (2019) 502-512.

[31] Y. Deng, W. Tang, W. Li, Y. Chen, MnO_2 -nanowire@ NiO -nanosheet core-shell hybrid nanostructure derived interfacile Effect for promoting catalytic oxidation activity, Catalysis Today. 308 (2018) 58-63.

[32] P. Li, C. He, J. Cheng, C.Y. Ma, B.J. Dou, Z.P. Hao, Catalytic oxidation of toluene over $\text{Pd}/\text{Co}_3\text{AlO}$ catalysts derived from hydrotalcite-like compounds: Effects of preparation methods, Applied Catalysis B-Environmental. 101 (2011) 570-579.

[33] B. Grzybowska, J. Słoczyński, R. Grabowski, K. Weisło, A. Kozłowska, J. Stoch, J. Zieliński, Chromium oxide/alumina catalysts in oxidative dehydrogenation of isobutane, Journal of Catalysis. 178 (1998) 687-700.

[34] C. He, Y. Yu, C. Chen, L. Yue, N. Qiao, Q. Shen, J. Chen, Z. Hao, Facile preparation of 3D ordered mesoporous $\text{CuO}_x\text{--CeO}_2$ with notably enhanced efficiency for the low temperature oxidation of heteroatom-containing volatile organic compounds, RSC Advances. 3 (2013) 19639-19656.

[35] D. Jampaiah, K.M. Tur, P. Venkataswamy, S.J. Ippolito, Y.M. Sabri, J. Tardio, S.K. Bhargava, B.M. Reddy, Catalytic oxidation and adsorption of elemental mercury over nanostructured $\text{CeO}_2\text{--MnO}_x$ catalyst, RSC Advances. 5 (2015) 30331-30341.

[36] F. Kapteijn, A.D. Vanlangeveld, J.A. Moulijn, A. Andreini, M.A. Vuurman, A.M. Turek, J.-M. Jehng, I.E. Wachs, Alumina-supported manganese oxide catalysts: I. Characterization: effect of precursor and loading, Journal of Catalysis. 150 (1994) 94-104.

[37] Y. Xiang, Y. Zhu, J. Lu, C. Zhu, M. Zhu, Q. Xie, T. Chen, $\text{Co}_3\text{O}_4/\alpha\text{-Fe}_2\text{O}_3$ catalyzed oxidative degradation of gaseous benzene: Preparation, characterization and its catalytic properties, Solid State Sciences .93 (2019) 79-86.

- [38] X. Xie, Y. Li, Z.Q. Liu, M. Haruta, W. Shen, Low-temperature oxidation of CO catalysed by Co_3O_4 nanorods, *Nature*. 458 (2009) 746.
- [39] S. Xie, J. Deng, S. Zang, H. Yang, G. Guo, H. Arandiyana, H. Dai, Au–Pd/3DOM Co_3O_4 : Highly active and stable nanocatalysts for toluene oxidation, *Journal of Catalysis*. 322 (2015) 38-48.
- [40] Z. Wu, J. Deng, S. Xie, H. Yang, X. Zhao, K. Zhang, H. Lin, H. Dai, G. Guo, Mesoporous Cr_2O_3 -supported Au–Pd nanoparticles: High-performance catalysts for the oxidation of toluene, *Microporous & Mesoporous Materials*. 224 (2016) 311-322.
- [41] W. Si, Y. Wang, S. Zhao, F. Hu, J. Li, A facile method for in situ preparation of the $\text{MnO}_2/\text{LaMnO}_3$ catalyst for the removal of toluene, *Environmental Science & Technology*. 50 (2016) 4572-4578.
- [42] H. Huang, D.Y. Leung, Complete oxidation of formaldehyde at room temperature using TiO_2 supported metallic Pd nanoparticles, *ACS Catalysis*. 1 (2011) 348-354.

CHAPTER 6 Conclusions and Prospects

6.1 Conclusions

Pollutant volatile organic compounds (VOCs) has already been widely concerned because of their harmful properties to both the environment and human beings. One of environmental and economical way to remove VOCs is the catalytic oxidation, by which VOCs could be efficiently converted into harmless substances of H_2O , CO_2 , and other less harmful chemicals. The catalytic oxidation of VOCs relates to three kinds of reaction mechanisms, i.e., Eley-Rideal (E-R) mechanism, Langmuir-Hinshelwood (L-H) mechanism and Mars-van Krevelen (MVK) mechanism which dependent on the applied catalysts and the types of the involved VOCs in the reactions. The important factor for VOCs catalytic oxidation is to design and prepare the catalysts, which should possess high catalytic activity, stability and low cost. Therefore, according to this, we developed transition metal oxides-based catalysts prepared by time-saving method of electrodeposition, the obtained results are summarized as the following:

(1) In the first work, we prepared hetero-metal doping Co-based catalysts by using facile UPED electrodeposition method for the catalytic oxidation of toluene. The experimental results showed that the hetero-metal doping significantly influenced the morphology and surface elemental compositions of Co-based catalyst when compared with pure $\text{Co}_3\text{O}_4/\text{NF}$ catalyst. The enhanced low-temperature reducibility and oxygen mobility of Co-Ni/NF, Co-Mn/NF and Co-Cu/NF catalysts were favorable to the catalytic oxidation of toluene. Among all the prepared catalysts, Co-Cu/NF catalyst achieved the best catalytic activity, stability and high selectivity to CO_2 for the toluene oxidation as a result of its low-temperature reducibility, increased surface and lattice oxygen species, and high content of active Co^{3+} species promoted by the interaction of the mixed metal oxides.

(2) Based on first work as it stated above, we tried to prepare cerium (Ce) modified cobalt (Co)-based (Co-Ce) mixed oxide catalysts on nickel foam (NF) with different Co/Ce molar ratios by electrodeposition method. The morphology of Co-Ce/NF catalysts was significantly influenced by

the increased Co/Ce molar ratio from 5:1 to 15:1, and Co-Ce mixed oxide with a well nanosheet structure when Co/Ce molar ratio was 10:1. The synergistic effect between Co and Ce improved the reducibility and the generation of surface and lattice oxygen species of the prepared Co-Ce/NF catalysts. For the catalytic oxidation of toluene, 10Co-Ce/NF catalyst prepared with a molar ratio of Co/Ce at 10 in the initial solution achieved the best catalytic performance among all the catalysts with a complete toluene conversion temperature of 268 °C and CO₂ selectivity of 100%. Moreover, the excellent stability and water resistance of 10Co-Ce/NF catalyst after long-term test was contributed to its stable physiochemical properties.

(3) Cerium oxide (CeO₂) has been proved to be active to the catalytic oxidation. Therefore, we fabricated CeO₂-containing catalysts of Ag-CeO₂@CNWs/CF with highly dispersed Ag nanoparticles by using a three-step electrochemical process. The supported Ag nanoparticles with suitable loading effectively enhanced the low-temperature reducibility, the generation of oxygen vacancies, and distribution of surface acid sites, which are favorable to the catalytic oxidation of toluene. For the best catalyst of 80Ag-CeO₂@CNWs/CF, which achieved the best catalytic activity with the T₁₀, T₅₀ and T₉₀ of toluene conversions at 222, 240 and 256 °C, respectively, these values were much lower than those of 3.7wt%Ag-CeO₂@CNWs/CF catalyst prepared by a general wet impregnation method. Consequently, the present electrodeposition method could be a promising way to prepare high-performance catalysts for the catalytic oxidation of VOCs.

(4) Finally, in order to investigate the influence of the catalyst supports of NF and CF on the catalytic performance of the prepared catalysts, Mn-Co oxides based catalysts were prepared for the catalytic oxidation of VOCs. The results demonstrated that Mn-Co oxide composite were uniformly coated on the Cu nanowires, the nanowires provided advantages for the dispersion of the active species of Mn and Co, especially, the well-dispersed Mn and Co oxides and intimate contact of their nanocrystals exerted synergistic effect on the performance of final catalysts and therefore enhanced the catalytic performance of the catalyst. When the Mn/Co molar ratio was 10:1 in the initial solution for electrodeposition, the 0.10Mn-0.01Co/CF catalyst achieved the best catalytic activity with the

complete toluene conversion to CO_2 and H_2O at a temperature as low as 253 °C.

(5) Electrodeposition method is proved to be a facile and time-saving way to prepare active catalysts with stable physiochemical properties, excellent stability and water resistance for the catalytic oxidation of VOCs. As a result, compared with traditional methods such as impregnation, hydrothermal, co-deposition methods, it is expected that the electrodeposition method should be a more promising way to prepare highly active and stable transition metal-based catalysts with high utilization of metals and low cost for the efficient catalytic oxidation of VOCs.

6.2 Prospects

For the catalytic oxidation of VOCs, many efforts have already been made and we also got some achievements. However, it is worth noting that there is still great challenge for the development of novel catalysts with high catalytic activity, good stability, strong poisoning resistance and pretty cost for the catalytic oxidation of VOCs. In terms of noble-metal-based catalysts, noble metals are always supported on the support, as a result, their catalytic performance are not only related to the nature of the noble metal, but also closely associated with the physiochemical properties of the support. As stated above, the materials with porous structures and large specific surface areas can act as catalyst supports, which are favorable to the dispersion and stabilization of the supported noble metal, and thereby promoting their catalytic performance. Many researches concentrated on the noble metal based catalysts due to their high activity for the oxidation of VOCs. However, some such catalysts also have their poor resistance to poisoning and sintering, and the high costs limit their wide applications. In fact, in a practical industrial process, in addition to the high activity, the long-term stability is also an important factor. Consequently, current works pay more attentions on the long-term stability of the catalyst and have already made some achievement. Catalysts such as Pt-CeO₂/activated carbon, Pd/Co₃AlO and Au/Co₃O₄ have been confirmed to have good stability for VOCs oxidation during the long-term tests. Herein, mesoporous supports not only improved the adsorption and diffusion of the reactant molecules but also prevented the aggregation of the nanoparticles by confining them within their mesoporous structures. Nevertheless, VOCs derived

from industrial process always contain toxic substances such as sulfur or halogen, which could cause irreversible deactivation of the catalyst. Many efforts have been devoted to solve such issues. For instance, Pt/TiO₂-La₂O₃, Au/CeO₂-Al₂O₃, Pd/HAP and AuPd/CeO₂ catalysts have been developed, which demonstrated excellent poisoning resistance, especially for the catalytic oxidation of sulfur or chlorine containing VOCs. Importantly, the interaction between noble nanoparticles and porous support made a great contribution to the excellent stability of the catalyst. Thus, it can be concluded that noble metal with good resistance to poisoning and sintering could be well designed by using appropriate catalyst supports and preparation methods.

Moreover, it is always considered that the transition metal oxides based catalysts are more superior than the noble metal based ones because of their low cost, and strong poisoning resistance and high thermal stability for the heteroatom-containing VOCs oxidation. One of the advantages of transition metal oxides is that their morphologies can be easily controlled by applying different kinds of preparation methods. The special morphologies like rod, sheet, sphere, core-shell and so on, could expose more high-energy crystal faces, which are closely related to their catalytic performance. Meanwhile, the reported works have already proved that the transition metal oxides can be used as either catalysts or catalyst supports, especially the mixed metal oxides based catalysts have been found to have high capacity for the removal of VOCs efficiently at relatively low temperatures as a result of the improved low temperature reducibility and redox properties of the catalyst. For instance, catalysts of three-dimensional ordered mesoporous CuO_x-CeO₂, nanocube-shaped Co₃O₄, porous CeO₂-TiO₂ mixed oxides, sandwich-structured CeO₂@ZSM-5 hybrid composites and La modified HZSM-5 zeolite had high activity and stability for the chlorine and sulfur containing VOCs oxidation, demonstrating that transition metal oxides are the alternative and desirable catalysts with low cost for various VOCs oxidation when compared with the noble metal based ones. However, poisoning substances and coke formation still have some adverse effects on the catalyst. Especially, the adsorption of chlorine and sulfur species could result in the loss of active sites whereas the coke formation could block the pores and active sites of the catalysts. To solve chlorine or sulfur

poisoning, increasing reaction temperature and/or ozone treatment are considered as the effective way. Moreover, the formed coke can be easily removed by calcination in oxygen or air. Consequently, the transition metal oxides based catalysts could exhibit high poisoning resistance at relatively higher reaction temperatures and good thermal resistance capability.

As the mentioned above, both noble metal based catalysts and transition metal oxides based catalysts could be well designed and prepared according to the needs of the reaction, especially the combination of the noble metal and/or transition metal oxide with special morphology and porous structure could provide a possibility to apply noble metal based catalysts in a large scale with superior activity, high stability and low cost. At present, the investigation and application of porous materials have already been given a new prospect for the use of these catalysts in the catalytic oxidation of VOCs, and the superior nature of transition metals could make them widely used in practical processes.

List of publications and presentations

Publications

1. **Jing Wang**, Akihiro Yoshida, Peifen Wang, Tao Yu, Zhongde Wang, Xiaogang Hao, Abuliti Abudula, Guoqing Guan, “Catalytic oxidation of volatile organic compound over cerium modified cobalt-based mixed oxide catalysts synthesized by electrodeposition method”, *Applied Catalysis B: Environmental*, 271 (2020) 118941.
2. **Jing Wang**, Peifen Wang, Qiang Zhao, Tao Yu, Xiao Du, Xiaogang Hao, Abuliti Abudula, Guoqing Guan, “Highly dispersed Ag nanoparticles embedded on the surface of CeO₂/CF nanowires derived from three-dimensional structured Cu foam for toluene catalytic oxidation”, *Molecular Catalysis*, 486 (2020) 110879.
3. **Jing Wang**, Peifen Wang, Akihiro Yoshida, Qiang Zhao, Shasha Li, Xiaogang Hao, Abuliti Abudula, Guangwen Xu, Guoqing Guan, “Mn-Co oxide decorated on Cu nanowires as efficient catalysts for catalytic oxidation of toluene”, *Carbon Resources Conversions*, 3 (2020) 36-45.
4. **Jing Wang**, Peifen Wang, Qiang Zhao, Jing Shi, Xiao Du, Xiaogang Hao, Abuliti Abudula, Guoqing Guan, “Stable hetero-metal doped Co-based catalysts prepared by electrodeposition method for low temperature combustion of toluene”, *Carbon Resources Conversions*, 3 (2020) 95-103.
5. Peifen Wang, **Jing Wang**, Jin Shi, Xiao Du, Xiaogang Hao, Bing Tang, Abuliti Abudula, and Guoqing Guan, “Low content of samarium doped CeO₂ oxide catalysts derived from metal organic framework precursor for toluene oxidation”, *Molecular Catalysis*, 492 (2020)111027.
6. Zhijun Wu, Zhengkun Xie, **Jing Wang**, Tao Yu, Xiao Du, Zhongde Wang, Xiaogang Hao,

- Abuliti Abudula, and Guoqing Guan, “Simultaneously enhancing the thermal stability and electrochemical performance of solid polymer electrolytes by incorporating rod-like $\text{Zn}_2(\text{OH})\text{BO}_3$ particles”, *International Journal of Hydrogen Energy*, 2020, in press.
7. Zhijun Wu, Zhengkun Xie, Akihiro Yoshida, **Jing Wang**, Tao Yu, Zhongde Wang, Xiaogang Hao, Abuliti Abudula, and Guoqing Guan, “Nickel phosphate nanorod-enhanced polyethylene oxide-based composite polymer electrolytes for solid-state lithium batteries”, *Journal of Colloid and Interface Science*, 565 (2020) 110-118.
 8. Qiang Zhao, Junli Wang, Zuopeng Li, Yong Guo, **Jing Wang**, Bing Tang, Abuliti Abudula, and Guoqing Guan, “Heterostructured graphitic-carbon-nitride-nanosheets/copper(I) oxide composite as an enhanced visible light photocatalyst for decomposition of tetracycline antibiotics”, *Separation and Purification Technology*, 250(2020), 117238.
 9. Sang Dinh Ngo, Thi Tuong Vi Tran, Suwadee Kongparakul, Prasert Reubroycharoen, Pinit Kidkhuntod, Narong Chanlek, **Jing Wang**, Guoqing Guan, and Chantip Samart, “Catalytic pyrolysis of Napier grass with nickel-copper core-shell bi-functional catalyst”, *Journal of Analytical and Applied Pyrolysis*, 145 (2020) 104745.
 10. Wachiraporn Kettum, Thi Tuong Vi Tran, Suwadee Kongparakul, Prasert Reubroycharoen, **Jing Wang**, Guoqing Guan, Mingyue Ding, Chantip Samart, “High Selective Monoaromatic Hydrocarbon via Integrated Pyrolysis and Catalytic Upgrading of Napier Grass over Ca/Ni/Boronic acid/KIT-6”, *Biomass Conversion and Biorefinery*, 10 (2020) 423–434.

Patents

1. 王ジン、吉田曉弘、官国清、阿布里提、関和志、“VOC 除去用触媒の製造方法、VOC 除去用触媒及び VOC 除去方法”、日本特許、出願番号：特願 2018-157437、出願日：2018 年 8 月 24 日.
2. 王ジン、王佩芬、官国清、吉田曉弘、関和志、阿布里提、“VOC 除去用触媒の製造方法、VOC 除去用触媒及び VOC 除去方法”、日本特許、出願番号：特願 2019-082755、出願日：2019 年 4 月 24 日.
3. 王ジン、官国清、王佩芬、吉田曉弘、関和志、阿布里提、“VOC 除去用触媒の製造方法及び VOC 除去用触媒並びに VOC 除去方法”、日本特許、出願番号：特願 2019-155551、出願日：2019 年 8 月 28 日.
4. 王佩芬、王ジン、官国清、吉田曉弘、関和志、阿布里提、“金属酸化物触媒の製造方法及び VOC 除去方法”、日本特許、出願番号：特願 2019-081959、出願日：2019 年 4 月 23 日.
5. 王佩芬、官国清、王ジン、吉田曉弘、関和志、阿布里提、“VOC 除去触媒製造用前駆体、VOC 除去触媒及びその製造方法”、日本特許、出願番号：特願 2019-154653、出願日：2019 年 8 月 27 日.
6. 王佩芬、官国清、王ジン、関和志、阿布里提、“VOC 除去触媒及びその製造方法、” 出願番号：特願 2020-021327、出願日：2020 年 2 月 12 日.

International presentations

1. Peifen Wang, **Jing Wang**, Akihiro Yoshida, Suwadee Kongparakul, Chanatip Samart, Katsuki Kusakabe, Abuliti Abudula, and Guoqing Guan, “Enhanced toluene combustion

performance over Pt loaded Sm doping CeO₂ catalysts,” The 32nd International Symposium on Chemical Engineering (ISChE2019), at Chungnam National University, Daejeon, Korea, December 6-8, 2019.

Domestic presentations

1. **Jing Wang**, Akihiro Yoshida, Tao Yu, Abuliti Abudula, Guoqing Guan, “Catalytic combustion of toluene on Co-based catalysts synthesized by electrodeposition method”, 第 122 回触媒討論会 in 北海道教育大学,函館, 2018.
2. **Wang Jing**, Yu Tao, 吉田 曉弘, 阿布里提, 官 国清, “Catalytic combustion of toluene over Cu-Mn catalysts loaded on nickel foam by electrodeposition method”, 化学工学会第 84 年会, 芝浦工業大学, 2019.
3. 王 ジン, 王 佩芬, 吉田 曉弘, 阿布里提, 官 国清, “Mn-Co oxides supported on the nanowires of Cu foam for toluene catalytic combustion”, 化学工学会 横浜大会, 横浜国立大学, 2019.
4. **Jing Wang**, Peifen Wang, Akihiro Yoshida, Tao Yu, Abuliti Abudula, Guoqing Guan, “Low temperature catalytic oxidation of toluene over Ag-CeO₂/CF catalysts synthesized by novel electrodeposition method,” 化学工学会第 85 年会, 関西大学千里山キャンパス, 2020.
5. 王 佩芬, 王 ジン, 吉田 曉弘, 阿布里提, 官 国清, “A facile method to synthesize high performance Mn-Co oxides towards the oxidation of volatile organic compounds,” 化学工学会横浜大会, 横浜国立大学, 2019.
6. Peifen Wang, **Jing Wang**, Qiang Zhao, Tao Yu, Akihiro Yoshida, Abuliti Abudula,

Guoqing Guan, “Low-temperature catalytic combustion of toluene over Mn-Co oxides prepared by one-step agar-gel method,” 4 校交流会 in 一関工業高等専門学校, 2019.

Awards

1. Student Special Award (学生特別賞) at SCEJ Conference in Yokohama, 2019.
2. Excellent Student Recognition of Hirosaki University, 2020.